POLITECHNIKA RZESZOWSKA
im. Ignacego Łukasiewicza
WYDZIAŁ CHEMICZNY

PRACA DOKTORSKA

Synteza i analiza aktywności biologicznej zmodyfikowanych dendrymerów poliamidoaminowych generacji trzeciej podstawionych wybranymi związkami z grupy ksantonów, jako potencjalnych czynników w terapii przeciwnowotworowej i przeciwnicieniowej

mgr inż. Joanna Drozdowska

Promotorzy pracy:
Prof. dr hab. Wojciech Rode
Dr hab. Łukasz Uram, prof. PRz

Rzeszów, 2022

Dziękuję Panu dr hab. Łukaszowi Uramowi, prof. PRz za wspólną naukową drogę, która rozpoczęła się od pracy inżynierskiej, przez magisterską i trwała aż po doktorską. Dziękuję za wprowadzenie w fascynujący świat hodowli komórkowych, naukę metodyki pracy oraz przekazaną wiedzę i doświadczenie. Dziękuję za wszelkie rady, uwagi i wiarę w moje umiejętności. Miło będę wspominać nasze rozmowy i dyskusje podczas drogi do Laboratorium w Albigowej.

Dziękuję Panu prof. dr hab. Wojciechowi Rode za poświęcony czas i energię podczas opieki nad moją pracą doktorską, za dyskusje naukowe, wszelkie uwagi oraz doświadczenie, z którego mogłam czerpać podczas prowadzenia badań. Chcę podziękować także za możliwość odbycia stażu w Instytucie im. M. Nenckiego w Warszawie, gdzie poznałam techniki prowadzenia badań na organizmie modelowym nicieniu Caenorhabditis elegans.

Dziękuję Panu prof. dr hab. inż. Stanisławowi Wołowcowi za przekazaną wiedzę, doświadczenie oraz naukę syntezy dendrymerów i prowadzenia pomiarów NMR, a także za możliwość pracy w Profesora Laboratorium.

Dziękuję pracownikom i doktorantom z Katedry Chemii Nieorganicznej i Analitycznej oraz Katedry Polimerów i Biopolimerów za życzliwość oraz miłą atmosferę w pracy.

Dziękuję mojemu mężowi za nieustające wsparcie, wiarę we mnie, dodawanie otuchy w chwilach zwątpienia, cierpliwość oraz za pomoc w zachowaniu równowagi między pracą a życiem prywatnym.

Dziękuję moim rodzicom, rodzinie oraz przyjaciołom za wsparcie, wiarę we mnie oraz dopingowanie moich działań.

SPIS TREŚCI

Wykaz powiązanych tematycznie artykułów naukowych stanowiących rozprawę doktorską

Dla przedstawionych poniżej publikacji sumaryczny Impact Factor wynosi **20,403**, natomiast punktacja MEiN wynosi **480** punktów.

Publikacja 1 [P1]:

Markowicz Joanna*, Uram Łukasz, Sobich Justyna, Mangiardi Laura, Maj Piotr, Rode Wojciech. Antitumor and anti-nematode activities of α-mangostin. *European Journal of Pharmacology*. 2019 Nov 15;863:172678. doi: 10.1016/j.ejphar.2019.172678.

Impact Factor$_{2019}$: 3,263; Impact Factor$_{5\text{-letni}}$: 4,721; MEiN: 100 pkt; Liczba cytowań: 23

Publikacja 2 [P2]:

Maj Piotr, Mori Mattia, Sobich Justyna, **Markowicz Joanna**, Uram Łukasz, Zieliński Zbigniew, Quaglio Deborah, Calcaterra Andrea, Cau Ylenia, Botta Bruno, Rode Wojciech*. Alvaxanthone, a Thymidylate Synthase Inhibitor with Nematocidal and Tumoricidal Activities. *Molecules*. 2020 Jun 23;25(12):2894. doi: 10.3390/molecules25122894.

Impact Factor$_{2020}$: 4,412; Impact Factor$_{5\text{-letni}}$: 5,110; MEiN: 140 pkt; Liczba cytowań: 2

Publikacja 3 [P3]:

Markowicz Joanna*, Uram Łukasz, Wołowiec Stanisław, Rode Wojciech*. Biotin Transport-Targeting Polysaccharide-Modified PAMAM G3 Dendrimer as System Delivering α-Mangostin into Cancer Cells and *C. elegans* Worms. *International Journal of Molecular Sciences*. 2021 Nov 29;22(23):12925. doi: 10.3390/ijms222312925.

Impact Factor$_{2021}$: 6,208; Impact Factor$_{5\text{-letni}}$: 6,628; MEiN: 140 pkt; Liczba cytowań: 4

Publikacja 4 [P4]:

Markowicz Joanna*, Wołowiec Stanisław, Rode Wojciech, Uram Łukasz. Synthesis and Properties of α-Mangostin and Vadimezan Conjugates with Glucoheptoamidated and Biotinylated 3rd Generation Poly(amidoamine) Dendrimer, and Conjugation Effect on Their Anticancer and Anti-Nematode Activities. *Pharmaceutics*. 2022 March 10;14(3):606. doi: 10.3390/pharmaceutics14030606.

Impact Factor$_{2021}$: 6,525; Impact Factor$_{5\text{-letni}}$: 7,227; MEiN: 100 pkt; Liczba cytowań: 1

Streszczenie w języku polskim

Korzystne właściwości biologiczne ksantonów wykazane w wielu badaniach *in vitro* oraz *in vivo* potwierdzają ich potencjał do zastosowania w terapii między innymi chorób nowotworowych, pasożytniczych, czy zakażeń bakteryjnych. Jednakże częstym ograniczeniem tego typu związków są ich słabe parametry farmakokinetyczne, które uniemożliwiają wprowadzenie ksantonów do zastosowań klinicznych. Rozwiązaniem tego problemu może być użycie nośników leków, na przykład dendrymerów poliamidoaminowych (PAMAM), z którymi można związać cząsteczkę leku na drodze enkapsulacji bądź kowalencyjnie. Dendrymery PAMAM, będące super-rozgałęzionymi polimerami o wysokiej biokompatybilności, pozwalają usprawnić transport trudno rozpuszczalnych leków, zmniejszyć ich toksyczność oraz uzyskać efekt celowania w konkretne komórki, organella bądź szlaki metaboliczne. Dużym atutem dendrymerów jest ich poliwalentność, pozwalająca na równoczesne przyłączenie cząsteczek leku, cząsteczki adresującej, znacznika umożliwiającego obrazowanie lokalizacji tych nanocząstek oraz innych ligandów.

W niniejszej pracy po raz pierwszy opracowano koniugaty dendrymeru PAMAM generacji trzeciej (G3) z kowalencyjnie przyłączoną α-mangostyną lub vadimezanem. Wyboru tych dwóch związków dokonano na podstawie badań toksyczności grupy ośmiu ksantonów przeprowadzonych na dwóch liniach ludzkich komórek nowotworowych: komórkach raka płaskonabłonkowego z języka (SCC-15) i komórkach glejaka wielopostaciowego IV stopnia (U-118 MG) oraz porównawczo na komórkach prawidłowych fibroblastów skórnych linii BJ. Zsyntezowano szereg koniugatów dendrymerowych, w których reszty α-mangostyny (M) lub vadimezanu (V) przyłączono za pomocą wiązań amidowych lub estrowych. Dodatkowo, jako czynnik zwiększający wychwyt i kierujący do wybranych komórek nowotworowych zastosowano biotynę (B), a pozostałe wolne grupy aminowe na powierzchni nośnika zmodyfikowano resztami α-D-glukoheptono-1,4-laktonu (gh) w celu zmniejszenia natywnej cytotoksyczności dendrymeru. Otrzymano koniugaty amidowe o różnym stopniu postawienia resztami α-mangostyny: $\mathbf{G3^{2B12gh5M}}$ oraz $\mathbf{G3^{2B10gh17M}}$, a także koniugat estrowy $\mathbf{G3^{gh2B5M}}$. Zsyntezowano analogiczne koniugaty z vadimezanem: $\mathbf{G3^{2B12gh5V}}$ oraz $\mathbf{G3^{gh4B5V}}$. Związki $\mathbf{G3^{2B12gh}}$ oraz $\mathbf{G3^{gh}}$ stanowiły kontrolę w postaci nośnika, odpowiednio dla koniugatów amidowych oraz estrowych. Badania *in vitro* oraz *in vivo* na organizmie modelowym *C. elegans* wykazały brak toksyczności i działania antyproliferacyjnego tych nośników. Przyłączenie reszt α-mangostyny do dendrymeru $\mathbf{G3^{2B12gh}}$ istotnie zwiększyło aktywność biologiczną związku w zależności od stopnia

podstawienia, osiągając nawet 25-krotne wzmocnienie działania cytotoksycznego w przypadku koniugatu **G3^{2B10gh17M}**. Efekt wzmocnienia obserwowany był w przypadku każdego z badanych parametrów komórkowych (poziom ATP, aktywność kaspaz wykonawczych, stopień proliferacji i adhezji komórek) a także był widoczny w postaci spadku poziomu żywotności nicienia *C. elegans*. Koniugaty dendrymeru z amidowo przyłączoną α-mangostyną dodatkowo wyznakowano fluorescencyjnie, co pozwoliło wykazać, że związki te wnikały do badanych komórek i były zlokalizowane w pęcherzykach endocytarnych oraz częściowo w mitochondriach. Porównując aktywność amidowych oraz estrowych koniugatów α-mangostyny, zastosowanie obu typów wiązań zwiększyło aktywność związku, jednak silniejsze działanie wobec każdego z badanych parametrów uzyskano stosując wiązania amidowe. W przypadku vadimezanu, który nie wykazał toksyczności wobec badanych komórek i nicienia, przyłączenie związku do dendrymeru za pomocą wiązania estrowego nie zwiększyło jego aktywności. Natomiast uzyskano słabe, selektywne działanie antyproliferacyjne vadimezanu wobec komórek raka płaskonabłonkowego, które zostało zwielokrotnione poprzez przyłączenie związku wiązaniem amidowym do nośnika **G3^{2B12gh}**.

W prezentowanej pracy przedstawiono również wpływ wielkości oraz potencjału zeta koniugatów na badane parametry biologiczne. Na podstawie analizy pomiarów DLS oraz testów *in vitro* i *in vivo* można sformułować wniosek, że zastosowanie wiązań amidowych, częściowe zablokowanie powierzchniowych grup aminowych oraz zwiększona średnica i dodatni potencjał zeta, może stanowić zestaw modyfikacji dendrymeru PAMAM G3 niezbędny do zastosowania związku jako efektywnego nośnika leków.

Podsumowując, niniejsza praca doktorska dostarczyła informacji na temat działania przeciwnowotworowego i przeciwnicieniowego α-mangostyny, które może zostać wzmocnione poprzez zastosowanie nośnika w postaci odpowiednio zmodyfikowanego dendrymeru PAMAM G3. Opracowane nośniki pozostawały nietoksyczne wobec badanych komórek i nicieni, a aktywność przeciwnowotworowa oraz przeciwnicieniowa koniugatów była wynikiem działania transportowanego związku. Przedstawione badania na komórkach oraz *C. elegans* pozwalają stwierdzić, że otrzymane koniugaty α-mangostyny z nośnikiem dendrymerowym mogą stanowić nowe potencjalne terapeutyki do zastosowania w leczeniu chorób nowotworowych oraz zakażeń nicieniowych.

Streszczenie w języku angielskim

The favourable biological properties of xanthones demonstrated in many *in vitro* and *in vivo* studies confirm their potential for use in cancer therapy and bacterial or parasitic diseases. However, a common limitation of these types of compounds is their poor pharmacokinetic parameters, which prevent xanthones from being introduced into clinical use. The solution to this problem may be the use of drug carriers, for example poly(amidoamine) (PAMAM) dendrimers, to which the drug molecule can be covalently attached or encapsulated. The PAMAM dendrimers, which are hyper-branched polymers with high biocompatibility, allow to improve the transport of sparingly soluble drugs, reduce their toxicity and achieve the effect of targeting specific cells, organelles or metabolic pathways. A great advantage of dendrimers is their polyvalence allowing for the simultaneous attachment of drug molecules, a targeting molecules, a marker enabling the imaging of the location of these nanoparticles, and other ligands.

In this study, the third generation PAMAM dendrimer (G3) conjugates with covalently attached α-mangostin (M) or vadimezan (V) were developed for the first time. These two compounds were selected on the basis of toxicity studies of a group of eight xanthones performed on two human cancer cell lines: squamous cell carcinoma cells from the tongue (SCC-15) and grade IV glioblastoma multiforme cells (U-118 MG), and comparatively on normal skin fibroblast cells (line BJ). A number of dendrimer conjugates were synthesized with α-mangostin or vadimezan attached by amide or ester bonds. Additionally, biotin (B) was used as a targeting molecule to cancer cells, and the remaining free amine groups on the carrier surface were modified with α-D-glucoheptono-1,4-lactone (gh) to reduce the native dendrimer cytotoxicity. The amide conjugates with different amount of α-mangostin **G3^{2B12gh5M}** and **G3^{2B10gh17M}**, as well as the ester conjugate **G3^{gh2B5M}** were obtained. The equivalent conjugates were synthesized also with vadimezan: **G3^{2B12gh5V}** and **G3^{gh4B5V}**. The **G3^{2B12gh}** and **G3^{gh}** compounds were vehicle control for amide and ester conjugates, respectively. *In vitro* and *in vivo* studies on the *C. elegans* model organism revealed the lack of toxicity and antiproliferative effect of these vehicles. The attachment of α-mangostin to **G3^{2B12gh}** dendrimer significantly increased the biological activity of this compound depending on the degree of the dendrimer substitution by xanthone, with a 25-fold enhancement of the cytotoxic effect obtained in the case of the **G3^{2B10gh17M}** conjugate. The boost effect was observed for all studied cellular parameters (ATP level, activity of executioner caspases, degree of cells proliferation and adhesion) and was also visible as a decrease in the level of

C. elegans viability. The dendrimer conjugates with amide-bonded α-mangostin were additionally fluorescently labeled, which allowed to show that this compounds penetrate into the tested cells and accumulate in endocytic vesicles and partially in the mitochondria. Comparing the activity of the amide and ester α-mangostin conjugates, the use of both types of bonds increased the activity of the compound, but a stronger effect on each of the tested parameters was obtained in case of using amide bonds. In the case of vadimezan, which showed no toxicity against the tested cells and nematodes, the attachment to the dendrimer *via* an ester bond did not improve its activity. However, a weak selective antiproliferative activity of vadimezan against squamous carcinoma cells was obtained, which was multiplied by attaching the compound to the **G3**$^{\mathbf{2B12gh}}$ vehicle by amide bond.

The presented study also indicated the influence of the size and zeta potential of the synthesized conjugates on the tested biological parameters. Based on the analysis of DLS measurements and performed *in vitro* and *in vivo* studies, it can be concluded that the use of amide bonds, partial blockade of surface amine groups, and increased diameter and positive zeta potential may constitute a set of PAMAM G3 dendrimer modifications necessary for the use of the compound as an effective drug carrier.

To sum up, this PhD thesis provided information on the anticancer and antinematode activity of α-mangostin that can be strengthened using an appropriately modified PAMAM G3 dendrimer vehicle. The developed carriers remained non-toxic for studied cells and nematodes, and the anticancer and nematocidal activity of conjugates was the result of the mechanism of action of the transported compound. The presented studies allow to state that the obtained α-mangostin conjugates with a dendrimer carrier may be the new potential drugs for the treatment of cancer and nematode diseases.

1. Wprowadzenie teoretyczne

Związki pochodzenia naturalnego posiadają szereg korzystnych właściwości biologicznych, dzięki którym znalazły zastosowanie w przemyśle farmaceutycznym [1], kosmetycznym [2], rolniczym [3], a także nanotechnologii [4]. Struktura takich związków stanowi punkt wyjściowy do tworzenia licznych pochodnych o zmienionych, często korzystnych właściwościach, jak również do syntezy biopolimerów [5]. Na przestrzeni blisko czterech dekad (w latach 1981 – 2019) prawie 42% nowo wprowadzonych do obrotu leków stanowiły związki pochodzenia naturalnego lub ich syntetyczne pochodne, które znalazły zastosowanie w terapii chorób nowotworowych, chorób układu krążenia, cukrzycy, hemofilii i wielu innych [6]. Połowa nowych substancji o właściwościach przeciwbakteryjnych została opracowana na bazie związków naturalnych, co jest istotne ze względu na rosnący problem antybiotykooporności patogenów bakteryjnych [6,7].

Na szczególną uwagę zasługują ksantony, będące grupą ponad 1200-stu scharakteryzowanych, heterocyklicznych związków naturalnych, których cechą charakterystyczną jest obecność pierścienia dibenzo-γ-pironu (9*H*-ksanten-9-on) (Ryc. 1).

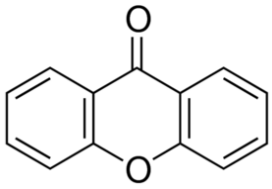

Ryc. 1. Struktura chemiczna cząsteczki ksantonu (9H-ksanten-9-onu) [własne, na podstawie [8]].

Większość przedstawicieli tej grupy (48%) można znaleźć w roślinach z rodziny kluzjowatych (*Clusiaceae* Lindl.), gdzie występują jako metabolity wtórne [8]. Mangostan właściwy (*Garcinia mangostana* L., *Clusiaceae*), drzewo z rodziny kluzjowatych, jest bogaty w izoprenylowane ksantony, wśród których najlepiej poznane są: α-, β-, γ-mangostyna, gartanina, 8-deoksygartanina oraz garcynon C i D [9]. Owocnia mangostanu (Ryc. 2A) była wykorzystywana w medycynie tradycyjnej w Azji Południowo-Wschodniej w formie maści, naparów, a także nalewek do leczenia stanów zapalnych, wrzodów, biegunki, infekcji skóry i ran [10].

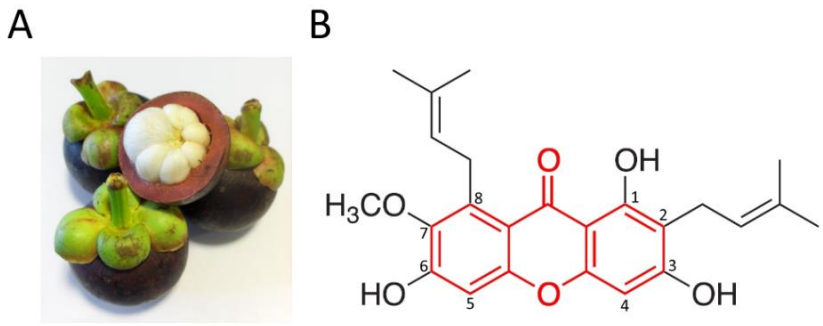

Ryc. 2. (A) Owocnia mangostanu [11] oraz (B) struktura chemiczna α-mangostyny [własne, na podstawie [12]].

Wiele współczesnych badań *in vitro* oraz *in vivo* pokazuje, że związki z grupy ksantonów posiadają różnorodne właściwości biologiczne: antyoksydacyjne, przeciwzapalne, przeciwbakteryjne, przeciwgrzybicze, przeciwmalaryczne oraz przeciwnowotworowe [13–16]. Ponadto podczas badań klinicznych pierwszej fazy, przeprowadzonych na zdrowych ochotnikach stwierdzono, że formulacje na bazie mangostanu znacząco zwiększają zdolność antyoksydacyjną organizmu oraz poprawiają funkcje układu odpornościowego, nie powodując skutków ubocznych [17,18].

Najwięcej uwagi, ze względu na korzystne właściwości przeciwnowotworowe, poświęca się obecnie α-mangostynie (1,3,6-trihydroksy-7-metoksy-2,8-bis(3-metylbut-2-en-1-yl)-9H-ksanten-9-on), która najobficiej występuje w owocni mangostanu [19]. W swojej strukturze (Ryc. 2B) α-mangostyna posiada trójpierścieniowy rdzeń ksantonowy, podstawiony dwiema grupami izoprenylowymi w pozycji C2 i C8, trzema grupami hydroksylowymi w pozycji C1, C3 i C6 oraz jedną grupą metoksylową w pozycji C7. α-Mangostyna swoją aktywność biologiczną zawdzięcza przede wszystkim obecności grup izoprenylowych oraz hydroksylowych, wśród których największe znaczenie dla właściwości przeciwnowotworowych ma grupa izoprenylowa przy węglu C8 [20,21].

Mechanizm działania przeciwnowotworowego α-mangostyny jest wielotorowy i na poziomie komórkowym opiera się głównie na (i) hamowaniu proliferacji komórek nowotworowych [22], (ii) zatrzymaniu ich cyklu komórkowego [23], (iii) indukcji apoptozy [24] oraz (iv) hamowaniu procesów angiogenezy [25]. Na poziomie organizmu skutkuje to spowolnieniem lub zatrzymaniem wzrostu guza [26] oraz ograniczeniem częstości przerzutowania do innych narządów [27]. Przedstawiona aktywność α-mangostyny została potwierdzona w badaniach komórkowych *in vitro* oraz na mysich modelach wielu typów nowotworów, między innymi: płuc [28], trzustki [26,29], piersi [30], jelita grubego [31,32], skóry [25] oraz krwi [33].

Poważnym ograniczeniem dla zastosowania α-mangostyny w farmakoterapii jest jej niska rozpuszczalność w wodzie, wynosząca 2,03 × 10^{-4} mg/L w 25 °C [34]. Powoduje to przede wszystkim słabą absorpcję oraz niską biodostępność leku w organizmie po podaniu doustnym, związaną z intensywną eliminacją leku w ramach efektu pierwszego przejścia [35]. W przypadku podania dożylnego α-mangostyna podlega szybkiej eliminacji z krwi, a następnie akumulacji w tkankach, głównie w nerkach, wątrobie, jelicie cienkim i płucach [36].

Vadimezan (kwas 5,6-dimetyloksantenon-4-octowy, DMXAA, ASA404) posiada dużo prostszą strukturę (Ryc. 3) niż α-mangostyna i pozbawiony jest przede wszystkim grup izoprenylowych przyłączonych do pierścienia ksantonowego.

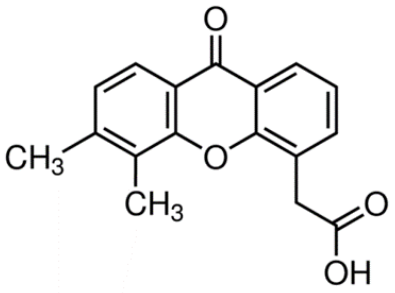

Ryc. 3. Struktura chemiczna vadimezanu [własne, na podstawie [37]].

Vadimezan zaliczany jest do grupy związków zaburzających strukturę naczyń krwionośnych w obrębie guzów nowotworowych (VDA, ang. *vascular disrupting agent*), przez co wykazuje wysoki potencjał działania przeciwnowotworowego zwłaszcza wobec nowotworów złośliwych, zdolnych do tworzenia przerzutów. Pośrednim skutkiem działania vadimezanu jest także aktywacja wrodzonej odpowiedzi immunologicznej, która prowadzi między innymi do produkcji cytokin prozapalnych i tlenku azotu oraz do zaburzenia metabolizmu energetycznego komórek guza [37]. Wyniki badań *in vitro* oraz *in vivo* vadimezanu były na tyle obiecujące, że związek trafił do etapu badań klinicznych, które jednak zakończyły się niepowodzeniem w III fazie, przez co związek nie został zatwierdzony jako lek [38]. Pomimo porażki vadimezanu jako czynnika VDA, podejmowane są dalsze próby wykorzystania jego pozostałych właściwości i zastosowania go zarówno w wolnej postaci, jak i z odpowiednim nośnikiem [39].

W celu poprawy właściwości farmakokinetycznych oraz biodystrybucji słabo rozpuszczalnych leków, przy równoczesnym zachowaniu ich aktywności biologicznej, wykorzystuje się systemy dostarczania bazujące na nośnikach. Stosuje się głównie nanocząstki, a także nanomicele, nanokryształy, nanorurki węglowe, hydrożele lub nośniki

krzemowe. Transportowany związek może być fizycznie enkapsulowany w nośniku, zaadsorbowany na jego powierzchni, a także związany kowalencyjnie lub na zasadzie oddziaływań elektrostatycznych [40]. Oprócz poprawy parametrów farmakokinetycznych, związanie leku z nośnikiem pozwala na zwiększenie jego stabilności oraz ukierunkowany transport do miejsca docelowego, któremu towarzyszyć będzie kontrolowane, spowolnione uwalnianie. Dzięki temu związek dociera do miejsca przeznaczenia w terapeutycznym stężeniu, a skutki uboczne związane z ogólnoustrojową toksycznością wobec prawidłowych tkanek są znacząco ograniczone [41]. Ukierunkowany transport leków jest podstawowym elementem terapii celowanej, która stanowi obiecującą metodę leczenia chorób nowotworowych oraz innych schorzeń.

Systemy transportu oparte na nanonośnikach projektowane są także dla α-mangostyny i mają na celu zwiększenie jej aktywności przeciwnowotworowej, selektywności oraz poprawę parametrów fizykochemicznych w porównaniu ze związkiem w wolnej postaci. W literaturze opisano przykłady zastosowania między innymi nanowłókien [42], nanomiceli [43], liposomów [44], a także nanocząstek polimerowych (wytwarzanych z polimerów naturalnych i syntetycznych) [45–47], lipidowych [48] oraz nanocząstek złota [49].

W prezentowanej pracy zaproponowano użycie dendrymeru poliamidoaminowego (PAMAM) jako nośnika dla α-mangostyny oraz vadimezanu. Dendrymery to globularne makrocząsteczki o wysoce rozgałęzionej, trójwymiarowej strukturze przypominającej drzewo (Ryc. 4), któremu zawdzięczają swoją nazwę (w języku greckim „*dendron*" oznacza drzewo, „*meros*" oznacza część). Osiągają średnicę w zakresie 1-100 nm. Rdzeń struktury dendrymeru stanowi atom lub cząsteczka, od którego odchodzą powtarzające się rozgałęzienia tworzące dendrony, na których powierzchni obecne są grupy funkcyjne [50].

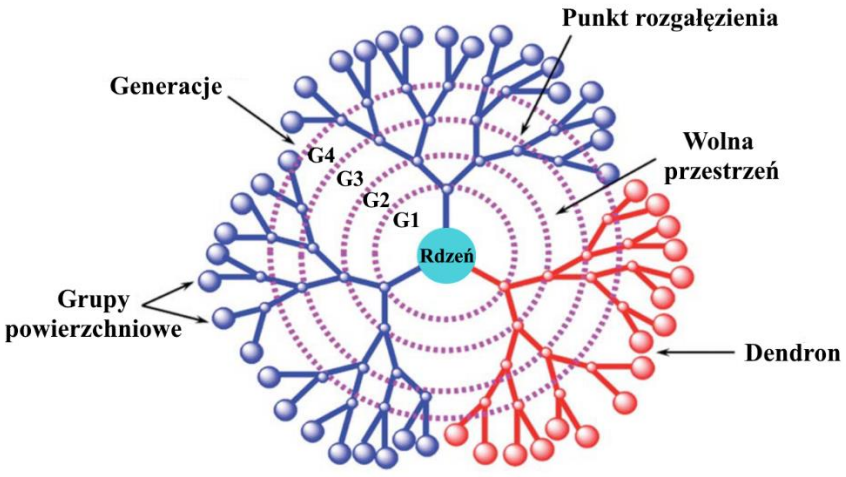

Ryc. 4. Schematyczne przedstawienie struktury dendrymeru [[51], zmienione].

Przewagą dendrymerów nad konwencjonalnymi polimerami liniowymi jest ściśle zdefiniowana struktura, z wielkością i monodyspersyjnością zbliżoną do białek; obecność licznych, łatwych do modyfikacji grup funkcyjnych na powierzchni; obecność wewnątrzcząsteczkowych jam pozwalających na enkapsulację; wysoka rozpuszczalność w wodzie; poliwalentność; biokompatybilność oraz relatywnie niska immunogenność. Dodatkowo globularny kształt dendrymerów pozwala na ich wydajne wnikanie do komórek łącznie z uzyskaniem efektu celowania, zmniejszony wychwyt przez makrofagi, a także łatwe przechodzenie przez bariery biologiczne na drodze transcytozy [52]. Wymienione właściwości dendrymerów sprawiły, że są one intensywnie badane i ulepszane przede wszystkim jako nośniki leków w terapii chorób nowotworowych [53], chorób neurodegeneracyjnych [54], choroby zwyrodnieniowej stawów [55], ale także jako nośniki innych substancji biologicznie aktywnych, użytecznych w terapii genowej [56], terapii fotodynamicznej [57], inżynierii tkankowej [58] oraz jako nośniki czynników kontrastowych stosowanych w różnych technikach obrazowania [59]. Dendrymery okazały się również pomocne jako adjuwanty w szczepionkach, zwiększając działanie immunostymulujące niskocząsteczkowych antygenów [60].

Dendrymery otrzymywane są metodami, które pozwalają na pełną kontrolę ich struktury na każdym etapie syntezy. Najczęściej stosowanymi są metoda rozbieżna oraz metoda zbieżna (Ryc. 5).

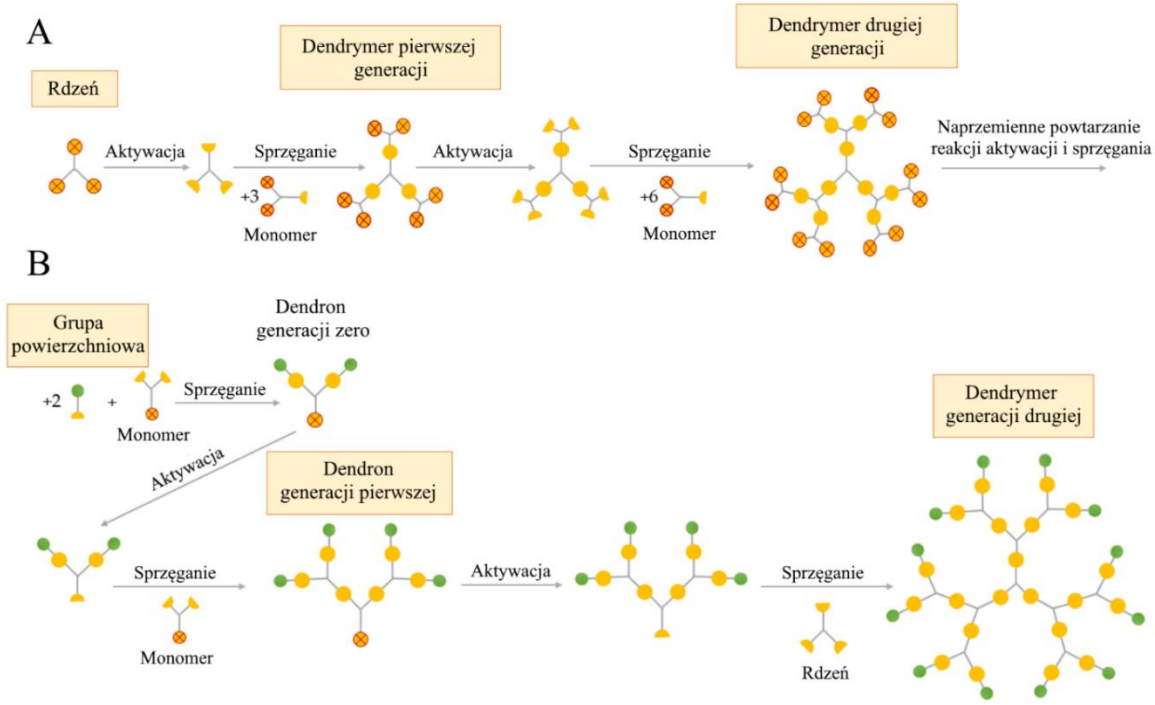

Ryc. 5. Uproszczony schemat syntezy dendrymerów metodą (A) rozbieżną oraz (B) zbieżną [[61], zmienione].

Metoda rozbieżna opracowana przez Tomalię i Newkome'a, polega na „wzroście" dendrymeru od wielofunkcyjnego rdzenia do obrzeży polimeru i na naprzemiennym powtarzaniu dwóch reakcji: aktywacji grup końcowych rdzenia (lub grup końcowych monomeru w dalszych etapach syntezy) oraz przyłączania cząsteczki monomeru. Przyłączenie monomeru do rdzenia pozwala otrzymać generację pierwszą dendrymeru (G1), po czym aktywacja grup funkcyjnych G1 i kolejne przyłączenie nowej cząsteczki monomeru prowadzi do powstania generacji drugiej (G2) i tak dalej. Ogólnie rzecz ujmując, każda nowa warstwa rozgałęzień daje nową generację [61]. Metoda rozbieżna w stosunkowo szybki sposób pozwala uzyskać wysoce symetryczne dendrymery, przy czym ze względu na ograniczenia wywołane zawadą steryczną oraz ryzyko uzyskania zdeformowanych rozgałęzień najwyższą generacją, jaką można otrzymać komercyjnie, jest generacja dziesiąta o średnicy 13,5 nm. Jedynie w skali laboratoryjnej zsyntezowano dendrymer triazynowy generacji trzynastej, który pozostawał stabilny w warunkach zmiennego pH, temperatury i polarności rozpuszczalnika [62].

Alternatywnym sposobem jest metoda zbieżna, zaproponowana przez Fréchet'a i Hawker'a w 1990 roku, w której synteza prowadzona jest od powierzchni do wnętrza dendrymeru, również poprzez naprzemienne powtarzanie reakcji sprzęgania oraz aktywacji. W pierwszym etapie grupy powierzchniowe (zwykle dwie) przyłączane są do monomeru, który następnie ulega aktywacji i reaguje z kolejnym monomerem, tworząc dendron generacji pierwszej, tzw. klin dendrytyczny. Procedura może być powtarzana kilkakrotnie w celu otrzymania bardziej rozgałęzionych dendronów wyższych generacji, które w ostatnim etapie syntezy zostaną przyłączone do wielofunkcyjnej cząsteczki rdzenia [61]. Strategia syntezy zbieżnej pozwala na większą kontrolę struktury dendrymeru oraz na otrzymanie produktu o wyższej czystości niż metoda rozbieżna. Ponadto, poprzez łączenie dendronów o różnej strukturze, możliwe jest otrzymanie dendrymerów asymetrycznych, charakteryzujących się niejednorodną morfologią [63]. Poważnym ograniczeniem metody zbieżnej jest fakt, że z zadowalającą wydajnością można otrzymać tylko dendrymery niższych generacji. Z tego powodu w komercyjnej produkcji dendrymerów preferowana jest metoda rozbieżna [64].

Metody syntezy dendrymerów są stale rozwijane, dzięki czemu powstają nowe strategie takie jak technika podwójnego wzrostu wykładniczego, dwustopniowa metoda zbieżna (podejście hiperrdzeniowe), metoda hipermonomerów (podejście rozgałęzionych monomerów), a także metody oparte na "clik-chemistry" [65,66].

Dendrymery poliamidoaminowe (PAMAM) zostały po raz pierwszy zsyntezowane w latach 80-tych XX w. przez Donalda Tomalię metodą syntezy rozbieżnej. Rdzeń dendrymeru PAMAM stanowi diamina (najczęściej stosowane są etylenodiamina, diaminododekan, diaminoheksan oraz diaminobutan), do której w reakcji addycji Michael'a przyłączany jest akrylan metylu, po czym następuje amidacja nadmiarem etylenodiaminy. Jeżeli synteza zostanie zakończona na etapie reakcji addycji akrylanu metylu powstanie dendrymer generacji połówkowej z powierzchniowymi grupami karboksylowymi. Jeśli zaś zakończenie nastąpi na etapie amidacji etylenodiaminą otrzymany zostanie dendrymer generacji pełnej z grupami aminowymi na powierzchni. Reakcje addycji Michael'a oraz amidacji prowadzone są naprzemiennie, aż do osiągnięcia makrocząsteczki o pożądanej wielkości, architekturze oraz charakterze grup końcowych, determinujących właściwości fizykochemiczne polimeru [63,67]. Wielkość, ciężar cząsteczkowy, ładunek powierzchniowy, hydrofobowość oraz obecność dodatkowych ligandów na powierzchni dendrymeru mają ogromny wpływ na jego farmakokinetykę [68]. Niezwykle istotną cechą dendrymerów PAMAM w kontekście zastosowania ich jako systemów transportu leków jest możliwość szczegółowego dopasowania wymienionych parametrów do rodzaju terapii, sposobu dostarczania, rodzaju tkanki, w jakiej mają się akumulować, czy pożądanego efektu terapeutycznego. Takie profilowanie pozwala na użycie tych nanocząstek w terapii spersonalizowanej.

Wielkość cząsteczki dendrymeru PAMAM, która zwykle jest wyznaczana poprzez pomiar średnicy, osiąga wartości w zakresie 1,1 – 15 nm, przyrastając liniowo o około 1 nm z każdą generacją. Dendrymery niższych generacji (poniżej G3) cechują się większą elastycznością oraz elipsoidalnym kształtem, podczas gdy wyższe generacje przybierają kształt sferyczny ze ściśle zdefiniowaną wewnętrzną architekturą. Na wielkość makrocząsteczki dendrymeru mocno wpływa polarność rozpuszczalnika. Silne oddziaływania rozpuszczalnika z cząsteczką dendrymeru powodują zwiększenie średnicy hydrodynamicznej polimeru, natomiast słabe oddziaływania prowadzą do zwiększenia gęstości struktur wewnętrznych dendrymeru i zmniejszenia jego średnicy [69]. Wielkość cząsteczki dendrymeru wpływa również na biodystrybucję, długość utrzymywania się w osoczu oraz czas eliminacji z organizmu. Cząsteczki o średnicy poniżej 3 nm (generacje G0-G2) łatwo przenikają do krwioobiegu, skąd rozprowadzane są po całym organizmie, a następnie usuwane przez nerki. Natomiast większe cząsteczki o średnicy do 12 nm charakteryzują się zwykle wydłużonym czasem przebywania w krwioobiegu oraz spowolnioną eliminacją przez wątrobę i nerki [70]. Dendrymery najwyższych generacji

(powyżej G10) są wydajniej wychwytywane i usuwane przez komórki układu immunologicznego, ponadto nie są w stanie przekroczyć bariery krew-guz (BTB – ang. *blood tumor barier*), która jest przepuszczalna dla makrocząsteczek o średnicy do 12 nm [68].

Wraz ze wzrostem generacji dendrymerów PAMAM rośnie ich stabilność metaboliczna, jednak z drugiej strony zwiększa się również ich cytotoksyczność. Jest to ściśle związane z liczbą oraz charakterem końcowych grup funkcyjnych polimeru, które determinują jego ładunek powierzchniowy. Grupy aminowe nadają cząsteczce dendrymeru charakter polikationowy, grupy karboksylowe – polianionowy, natomiast grupy hydroksylowe – obojętny. Dendrymery PAMAM obdarzone ładunkiem powierzchniowym ujemnym lub neutralnym wykazują istotnie niższą cytotoksyczność oraz słabszą przenikalność przez błony komórkowe niż dendrymery z ładunkiem dodatnim [71]. Obecność dodatniego ładunku na powierzchni cząsteczki dendrymeru pozwala na jej oddziaływanie z ujemnie naładowanymi błonami komórkowymi oraz białkami, co z kolei wpływa na szybkość wychwytu oraz rodzaj mechanizmu wnikania do komórki. Jednakże oddziaływanie polikationowych dendrymerów PAMAM wyższych generacji powoduje dezintegrację błony komórkowej, tworzenie w niej nanoporów oraz miejscowych ubytków, co może prowadzić do wycieku zawartości komórki i w konsekwencji do apoptozy. Z kolei dendrymery PAMAM niższych generacji (poniżej G5) zwykle są adsorbowane na powierzchni błony komórkowej lub wbudowują się w jej strukturę [72–74]. Ładunek powierzchniowy ma również wpływ na mechanizm wnikania i transportu dendrymeru PAMAM do wnętrza komórki, który odbywa się głównie na drodze mechanizmów endocytozy, specyficznych dla poszczególnych typów komórek [75,76].

Odpowiednia modyfikacja powierzchniowych grup funkcyjnych oraz optymalizacja wielkości cząsteczek dendrymeru PAMAM stanowią główne strategie mające na celu zmniejszenie jego natywnej cytotoksyczności, a tym samym poprawę jego biokompatybilności, jak również umożliwienie aktywnego i ukierunkowanego transportu do komórki. Do modyfikacji powierzchni dendrymerów PAMAM stosuje się między innymi: poli(tlenek etylenu) (PEG) [77,78], bezwodnik octowy [79], sacharydy (glukozę, mannozę, galaktozę [80], β-cyklodekstrynę [81], kwas hialuronowy [82]), aminokwasy (serynę, cysteinę [83]) oraz lipidy (kwas laurynowy [84]). Przyłączenie takich związków z jednej strony zmniejsza cytotoksyczność poprzez obniżenie ładunku powierzchniowego, a z drugiej może służyć jako czynnik kierujący do komórek nowotworowych, tym samym zwiększając selektywność oraz efekt terapeutyczny koniugatu. Wiele badań porównujących działanie natywnych dendrymerów PAMAM z ich odpowiednikami o zmodyfikowanej powierzchni wykazało zwiększony wychwyt tych drugich przez komórki nowotworowe

[85,86]. Bardzo dobrym przykładem jest zastosowanie cząsteczek glukozy, która oprócz obniżenia ładunku powierzchniowego zwiększa wychwyt dendrymeru przez komórki nowotworowe, które ze względu na przyspieszony metabolizm i proliferację wykazują znacznie większe zapotrzebowanie na glukozę niż komórki prawidłowe [87]. Innym rozwiązaniem jest zastosowanie dodatkowego liganda, skierowanego na konkretne receptory obecne na powierzchni komórek nowotworowych, które często ulegają nadekspresji, bądź na ich szlaki metaboliczne. Najczęściej stosowanymi związkami są witaminy (kwas foliowy [88,89], biotyna, kwas retinowy [90]), na które, podobnie jak na glukozę, komórki nowotworowe wykazują większe zapotrzebowanie. Używane są także peptydy [91] oraz przeciwciała [92]. Według publikacji autorstwa Maiti i Paira [93] najbardziej obiecującą cząsteczką adresującą wśród witamin wydaje się być biotyna (witamina B7, H). Biotyna stymuluje wzrost i rozwój komórek poprzez udział w procesach glukoneogenezy, biosyntezy kwasów tłuszczowych, metabolizmu aminokwasów oraz organizacji chromatyny, będąc koenzymem dla pięciu enzymów z grupy karboksylaz [93]. Dostarczana jest do komórek ssaczych poprzez specyficzne transportery, takie jak zależny od sodu transporter multiwitaminowy SMVT (ang. *sodium-dependent multivitamin transporter*) oraz transporter monokarboksylowy MCT-1 (ang. *monocarboxylate transporter*) [94]. Zwiększoną ekspresję tych receptorów oraz nasilony wychwyt biotyny wykazano w komórkach wielu typów nowotworów, między innymi jajnika, jelita grubego, piersi, płuc, nerki oraz białaczki [95]. Biotyna została wykorzystana między innymi w systemie celowanego transportu znanych chemioterapeutyków, takich jak cisplatyna [96], paklitaksel [97,98], doksorubicyna [99,100], chlorambucyl [101], gemcytabina [102], a także niesteroidowych leków przeciwzapalnych [103,104] oraz krótkich interferujących RNA (siRNA - ang. *small interfering RNA*) [105]. Dodatkowym atutem użycia biotyny jest jej zdolność do przechodzenia przez barierę krew-mózg (BBB, ang. *blood-brain barrier*), co pozwala na zastosowanie jej w terapii nowotworów centralnego układu nerwowego [106]. Szereg wyników naszego zespołu potwierdziło użyteczność biotyny jako cząsteczki ułatwiającej przenikanie dendrymerów do komórek nowotworowych [103,107,108].

Należy jednak pamiętać, że niektóre prawidłowe komórki, zwłaszcza o przyspieszonej proliferacji (np. hepatocyty) także mogą wykazywać zwiększone zapotrzebowanie na witaminy i wykazywać nadekspresję specyficznych dla nich receptorów, przez co w przypadku wyboru czynnika adresującego trzeba przede wszystkim kierować się specyfiką nowotworu oraz sposobem podania leku (miejscowo lub ogólnoustrojowo). Należy również wziąć pod uwagę fakt, że całkowita redukcja kationowego ładunku na powierzchni

dendrymeru często może prowadzić do utraty jego pożądanych właściwości, np. zdolności do oddziaływania z błonami czy kwasami nukleinowymi. Dlatego warto rozważyć tylko częściową modyfikację powierzchniowych grup funkcyjnych w celu osiągnięcia równowagi między zmniejszeniem cytotoksyczności a zachowaniem aktywności dendrymeru [109].

Dendrymery PAMAM jako potencjalne nośniki posiadają korzystne właściwości typu gospodarz-gość (ang. *host-guest*) determinowane przez hydrofobowy rdzeń oraz hydrofilowe warstwy końcowe. Cząsteczki transportowanego leku mogą zostać enkapsulowane we wnętrzu cząsteczki dendrymeru lub przyłączone do powierzchniowych grup funkcyjnych na zasadzie oddziaływań elektrostatycznych lub poprzez wiązania kowalencyjne [110]. Wydajność enkapsulacji ściśle zależy od wielkości cząsteczek oraz stężenia dendrymeru, które wpływają na liczbę dostępnych wolnych przestrzeni w strukturze polimeru. Miejsce oraz efektywność uwalniania enkapsulowanego leku uwarunkowane są zdolnością dendrymerów do akumulacji w tkance nowotworowej dzięki zwiększonej przepuszczalności naczyń krwionośnych guza oraz zmniejszonej drożności naczyń limfatycznych, co określane jest jako efekt zwiększonej przepuszczalności i retencji EPR (ang. *enhanced permeability and retention effect*) [111]. Z kolei przyłączenie leku do powierzchni dendrymeru za pomocą odpowiedniego wiązania bądź linkera pozwala na uzyskanie nośnika reagującego na określone bodźce, zarówno endogenne, jak i egzogenne, takie jak: zmiana pH, temperatury, potencjału redox, obecność enzymu lub fotoinicjatora. Zaletą systemu wrażliwego na bodźce jest uzyskanie efektu włącz-wyłącz, przez co możliwe jest kontrolowane uwalnianie leku w określonym czasie i pożądanym miejscu w zależności od rodzaju bodźca [112]. Najprostszą, a zarazem najczęściej stosowaną strategią uwalniania leku z makrocząsteczki nośnika jest wykorzystanie linkerów wrażliwych na pH oraz obecność enzymów hydrolitycznych. Główną zaletą takiego podejścia jest brak konieczności stosowania dodatkowych czynników zewnętrznych inicjujących proces uwalniania. Wartość pH tkanek prawidłowych oscyluje zwykle między neutralnym a lekko zasadowym, natomiast w środowisku guza nowotworowego nieznacznie spada do poziomu 6,5-6,8. W endosomach i lizosomach osiąga zaś poziom 4-6. Zatem zastosowanie wiązania wrażliwego na kwasowe pH spowoduje, że w krwioobiegu koniugat nośnik-lek będzie stabilny, a uwolnienie leku zostanie zainicjowane w środowisku tkanki nowotworowej i nasilone na etapie wnikania do komórek na drodze endocytozy podczas obniżenia pH w endosomie lub lizosomie [113]. Ponadto w endosomach oraz lizosomach znajdują się specyficzne enzymy zdolne do hydrolizy wiązań i uwolnienia cząsteczki leku. Co więcej, w środowisku guza zachodzi zwiększona ekspresja takich enzymów jak: metaloproteinazy macierzy pozakomórkowej,

hialuronidazy, esterazy oraz katepsyna B, które katalizują rozerwanie określonych sekwencji peptydowych oraz wiązań estrowych [114]. Spośród wiązań kowalencyjnych, do związania leku z dendrymerem, stosuje się wiązania amidowe, estrowe, disiarczkowe, hydrazonowe, azowe, a także różne linkery peptydowe.

Poliwalentność dendrymerów PAMAM umożliwia stworzenie nośnika „szytego na miarę" potrzeb określonej terapii, pozwalając na równoczesne przyłączenie leku bądź kilku leków (dla uzyskania efektu synergicznego), dodatkowych ligandów oraz czynników adresujących. Odpowiedni dobór parametrów fizykochemicznych polimeru, stosowanych ligandów oraz linkerów pozwala na uzyskanie aktywnego, ukierunkowanego transportu leku z kontrolowanym uwalnianiem w docelowym miejscu, przy równoczesnej minimalizacji kontaktu z prawidłowymi tkankami. Do zastosowań medycznych wybór dendrymerów generacji G3-G5 wydaje się być optymalnym rozwiązaniem pod kątem wielkości cząsteczki, liczby powierzchniowych grup funkcyjnych zdolnych do przyłączenia ligandów oraz leków, a także pod kątem wielkości wolnych przestrzeni między rozgałęzieniami zdolnych do enkapsulacji leku.

Niezbędnym etapem procesu tworzenia nowych leków i systemów dostarczania jest testowanie skuteczności ich działania na modelach chorób *in vitro* oraz *in vivo*. Aktywność przeciwnowotworowa określana jest przy pomocy badań na hodowlach ludzkich komórek nowotworowych oraz na myszach lub szczurach ksenogenicznych w odniesieniu do grupy kontrolnej, którą stanowią odpowiednio ludzkie komórki prawidłowe i zdrowe gryzonie. Do badań nad lekami o działaniu przeciwpasożytniczym często jako model wykorzystywany jest wolno żyjący nicień *Caenorhabditis elegans* [115]. Organizm ten ma zastosowanie również w naukach biomedycznych do określenia między innymi genotoksyczności oraz neurotoksyczności związków chemicznych [116].

2. Cele naukowe pracy

W prezentowanej pracy postawiono następujące cele naukowe:

1. Zbadanie potencjału przeciwnowotworowego i przeciwnicieniowego wybranych związków z grupy ksantonów jako kandydatów do związania z nośnikiem polimerowym.
2. Synteza szeregu koniugatów dendrymeru poliamidoaminowego generacji trzeciej ze związkami z grupy ksantonów (α-mangostyna i vadimezan) z uwzględnieniem:
    - 2.a) użycia α-D-glukoheptono-1,4-laktonu w celu zmniejszenia natywnej toksyczności nośnika,
    - 2.b) zastosowania biotyny jako cząsteczki adresującej i/lub zwiększającej wychwyt przez komórki,
    - 2.c) różnych sposobów wiązania ksantonów do dendrymeru (poprzez wiązania amidowe lub estrowe),
    - 2.d) różnego stopnia podstawienia resztami α-mangostyny.
3. Charakterystyka otrzymanych koniugatów metodami NMR oraz DLS.
4. Analiza aktywności biologicznej otrzymanych koniugatów w warunkach:
    - 4.a) *in vitro* wobec ludzkich komórek nowotworowych oraz prawidłowych,
    - 4.b) *in vivo* wobec organizmu modelowego – nicienia *Caenorhabditis elegans*, traktowanego jako model nicienia pasożytniczego.

3. Część eksperymentalna

3.1. Zbadanie potencjału przeciwnowotworowego i przeciwnicieniowego wybranych związków z grupy ksantonów jako kandydatów do związania z nośnikiem polimerowym [P1, P2]

Moje zainteresowanie tematyką ksantonów zrodziło się w wyniku współpracy promotora mojej pracy doktorskiej prof. dr hab. Wojciecha Rode z zespołem prof. Bruno Botty z Uniwersytetu La Sapienza w Rzymie. Naukowcy z Włoch posiadają własną bibliotekę około tysiąca związków pochodzenia naturalnego i ich pochodnych, które mogą posłużyć jako źródło kandydatów oraz cząsteczek wiodących w procesie projektowania i rozwoju nowych leków. Wspomniana biblioteka została wykorzystana do poszukiwania potencjalnych inhibitorów syntazy tymidylanowej (TS, ang. *thymidylate synthase,* EC 2.1.1.45). Syntaza tymidylanowa to enzym należący do metylotransferaz, będący celem molekularnym w terapii przeciwnowotworowej, przeciwwirusowej, przeciwgrzybicznej i przeciwpierwotniaczej, ponieważ reakcja którą katalizuje jest jedynym źródłem *de novo* 2'-deoksytymidylanu (dTMP, ang. *2'-deoxythymidine monophosphate*) w komórce eukariotycznej [117]. Prace badawcze zespołu prof. dr hab. Wojciecha Rode skupiają się na szczegółowym poznaniu molekularnego mechanizmu reakcji katalizowanej przez TS oraz znalezieniu dla niej nowych inhibitorów. Badania te dostarczyły wielu struktur krystalograficznych rekombinowanej TS w kompleksach z substratem i/lub inhibitorem (m. in. PDB 4E5O, PDB 4EB4, PDB 4EIN). Jedna z takich struktur krystalograficznych – syntaza tymidylanowa nicienia *Caenorhabditis elegans* w kompleksie z 2'-deoksyurydyno-5'-monofosforanem (dUMP, ang. *2'-deoxyuridine-5'-monophosphate*) i niskocząsteczkowym inhibitorem Tomudex (PDB 4IQQ), posłużyła jako receptor do przeszukiwania biblioteki związków naturalnych techniką dokowania molekularnego. Ostatecznie wybrano dwadzieścia związków (Tabela 1 w [P2]) do dalszej analizy aktywności biologicznej wobec czterech wariantów rekombinowanej syntazy tymidylanowej (ludzkiej, mysiej oraz nicieni *Trichinella spiralis* i *C. elegans*). Badanie przesiewowe związków *in silico* oraz analiza ich aktywności jako inhibitorów enzymu została wykonana przez pracowników Uniwersytetu La Sapienza w Rzymie oraz Instytutu Biologii Doświadczalnej im. M. Nenckiego PAN w Warszawie. Następnie sześć najbardziej obiecujących związków: alwaksanton, 1,3-dihydroksy-2-metoksyksanton, rhediaksanton B, rhediaksanton C, 1-hydroksy-7-metoksyksanton oraz 2-metoksyksanton wykorzystałam do badań na hodowlach komórkowych [P2], chcąc sprawdzić ich potencjalną

aktywność przeciwnowotworową *in vitro*. Po przeprowadzonym przeze mnie przeglądzie literaturowym dotyczącym ksantonów, zdecydowałam również o sprawdzeniu aktywności dostępnej komercyjnie α-mangostyny [P1], której struktura chemiczna jest zbliżona do struktury alwaksantonu.

Badania potencjału przeciwnowotworowego wybranych sześciu związków oraz α-mangostyny prowadziłam na trzech liniach komórek ludzkich:

- U-118 MG – komórkach glejaka wielopostaciowego IV stopnia złośliwości,
- SCC-15 – komórkach raka płaskonabłonkowego z języka,
- BJ – prawidłowych fibroblastach skórnych, użytych jako odniesienie do komórek nowotworowych.

Szczegóły metody prowadzenia hodowli komórkowych, stosowane odczynniki oraz wykonywane testy opisałam w rozdziale Materiały i Metody w publikacji [P1] oraz [P2].

Wstępną ocenę wpływu wybranych ksantonów na badane komórki po 48-godzinnej inkubacji przeprowadziłam za pomocą testu wychwytu czerwieni obojętnej (NR, ang. *neutral red*). Jest to jeden z najczęściej wykorzystywanych testów na cytotoksyczność, ze względu na wysoką czułość i niską cenę. Czerwień obojętna posiada niski kationowy ładunek w fizjologicznym pH, dlatego przenika przez błony komórkowe na zasadzie biernej dyfuzji i ulega akumulacji w lizosomach. Ze względu na fakt, że żywe, nieuszkodzone komórki mają zdolność do wychwytu barwnika, a martwe nie, test NR służy przede wszystkim do określenia poziomu żywotności komórek w hodowli, ale także do określenia przepuszczalności błony komórkowej oraz aktywności lizosomów [118]. Otrzymane wyniki pozwoliły na wyznaczenie dla części związków wartości IC_{50} (ang. *the half maximal inhibitory concentration*) – stężenia hamującego wzrost komórek do 50% wzrostu komórek kontrolnych.

Po wstępnej analizie cytotoksyczności do dalszych badań wybrałam 3 związki: α-mangostynę, alwaksanton oraz rhediaksanton B, które wykazywały najwyższy potencjał przeciwnowotworowy wobec analizowanych linii komórkowych. Dla tych związków wykonałam bardziej szczegółowe analizy określające ich wpływ na proliferację komórek, kondycję mitochondriów, indukcję apoptozy oraz zdolność komórek do adhezji i migracji. W trakcie prowadzenia wymienionych badań oraz na podstawie analizy literatury zdecydowałam o dołączeniu do grupy wybranych ksantonów jeszcze jednego związku – vadimezanu, jako związku o najmniej złożonej budowie chemicznej w porównaniu do pozostałych ksantonów.

Test redukcji soli tetrazoliowych XTT (sodowa sól 2,3-bis[2-metoksy-4-nitro-5-sulfofenylo]-2H-tetrazolio-5-karboksyanilidu) również jest stosowany do oznaczenia poziomu żywotności komórek. W związku z tym, że sól XTT ulega redukcji do pochodnej formazanu pod wpływem dehydrogenaz i oksygenaz mitochondrialnych prawidłowo funkcjonujących komórek [119], wykorzystałam ten test w celu oceny kondycji mitochondriów badanych komórek po 48-godzinnej inkubacji z wymienionymi wyżej związkami.

Wpływ α-mangostyny, alwaksantonu, rhediaksantonu B oraz vadimezanu na proliferację komórek badałam wykorzystując metodę ilościowego oznaczenia DNA komórek, polegającą na zastosowaniu barwnika fluorescencyjnego specyficznego dla określonych zasad azotowych. W tym przypadku wydłużyłam czas inkubacji do 72 godzin tak, aby sprawdzić czy badane związki wpływały na częstotliwość podziałów komórkowych.

Kolejnym analizowanym parametrem była zdolność badanych ksantonów do indukcji apoptozy. W tym celu zastosowałam zestaw odczynników, który mierzy aktywność enzymatyczną kaspazy 3 i 7 – proteaz cysteinowych odpowiedzialnych za degradację białek strukturalnych oraz enzymów komórki w końcowej fazie apoptozy (fazie wykonawczej) [120]. Głównym elementem zestawu jest rodamina 110 z przyłączoną sekwencją peptydową DEVD (Asp-Glu-Val-Asp), która jest specyficznie rozpoznawana przez kaspazę 3 i 7.

Ekspresja oraz biosynteza kaspaz wykonawczych, a także innych białek jest ściśle uzależniona od ilości ATP (adenozyno-5'-trifosforan) w komórce. Zatem w celu sprawdzenia wydajności energetycznej komórek po inkubacji z badanymi związkami wykonałam oznaczenie poziomu wewnątrzkomórkowego ATP. Analiza opierała się na reakcji monooksygenacji lucyferyny katalizowanej przez termostabilną lucyferazę w obecności jonów magnezu, cząsteczkowego tlenu oraz ATP, dostarczanego przez aktywne metabolicznie komórki. Produktem tej reakcji są kwanty światła w formie luminescencji, której mierzony sygnał jest wprost proporcjonalny do ilości ATP w badanych komórkach.

Ruchliwość komórek nowotworowych jest istotnym parametrem informującym o zdolności do metastazy. Jest to złożony proces, na który składają się migracja oraz adhezja komórek do macierzy pozakomórkowej (ECM, ang. *extracellular matrix*) [121]. Analizę adhezji komórek po traktowaniu badanymi ksantonami wykonałam przy użyciu fioletu krystalicznego (CV, ang. *crystal violet*), który barwi DNA komórek związanych z dnem płytki poprzez białka. Komórki uszkodzone lub martwe, które tracą przyczepność są usuwane na etapie przemywania buforem, zatem mierzona absorbancja fioletu jest wprost

proporcjonalna do liczby komórek adherentnych [122]. Zdolność komórek do migracji była analizowana z wykorzystaniem testu gojenia ran, znanym także jako test rysy (ang. *wound-healing assay*, *scratch assay*). Polega on na wykonaniu sterylną końcówką pipety automatycznej rysy na powierzchni hodowli komórkowej o pełnej konfluencji i obserwacji stopnia migracji komórek do obszaru rysy [123].

Toksyczność wybranych ksantonów z biblioteki udostępnionej przez partnerów z Włoch wobec modelowego organizmu wielokomórkowego – wolno żyjącego nicienia *Caenorhabditis elegans* została zbadana przez Panią dr Justynę Sobich w Instytucie Biologii Doświadczalnej im. M. Nenckiego PAN w Warszawie. Analiza była prowadzona na populacji mieszanej nicieni (wszystkie stadia rozwoju) przez 7 dni, a uzyskane wyniki pozwoliły na wyznaczenie wartości LC_{50} (ang. *the half maximal lethal concentration*) – stężenia powodującego śmierć połowy nicieni w badanej populacji.

Działanie α-mangostyny i vadimezanu dodatkowo zbadałam na synchronicznej hodowli dorosłych nicieni (stadium L4). Opis prowadzenia hodowli, stosowane odczynniki oraz szczegóły analiz przedstawiłam w Materiałach i Metodach w publikacji [P3]. W celu uzyskania populacji dorosłych osobników nicieni wykonałam synchronizację mieszanej populacji metodą jałowienia. W wyniku tej procedury otrzymałam wyłącznie jaja nicieni, z których po całonocnej inkubacji wykluły się młode larwy (stadium L1). Dodatkowa inkubacja larw L1 na szalkach z bakteriami jako pożywieniem pozwoliła na uzyskanie osobników dorosłych w stadium L4, które następnie były inkubowane z badanymi związkami przez 7 dni. Począwszy od pierwszego do ostatniego dnia inkubacji codziennie analizowałam liczbę żywych oraz martwych nicieni przy użyciu mikroskopu odwróconego, zwracając uwagę na ich ruchliwość oraz morfologię.

Wszystkie wymienione testy *in vitro* z uwzględnieniem grupy kontrolnej (komórek nieinkubowanych z badanymi związkami) wykonałam w trzech niezależnych eksperymentach, a każdy z nich w trzech powtórzeniach. Dodatkowo przeprowadziłam analizę statystyczną wyników wykorzystując narzędzia programu Statistica 13.3 firmy Statsoft Polska. Ze względu na brak rozkładu normalnego danych zastosowałam testy nieparametryczne: test Kruskala-Wallisa oraz test U Manna Whitney'a. Natomiast w przypadku analizy przeżycia nicieni, w celu wyznaczenia istotnego statystycznie spadku przeżywalności w odniesieniu do kontroli, wykonałam nieparametryczny test Gehana-Wilcoxona. Wyniki, dla których wartość prawdopodobieństwa testowego p wynosiła mniej niż 0,05 uznałam za istotne statystycznie.

3.2. Synteza koniugatów dendrymeru PAMAM G3 z α-mangostyną lub vadimezanem zmodyfikowanych resztami α-D-glukoheptono-1,4-laktonu oraz biotyny [P3, P4]

Ścieżki syntezy koniugatów, stosowane odczynniki, warunki prowadzenia reakcji, a także oczyszczania produktów i półproduktów szczegółowo opisałam w publikacjach [P3] i [P4] w sekcji Materiały i metody. Do syntezy wszystkich koniugatów wykorzystałam dendrymer PAMAM generacji trzeciej, którego metanolowy roztwór o stężeniu 20.1 mM został przygotowany w większej ilości przez prof. dr hab. inż. Stanisława Wołowca według protokołu Donalda Tomalii [124]. Wszystkie reakcje prowadziłam w DMSO (dimetylosulfotlenek), dlatego przed przystąpieniem do syntezy poszczególnych koniugatów metanol był odparowywany. Produkty oraz półprodukty syntez oczyszczałam wykonując 3-4 dniową dializę wobec wody. Rozpuszczalnik usuwałam pod próżnią na wyparce obrotowej, a następnie produkt suszyłam przez kilkanaście godzin przy pomocy pompy próżniowej.

3.2.1. Synteza biotynylowanych koniugatów dendrymeru PAMAM G3 z amidowo przyłączoną α-mangostyną lub vadimezanem

Pierwszym etapem syntezy była biotynylacja powierzchniowych grup aminowych natywnego dendrymeru PAMAM G3. W tym celu zastosowałam NHS-biotynę, czyli biotynę w formie estru N-sukcynoimidylowego (NHS, ang. – *N-hydroxysuccinimide*), aby poprzez reakcję aminolizy uzyskać wiązanie amidowe między biotyną a dendrymerem. Stechiometria reakcji była obliczona tak, aby uzyskać podstawienie dendrymeru dwoma resztami biotyny (**G3^{2B}**). W kolejnym kroku przeprowadziłam aktywację grup hydroksylowych α-mangostyny za pomocą chloromrówczanu 4-nitrofenylu (NPCF, ang. 4-*nitrophenyl chloroformate*), otrzymując diester węglanowy α-mangostyny i *p*-nitrofenolu, który następnie stanowił substrat w reakcji z **G3^{2B}**. Zastosowanie NPCF pozwoliło na wprowadzenie jednowęglowego linkera między grupą hydroksylową α-mangostyny a grupą aminową dendrymeru, a tym samym utworzenie wiązania karbamidowego. Reakcję przyłączenia α-mangostyny do biotynylowanego dendrymeru prowadziłam ze stechiometrią obliczoną dla niższego oraz wyższego podstawienia grup aminowych dendrymeru, otrzymując koniugaty z pięcioma lub siedemnastoma resztami ksantonu (**G3^{2B5M}** oraz **G3^{2B17M}**). Ostatnim etapem było

podstawienie pozostałych wolnych grup aminowych na powierzchni dendrymeru resztami α-D-glukoheptono-1,4-laktonu (GHL). W przypadku koniugatu **G3^{2B5M}** wykonałam podstawienie połowy wolnych grup aminowych, natomiast w przypadku koniugatu **G3^{2B17M}** wszystkich grup aminowych, jakie pozostały dostępne. W ten sposób otrzymałam koniugat **G3^{2B12gh5M}** oraz **G3^{2B10gh17M}**. Analogiczne podstawienie resztami GHL-u wykonałam dla biotynylowanego dendrymeru **G3^{2B}** w celu uzyskania **G3^{2B12gh}** – nośnika stanowiącego kontrolę do badań biologicznych. Dodatkowo dla osobnych porcji koniugatów z α-mangostyną przeprowadziłam znakowanie fluorescencyjne. Do tego celu wykorzystałam fluoresceinę związaną z kwasem 5(6)-karboksyamidoheksanowym (FCH, ang. *6-[fluorescein-5(6)-carboxamido]hexanoic acid*), ze względu na dużą dostępność grup hydroksylowych pochodzących od przyłączonych łańcuchów GHL, do których FCH mógł się przyłączyć.

Syntezę koniugatu dendrymeru z amidowo związanym vadimezanem przeprowadziłam w dwóch etapach ze stechiometrią obliczoną na otrzymanie związku **G3^{2B12gh5V}** – analogicznego do **G3^{2B12gh5M}**. Pierwszym krokiem była reakcja natywnego dendrymeru PAMAM G3 z biotyną i vadimezanem równocześnie. Ze względu na obecność grupy karboksylowej w obu związkach, do syntezy użyłam odczynnika Mukaiyama (jodek 2-chloro-1-metylopirydyny), który służy do aktywacji grup hydroksylowych kwasów karboksylowych i alkoholi, przez co często jest wykorzystywany do syntezy estrów, laktonów, amidów oraz ketenów [125]. W drugim kroku wykonałam reakcję podstawienia dwunastu wolnych grup aminowych resztami GHL-u.

3.2.2. Synteza biotynylowanych koniugatów dendrymeru PAMAM G3 z estrowo przyłączoną α-mangostyną lub vadimezanem

Natywny dendrymer PAMAM G3 poddałam reakcji z nadmiarem GHL-u, aby otrzymać podstawienie wszystkich powierzchniowych grup aminowych dendrymeru przez łańcuchy sacharydowe. Otrzymany związek **G3^{gh}** stanowił zarówno substrat do kolejnych reakcji, jak i kontrolę nośnika do badań biologicznych. Następnie, aby umożliwić związanie α-mangostyny do **G3^{gh}**, przeprowadziłam aktywację związku bezwodnikiem bursztynowym otrzymując ester α-mangostyny i kwasu bursztynowego. Uzyskaną pochodną α-mangostyny oraz biotynę przyłączyłam do dendrymeru **G3^{gh}** w jednej reakcji z użyciem odczynnika Mukaiyama jako aktywatora grup karboksylowych. Wspomniana reakcja była prowadzona

ze stechiometrią obliczoną na uzyskanie koniugatu z dwoma resztami biotyny oraz pięcioma resztami α-mangostyny (**G3^{gh2B5M}**). Analogiczną reakcję przeprowadziłam dla vadimezanu oraz biotyny, otrzymując koniugat **G3^{gh4B5V}**.

3.3. Charakterystyka fizykochemiczna otrzymanych koniugatów

Do potwierdzenia struktury uzyskanych produktów wykorzystałam spektroskopię magnetycznego rezonansu jądrowego NMR (ang. *nuclear magnetic resonance*). Wykonałam pomiary widm jednowymiarowych protonowych ^{1}H oraz węglowych ^{13}C, a także dwuwymiarowe pomiary korelacyjne: COSY (ang. *corelated spectroscopy*), HSQC (ang. *heteronuclear single-quantum correlation spectroscopy*) oraz HMBC (ang. *heteronuclear multiple-bond correlation spectroscopy*). Wszystkie pomiary prowadziłam w deuterowanym DMSO na spektrometrze 300 MHz firmy Bruker, natomiast analizę widm wykonałam w programie dedykowanym dla urządzenia.

W celu określenia średnicy oraz potencjału zeta (ζ) koniugatów zastosowałam technikę odpowiednio dynamicznego oraz elektroforetycznego rozpraszania światła (DLS oraz ELS, ang. *Dynamic Light Scattering*, *Electroforetic Light Scattering*). Pomiary tych parametrów wykonałam przy pomocy urządzenia Zetasizer Nano firmy Malvern w pH 7 oraz pH 5.

3.4. Analiza aktywności biologicznej otrzymanych koniugatów w warunkach *in vitro* oraz *in vivo*

Właściwości biologiczne zsyntezowanych koniugatów dendrymeru PAMAM G3 z α-mangostyną i vadimezanem badałam na hodowlach ludzkich komórek nowotworowych linii U-118 MG i SCC-15 oraz prawidłowych fibroblastów – linia BJ. W celu porównania aktywności α-mangostyny oraz vadimezanu związanych z nośnikiem dendrymerowym, z aktywnością tych związków w wolnej postaci wykonałam te same testy komórkowe, które opisałam w rozdziale 3.1. Dodatkowo przeprowadziłam obserwację dystrybucji oraz lokalizacji znakowanych fluorescencyjnie koniugatów **G3^{2B12gh5M}** oraz **G3^{2B12gh17M}** wewnątrz badanych komórek przy pomocy mikroskopu konfokalnego Olympus Fluoview FV10i. Obrazy mikroskopowe zebrane w trzech kanałach (niebieski – jądra komórkowe, czerwony – mitochondria, zielony – fluoresceina) analizowałam przy użyciu programu ImageJ.

Wykorzystując hodowlę nicienia *C. elegans*, wykonałam analizę toksyczności oraz wpływu na przeżywalność dorosłych osobników po 7-dniowej inkubacji nicieni zarówno z koniugatami dendrymeru z α-mangostyną i vadimezanem, jak i z odpowiednimi związkami w wolnej postaci. Synchronizację hodowli oraz badania z wymienionymi związkami przeprowadziłam według procedury opisanej w rozdziale 3.1.

Analizę statystyczną wyników badań przeprowadzonych na hodowlach komórkowych oraz hodowli nicienia *C. elegans* wykonałam metodami opisanymi również w rozdziale 3.1.

4. Wyniki badań

Analiza właściwości biologicznych, zawarta w publikacji [P1] wykazała, że α-mangostyna posiada potencjał przeciwnowotworowy. Najsilniejsze działanie toksyczne α-mangostyny, badane za pomocą testów NR oraz XTT (Fig. 2A, 2B oraz 2C w [P1]), zaobserwowałam wobec komórek raka płaskonabłonkowego SCC-15. Mniej wrażliwe okazały się komórki glejaka U-118 MG oraz komórki prawidłowych fibroblastów ludzkich BJ, których żywotność utrzymywała się na podobnym poziomie. Wyniki badań wpływu α-mangostyny na proliferację (Fig. 2D w [P1]) wykazały korelację z wynikami analizy cytotoksyczności. Natomiast najsłabszy efekt antyproliferacyjny wystąpił w przypadku komórek prawidłowych. Oprócz wpływu na podziały komórkowe, działanie cytotoksyczne α-mangostyny przejawiało się również poprzez indukcję apoptozy oraz spadek poziomu ATP (Fig. 5 w [P1]). Istotny wzrost aktywności kaspazy 3 oraz 7 zaobserwowałam w obu liniach komórek nowotworowych od stężenia 10 μM, natomiast w przypadku komórek prawidłowych taki wzrost był widoczny tylko w najwyższym stężeniu 20 μM. Aktywacja oraz przeprowadzenie procesu programowanej śmierci wymaga od komórki dużych nakładów energii. Z tego powodu przebieg zmian poziomu ATP w komórkach po inkubacji z α-mangostyną zestawiłam ze zmianami poziomu aktywności kaspaz. Istotny spadek poziomu ATP nastąpił tylko w przypadku komórek raka płaskonabłonkowego SCC-15. W fibroblastach pozostawał na poziomie zbliżonym do kontroli w całym zakresie badanych stężeń, natomiast w komórkach glejaka odnotowałam istotny wzrost jego poziomu w stężeniach nietoksycznych oraz powrót do poziomu kontroli w stężeniu 20 μM. Można przypuszczać, że zwiększona ilość ATP w komórkach glejaka mogła wynikać ze zwiększonego zapotrzebowania komórek na energię do syntezy między innymi kaspaz, a także innych białek zaangażowanych w proces apoptozy. α-Mangostyna wykazała także wpływ na ruchliwość komórek, którą analizowałam badając dwa parametry – adhezję oraz migrację. Podobnie jak w przypadku wcześniej omówionych parametrów, największą redukcję adhezji obserwowałam w komórkach SCC-15 (Fig. 3 w [P1]). Migracja komórek wszystkich trzech linii była istotnie zahamowana tylko w stężeniach toksycznych, podczas gdy w niższych, mniej toksycznych stężeniach słabszą zdolność do migracji wykazały tylko komórki prawidłowe (Fig. 4 w [P1]). Można więc wnioskować, że redukcja adhezji oraz migracji komórek była wynikiem działania toksycznego α-mangostyny, skutkującego śmiercią komórek oraz utratą przyczepności, a nie potencjalnego działania antymetastatycznego. Pomimo tego silniejsze działanie związku wobec komórek raka

płaskonabłonkowego pozwala stwierdzić, że α-mangostyna wykazuje potencjał do zastosowania w terapii niektórych nowotworów. Jej toksyczność była dodatkowo badana na organizmie modelowym – nicieniu *Caenorhabditis elegans*. Związek hamował wzrost mieszanej populacji nicieni z LC_{50} równym 3,8 μM ± 0,5 μM, co jest zbliżoną wartością do LC_{50} mebendazolu, znanego leku przeciwpasożytniczego [P1]. Co ciekawe, α-mangostyna wykazała słabsze działanie wobec populacji dorosłych nicieni, osiągając wartość LC_{50} równą 18,74 μM (Tabela 3 w [P3]).

W publikacji [P2] zbadałam właściwości biologiczne sześciu ksantonów, wyselekcjonowanych z biblioteki związków naturalnych. Działanie toksyczne w badanym zakresie stężeń wobec analizowanych komórek wykazały tylko trzy związki: alwaksanton, rhediaksanton B oraz rhediaksanton C (Tabela 2 w [P2]). Jednak do dalszej analizy wybrałam tylko dwa związki, odrzucając rhediaksanton C, ponieważ wykazywał 2-3 krotnie silniejsze działanie toksyczne wobec prawidłowych fibroblastów w porównaniu do komórek nowotworowych obu linii, co wykluczało jego selektywność. Dalsza analiza cytotoksyczności alwaksantonu oraz rhediaksantonu B za pomocą testu NR (Fig. 1A w [P2]) wykazała, że rhediaksanton B był bardziej toksyczny, osiągając wartości IC_{50} poniżej 10 μM. Z kolei wyniki testu XTT (Fig. 1C w [P2]) wskazały na silniejsze działanie alwaksantonu wobec komórek nowotworowych niż prawidłowych, przy czym komórki SCC-15 były najbardziej wrażliwe. Na podstawie analizy dwóch testów na cytotoksyczność podjęłam próbę określenia prawdopodobnego mechanizmu działania alwaksantonu na badane komórki. W przypadku fibroblastów oraz komórek glejaka prawdopodobnie było to uszkodzenie błony komórkowej oraz lizosomalnej, natomiast w przypadku komórek raka płaskonabłonkowego do tych procesów dochodzi silny wpływ na funkcjonalność mitochondriów. Obydwa związki wykazały działanie antyproliferacyjne wobec wszystkich trzech badanych linii komórkowych, przy czym rhediaksanton B działał silniej w zakresie niższych stężeń niż alwaksanton, który z kolei w stężeniu powyżej 10 μM wykazał selektywność wobec komórek U-118 MG oraz SCC-15 (Fig. 2 w [P2]). Działanie cytotoksyczne obu związków przejawiało się również poprzez utratę adhezji komórek. Alwaksanton istotnie zmniejszył przyczepność komórek SCC-15 oraz BJ w wyższych stężeniach, podobnie jak rhediaksanton B w niższym zakresie stężeń (Fig. 3 w [P2]). Badane związki indukowały także zmiany poziomu wewnątrzkomórkowego ATP, jednak odmiennie od siebie oraz w sposób zależny od linii komórkowej. Inkubacja komórek glejaka z alwaksantonem nie wpłynęła na zmianę poziomu ATP w tych komórkach wobec nietraktowanej lekiem kontroli. Nieznaczne obniżenie poziomu ATP w najwyższych stężeniach było widoczne w fibroblastach, natomiast nagła

redukcja ilości ATP nastąpiła w komórkach SCC-15. Rhediaksanton B spowodował zmniejszenie poziomu energii do 30% w komórkach U-118 MG oraz BJ, natomiast do 20% w komórkach SCC-15 w porównaniu do kontroli. W tej publikacji również zestawiłam poziom wewnątrzkomórkowego ATP z poziomem aktywności kaspaz (Fig. 4 w [P2]). Obydwa analizowane ksantony zwiększyły aktywność kaspazy 3 i 7, przy czym w większym stopniu w komórkach nowotworowych niż w prawidłowych.

Ostatnim badanym związkiem był vadimezan, którego analizę aktywności biologicznej przeprowadziłam ze względu na jego uproszczoną strukturę chemiczną w porównaniu do poprzednich związków oraz brak grup izoprenylowych. W badanym zakresie stężeń (do 200 μM) żywotność komórek wszystkich trzech linii oznaczona testami NR i XTT pozostawała na poziomie zbliżonym do kontroli, a otrzymane wyniki nie pozwoliły na wyznaczenie wartości IC_{50} (Tabela 2 w [P4]). Chcąc upewnić się o braku aktywności vadimezanu wobec badanych komórek, przeprowadziłam test na proliferację z czasem inkubacji 72 godzin. Vadimezan wykazał istotne statystycznie działanie antyproliferacyjne tylko w przypadku komórek raka płaskonabłonkowego w 100 oraz 200 μM stężeniu (Fig. 5 w [P4]).

Dalsza część mojej pracy polegała na sprzęgnięciu modyfikowanych biotyną i α-D-glukoheptono-1,4-laktonem dendrymerów PAMAM G3 z wyselekcjonowanymi, badanymi wcześniej związkami. Finalnie do związania z dendrymerem PAMAM generacji trzeciej wybrałam α-mangostynę oraz vadimezan. Zdecydowało o tym kilka czynników, przede wszystkim: zadowalające wyniki badań biologicznych α-mangostyny oraz jej nieznaczna, ale zauważalna selektywność wobec komórek raka płaskonabłonkowego (Tabela 1), uproszczona struktura chemiczna vadimezanu w stosunku do pozostałych ksantonów, brak aktywności vadimezanu wobec badanych komórek oraz duża komercyjna dostępność obu związków.

Tabela 1. Wartości IC_{50} obliczone na podstawie wyników testów cytotoksyczności NR [P1, P2, P4].

IC_{50} [μM] / **Badany związek**	**BJ**	**U-118 MG**	**SCC-15**
α-Mangostyna	8,97	9,59	6,43
Alwaksanton	15,76	13,07	17,66
Rhediaksanton B	5,5	4,75	9,2
Vadimezan	>>200	>>200	>>200

W publikacji [P3] przedstawiłam syntezę, charakterystykę fizykochemiczną oraz analizę właściwości biologicznych koniugatów dendrymeru PAMAM G3 z amidowo związanymi α-mangostyną oraz biotyną. Stosując zaprezentowaną w publikacji ścieżkę syntezy (Schemat 1 w [P3]) otrzymałam dwa biotynylowane koniugaty PAMAM G3 z 5 lub 17 resztami α-mangostyny. W przypadku koniugatu z 5 resztami ksantonu dodatkowo zablokowałam 12 powierzchniowych grup aminowych przy pomocy reszt α-D-glukoheptono-1,4-laktonu (GHL), otrzymując koniugat **G3^{2B12gh5M}**. Na powierzchni koniugatu z 17 resztami α-mangostyny pozostało 13 wolnych grup NH_2, dla których wykonałam analogiczny zabieg, jednak prawdopodobnie ze względu na dużą zawadę steryczną tworzoną przez sztywną strukturę α-mangostyny reakcji uległo tylko 10 grup aminowych. Z tego względu otrzymałam koniugat **G3^{2B10gh17M}**. Reakcję przyłączenia GHL-u wykonałam w celu zmniejszenia liczby powierzchniowych grup aminowych, odpowiedzialnych za natywną, nieselektywną cytotoksyczność dendrymerów PAMAM G3. Synteza koniugatów o niższym oraz wyższym stopniu podstawienia dendrymeru resztami α-mangostyny miała na celu wykorzystanie cechy poliwalentności, która jest atutem rozgałęzionych struktur dendrymerycznych. Natomiast obecność biotyny w każdym z koniugatów była podyktowana jej korzystnymi właściwościami jako cząsteczki zwiększającej wychwyt komórkowy oraz kierującej do niektórych typów komórek nowotworowych. W celu określenia aktywności biologicznej samego nośnika zsyntezowałam koniugat bez przyłączonej α-mangostyny – **G3^{2B12gh}**.

Oba koniugaty z α-mangostyną wykazały wysoki stopnień asocjacji, tworząc cząstki o średnicy powyżej 100 nm (Tabela 1 oraz Fig. 3 w [P3]). Największe asocjaty (> 1260 nm) zaobserwowałam w przypadku **G3^{2B12gh5M}** w pH 7, które pod wpływem obniżenia pH do 5 uległy rozbiciu do mniejszych cząstek o średnicy w zakresie 114-180 nm. Asocjaty związku **G3^{2B10gh17M}** w pH 7 okazały się być znacznie mniejsze (średnica w zakresie 111-150 nm), jednak zmiana pH z obojętnego na kwasowe nie przyniosła znaczących zmian w ich średnicy. Jedynie sam nośnik **G3^{2B12gh}** pozostawał w formie monomolekularnej osiągając średnicę około 1 nm w pH 7, która w wyniku zakwaszenia środowiska zwiększyła się do około 4 nm. Wzrost średnicy hydrodynamicznej w miarę obniżania pH jest powszechnie znanym zjawiskiem w przypadku dendrymerów PAMAM, często też nazywanym efektem puchnięcia, a odpowiedzialna za ten proces jest protonacja wewnętrznych, trzeciorzędowych grup aminowych dendrymeru [126]. Wszystkie badane koniugaty osiągnęły dodatni potencjał zeta, który okazał się ściśle zależeć od pH (Tabela 1 oraz Fig. 4 w [P3]). W środowisku kwaśnym wartości potencjału zeta wszystkich trzech związków wzrosły niemal dwukrotnie w porównaniu do wartości w środowisku obojętnym. Przyłączenie α-mangostyny do nośnika

spowodowało również dwukrotne zwiększenie potencjału zeta całego koniugatu, niezależnie od liczby przyłączonych reszt ksantonu.

Wykonując testy toksyczności NR i XTT oraz test na proliferację komórek wykazałam, że nośnik **G3^{2B12gh}** był nietoksyczny wobec wszystkich trzech badanych linii komórkowych (Fig. 5, 6 i 9 w [P3]). Siedmiodniowa inkubacja *C. elegans* z nośnikiem także nie wykazała istotnego spadku żywotności nicieni (Fig. 7 w [P3]).

Przyłączenie α-mangostyny do nośnika istotnie zwiększyło toksyczność otrzymanego koniugatu wobec testowanych komórek oraz nicienia w porównaniu z wolną postacią α-mangostyny, a efekt ten był ściśle zależny od stopnia podstawienia nośnika przez badany lek. W przypadku koniugatu **G3^{2B12gh5M}** zaobserwowałam 5,2-krotne zwiększenie toksyczności wobec komórek glejaka oraz 4,5-krotne zwiększenie toksyczności wobec komórek raka płaskonabłonkowego oraz prawidłowych fibroblastów w porównaniu do wolnej postaci α-mangostyny. Koniugat **G3^{2B10gh17M}** jeszcze bardziej wzmocnił efekt toksyczny, będąc 21-25 razy bardziej aktywny wobec komórek nowotworowych obu linii. Działanie toksyczne α-mangostyny wobec nicienia *C. elegans* również zostało wzmocnione poprzez przyłączenie związku do nośnika, osiągając 2,4-krotne wzmocnienie w przypadku koniugatu **G3^{2B12gh5M}** oraz 13,6-krotne w przypadku koniugatu **G3^{2B10gh17M}** (Fig. 11 oraz Tabela 3 w [P3]). Dla pozostałych badanych parametrów komórkowych (proliferacja, adhezja, poziom ATP oraz aktywność kaspaz 3 i 7) również uzyskałam wyniki wskazujące na silniejsze działanie α-mangostyny związanej z nośnikiem dendrymerowym niż α-mangostyny w wolnej postaci, a porównując oba koniugaty wyższą aktywność w każdym z testów wykazywał podstawiony większą liczbą reszt α-mangostyny **G3^{2B10gh17M}** (Fig. 8, 9 i 10 w [P3]).

Znakowane fluorescencyjnie koniugaty badałam pod kątem akumulacji oraz lokalizacji we wnętrzu badanych komórek. Tworzenie asocjatów przez badane koniugaty z α-mangostyną wpłynęło na szybkość ich wnikania do komórek, na co wskazał fakt, że po 4-godzinnej inkubacji nie było możliwe zaobserwowanie znakowanych fluorescencyjnie dendrymerów w komórkach. Z tego powodu wydłużyłam inkubację do 48 godzin. Po tym czasie zarówno koniugat z 5-cioma, jak i 17-stoma resztami α-mangostyny wniknął do badanych komórek, przy czym stopień akumulacji związków w komórkach fibroblastów był wyższy niż w komórkach nowotworowych. Ponadto w programie ImageJ dokonałam nałożenia kanałów fluorescencyjnych pochodzących od znacznika mitochondriów (Mito Tracker), znacznika jąder komórkowych (DAPI) oraz fluoresceiny związanej z koniugatami (FCH), co pozwoliło na uzyskanie informacji na temat lokalizacji koniugatów w tych

organellach komórkowych (Fig. 7 w [P3]). Analiza otrzymanych obrazów pozwoliła stwierdzić, że badane koniugaty **G3^{2B12gh5M}** oraz **G3^{2B10gh17M}** wnikały wydajniej do mitochondriów komórek raka płaskonabłonkowego oraz prawidłowych fibroblastów, natomiast w niższym stopniu do mitochondriów komórek glejaka.

W pracy [P4] zaprezentowałam syntezę, charakterystykę fizykochemiczną oraz analizę właściwości biologicznych koniugatu dendrymeru PAMAM G3 z estrowo związanymi α-mangostyną oraz biotyną, analogicznego koniugatu z estrowo związanym vadimezanem, a także koniugatu z vadimezanem związanym amidowo. Synteza koniugatów z amidowo oraz estrowo związanymi ksantonami miała na celu sprawdzenie wpływu rodzaju wiązania na aktywność biologiczną badanych związków, odkąd wiązanie estrowe uważane jest za bardziej labilne [127]. W celu umożliwienia przyłączenia zarówno α-mangostyny, jak i vadimezanu wiązaniem estrowym do dendrymeru, w pierwszym kroku otrzymałam nośnik **G3^{gh}**, w którym wszystkie powierzchniowe grupy aminowe zostały podstawione resztami GHL. Następnie, aby związek porównać z amidowym koniugatem **G3^{2B12gh5M}**, do **G3^{gh}** przyłączyłam estrowo 2 reszty biotyny oraz 5 reszt α-mangostyny, uzyskując **G3^{gh2B5M}** (Schemat 2 w [P4]). W przypadku vadimezanu zsyntezowałam dwa koniugaty: z amidowo przyłączonym związkiem – **G3^{2B12gh5V}** oraz estrowo – **G3^{gh4B5V}** (Schemat 2 i 3 w [P4]). Ponadto, otrzymane pary koniugatów mogłam analizować pod kątem obecności lub braku wolnych grup aminowych na powierzchni, co dostarczyło istotnych informacji z uwagi na stosowany zabieg tylko częściowego podstawienia grup aminowych.

Nośnik koniugatów zawierających wiązania estrowe – **G3^{gh}**, podobnie jak amidowe **G3^{2B12gh}**, pozostawał w pH obojętnym w postaci monomolekularnej osiągając średnicę 1,5-1,7 nm, zwiększając ją do około 4 nm po obniżeniu pH do wartości równej 5 (Tabela 1 w [P4]). Koniugat z estrowo związanymi resztami α-mangostyny (**G3^{gh2B5M}**) tworzył asocjaty zarówno w pH obojętnym, jak i kwasowym, a zmiana odczynu środowiska nie wpłynęła na zmianę średnicy wspomnianych asocjatów, która utrzymywała się w zakresie 113-213 nm. Co ciekawe, koniugat z estrowo przyłączonym vadimezanem (**G3^{gh4B5V}**), w przeciwieństwie do amidowego odpowiednika (**G3^{2B12gh5V}**), nie tworzył asocjatów. Jego średnica w pH 7 pozostawała w zakresie 2,9-3,7 nm, wzrastając do około 4,5 nm w pH 5. Natomiast koniugat zawierający amidowo związane reszty vadimezanu, podobnie jak jego amidowy odpowiednik z α-mangostyną, wykazał wysoki stopień asocjacji cząsteczek uzyskując średnicę w zakresie 924-1166 nm. Wszystkie zsyntezowane koniugaty posiadały dodatni potencjał zeta, który dla związków w postaci monomolekularnej był stosunkowo niski i miał wartość <8 mV, a dla związków tworzących asocjaty wzrastał powyżej 20 mV.

Związanie vadimezanu z biotynylowanym dendrymerem PAMAM G3 poprzez wiązanie amidowe czy estrowe nie zwiększyło istotnie toksyczności związku wobec żadnych z analizowanych linii komórkowych oraz nicienia *C. elegans*. Interesujące jednak, że działanie antyproliferacyjne vadimezanu w wolnej postaci, które obserwowałam w stężeniu 200 μM wobec komórek nowotworowych, zostało spotęgowane przyłączeniem związku do dendrymeru wiązaniem amidowym (koniugat **G3^{2B12gh5V}**) (Fig. 5 w [P4]). Najbardziej wrażliwe okazały się komórki raka płaskonabłonkowego, dla których uzyskałam efekt 50-krotnego wzmocnienia aktywności antyproliferacyjnej vadimezanu. Analogicznego efektu nie zaobserwowałam w przypadku koniugatu z estrowo związanym vadimezanem (**G3^{gh4B5V}**). Tak duża różnica w aktywności między koniugatami vadimezanu może wynikać z różnic w wielkości cząstek oraz wielkości ładunku powierzchniowego, a także pośrednio z obecności niezablokowanych grup aminowych na powierzchni koniugatu zawierającego wiązania amidowe.

Wzmocnienie aktywności α-mangostyny pod wpływem przyłączenia do nośnika dendrymerowego wiązaniem amidowym wykazałam w publikacji [P3]. Zatem nie zdziwił fakt, że zastosowanie nośnika **G3^{gh}** oraz wiązania estrowego również zwiększyło aktywność analizowanego ksantonu (2,5–9-cio krotnie w zależności od rodzaju komórek). Najsilniejsze działanie, zarówno toksyczne, jak i antyproliferacyjne koniugatu **G3^{gh2B5M}** zawierającego wiązania estrowe zaobserwowałam wobec komórek raka płaskonabłonkowego SCC-15. Jednak silniejszy wpływ zarówno na integralność błon komórkowych, kondycję mitochondriów, czy intensywność podziałów komórkowych wszystkich trzech analizowanych typów komórek wykazał koniugat zawierający wiązania amidowe (**G3^{2B12gh5M}**) niż estrowe (**G3^{gh2B5M}**). W przypadku tej pary koniugatów, różnice w aktywności również mogły wynikać z obecności wolnych grup aminowych, odpowiedzialnych za wyższy potencjał zeta koniugatu amidowego niż estrowego. Warto również podkreślić, że podobnie jak w przypadku nośnika **G3^{2B12gh}**, nośnik dla koniugatów estrowych **G3^{gh}** nie wykazał działania toksycznego ani antyproliferacyjnego wobec badanych komórek (Fig. S7 w materiałach dodatkowych do [P4]).

Wzrost toksyczności, wynikający z estrowego związania α-mangostyny z nośnikiem dendrymerowym **G3^{gh}**, zaobserwowałam również wobec nicienia *C. elegans* (Fig. 6 w [P4]). W tym przypadku porównanie działania koniugatu zawierającego wiązania estrowe z odpowiednikiem posiadającym wiązania amidowe także wykazało silniejszy wpływ związku **G3^{2B12gh5M}** na spadek przeżywalności badanych nicieni.

5. Podsumowanie

W niniejszej pracy doktorskiej wykazałam potencjał przeciwnowotworowy *in vitro* i przeciwnicieniowy związków z grupy ksantonów oraz skuteczność i użyteczność zastosowania biotynylowanych dendrymerów poliamidoaminowych generacji trzeciej o zmodyfikowanej powierzchni, jako nośników mających zdolność wzmacniania efektów działania wybranych ksantonów.

W pierwszym etapie pracy dokonałam analizy właściwości biologicznych ośmiu ksantonów pod kątem oceny ich potencjału przeciwnowotworowego oraz przeciwnicieniowego. Dla najbardziej aktywnej z tej grupy α-mangostyny oraz najmniej aktywnego vadimezanu opracowałam nośnik polimerowy, składający się z dendrymeru PAMAM G3 z dodatkowo przyłączonymi resztami biotyny jako cząsteczkami kierującymi do niektórych komórek nowotworowych oraz resztami α-D-glukoheptono-1,4-laktonu przyłączonymi w celu zmniejszenia natywnej toksyczności samego dendrymeru. Wybrane ksantony (α-mangostyna i vadimezan) związałam kowalencyjnie z nośnikiem za pomocą wiązania amidowego lub estrowego. Ponadto zsyntezowałam amidowe koniugaty dendrymeru podstawione resztami α-mangostyny w różnym stopniu. Z racji tego, że dotąd w literaturze opisano jedynie koniugaty dendrymerów PAMAM z enkapsulowaną α-mangostyną oraz brak jest doniesień dotyczących koniugatów dendrymerów z vadimezanem, przedstawione przeze mnie ścieżki syntez są oryginalne i przedstawiają sposób kowalencyjnego związania tych związków z nośnikiem dendrymerowym.

Związanie α-mangostyny z dendrymerem PAMAM G3 zarówno przez wiązanie amidowe, jak i estrowe istotnie zwiększyło aktywność związku wobec analizowanych komórek oraz nicienia, przy czym najsilniejsze działanie wykazały koniugaty amidowe. Warto podkreślić, że mechanizm działania α-mangostyny w postaci koniugatu z dendrymerem pozostał charakterystyczny dla związku w wolnej postaci, wykazując skuteczność w znacznie niższym zakresie stężeń, jednak w przybliżeniu proporcjonalnym do liczby użytych cząsteczek ksantonu. Najbardziej wrażliwymi wobec badanych koniugatów z α-mangostyną okazały się komórki raka płaskonabłonkowego linii SCC-15, jednak zbliżoną toksyczność uzyskałam również w przypadku komórek prawidłowych BJ, co wyklucza selektywność otrzymanych koniugatów wobec badanych komórek nowotworowych. Jednak co ciekawe, przyłączenie vadimezanu wiązaniem amidowym do nośnika zwiększyło antyproliferacyją aktywność tego związku w sposób selektywny wobec komórek raka

płaskonabłonkowego, podczas gdy koniugat zawierający wiązania estrowe nie wywołał żadnego efektu wobec badanych komórek oraz nicienia. Oprócz wpływu rodzaju wiązania oraz liczby reszt α-mangostyny na aktywność biologiczną koniugatów, istotne znaczenie miały także ich średnica oraz potencjał zeta.

Zatem, w przedstawionej pracy wykazałam, że biotynylowane dendrymery PAMAM G3 o odpowiednio zaprojektowanej architekturze mają zdolność do zwiększania aktywności biologicznej transportowanych związków i jednocześnie same nie wykazują toksyczności, co sprawia, że mogą być wykorzystane jako bezpieczne nośniki substancji aktywnych biologicznie. Ponadto wyniki zawartych w rozprawie badań wskazują na możliwość potencjalnego zastosowania otrzymanych koniugatów z α-mangostyną w lokalnej terapii przeciwnowotworowej oraz przeciwnicieniowej.

Warto również zwrócić uwagę na to, że prezentowana praca doktorska stanowi swego rodzaju przedstawienie procesu tworzenia potencjalnych leków w skali laboratoryjnej. Praca posiada etapy takie jak: selekcja związków-kandydatów, poprawa ich właściwości poprzez związanie z nośnikiem polimerowym, analiza właściwości biologicznych na modelach *in vitro* oraz *in vivo*, które noszą cechy standardowych etapów procesu odkrywania leków: fazy koncepcyjnej, fazy odkrywania oraz fazy badań przedklinicznych.

6. Bibliografia

1. Atanasov, A.G.; Zotchev, S.B.; Dirsch, V.M.; Supuran, C.T. Natural Products in Drug Discovery: Advances and Opportunities. *Nat Rev Drug Discov* **2021**, *20*, 200–216, doi:10.1038/s41573-020-00114-z.
2. de Lima Cherubim, D.J.; Buzanello Martins, C.V.; Oliveira Fariña, L.; da Silva de Lucca, R.A. Polyphenols as Natural Antioxidants in Cosmetics Applications. *Journal of Cosmetic Dermatology* **2020**, *19*, 33–37, doi:10.1111/jocd.13093.
3. Mishra, P.; Tripathi, A.; Dikshit, A.; Pandey, A. Insecticides Derived from Natural Products: Diversity and Potential Applications. In *Natural Bioactive Products in Sustainable Agriculture*; Singh, J., Yadav, A.N., Eds.; Springer: Singapore, 2020; pp. 83–99 ISBN 9789811530241.
4. Koyande, A.K.; Chew, K.W.; Manickam, S.; Chang, J.-S.; Show, P.-L. Emerging Algal Nanotechnology for High-Value Compounds: A Direction to Future Food Production. *Trends in Food Science & Technology* **2021**, *116*, 290–302, doi:10.1016/j.tifs.2021.07.026.
5. Kaczmarek, B. Tannic Acid with Antiviral and Antibacterial Activity as A Promising Component of Biomaterials—A Minireview. *Materials* **2020**, *13*, 3224, doi:10.3390/ma13143224.
6. Newman, D.J.; Cragg, G.M. Natural Products as Sources of New Drugs over the Nearly Four Decades from 01/1981 to 09/2019. *J. Nat. Prod.* **2020**, *83*, 770–803, doi:10.1021/acs.jnatprod.9b01285.
7. Álvarez-Martínez, F.J.; Barrajón-Catalán, E.; Micol, V. Tackling Antibiotic Resistance with Compounds of Natural Origin: A Comprehensive Review. *Biomedicines* **2020**, *8*, 405, doi:10.3390/biomedicines8100405.
8. Klein-Júnior, L.C.; Campos, A.; Niero, R.; Corrêa, R.; Heyden, Y.V.; Filho, V.C. Xanthones and Cancer: From Natural Sources to Mechanisms of Action. *Chemistry & Biodiversity* **2020**, *17*, e1900499, doi:10.1002/cbdv.201900499.
9. Ovalle-Magallanes, B.; Eugenio-Pérez, D.; Pedraza-Chaverri, J. Medicinal Properties of Mangosteen (Garcinia Mangostana L.): A Comprehensive Update. *Food Chem. Toxicol.* **2017**, *109*, 102–122, doi:10.1016/j.fct.2017.08.021.
10. Wang, M.-H.; Zhang, K.-J.; Gu, Q.-L.; Bi, X.-L.; Wang, J.-X. Pharmacology of Mangostins and Their Derivatives: A Comprehensive Review. *Chin J Nat Med* **2017**, *15*, 81–93, doi:10.1016/S1875-5364(17)30024-9.
11. Akao, Y.; Nakagawa, Y.; Nozawa, Y. Anti-Cancer Effects of Xanthones from Pericarps of Mangosteen. *International Journal of Molecular Sciences* **2008**, *9*, 355–370, doi:10.3390/ijms9030355.
12. Buravlev, E.V.; Shevchenko, O.G.; Anisimov, A.A.; Suponitsky, K.Y. Novel Mannich Bases of α- and γ-Mangostins: Synthesis and Evaluation of Antioxidant and Membrane-Protective Activity. *European Journal of Medicinal Chemistry* **2018**, *152*, 10–20, doi:10.1016/j.ejmech.2018.04.022.
13. Nauman, M.C.; Johnson, J.J. The Purple Mangosteen (Garcinia Mangostana): Defining the Anticancer Potential of Selected Xanthones. *Pharmacological Research* **2022**, *175*, 106032, doi:10.1016/j.phrs.2021.106032.
14. Mohamed, G.A.; Al-Abd, A.M.; El-halawany, A.M.; Abdallah, H.M.; Ibrahim, S.R.M. New Xanthones and Cytotoxic Constituents from Garcinia Mangostana Fruit Hulls against Human Hepatocellular, Breast, and Colorectal Cancer Cell Lines. *Journal of Ethnopharmacology* **2017**, *198*, 302–312, doi:10.1016/j.jep.2017.01.030.
15. Araújo, J.; Fernandes, C.; Pinto, M.; Tiritan, M.E. Chiral Derivatives of Xanthones with Antimicrobial Activity. *Molecules* **2019**, *24*, 314, doi:10.3390/molecules24020314.

16. Feng, Z.; Lu, X.; Gan, L.; Zhang, Q.; Lin, L. Xanthones, A Promising Anti-Inflammatory Scaffold: Structure, Activity, and Drug Likeness Analysis. *Molecules* **2020**, *25*, 598, doi:10.3390/molecules25030598.
17. Xie, Z.; Sintara, M.; Chang, T.; Ou, B. Daily Consumption of a Mangosteen-Based Drink Improves in Vivo Antioxidant and Anti-Inflammatory Biomarkers in Healthy Adults: A Randomized, Double-Blind, Placebo-Controlled Clinical Trial. *Food Science & Nutrition* **2015**, *3*, 342–348, doi:10.1002/fsn3.225.
18. Tang, Y.-P.; Li, P.-G.; Kondo, M.; Ji, H.-P.; Kou, Y.; Ou, B. Effect of a Mangosteen Dietary Supplement on Human Immune Function: A Randomized, Double-Blind, Placebo-Controlled Trial. *Journal of Medicinal Food* **2009**, *12*, 755–763, doi:10.1089/jmf.2008.0204.
19. Muchtaridi, M.; Aprillianie Wijaya, C. Anticancer Potential of α-Mangostin. *Asian Journal of Pharmaceutical and Clinical Research* **2017**, *10*, 440, doi:10.22159/ajpcr.2017.v10i12.20812.
20. Chi, X.-Q.; Zi, C.-T.; Li, H.-M.; Yang, L.; Lv, Y.-F.; Li, J.-Y.; Hou, B.; Ren, F.-C.; Hu, J.-M.; Zhou, J. Design, Synthesis and Structure–Activity Relationships of Mangostin Analogs as Cytotoxic Agents. *RSC Advances* **2018**, *8*, 41377–41388, doi:10.1039/C8RA08409B.
21. Nauman, M.C.; Tocmo, R.; Vemu, B.; Veenstra, J.P.; Johnson, J.J. Inhibition of CDK2/CyclinE1 by Xanthones from the Mangosteen (Garcinia Mangostana): A Structure-Activity Relationship Study. *Natural Product Research* **2021**, *35*, 5429–5433, doi:10.1080/14786419.2020.1777413.
22. Kritsanawong, S.; Innajak, S.; Imoto, M.; Watanapokasin, R. Antiproliferative and Apoptosis Induction of α-Mangostin in T47D Breast Cancer Cells. *International Journal of Oncology* **2016**, *48*, 2155–2165, doi:10.3892/ijo.2016.3399.
23. Kurose, H.; Shibata, M.-A.; Iinuma, M.; Otsuki, Y. Alterations in Cell Cycle and Induction of Apoptotic Cell Death in Breast Cancer Cells Treated with *α* -Mangostin Extracted from Mangosteen Pericarp. *Journal of Biomedicine and Biotechnology* **2012**, *2012*, 1–9, doi:10.1155/2012/672428.
24. Lee, C.-H.; Ying, T.-H.; Chiou, H.-L.; Hsieh, S.-C.; Wen, S.-H.; Chou, R.-H.; Hsieh, Y.-H. Alpha-Mangostin Induces Apoptosis through Activation of Reactive Oxygen Species and ASK1/P38 Signaling Pathway in Cervical Cancer Cells. *Oncotarget* **2017**, *8*, 47425–47439, doi:10.18632/oncotarget.17659.
25. Wang, J.J.; Sanderson, B.J.S.; Zhang, W. Significant Anti-Invasive Activities of α-Mangostin from the Mangosteen Pericarp on Two Human Skin Cancer Cell Lines. *Anticancer Research* **2012**, *32*, 3805–3816.
26. Hafeez, B.B.; Mustafa, A.; Fischer, J.W.; Singh, A.; Zhong, W.; Shekhani, M.O.; Meske, L.; Havighurst, T.; Kim, K.; Verma, A.K. α-Mangostin: A Dietary Antioxidant Derived from the Pericarp of Garcinia Mangostana L. Inhibits Pancreatic Tumor Growth in Xenograft Mouse Model. *Antioxidants & Redox Signaling* **2014**, *21*, 682–699, doi:10.1089/ars.2013.5212.
27. Shibata, M.-A.; Iinuma, M.; Morimoto, J.; Kurose, H.; Akamatsu, K.; Okuno, Y.; Akao, Y.; Otsuki, Y. α-Mangostin Extracted from the Pericarp of the Mangosteen (Garcinia Mangostana Linn) Reduces Tumor Growth and Lymph Node Metastasis in an Immunocompetent Xenograft Model of Metastatic Mammary Cancer Carrying a P53 Mutation. *BMC Medicine* **2011**, *9*, 69, doi:10.1186/1741-7015-9-69.
28. Zhang, C.; Yu, G.; Shen, Y. The Naturally Occurring Xanthone α-Mangostin Induces ROS-Mediated Cytotoxicity in Non-Small Scale Lung Cancer Cells. *Saudi J Biol Sci* **2018**, *25*, 1090–1095, doi:10.1016/j.sjbs.2017.03.005.
29. Ma, Y.; Yu, W.; Shrivastava, A.; Srivastava, R.K.; Shankar, S. Inhibition of Pancreatic Cancer Stem Cell Characteristics by α-Mangostin: Molecular Mechanisms Involving

Sonic Hedgehog and Nanog. *Journal of Cellular and Molecular Medicine* **2019**, *23*, 2719–2730, doi:10.1111/jcmm.14178.
30. Li, P.; Tian, W.; Ma, X. Alpha-Mangostin Inhibits Intracellular Fatty Acid Synthase and Induces Apoptosis in Breast Cancer Cells. *Molecular Cancer* **2014**, *13*, 138, doi:10.1186/1476-4598-13-138.
31. Watanapokasin, R.; Jarinthanan, F.; Nakamura, Y.; Sawasjirakij, N.; Jaratrungtawee, A.; Suksamrarn, S. Effects of α-Mangostin on Apoptosis Induction of Human Colon Cancer. *World J Gastroenterol* **2011**, *17*, 2086–2095, doi:10.3748/wjg.v17.i16.2086.
32. Chitchumroonchokchai, C.; Thomas-Ahner, J.M.; Li, J.; Riedl, K.M.; Nontakham, J.; Suksumrarn, S.; Clinton, S.K.; Kinghorn, A.D.; Failla, M.L. Anti-Tumorigenicity of Dietary α-Mangostin in an HT-29 Colon Cell Xenograft Model and the Tissue Distribution of Xanthones and Their Phase II Metabolites. *Molecular Nutrition & Food Research* **2013**, *57*, 203–211, doi:10.1002/mnfr.201200539.
33. Chen, J.-J.; Long, Z.-J.; Xu, D.-F.; Xiao, R.-Z.; Liu, L.-L.; Xu, Z.-F.; Qiu, S.X.; Lin, D.-J.; Liu, Q. Inhibition of Autophagy Augments the Anticancer Activity of α-Mangostin in Chronic Myeloid Leukemia Cells. *Leukemia & Lymphoma* **2014**, *55*, 628–638, doi:10.3109/10428194.2013.802312.
34. PubChem Alpha-Mangostin Available online: https://pubchem.ncbi.nlm.nih.gov/compound/5281650#section=Solubility (accessed on 28 March 2021).
35. Li, L.; Brunner, I.; Han, A.-R.; Hamburger, M.; Kinghorn, A.D.; Frye, R.; Butterweck, V. Pharmacokinetics of α-Mangostin in Rats after Intravenous and Oral Application. *Molecular Nutrition & Food Research* **2011**, *55*, S67–S74, doi:10.1002/mnfr.201000511.
36. Han, S.Y.; You, B.H.; Kim, Y.C.; Chin, Y.-W.; Choi, Y.H. Dose-Independent ADME Properties and Tentative Identification of Metabolites of α-Mangostin from Garcinia Mangostana in Mice by Automated Microsampling and UPLC-MS/MS Methods. *PLOS ONE* **2015**, *10*, e0131587, doi:10.1371/journal.pone.0131587.
37. Daei Farshchi Adli, A.; Jahanban-Esfahlan, R.; Seidi, K.; Samandari-Rad, S.; Zarghami, N. An Overview on Vadimezan (DMXAA): The Vascular Disrupting Agent. *Chemical Biology & Drug Design* **2018**, *91*, 996–1006, doi:10.1111/cbdd.13166.
38. Le Naour, J.; Zitvogel, L.; Galluzzi, L.; Vacchelli, E.; Kroemer, G. Trial Watch: STING Agonists in Cancer Therapy. *OncoImmunology* **2020**, *9*, 1777624, doi:10.1080/2162402X.2020.1777624.
39. Zheng, C.; Zhang, W.; Wang, J.; Zhai, Y.; Xiong, F.; Cai, Y.; Gong, X.; Zhu, B.; Zhu, H.H.; Wang, H.; et al. Lenvatinib- and Vadimezan-Loaded Synthetic High-Density Lipoprotein for Combinational Immunochemotherapy of Metastatic Triple-Negative Breast Cancer. *Acta Pharmaceutica Sinica B* **2022**, *12*, 3726–3738, doi:10.1016/j.apsb.2022.02.021.
40. Manzari, M.T.; Shamay, Y.; Kiguchi, H.; Rosen, N.; Scaltriti, M.; Heller, D.A. Targeted Drug Delivery Strategies for Precision Medicines. *Nat Rev Mater* **2021**, *6*, 351–370, doi:10.1038/s41578-020-00269-6.
41. Dang, Y.; Guan, J. Nanoparticle-Based Drug Delivery Systems for Cancer Therapy. *Smart Materials in Medicine* **2020**, *1*, 10–19, doi:10.1016/j.smaim.2020.04.001.
42. Pham, D.T.; Saelim, N.; Tiyaboonchai, W. Alpha Mangostin Loaded Crosslinked Silk Fibroin-Based Nanoparticles for Cancer Chemotherapy. *Colloids and Surfaces B: Biointerfaces* **2019**, *181*, 705–713, doi:10.1016/j.colsurfb.2019.06.011.
43. Yang, S.; Gao, X.; He, Y.; Hu, Y.; Xu, B.; Cheng, Z.; Xiang, M.; Xie, Y. Applying an Innovative Biodegradable Self-Assembly Nanomicelles to Deliver α-Mangostin for Improving Anti-Melanoma Activity. *Cell Death Dis* **2019**, *10*, 1–14, doi:10.1038/s41419-019-1323-9.
44. Trang Phan, T.K.; Tran, T.Q.; Nguyen Pham, D.T.; Nguyen, D.T. Characterization, Release Pattern, and Cytotoxicity of Liposomes Loaded With α-Mangostin Isolated From

Pericarp of Mangosteen (Garcinia Mangostana L.). *Natural Product Communications* **2020**, *15*, 1934578X20974559, doi:10.1177/1934578X20974559.
45. Chandra Boinpelly, V.; Verma, R.K.; Srivastav, S.; Srivastava, R.K.; Shankar, S. α-Mangostin-Encapsulated PLGA Nanoparticles Inhibit Colorectal Cancer Growth by Inhibiting Notch Pathway. *Journal of Cellular and Molecular Medicine* **2020**, *24*, 11343–11354, doi:10.1111/jcmm.15731.
46. Samprasit, W.; Opanasopit, P.; Chamsai, B. Mucoadhesive Chitosan and Thiolated Chitosan Nanoparticles Containing Alpha Mangostin for Possible Colon-Targeted Delivery. *Pharmaceutical Development and Technology* **2021**, *26*, 362–372, doi:10.1080/10837450.2021.1873370.
47. Doan, V.T.H.; Takano, S.; Doan, N.A.T.; Nguyen, P.T.M.; Nguyen, V.A.T.; Pham, H.T.T.; Nakazawa, K.; Fujii, S.; Sakurai, K. Anticancer Efficacy of Cyclodextrin-Based Hyperbranched Polymer Nanoparticles Containing Alpha-Mangostin. *Polym J* **2021**, *53*, 481–492, doi:10.1038/s41428-020-00441-3.
48. Bonafè, F.; Pazzini, C.; Marchionni, S.; Guarnieri, C.; Muscari, C. Complete Disaggregation of MCF-7-Derived Breast Tumour Spheroids with Very Low Concentrations of α-Mangostin Loaded in CD44 Thioaptamer-Tagged Nanoparticles. *Int. J. Med. Sci.* **2019**, *16*, 33–42, doi:10.7150/ijms.28135.
49. Qiu, S.; Granet, R.; Mbakidi, J.-P.; Brégier, F.; Pouget, C.; Micallef, L.; Sothea-Ouk, T.; Leger, D.Y.; Liagre, B.; Chaleix, V.; et al. Delivery of Tanshinone IIA and α-Mangostin from Gold/PEI/Cyclodextrin Nanoparticle Platform Designed for Prostate Cancer Chemotherapy. *Bioorg Med Chem Lett* **2016**, *26*, 2503–2506, doi:10.1016/j.bmcl.2016.03.097.
50. Dias, A.P.; da Silva Santos, S.; da Silva, J.V.; Parise-Filho, R.; Igne Ferreira, E.; Seoud, O.E.; Giarolla, J. Dendrimers in the Context of Nanomedicine. *International Journal of Pharmaceutics* **2020**, *573*, 118814, doi:10.1016/j.ijpharm.2019.118814.
51. Jain, V.; Bharatam, P.V. Pharmacoinformatic Approaches to Understand Complexation of Dendrimeric Nanoparticles with Drugs. *Nanoscale* **2014**, *6*, 2476–2501, doi:10.1039/C3NR05400D.
52. Nikzamir, M.; Hanifehpour, Y.; Akbarzadeh, A.; Panahi, Y. Applications of Dendrimers in Nanomedicine and Drug Delivery: A Review. *J Inorg Organomet Polym* **2021**, *31*, 2246–2261, doi:10.1007/s10904-021-01925-2.
53. Ambekar, R.S.; Choudhary, M.; Kandasubramanian, B. Recent Advances in Dendrimer-Based Nanoplatform for Cancer Treatment: A Review. *European Polymer Journal* **2020**, *126*, 109546, doi:10.1016/j.eurpolymj.2020.109546.
54. Igartúa, D.E.; Martinez, C.S.; Temprana, C.F.; Alonso, S. del V.; Prieto, M.J. PAMAM Dendrimers as a Carbamazepine Delivery System for Neurodegenerative Diseases: A Biophysical and Nanotoxicological Characterization. *International Journal of Pharmaceutics* **2018**, *544*, 191–202, doi:10.1016/j.ijpharm.2018.04.032.
55. Hu, Q.; Ding, B.; Yan, X.; Peng, L.; Duan, J.; Yang, S.; Cheng, L.; Chen, D. Polyethylene Glycol Modified PAMAM Dendrimer Delivery of Kartogenin to Induce Chondrogenic Differentiation of Mesenchymal Stem Cells. *Nanomedicine: Nanotechnology, Biology and Medicine* **2017**, *13*, 2189–2198, doi:10.1016/j.nano.2017.05.011.
56. Perisé-Barrios, A.J.; Jiménez, J.L.; Domínguez-Soto, A.; de la Mata, F.J.; Corbí, A.L.; Gomez, R.; Muñoz-Fernandez, M.Á. Carbosilane Dendrimers as Gene Delivery Agents for the Treatment of HIV Infection. *Journal of Controlled Release* **2014**, *184*, 51–57, doi:10.1016/j.jconrel.2014.03.048.
57. Narsireddy, A.; Vijayashree, K.; Adimoolam, M.G.; Manorama, S.V.; Rao, N.M. Photosensitizer and Peptide-Conjugated PAMAM Dendrimer for Targeted in Vivo Photodynamic Therapy. *Int J Nanomedicine* **2015**, *10*, 6865–6878, doi:10.2147/IJN.S89474.

58. Desai, P.N.; Yuan, Q.; Yang, H. Synthesis and Characterization of Photocurable Polyamidoamine Dendrimer Hydrogels as a Versatile Platform for Tissue Engineering and Drug Delivery. *Biomacromolecules* **2010**, *11*, 666–673, doi:10.1021/bm901240g.
59. Markowicz-Piasecka, M.; Sikora, J.; Szymański, P.; Kozak, O.; Studniarek, M.; Mikiciuk-Olasik, E. PAMAM Dendrimers as Potential Carriers of Gadolinium Complexes of Iminodiacetic Acid Derivatives for Magnetic Resonance Imaging. *Journal of Nanomaterials* **2015**, *2015*, e394827, doi:10.1155/2015/394827.
60. Chowdhury, S.; Toth, I.; Stephenson, R.J. Dendrimers in Vaccine Delivery: Recent Progress and Advances. *Biomaterials* **2022**, *280*, 121303, doi:10.1016/j.biomaterials.2021.121303.
61. Santos, A.; Veiga, F.; Figueiras, A. Dendrimers as Pharmaceutical Excipients: Synthesis, Properties, Toxicity and Biomedical Applications. *Materials* **2020**, *13*, 65, doi:10.3390/ma13010065.
62. Lim, J.; Kostiainen, M.; Maly, J.; da Costa, V.C.P.; Annunziata, O.; Pavan, G.M.; Simanek, E.E. Synthesis of Large Dendrimers with the Dimensions of Small Viruses. *J. Am. Chem. Soc.* **2013**, *135*, 4660–4663, doi:10.1021/ja400432e.
63. Pan, J.; Attia, S.A.; Filipczak, N.; Torchilin, V.P. 10 - Dendrimers for Drug Delivery Purposes. In *Nanoengineered Biomaterials for Advanced Drug Delivery*; Mozafari, M., Ed.; Woodhead Publishing Series in Biomaterials; Elsevier, 2020; pp. 201–242 ISBN 978-0-08-102985-5.
64. Gupta, V.; Nayak, S. Dendrimers: A Review on Synthetic Approaches. *J App Pharm Sci* **2015**, 117–122, doi:10.7324/JAPS.2015.50321.
65. Kesharwani, S.; Jaiswal, P.K.; Kesharwani, R.; kumar, V.; Patel, D.K. DENDRIMER: A NOVEL APPROACH FOR DRUG DELIVERY. *J. Pharm. Sci. Innov.* **2016**, *5*, 54–62, doi:10.7897/2277-4572.05212.
66. Gawande, V.; Choudhury, H.; Kesharwani, P. Chapter 6 - Dendrimer Nomenclature and Synthesis Methods. In *Dendrimer-Based Nanotherapeutics*; Kesharwani, P., Ed.; Academic Press, 2021; pp. 75–94 ISBN 978-0-12-821250-9.
67. Tripathi, P.K.; Tripathi, S. 6 - Dendrimers for Anticancer Drug Delivery. In *Pharmaceutical Applications of Dendrimers*; Chauhan, A., Kulhari, H., Eds.; Micro and Nano Technologies; Elsevier, 2020; pp. 131–150 ISBN 978-0-12-814527-2.
68. Tunki, L.; Kulhari, H.; Bhargava, S.K.; Pooja, D. 4 - Pharmacokinetic Considerations in Design of Dendrimer-Based Nanomedicines. In *Pharmaceutical Applications of Dendrimers*; Chauhan, A., Kulhari, H., Eds.; Micro and Nano Technologies; Elsevier, 2020; pp. 93–106 ISBN 978-0-12-814527-2.
69. Mekuria, S.L.; Debele, T.A.; Tsai, H.-C. PAMAM Dendrimer Based Targeted Nano-Carrier for Bio-Imaging and Therapeutic Agents. *RSC Adv.* **2016**, *6*, 63761–63772, doi:10.1039/C6RA12895E.
70. Sadekar, S.; Ray, A.; Janàt-Amsbury, M.; Peterson, C.M.; Ghandehari, H. Comparative Biodistribution of PAMAM Dendrimers and HPMA Copolymers in Ovarian-Tumor-Bearing Mice. *Biomacromolecules* **2011**, *12*, 88–96, doi:10.1021/bm101046d.
71. Menjoge, A.R.; Kannan, R.M.; Tomalia, D.A. Dendrimer-Based Drug and Imaging Conjugates: Design Considerations for Nanomedical Applications. *Drug Discovery Today* **2010**, *15*, 171–185, doi:10.1016/j.drudis.2010.01.009.
72. Fox, L.J.; Richardson, R.M.; Briscoe, W.H. PAMAM Dendrimer - Cell Membrane Interactions. *Advances in Colloid and Interface Science* **2018**, *257*, 1–18, doi:10.1016/j.cis.2018.06.005.
73. Mecke, A.; Majoros, I.J.; Patri, A.K.; Baker, J.R.; Holl, M.M.B.; Orr, B.G. Lipid Bilayer Disruption by Polycationic Polymers: The Roles of Size and Chemical Functional Group. *Langmuir* **2005**, *21*, 10348–10354, doi:10.1021/la050629l.

74. Chis, A.A.; Dobrea, C.; Morgovan, C.; Arseniu, A.M.; Rus, L.L.; Butuca, A.; Juncan, A.M.; Totan, M.; Vonica-Tincu, A.L.; Cormos, G.; et al. Applications and Limitations of Dendrimers in Biomedicine. *Molecules* **2020**, *25*, 3982, doi:10.3390/molecules25173982.
75. Vidal, F.; Vásquez, P.; Díaz, C.; Nova, D.; Alderete, J.; Guzmán, L. Mechanism of PAMAM Dendrimers Internalization in Hippocampal Neurons. *Mol. Pharmaceutics* **2016**, *13*, 3395–3403, doi:10.1021/acs.molpharmaceut.6b00381.
76. Sokol, M.B.; Faustova, M.R.; Nikolskaya, E.D.; Zhunina, O.A.; Fomicheva, M.V.; Petrov, R.V.; Yabbarov, N.G. Cellular Internalization of Targeted and Non-Targeted Delivery Systems for Contrast Agents Based on Polyamidoamine Dendrimers. *Russ Chem Bull* **2020**, *69*, 793–803, doi:10.1007/s11172-020-2835-2.
77. Sahoo, R.K.; Gothwal, A.; Rani, S.; Nakhate, K.T.; Ajazuddin; Gupta, U. PEGylated Dendrimer Mediated Delivery of Bortezomib: Drug Conjugation versus Encapsulation. *International Journal of Pharmaceutics* **2020**, *584*, 119389, doi:10.1016/j.ijpharm.2020.119389.
78. Luong, D.; Kesharwani, P.; Deshmukh, R.; Mohd Amin, M.C.I.; Gupta, U.; Greish, K.; Iyer, A.K. PEGylated PAMAM Dendrimers: Enhancing Efficacy and Mitigating Toxicity for Effective Anticancer Drug and Gene Delivery. *Acta Biomaterialia* **2016**, *43*, 14–29, doi:10.1016/j.actbio.2016.07.015.
79. Kolhatkar, R.B.; Kitchens, K.M.; Swaan, P.W.; Ghandehari, H. Surface Acetylation of Polyamidoamine (PAMAM) Dendrimers Decreases Cytotoxicity While Maintaining Membrane Permeability. *Bioconjugate Chem.* **2007**, *18*, 2054–2060, doi:10.1021/bc0603889.
80. Sharma, R.; Liaw, K.; Sharma, A.; Jimenez, A.; Chang, M.; Salazar, S.; Amlani, I.; Kannan, S.; Kannan, R.M. Glycosylation of PAMAM Dendrimers Significantly Improves Tumor Macrophage Targeting and Specificity in Glioblastoma. *Journal of Controlled Release* **2021**, *337*, 179–192, doi:10.1016/j.jconrel.2021.07.018.
81. Pooresmaeil, M.; Namazi, H.; Salehi, R. Synthesis of Photoluminescent Glycodendrimer with Terminal β-Cyclodextrin Molecules as a Biocompatible PH-Sensitive Carrier for Doxorubicin Delivery. *Carbohydrate Polymers* **2020**, *246*, 116658, doi:10.1016/j.carbpol.2020.116658.
82. Han, M.; Lv, Q.; Tang, X.-J.; Hu, Y.-L.; Xu, D.-H.; Li, F.-Z.; Liang, W.-Q.; Gao, J.-Q. Overcoming Drug Resistance of MCF-7/ADR Cells by Altering Intracellular Distribution of Doxorubicin via MVP Knockdown with a Novel SiRNA Polyamidoamine-Hyaluronic Acid Complex. *J Control Release* **2012**, *163*, 136–144, doi:10.1016/j.jconrel.2012.08.020.
83. Navath, R.S.; Menjoge, A.R.; Wang, B.; Romero, R.; Kannan, S.; Kannan, R.M. Amino Acid-Functionalized Dendrimers with Heterobifunctional Chemoselective Peripheral Groups for Drug Delivery Applications. *Biomacromolecules* **2010**, *11*, 1544–1563, doi:10.1021/bm100186b.
84. Saovapakhiran, A.; D'Emmanuele, A.; Attwood, D.; Penny, J. Surface Modification of PAMAM Dendrimers Modulates the Mechanism of Cellular Internalization. *Bioconjugate Chemistry* **2009**, *20*, 693–701, doi:10.1021/bc800234.
85. Jia, L.; Xu, J.-P.; Wang, H.; Ji, J. Polyamidoamine Dendrimers Surface-Engineered with Biomimetic Phosphorylcholine as Potential Drug Delivery Carriers. *Colloids Surf B Biointerfaces* **2011**, *84*, 49–54, doi:10.1016/j.colsurfb.2010.12.012.
86. Teow, H.M.; Zhou, Z.; Najlah, M.; Yusof, S.R.; Abbott, N.J.; D'Emanuele, A. Delivery of Paclitaxel across Cellular Barriers Using a Dendrimer-Based Nanocarrier. *Int J Pharm* **2013**, *441*, 701–711, doi:10.1016/j.ijpharm.2012.10.024.
87. Torres-Pérez, S.A.; Ramos-Godínez, M. del P.; Ramón-Gallegos, E. Glycosylated One-Step PAMAM Dendrimers Loaded with Methotrexate for Target Therapy in Breast Cancer Cells MDA-MB-231. *Journal of Drug Delivery Science and Technology* **2020**, *58*, 101769, doi:10.1016/j.jddst.2020.101769.

88. Zong, H.; Thomas, T.P.; Lee, K.-H.; Desai, A.M.; Li, M.; Kotlyar, A.; Zhang, Y.; Leroueil, P.R.; Gam, J.J.; Banaszak Holl, M.M.; et al. Bifunctional PAMAM Dendrimer Conjugates of Folic Acid and Methotrexate with Defined Ratio. *Biomacromolecules* **2012**, *13*, 982–991, doi:10.1021/bm201639c.
89. Xu, L.; Kittrell, S.; Yeudall, W.A.; Yang, H. Folic Acid-Decorated Polyamidoamine Dendrimer Mediates Selective Uptake and High Expression of Genes in Head and Neck Cancer Cells. *Nanomedicine* **2016**, *11*, 2959–2973, doi:10.2217/nnm-2016-0244.
90. Yalçın, S.; Erkan, M.; Ünsoy, G.; Parsian, M.; Kleeff, J.; Gündüz, U. Effect of Gemcitabine and Retinoic Acid Loaded PAMAM Dendrimer-Coated Magnetic Nanoparticles on Pancreatic Cancer and Stellate Cell Lines. *Biomedicine & Pharmacotherapy* **2014**, *68*, 737–743, doi:10.1016/j.biopha.2014.07.003.
91. Han, L.; Huang, R.; Liu, S.; Huang, S.; Jiang, C. Peptide-Conjugated PAMAM for Targeted Doxorubicin Delivery to Transferrin Receptor Overexpressed Tumors. *Mol. Pharmaceutics* **2010**, *7*, 2156–2165, doi:10.1021/mp100185f.
92. Kulhari, H.; Pooja, D.; Shrivastava, S.; Kuncha, M.; Naidu, V.G.M.; Bansal, V.; Sistla, R.; Adams, D.J. Trastuzumab-Grafted PAMAM Dendrimers for the Selective Delivery of Anticancer Drugs to HER2-Positive Breast Cancer. *Sci Rep* **2016**, *6*, 23179, doi:10.1038/srep23179.
93. Maiti, S.; Paira, P. Biotin Conjugated Organic Molecules and Proteins for Cancer Therapy: A Review. *European Journal of Medicinal Chemistry* **2018**, *145*, 206–223, doi:10.1016/j.ejmech.2018.01.001.
94. Azhar, A.; Booker, G.W.; Polyak, S.W. Mechanisms of Biotin Transport. *Biochem Anal Biochem* **2015**, *04*, doi:10.4172/2161-1009.1000210.
95. Ren, W.X.; Han, J.; Uhm, S.; Jang, Y.J.; Kang, C.; Kim, J.-H.; Kim, J.S. Recent Development of Biotin Conjugation in Biological Imaging, Sensing, and Target Delivery. *Chem. Commun.* **2015**, *51*, 10403–10418, doi:10.1039/C5CC03075G.
96. Yellepeddi, V.K.; Kumar, A.; Maher, D.M.; Chauhan, S.C.; Vangara, K.K.; Palakurthi, S. Biotinylated PAMAM Dendrimers for Intracellular Delivery of Cisplatin to Ovarian Cancer: Role of SMVT. *Anticancer Res* **2011**, *31*, 897–906.
97. Rompicharla, S.V.K.; Kumari, P.; Bhatt, H.; Ghosh, B.; Biswas, S. Biotin Functionalized PEGylated Poly(Amidoamine) Dendrimer Conjugate for Active Targeting of Paclitaxel in Cancer. *International Journal of Pharmaceutics* **2019**, *557*, 329–341, doi:10.1016/j.ijpharm.2018.12.069.
98. Yao, H.; Ma, J. Dendrimer-Paclitaxel Complexes for Efficient Treatment in Ovarian Cancer: Study on OVCAR-3 and HEK293T Cells. *Acta Biochimica Polonica* **2018**, *65*, 219–225, doi:10.18388/abp.2017_2331.
99. Yuan, H.; Luo, K.; Lai, Y.; Pu, Y.; He, B.; Wang, G.; Wu, Y.; Gu, Z. A Novel Poly(l-Glutamic Acid) Dendrimer Based Drug Delivery System with Both PH-Sensitive and Targeting Functions. *Mol. Pharmaceutics* **2010**, *7*, 953–962, doi:10.1021/mp1000923.
100. Pu, Y.; Chang, S.; Yuan, H.; Wang, G.; He, B.; Gu, Z. The Anti-Tumor Efficiency of Poly(L-Glutamic Acid) Dendrimers with Polyhedral Oligomeric Silsesquioxane Cores. *Biomaterials* **2013**, *34*, 3658–3666, doi:10.1016/j.biomaterials.2013.01.082.
101. Seixas, N.; Ravanello, B.B.; Morgan, I.; Kaluđerović, G.N.; Wessjohann, L.A. Chlorambucil Conjugated Ugi Dendrimers with PAMAM-NH2 Core and Evaluation of Their Anticancer Activity. *Pharmaceutics* **2019**, *11*, 59, doi:10.3390/pharmaceutics11020059.
102. Hanurry, E.Y.; Mekonnen, T.W.; Andrgie, A.T.; Darge, H.F.; Birhan, Y.S.; Hsu, W.-H.; Chou, H.-Y.; Cheng, C.-C.; Lai, J.-Y.; Tsai, H.-C. Biotin-Decorated PAMAM G4.5 Dendrimer Nanoparticles to Enhance the Delivery, Anti-Proliferative, and Apoptotic Effects of Chemotherapeutic Drug in Cancer Cells. *Pharmaceutics* **2020**, *12*, 443, doi:10.3390/pharmaceutics12050443.

103. Uram, Ł.; Filipowicz, A.; Misiorek, M.; Pieńkowska, N.; Markowicz, J.; Wałajtys-Rode, E.; Wołowiec, S. Biotinylated PAMAM G3 Dendrimer Conjugated with Celecoxib and/or Fmoc-l-Leucine and Its Cytotoxicity for Normal and Cancer Human Cell Lines. *European Journal of Pharmaceutical Sciences* **2018**, *124*, 1–9, doi:10.1016/j.ejps.2018.08.019.
104. Uram, Ł.; Filipowicz-Rachwał, A.; Misiorek, M.; Winiarz, A.; Wałajtys-Rode, E.; Wołowiec, S. Synthesis and Different Effects of Biotinylated PAMAM G3 Dendrimer Substituted with Nimesulide in Human Normal Fibroblasts and Squamous Carcinoma Cells. *Biomolecules* **2019**, *9*, 437, doi:10.3390/biom9090437.
105. Tietze, S.; Schau, I.; Michen, S.; Ennen, F.; Janke, A.; Schackert, G.; Aigner, A.; Appelhans, D.; Temme, A. A Poly(Propyleneimine) Dendrimer-Based Polyplex-System for Single-Chain Antibody-Mediated Targeted Delivery and Cellular Uptake of SiRNA. *Small* **2017**, *13*, 1700072, doi:10.1002/smll.201700072.
106. Hemmer, R.; Hall, A.; Spaulding, R.; Rossow, B.; Hester, M.; Caroway, M.; Haskamp, A.; Wall, S.; Bullen, H.A.; Morris, C.; et al. Analysis of Biotinylated Generation 4 Poly(Amidoamine) (PAMAM) Dendrimer Distribution in the Rat Brain and Toxicity in a Cellular Model of the Blood-Brain Barrier. *Molecules* **2013**, *18*, 11537–11552, doi:10.3390/molecules180911537.
107. Uram, Ł.; Szuster, M.; Filipowicz, A.; Zaręba, M.; Wałajtys-Rode, E.; Wołowiec, S. Cellular Uptake of Glucoheptoamidated Poly(Amidoamine) PAMAM G3 Dendrimer with Amide-Conjugated Biotin, a Potential Carrier of Anticancer Drugs. *Bioorganic & Medicinal Chemistry* **2017**, *25*, 706–713, doi:10.1016/j.bmc.2016.11.047.
108. Uram, Ł.; Misiorek, M.; Pichla, M.; Filipowicz-Rachwał, A.; Markowicz, J.; Wołowiec, S.; Wałajtys-Rode, E. The Effect of Biotinylated PAMAM G3 Dendrimers Conjugated with COX-2 Inhibitor (Celecoxib) and PPARγ Agonist (Fmoc-L-Leucine) on Human Normal Fibroblasts, Immortalized Keratinocytes and Glioma Cells in Vitro. *Molecules* **2019**, *24*, 3801, doi:10.3390/molecules24203801.
109. Janaszewska, A.; Lazniewska, J.; Trzepiński, P.; Marcinkowska, M.; Klajnert-Maculewicz, B. Cytotoxicity of Dendrimers. *Biomolecules* **2019**, *9*, doi:10.3390/biom9080330.
110. Kharwade, R.; More, S.; Warokar, A.; Agrawal, P.; Mahajan, N. Starburst Pamam Dendrimers: Synthetic Approaches, Surface Modifications, and Biomedical Applications. *Arabian Journal of Chemistry* **2020**, *13*, 6009–6039, doi:10.1016/j.arabjc.2020.05.002.
111. Nakamura, Y.; Mochida, A.; Choyke, P.L.; Kobayashi, H. Nanodrug Delivery: Is the Enhanced Permeability and Retention Effect Sufficient for Curing Cancer? *Bioconjugate Chem.* **2016**, *27*, 2225–2238, doi:10.1021/acs.bioconjchem.6b00437.
112. Ghaffari, M.; Dehghan, G.; Abedi-Gaballu, F.; Kashanian, S.; Baradaran, B.; Ezzati Nazhad Dolatabadi, J.; Losic, D. Surface Functionalized Dendrimers as Controlled-Release Delivery Nanosystems for Tumor Targeting. *European Journal of Pharmaceutical Sciences* **2018**, *122*, 311–330, doi:10.1016/j.ejps.2018.07.020.
113. Wang, H.; Huang, Q.; Chang, H.; Xiao, J.; Cheng, Y. Stimuli-Responsive Dendrimers in Drug Delivery. *Biomater. Sci.* **2016**, *4*, 375–390, doi:10.1039/C5BM00532A.
114. Mo, R.; Gu, Z. Tumor Microenvironment and Intracellular Signal-Activated Nanomaterials for Anticancer Drug Delivery. *Materials Today* **2016**, *19*, 274–283, doi:10.1016/j.mattod.2015.11.025.
115. Burns, A.R.; Luciani, G.M.; Musso, G.; Bagg, R.; Yeo, M.; Zhang, Y.; Rajendran, L.; Glavin, J.; Hunter, R.; Redman, E.; et al. Caenorhabditis Elegans Is a Useful Model for Anthelmintic Discovery. *Nat Commun* **2015**, *6*, 7485, doi:10.1038/ncomms8485.
116. Honnen, S. Caenorhabditis Elegans as a Powerful Alternative Model Organism to Promote Research in Genetic Toxicology and Biomedicine. *Archives of Toxicology* **2017**, *91*, 2029–2044, doi:10.1007/s00204-017-1944-7.

117. Rode, W.; Jarmuła, A. Mechanizm reakcji katalizowanej przez syntazę tymidylanową. *Postępy Biochemii* **2015**, 10.
118. Repetto, G.; del Peso, A.; Zurita, J.L. Neutral Red Uptake Assay for the Estimation of Cell Viability/Cytotoxicity. *Nat Protoc* **2008**, *3*, 1125–1131, doi:10.1038/nprot.2008.75.
119. Berridge, M.V.; Herst, P.M.; Tan, A.S. Tetrazolium Dyes as Tools in Cell Biology: New Insights into Their Cellular Reduction. *Biotechnol Annu Rev* **2005**, *11*, 127–152, doi:10.1016/S1387-2656(05)11004-7.
120. D'Arcy, M.S. Cell Death: A Review of the Major Forms of Apoptosis, Necrosis and Autophagy. *Cell Biology International* **2019**, *43*, 582–592, doi:10.1002/cbin.11137.
121. Gkretsi, V.; Stylianopoulos, T. Cell Adhesion and Matrix Stiffness: Coordinating Cancer Cell Invasion and Metastasis. *Front. Oncol.* **2018**, *8*, 145, doi:10.3389/fonc.2018.00145.
122. Feoktistova, M.; Geserick, P.; Leverkus, M. Crystal Violet Assay for Determining Viability of Cultured Cells. *Cold Spring Harb Protoc* **2016**, *2016*, pdb.prot087379, doi:10.1101/pdb.prot087379.
123. Liang, C.-C.; Park, A.Y.; Guan, J.-L. *In Vitro* Scratch Assay: A Convenient and Inexpensive Method for Analysis of Cell Migration *in Vitro*. *Nature Protocols* **2007**, *2*, 329–333, doi:10.1038/nprot.2007.30.
124. Tomalia, D.A.; Baker, H.; Dewald, J.; Hall, M.; Kallos, G.; Martin, S.; Roeck, J.; Ryder, J.; Smith, P. A New Class of Polymers: Starburst-Dendritic Macromolecules. *Polymer Journal* **1985**, *17*, 117–132, doi:10.1295/polymj.17.117.
125. Crosignani, S.; Gonzalez, J.; Swinnen, D. Polymer-Supported Mukaiyama Reagent: A Useful Coupling Reagent for the Synthesis of Esters and Amides. *Organic Letters* **2004**, *6*, 4579–4582, doi:10.1021/ol0480372.
126. Maiti, P.K.; Çağın, T.; Lin, S.-T.; Goddard, W.A. Effect of Solvent and PH on the Structure of PAMAM Dendrimers. *Macromolecules* **2005**, *38*, 979–991, doi:10.1021/ma049168l.
127. Klein, V.G.; Bond, A.G.; Craigon, C.; Lokey, R.S.; Ciulli, A. Amide-to-Ester Substitution as a Strategy for Optimizing PROTAC Permeability and Cellular Activity. *J. Med. Chem.* **2021**, *64*, 18082–18101, doi:10.1021/acs.jmedchem.1c01496.

7. Wykaz rycin i tabel

Wykaz osiągnięć naukowych doktoranta

I. Publikacje naukowe (podkreśleniem oznaczono publikacje należące do cyklu artykułów stanowiących rozprawę doktorską)

1) **Markowicz J***, Wołowiec S, Rode W, Uram Ł. Synthesis and Properties of α-Mangostin and Vadimezan Conjugates with Glucoheptoamidated and Biotinylated 3rd Generation Poly(amidoamine) Dendrimer, and Conjugation Effect on Their Anticancer and Anti-Nematode Activities. *Pharmaceutics*. 2022 March 10;14(3):606. Doi: 10.3390/pharmaceutics14030606.

2) Wróbel K, Wołowiec S, **Markowicz J**, Wałajtys-Rode E, Uram Ł*. Synthesis of Biotinylated PAMAM G3 Dendrimers Substituted with R-Glycidol and Celecoxib/Simvastatin as Repurposed Drugs and Evaluation of Their Increased Additive Cytotoxicity for Cancer Cell Lines. *Cancers (Basel)*. 2022 Jan 29;14(3):714. Doi: 10.3390/cancers14030714.

3) **Markowicz J***, Uram Ł, Wołowiec S, Rode W*. Biotin Transport-Targeting Polysaccharide-Modified PAMAM G3 Dendrimer as System Delivering α-Mangostin into Cancer Cells and *C. elegans* Worms. *International Journal of Molecular Sciences*. 2021 Nov 29;22(23):12925. Doi: 10.3390/ijms222312925.

4) Uram Ł*, **Markowicz J**, Misiorek M, Filipowicz-Rachwał A, Wołowiec, S, Wałajtys-Rode E. Celecoxib substituted biotinylated poly(amidoamine) G3 dendrimer as potential treatment for temozolomide resistant glioma therapy and anti-nematode agent. *European Journal of Pharmaceutical Sciences*. 2020 Sep 1;152:105439. Doi: 10.1016/j.ejps.2020.105439.

5) Maj P, Mori M, Sobich J, **Markowicz J**, Uram Ł, Zieliński Z, Quaglio D, Calcaterra A, Cau Y, Botta B, Rode W*. Alvaxanthone, a Thymidylate Synthase Inhibitor with Nematocidal and Tumoricidal Activities. *Molecules.* 2020 Jun 23;25(12):2894. Doi: 10.3390/molecules25122894.

6) **Markowicz J***, Uram Ł, Sobich J, Mangiardi L, Maj P, Rode W. Antitumor and anti-nematode activities of α-mangostin. *European Journal of Pharmacology*. 2019 Nov 15;863:172678. Doi: 10.1016/j.ejphar.2019.172678.

7) Uram Ł*, Misiorek M, Pichla M, Filipowicz-Rachwał A, **Markowicz J**, Wołowiec S, Wałajtys-Rode E. The Effect of Biotinylated PAMAM G3 Dendrimers Conjugated with COX-2 Inhibitor (celecoxib) and PPARγ Agonist (Fmoc-L-Leucine) on Human Normal Fibroblasts, Immortalized Keratinocytes and Glioma Cells in Vitro. *Molecules*. 2019 Oct 22;24(20):3801. Doi: 10.3390/molecules24203801.

8) Uram Ł*, Filipowicz A, Misiorek M, Pieńkowska N, **Markowicz J**, Wałajtys-Rode E, Wołowiec S. Biotinylated PAMAM G3 dendrimer conjugated with celecoxib and/or Fmoc-l-Leucine and its cytotoxicity for normal and cancer human cell lines. *European Journal of Pharmaceutical Sciences*. 2018 Nov 1;124:1-9. Doi: 10.1016/j.ejps.2018.08.019.

II. Udział w konferencjach ogólnopolskich i międzynarodowych

24-25.06.2021 Chemistry & Biotechnology International Conference, Politechnika Wrocławska, Wrocław (konferencja online)
Markowicz Joanna, Uram Łukasz: ”Biotin labelled PAMAM G3 dendrimers as a delivery system for α-mangostin into squamous carcinoma cells” (referat ustny)

24-25.06.2021 Chemistry & Biotechnology International Conference, Politechnika Wrocławska, Wrocław (konferencja online)
Uram Łukasz, Markowicz Joanna: ”Celecoxib substituted biotinylated poly(amidoamine) G3 dendrimer as therapeutic agent for temozolomide resistant glioma therapy” (poster)

30-31.05.2019 V Ogólnopolska Konferencja Doktorantów Nauk o Życiu BioOpen, Wydział Biologii i Ochrony Środowiska Uniwersytet Łódzki, Łódź
Markowicz Joanna, Uram Łukasz: „Potencjał przeciwnowotworowy α-mangostyny wobec komórek raka płaskonabłonkowego na podstawie badań wybranych parametrów komórkowych” (referat ustny)

17-19.05.2019 8th Intercollegiate Biotechnology Symposium "Symbioza", Warszawa
Markowicz Joanna, Uram Łukasz: “α-mangostin, a natural compound from Garcinia mangostana Linn, exerts selective toxic

activity against squamous carcinoma cells through inhibition of proliferation, adhesion and apoptosis induction" (poster)

10-12.05.2019 5th International Conference of Cell Biology, Kraków
Markowicz Joanna, Uram Łukasz: "Biotinylated PAMAM G3 dendrimer conjugated with celecoxib as potential nanoparticle delivery system in therapy of glioblastoma multiforme" (poster)

18.05.2018 I Ogólnopolska Konferencja Naukowa "Polimery w Medycynie",Łódź
Markowicz Joanna, Pieńkowska Natalia: „Analiza właściwości przeciwnowotworowych biotynylowanego dendrymeru PAMAM generacji trzeciej, podstawionego Celekoksybem - badania *in vitro*" (poster)

02-03.12.2017 IV Ogólnopolskie Sympozjum Biomedyczne ESKULAP, Lublin
Markowicz Joanna, Uram Łukasz: „Celekoksyb i Fmoc-L-Leucyna skoniugowane z biotynylowanym dendrymerem PAMAM G3 jako konstrukt lekowy do zastosowania w przeciwnowotworowej terapii celowanej" (referat ustny)

III. Staże naukowe

08.01.2018 – 08.02.2018 Miesięczny staż naukowy w Instytucie Biologii Doświadczalnej im. M. Nenckiego PAN, Warszawa

IV. Nagrody za działalność naukową

2020/2021 Stypendium Fundacji Czesława M. Rodkiewicza – Edycja 2021 dla doktorantów prowadzących badania w dziedzinie powiązania techniki z naukami medycznymi

2020/2021 Stypendium dla najlepszych doktorantów na kierunku Technologia chemiczna z dotacji projakościowej

2017 – 2022 Stypendium rektora dla najlepszych doktorantów na kierunku Technologia chemiczna

V. Inna działalność w trakcie studiów doktoranckich

2017 – 2019	Przygotowanie oraz prowadzenie pokazów naukowych o tematyce biotechnologicznej wraz z kołem naukowym INSERT podczas Seminariów „Wybrane Problemy Chemii", Dni Otwartych Politechniki Rzeszowskiej oraz Nocnych Spotkań z Nauką.
2017/2018	Realizacja autorskich pokazów naukowych dla uczniów szkół ponadgimnazjalnych w ramach Roadshow 4. edycji programu ADAMED SmartUP – projektu naukowo-edukacyjnego popularyzującego nauki ścisłe i przyrodnicze.
2017 – 2022	Działalność w Kole Naukowym Studentów Biotechnologii INSERT

VI. Informacje naukometryczne

Wg bazy Web of Science (dane na dzień 24.10.2022):

- Łączny Impact Factor prac: 38,161
- Łączna liczba cytacji: bez autocytacji – 53, z autocytacjami – 67
- Indeks Hirscha: 4

Wg Google Scholar (dane na dzień 24.10.2022):

- Łączna liczba cytacji: 84
- Indeks Hirscha: 4

Oświadczenie doktoranta dotyczące merytorycznego i procentowego udziału w powstaniu artykułów naukowych

POLITECHNIKA RZESZOWSKA
im. IGNACEGO ŁUKASIEWICZA

al. Powstańców Warszawy 12, 35-959 Rzeszów
tel.: +48 17 865 1100, e-mail: kancelaria@prz.edu.pl
www.prz.edu.pl

Mgr inż. Joanna Drozdowska
Wydział Chemiczny, Politechnika Rzeszowska
Katedra Chemii Nieorganicznej i Analitycznej
al. Powstańców Warszawy 6, 35-959 Rzeszów
e-mail: d409@stud.prz.edu.pl

Rzeszów, 28.09.2022

OŚWIADCZENIE

Oświadczam, że w niżej wymienionych pracach mój udział merytoryczny oraz procentowy był następujący:

Lp.	Tytuł publikacji oraz informacje bibliograficzne	Udział merytoryczny	Udział %
[P1]	Markowicz Joanna, Uram Łukasz, Sobich Justyna, Mangiardi Laura, Maj Piotr, Rode Wojciech. Antitumor and anti-nematode activities of α-mangostin. *European Journal of Pharmacology*. 2019 Nov 15;863:172678. doi: 10.1016/j.ejphar.2019.172678	- współtworzenie koncepcji publikacji, - wybór metodologii badań, - przeprowadzenie eksperymentów na hodowlach komórkowych, - analiza, wizualizacja i opracowanie statystyczne wyników, - zredagowanie i edycja treści manuskryptu, - odniesienie się do uwag recenzentów i zredagowanie końcowej formy publikacji, - pełnienie funkcji autora korespondencyjnego	50%
[P2]	Maj Piotr, Mori Mattia, Sobich Justyna, Markowicz Joanna, Uram Łukasz, Zieliński Zbigniew, Quaglio Deborah, Calcaterra Andrea, Cau Ylenia, Botta Bruno, Rode Wojciech. Alvaxanthone, a	- przeprowadzenie eksperymentów na hodowlach komórkowych, - analiza, wizualizacja i opracowanie statystyczne wyników z części biologicznej	14%

Joanna Drozdowska

WYDZIAŁ CHEMICZNY
POLITECHNIKA RZESZOWSKA

al. Powstańców Warszawy 6, 35-959 Rzeszów
tel.: +48 17 865 1652, e-mail: chemia@prz.edu.pl
www.wch.prz.edu.pl

al. Powstańców Warszawy 12, 35-959 Rzeszów
tel.: +48 17 865 1100, e-mail: kancelaria@prz.edu.pl
www.prz.edu.pl

	Thymidylate Synthase Inhibitor with Nematocidal and Tumoricidal Activities. *Molecules*. 2020 Jun 23;25(12):2894. doi: 10.3390/molecules25122894		
[P3]	Markowicz Joanna, Uram Łukasz, Wołowiec Stanisław, Rode Wojciech. Biotin Transport-Targeting Polysaccharide-Modified PAMAM G3 Dendrimer as System Delivering α-Mangostin into Cancer Cells and *C. elegans* Worms. *International Journal of Molecular Sciences*. 2021 Nov 29;22(23):12925. doi: 10.3390/ijms222312925	- współtworzenie koncepcji publikacji, - przeprowadzenie eksperymentów (syntezy chemiczne koniugatów, pomiary NMR oraz DLS, badania na hodowlach komórkowych oraz hodowli nicienia), - analiza, wizualizacja i opracowanie statystyczne wyników, - analiza obrazów mikroskopowych, - zredagowanie i edycja treści manuskryptu, - odniesienie się do uwag recenzentów i opracowanie końcowej formy publikacji, - pełnienie funkcji autora korespondencyjnego	60%
[P4]	Markowicz Joanna, Wołowiec Stanisław, Rode Wojciech, Uram Łukasz. Synthesis and Properties of α-Mangostin and Vadimezan Conjugates with Glucoheptoamidated and Biotinylated 3rd Generation Poly(amidoamine) Dendrimer, and Conjugation Effect on Their Anticancer and Anti-Nematode Activities. *Pharmaceutics*. 2022 March 10;14(3):606. doi: 10.3390/pharmaceutics14030606	- współtworzenie koncepcji publikacji, - przeprowadzenie eksperymentów (syntezy chemiczne koniugatów, pomiary NMR oraz DLS, badania na hodowlach komórkowych oraz hodowli nicienia), - analiza, wizualizacja i opracowanie statystyczne wyników, - zredagowanie i edycja treści manuskryptu, - odniesienie się do uwag recenzentów i współopracowanie końcowej formy pracy, - pełnienie funkcji autora korespondencyjnego	60%

Joanna Drozdowska

al. Powstańców Warszawy 6, 35-959 Rzeszów
tel.: +48 17 865 1652, e-mail: chemia@prz.edu.pl
www.wch.prz.edu.pl

Oświadczenia współautorów artykułów naukowych

POLITECHNIKA RZESZOWSKA
im. IGNACEGO ŁUKASIEWICZA

al. Powstańców Warszawy 12, 35-959 Rzeszów
tel.: +48 17 865 1100, e-mail: kancelaria@prz.edu.pl
www.prz.edu.pl

Dr hab. Łukasz Uram, prof. PRz
Wydział Chemiczny, Politechnika Rzeszowska
Katedra Chemii Nieorganicznej i Analitycznej
al. Powstańców Warszawy 6, 35-959 Rzeszów
tel: (17) 743 20 12, e-mail: luram@prz.edu.pl

Rzeszów, 28.09.2022

OŚWIADCZENIE

Oświadczam, że w niżej wymienionych pracach mój udział merytoryczny oraz procentowy był następujący:

Lp.	Tytuł publikacji oraz informacje bibliograficzne	Udział merytoryczny	Udział %
[P1]	Markowicz Joanna, Uram Łukasz, Sobich Justyna, Mangiardi Laura, Maj Piotr, Rode Wojciech. Antitumor and anti-nematode activities of α-mangostin. *European Journal of Pharmacology*. 2019 Nov 15;863:172678. doi: 10.1016/j.ejphar.2019.172678	- wybór metodologii badań na hodowlach komórkowych, - przeprowadzenie testu migracji komórek, - korekta treści manuskryptu, - odniesienie się do uwag recenzentów i współopracowanie końcowej formy pracy, - pozyskanie środków na badania	30%
[P2]	Maj Piotr, Mori Mattia, Sobich Justyna, Markowicz Joanna, Uram Łukasz, Zieliński Zbigniew, Quaglio Deborah, Calcaterra Andrea, Cau Ylenia, Botta Bruno, Rode Wojciech. Alvaxanthone, a Thymidylate Synthase Inhibitor with Nematocidal and Tumoricidal Activities. *Molecules*. 2020 Jun 23;25(12):2894.	- przeprowadzenie obserwacji mikroskopowych, - zredagowanie i edycja treści publikacji	14%

Łukasz Uram

WYDZIAŁ CHEMICZNY
POLITECHNIKI RZESZOWSKIEJ

al. Powstańców Warszawy 6, 35-959 Rzeszów
tel.: +48 17 865 1652, e-mail: chemia@prz.edu.pl
www.wch.prz.edu.pl

al. Powstańców Warszawy 12, 35-959 Rzeszów
tel.: +48 17 865 1100, e-mail: kancelaria@prz.edu.pl
www.prz.edu.pl

	doi: 10.3390/molecules25122894		
[P3]	Markowicz Joanna, Uram Łukasz, Wołowiec Stanisław, Rode Wojciech. Biotin Transport-Targeting Polysaccharide-Modified PAMAM G3 Dendrimer as System Delivering α-Mangostin into Cancer Cells and *C. elegans* Worms. *International Journal of Molecular Sciences*. 2021 Nov 29;22(23):12925. doi: 10.3390/ijms222312925	- współtworzenie koncepcji publikacji, - wybór metodologii badań biologicznych, - przeprowadzenie obserwacji z wykorzystaniem mikroskopu konfokalnego, - korekta treści części biologicznej publikacji, - odniesienie się do uwag recenzentów i współopracowanie końcowej formy pracy	25%
[P4]	Markowicz Joanna, Wołowiec Stanisław, Rode Wojciech, Uram Łukasz. Synthesis and Properties of α-Mangostin and Vadimezan Conjugates with Glucoheptoamidated and Biotinylated 3rd Generation Poly(amidoamine) Dendrimer, and Conjugation Effect on Their Anticancer and Anti-Nematode Activities. *Pharmaceutics*. 2022 March 10;14(3):606. doi: 10.3390/pharmaceutics14030606	- współtworzenie koncepcji publikacji, - wybór metodologii badań biologicznych, - korekta treści części biologicznej publikacji, - odniesienie się do uwag recenzentów i współopracowanie końcowej formy pracy	20%

Łukasz Chem

Prof. dr hab. Wojciech Rode
Instytut Biologii Doświadczalnej im. M. Nenckiego PAN
ul. Ludwika Pasteura 3, 02-093 Warszawa
e-mail: w.rode@nencki.edu.pl

Rzeszów, 28.09.2022

OŚWIADCZENIE

Oświadczam, że w niżej wymienionych pracach mój udział merytoryczny oraz procentowy był następujący:

Lp.	Tytuł publikacji oraz informacje bibliograficzne	Udział merytoryczny	Udział %
[P1]	Markowicz Joanna, Uram Łukasz, Sobich Justyna, Mangiardi Laura, Maj Piotr, Rode Wojciech. Antitumor and anti-nematode activities of α-mangostin. *European Journal of Pharmacology*. 2019 Nov 15;863:172678. doi: 10.1016/j.ejphar.2019.172678	- współtworzenie koncepcji publikacji, - korekta treści publikacji, - odniesienie się do części uwag recenzentów, - pozyskanie środków na badania	5%
[P2]	Maj Piotr, Mori Mattia, Sobich Justyna, Markowicz Joanna, Uram Łukasz, Zieliński Zbigniew, Quaglio Deborah, Calcaterra Andrea, Cau Ylenia, Botta Bruno, Rode Wojciech. Alvaxanthone, a Thymidylate Synthase Inhibitor with Nematocidal and Tumoricidal Activities. *Molecules*. 2020 Jun 23;25(12):2894. doi: 10.3390/molecules25122894	- współtworzenie koncepcji publikacji, - redagowanie i edycja treści manuskryptu, - odniesienie się do części uwag recenzentów, - pełnienie funkcji autora korespondencyjnego, - pozyskanie środków na badania i publikację	5%
[P3]	Markowicz Joanna, Uram Łukasz, Wołowiec Stanisław, Rode Wojciech. Biotin Transport-Targeting Polysaccharide-Modified PAMAM G3 Dendrimer as System Delivering α-Mangostin into Cancer Cells and *C. elegans* Worms. *International Journal of Molecular Sciences*. 2021 Nov 29;22(23):12925. doi: 10.3390/ijms222312925	- współtworzenie koncepcji publikacji, - korekta treści publikacji, - odniesienie się do części uwag recenzentów, - pozyskanie środków na badania i publikację	5%
[P4]	Markowicz Joanna, Wołowiec Stanisław, Rode Wojciech, Uram Łukasz. Synthesis and Properties of α-Mangostin and Vadimezan Conjugates with Glucoheptoamidated and Biotinylated 3rd Generation Poly(amidoamine) Dendrimer, and Conjugation Effect on Their Anticancer and Anti-Nematode Activities. *Pharmaceutics*. 2022 March 10;14(3):606. doi: 10.3390/pharmaceutics14030606	- współtworzenie koncepcji publikacji, - korekta treści publikacji, - odniesienie się do części uwag recenzentów, - pozyskanie środków na badania i publikację	10%

Prof. dr hab. inż. Stanisław Wołowiec

Kolegium Nauk Medycznych, Uniwersytet Rzeszowski

Zakład Biochemii i Chemii Ogólnej, Instytut Nauk Medycznych

ul. Warzywna 1a, 35-310 Rzeszów

e-mail: swolowiec@ur.edu.pl

Rzeszów, 28.09.2022

OŚWIADCZENIE

Oświadczam, że w niżej wymienionych pracach mój udział merytoryczny oraz procentowy był następujący:

Lp.	Tytuł publikacji oraz informacje bibliograficzne	Udział merytoryczny	Udział %
[P3]	Markowicz Joanna, Uram Łukasz, Wołowiec Stanisław, Rode Wojciech. Biotin Transport-Targeting Polysaccharide-Modified PAMAM G3 Dendrimer as System Delivering α-Mangostin into Cancer Cells and *C. elegans* Worms. *International Journal of Molecular Sciences*. 2021 Nov 29;22(23):12925. doi: 10.3390/ijms222312925	- wybór metodologii badań w zakresie syntez chemicznych, - przeprowadzenie syntezy natywnego dendrymeru PAMAM G3, - przeprowadzenie części pomiarów NMR, - korekta treści części chemicznej manuskryptu, - odniesienie się do części uwag recenzentów dotyczących syntez chemicznych	10%
[P4]	Markowicz Joanna, Wołowiec Stanisław, Rode Wojciech, Uram Łukasz. Synthesis and Properties of α-Mangostin and Vadimezan Conjugates with Glucoheptoamidated and Biotinylated 3rd	- wybór metodologii badań w zakresie syntez chemicznych, - dostarczenie natywnego dendrymeru PAMAM G3,	10%

Stanisław Wołowiec

	Generation Poly(amidoamine) Dendrimer, and Conjugation Effect on Their Anticancer and Anti-Nematode Activities. *Pharmaceutics*. 2022 March 10;14(3):606. doi: 10.3390/pharmaceutics14030606	- przeprowadzenie części pomiarów NMR, - korekta treści części chemicznej manuskryptu, - odniesienie się do części uwag recenzentów dotyczących syntez chemicznych	

Stanisław Wołowiec

Dr Justyna Sobich

Instytut Parazytologii im. W. Stefańskiego PAN

ul. Twarda 51/55, 00-818 Warszawa

e-mail: jsobich@twarda.pan.pl

Warszawa, 28.09.2022

OŚWIADCZENIE

Oświadczam, że w niżej wymienionych pracach mój udział merytoryczny oraz procentowy był następujący:

Lp.	Tytuł publikacji oraz informacje bibliograficzne	Udział merytoryczny	Udział %
[P1]	Markowicz Joanna, Uram Łukasz, Sobich Justyna, Mangiardi Laura, Maj Piotr, Rode Wojciech. Antitumor and anti-nematode activities of α-mangostin. *European Journal of Pharmacology*. 2019 Nov 15;863:172678. doi: 10.1016/j.ejphar.2019.172678	- wybór metodologii badań na hodowli nicieni *C. elegans*, - przeprowadzenie eksperymentu z wykorzystaniem hodowli nicieni oraz analiza jego wyników	10%
[P2]	Maj Piotr, Mori Mattia, Sobich Justyna, Markowicz Joanna, Uram Łukasz, Zieliński Zbigniew, Quaglio Deborah, Calcaterra Andrea, Cau Ylenia, Botta Bruno, Rode Wojciech. Alvaxanthone, a Thymidylate Synthase Inhibitor with Nematocidal and Tumoricidal Activities. *Molecules*. 2020 Jun 23;25(12):2894. doi: 10.3390/molecules25122894	- przeprowadzenie eksperymentów z wykorzystaniem hodowli nicieni, - analiza, wizualizacja i opracowanie wyników badań na *C. elegans*	14%

Justyna Sobich

Warszawa, 28.09.2022

Dr Piotr Maj
Uniwersytet w Göteborgu, Wydział Chemii i Biologii Molekularnej
Uniwersytet w Uppsali, Wydział Chemii – Centrum Biomedyczne
Email: piotr.maj@gu.se, piotr.maj@kemi.uu.se

OŚWIADCZENIE

Oświadczam, że w niżej wymienionych pracach mój udział merytoryczny oraz procentowy był następujący:

Lp.	Tytuł publikacji oraz informacje bibliograficzne	Udział merytoryczny	Udział %
[P1]	Markowicz Joanna, Uram Łukasz, Sobich Justyna, Mangiardi Laura, Maj Piotr, Rode Wojciech. Antitumor and anti-nematode activities of α-mangostin. *European Journal of Pharmacology*. 2019 Nov 15;863:172678. doi: 10.1016/j.ejphar.2019.172678	- udział w przygotowaniu metodyki badań wykorzystujących model *C. elegans*.	3%
[P2]	Maj Piotr, Mori Mattia, Sobich Justyna, Markowicz Joanna, Uram Łukasz, Zieliński Zbigniew, Quaglio Deborah, Calcaterra Andrea, Cau Ylenia, Botta Bruno, Rode Wojciech. Alvaxanthone, a Thymidylate Synthase Inhibitor with Nematocidal and Tumoricidal Activities. *Molecules*. 2020 Jun 23;25(12):2894. doi: 10.3390/molecules25122894	- przeprowadzenie oznaczenia aktywności badanych związków jako inhibitorów syntazy tymidylanowej, - analiza, wizualizacja i opracowanie wyników dotyczących aktywności inhibitorów syntazy tymidylanowej	14%

P. Maj

Dr Zbigniew Zieliński

Instytut Biologii Doświadczalnej im. M. Nenckiego PAN

ul. Ludwika Pasteura 3, 02-093 Warszawa

e-mail: z.zielinski@nencki.edu.pl

Warszawa, 28.09.2022

OŚWIADCZENIE

Oświadczam, że w niżej wymienionych pracach mój udział merytoryczny oraz procentowy był następujący:

Lp.	Tytuł publikacji oraz informacje bibliograficzne	Udział merytoryczny	Udział %
[P2]	Maj Piotr, Mori Mattia, Sobich Justyna, Markowicz Joanna, Uram Łukasz, Zieliński Zbigniew, Quaglio Deborah, Calcaterra Andrea, Cau Ylenia, Botta Bruno, Rode Wojciech. Alvaxanthone, a Thymidylate Synthase Inhibitor with Nematocidal and Tumoricidal Activities. *Molecules*. 2020 Jun 23;25(12):2894. doi: 10.3390/molecules25122894	- udział w eksperymentach enzymologicznych.	5%

Dr Zbigniew Zieliński

UNIVERSITÀ
DI SIENA
1240

DIPARTIMENTO DI BIOTECNOLOGIE,
CHIMICA E FARMACIA

Siena, 7 October 2022

To whom it may concern

STATEMENT

I declare that in the paper mentioned below, my substantive participation and percentage share was as follows:

No.	Publication title and bibliographic information	Substantive participation	% share
[P2]	Maj Piotr, Mori Mattia, Sobich Justyna, Markowicz Joanna, Uram Łukasz, Zieliński Zbigniew, Quaglio Deborah, Calcaterra Andrea, Cau Ylenia, Botta Bruno, Rode Wojciech. Alvaxanthone, a Thymidylate Synthase Inhibitor with Nematocidal and Tumoricidal Activities. *Molecules*. 2020 Jun 23;25(12):2894. doi: 10.3390/molecules25122894	- conducting in silico experiments and retrieving the substances for biological testing - writing and editing of the manuscript	14%

Yours sincerely,
Mattia Mori

Associate Professor in Medicinal Chemistry
University of Siena, Department of Biotechnology, Chemistry and Pharmacy
Via Aldo Moro 2, 53100 Siena. Italy

Phone: +39 0577 232360 (office)
Phone: +39 0577 232488 (lab)
E-mail: mattia.mori@unisi.it

Professor Bruno Botta

Department of Chemistry and Technology of Drugs, Department of Excellence 2018-2022

Sapienza University of Rome

Piazzale Aldo Moro 5, 00185 Rome, Italy

e-mail: bruno.botta@uniroma1.it

Rome, 10th October 2022

STATEMENT

I declare that in the paper mentioned below, my substantive participation and percentage share was as follows:

No.	Publication title and bibliographic information	Substantive participation	% share
[P2]	Maj Piotr, Mori Mattia, Sobich Justyna, Markowicz Joanna, Uram Łukasz, Zieliński Zbigniew, Quaglio Deborah, Calcaterra Andrea, Cau Ylenia, Botta Bruno, Rode Wojciech. Alvaxanthone, a Thymidylate Synthase Inhibitor with Nematocidal and Tumoricidal Activities. *Molecules*. 2020 Jun 23;25(12):2894. doi: 10.3390/molecules25122894	- co-creating the concept of the publication, - writing and editing of the manuscript	5%

Bruno Botta

Deborah Quaglio, PhD

Department of Chemistry and Technology of Drugs, Department of Excellence 2018-2022

Sapienza University of Rome

Piazzale Aldo Moro 5, 00185 Rome, Italy

e-mail: deborah.quaglio@uniroma1.it

Rome, October 10, 2022

Sincerely yours,

Deborah Quaglio

STATEMENT

I declare that in the paper mentioned below, my substantive participation and percentage share was as follows:

No.	Publication title and bibliographic information	Substantive participation	% share
[P2]	Maj Piotr, Mori Mattia, Sobich Justyna, Markowicz Joanna, Uram Łukasz, Zieliński Zbigniew, Quaglio Deborah, Calcaterra Andrea, Cau Ylenia, Botta Bruno, Rode Wojciech. Alvaxanthone, a Thymidylate Synthase Inhibitor with Nematocidal and Tumoricidal Activities. *Molecules*. 2020 Jun 23;25(12):2894. doi: 10.3390/molecules25122894	- delivering of natural products	5%

Andrea Calcaterra, PhD

Department of Chemistry and Technology of Drugs, Department of Excellence 2018-2022

Sapienza University of Rome

Piazzale Aldo Moro 5, 00185 Rome, Italy

e-mail: andrea.calcaterra@uniroma1.it

Rome, 10th October 2022

STATEMENT

I declare that in the paper mentioned below, my substantive participation and percentage share was as follows:

No.	Publication title and bibliographic information	Substantive participation	% share
[P2]	Maj Piotr, Mori Mattia, Sobich Justyna, Markowicz Joanna, Uram Łukasz, Zieliński Zbigniew, Quaglio Deborah, Calcaterra Andrea, Cau Ylenia, Botta Bruno, Rode Wojciech. Alvaxanthone, a Thymidylate Synthase Inhibitor with Nematocidal and Tumoricidal Activities. *Molecules*. 2020 Jun 23;25(12):2894. doi: 10.3390/molecules25122894	- delivering of natural products	5%

Sincerely

Andrea Calcaterra

Kopie artykułów naukowych stanowiących rozprawę doktorską

European Journal of Pharmacology 863 (2019) 172678

Contents lists available at ScienceDirect

European Journal of Pharmacology

journal homepage: www.elsevier.com/locate/ejphar

Full length article

Antitumor and anti-nematode activities of α-mangostin

Joanna Markowicz[a,*], Łukasz Uram[a], Justyna Sobich[b], Laura Mangiardi[c], Piotr Maj[b], Wojciech Rode[a,b]

[a] Faculty of Chemistry, Rzeszów University of Technology, 6 Powstańców Warszawy Ave, 35-959, Rzeszów, Poland
[b] Nencki Institute of Experimental Biology, 3 Pasteur Street, 02-093, Warsaw, Poland
[c] Center for Life NanoScience, CLNS@Sapienza, Italian Institute of Technology (IIT), Viale Regina Elena 291, 00161 Rome, Italy and Dipartimento di Chimica e Tecnologie del Farmaco, Sapienza Università di Roma, Piazzale Aldo Moro 5, 00185, Rome, Italy

ARTICLE INFO

Keywords:
α-Mangostin
Glioblastoma multiforme
Squamous carcinoma
Caenorhabditis elegans
Biological activity

ABSTRACT

α-Mangostin, one of the major xanthones isolated from pericarp of mangosteen (*Garcinia mangostana* Linn), exhibits a wide range of pharmacological activities, including antioxidant, anti-inflammatory, antimicrobial as well as anticancer, both in *in vitro* and *in vivo* studies. In the present study, α-mangostin' anti-cancer and anti-parasitic properties were tested *in vitro* against three human cell lines, including squamous carcinoma (SCC-15) and glioblastoma multiforme (U-118 MG), compared to normal skin fibroblasts (BJ), and *in vivo* against *Caenorhabditis elegans*. The drug showed cytotoxic activity, manifested by decrease of cell viability, inhibition of proliferation, induction of apoptosis and reduction of adhesion at concentrations lower than 10 μM (the IC_{50} values were 6.43, 9.59 and 8.97 μM for SCC-15, U-118 MG and BJ, respectively). The toxicity, causing cell membrane disruption and mitochondria impairment, was selective against squamous carcinoma with regard to normal cells. Moreover, for the first time anti-nematode activity of α-mangostin toward *C. elegans* was described (the LC_{50} = 3.8 ± 0.5 μM), with similar effect exerted by mebendazole, a well-known anthelmintic drug.

1. Introduction

α-Mangostin belongs to the major xanthones isolated from pericarp of mangosteen (*Garcinia mangostana* L.), which has long been used in traditional medicine in South East Asia to treat inflammation, skin infection, wounds and chronic ulcer. Numerous *in vitro* and *in vivo* studies revealed α-mangostin exhibits a wide range of pharmacological activities, including antioxidant, anti-inflammatory, antimicrobial and anthelmintic (Ibrahim et al., 2016; Ovalle-Magallanes et al., 2017; Zhang et al., 2017). Since cancer treatment still remains a challenge, anticancer activity is particularly interesting and α-mangostin was demonstrated to inhibit cancer cells proliferation and metastasis, as well to induce apoptosis in certain human malignancies such as skin (Wang et al., 2011), breast (Won et al., 2014), brain (Chao et al., 2011) and digestive system (Shan et al., 2014) cancers.

α-Mangostin has been reported also to exert anticancer activity *in vivo,* with significant reduction of tumor growth through induction of apoptosis and cell cycle arrest (Zhang et al., 2017). In tongue mucoepidermoid carcinoma (YD-15) xenografts, α-mangostin increased the levels of pro-apoptotic factors (LEE et al., 2016). Mitochondria-mediated apoptosis was observed in hepatocellular carcinoma (Sk-Hep-1) xenograft mice (Hsieh et al., 2013). Cell cycle arrest induced by α-mangostin has been proven by Johnson et al. (2012) on athymic nude mice bearing prostate cancer.

Parasitic worms cause diseases mainly in developing countries with over two billions of infected (Hotez et al., 2008). Due to the relatively low number of available anthelmintics (Hu et al., 2013) and reports of increasing resistance to these drugs among human parasites (Geary, 2012; Sutherland and Leathwick, 2011), potential α-mangostin activity of this type seems also worthwhile to seek (Keiser et al., 2012). Considering several common features of cancers and parasites, as well as antiparasitic properties of certain anticancer drugs and anticancer activity of some antiparasitics (Dorosti et al., 2014; Klinkert and Heussler, 2006), potential mutual action should be taken into account. Moreover, due to an increasing necessity to reduce testing on animals, *Caenorhabditis elegans* has emerged as *in vivo* model organism for anticancer drug screening without the limitations of ethical boundaries. Importantly, 60–80% of *C. elegans* genes have human homologs and many similar conservative biological processes are described in both (Artal-Sanz et al., 2006; Kobet et al., 2014; Kyriakakis et al., 2015).

Such a wide range of biological properties of α-mangostin are related to its chemical structure (see Fig. 1). The position and the number

* Corresponding author. Faculty of Chemistry, Rzeszow University of Technology, 6 Powstańców Warszawy Ave, 35-959, Rzeszów, Poland.
E-mail address: jmarkowicz@stud.prz.edu.pl (J. Markowicz).

https://doi.org/10.1016/j.ejphar.2019.172678
Received 3 July 2019; Received in revised form 12 September 2019; Accepted 18 September 2019
Available online 19 September 2019

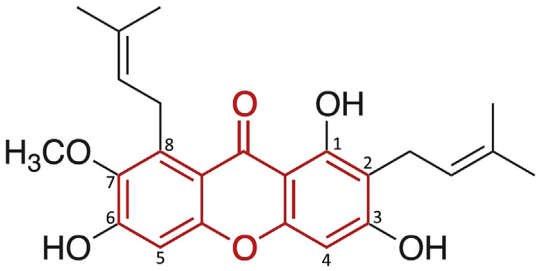

Fig. 1. Chemical structure of α-mangostin. The 9H-Xanthen-9-one ring is marked in red with a numbering of carbons.

of attached prenyl and hydroxyl groups determine its anticancer properties (Cai et al., 2016). Phenol groups on C3 and C6 are critical to anti-proliferative activity and C4 modification is capable to improve both anti-cancer and drug-like properties (Fei et al., 2014). Moreover, considering the drug's potential target, the crystal structure of α-mangostin complex (PDB 6AA4) with MTH1 hydrolase should be mentioned. MTH1 hydrolyzes oxidized nucleoside triphosphates and prevents their incorporation into DNA, making this enzyme crucial for cancer cells in oxidative stress defense and becoming a potential target for anticancer therapy (Yokoyama et al., 2019).

The present paper is aimed at assessing anti-cancer potential of α-mangostin, tested against squamous carcinoma (SCC-15) and glioblastoma multiforme (U-118 MG) cell lines, representing the most malignant and lethal types of human tumors, especially glioma (5-year survival of 5% of patients) (Ostrom et al., 2014). Studies were performed in comparison to normal fibroblasts. Cytotoxic, anti-proliferative, anti-motile and pro-apoptotic properties, as well as intracellular ATP level changes accompanying metabolic disturbances were examined. Furthermore, the drug's anti-nematode potential was checked, using *Caenorhabditis elegans* as a model of parasitic nematodes (Bürglin et al., 1998).

2. Materials and methods

2.1. Materials

α-Mangostin (purity ≥ 98% (HPLC)) was purchased from Sigma Aldrich (St Luis, MO, USA) and dissolved in dimethylsulfoxide (DMSO) to obtain 80 mM stock solution. The tested solutions of α-mangostin were prepared from stock solution in a corresponding cell culture media with adjusting the DMSO concentration to ≤0.05%, which had no significant effect on treated cells.

Human glioblastoma (U-118 MG, ATCC® HTB-15), human squamous cell carcinoma (SCC-15, ATCC® CRL-1623) and human normal fibroblast (BJ, ATCC® CRL-2522) cell lines, Dulbecco's Modified Eagle's Media (DMEM and DMEM: F-12), Eagle's Minimum Essential Medium (EMEM), fetal bovine serum (FBS), penicillin and streptomycin solution were obtained from American Type Culture Collection (ATCC, Manassas, VA, USA). Trypsin-EDTA solution, phosphate-buffered saline (PBS) with and without magnesium and calcium ions, hydrocortisone, 0.33% neutral red solution (3-amino-m-dimethylamino-2-methyl-phenazine hydrochloride), XTT sodium salt (2,3-bis[2-methoxy-4-nitro-5-sulfophenyl]-2H-tetrazolium-5-carboxanilide inner salt), phenazine-methosulfate (PMS), 0.4% trypan blue solution, dimethylsulfoxide (DMSO) and other chemicals and buffers were provided by Sigma-Aldrich (St Louis, MO, USA). DAPI (4′,6-diamidino-2-phenylindole, dihydrochloride) and CyQUANT® GR Cell Proliferation Assay Kit were purchased from Life Technologies (Carlsbad, CA, USA). CellTiter-Glo® Luminescent Cell Viability Assay for ATP level determination and Apo-ONE® Homogenous Caspase-3/7 Assay were obtained from Promega Corporation (Madison, WI, USA). All other cell culture materials were from Corning Incorporated (Corning, NY, USA), Greiner (Austria) or Nunc (Denmark).

2.2. Cell cultures

Human glioblastoma cells U-118 MG (doubling time 37 h) were cultured in DMEM, human squamous carcinoma cells SCC-15 (doubling time 48 h) were grown in DMEM: F-12 supplemented with hydrocortisone (400 ng/ml) and normal human skin fibroblasts (doubling time 1.9 day) were cultured in EMEM. All culture media contained 10% heat-inactivated FBS and 100 U/ml penicillin and 100 µg/ml streptomycin. All cell lines were cultured at 37 °C in humidified 95% air, containing 5% CO_2, with media changed every 2–3 days. Cells were passaged at 80–85% confluence after treatment with 0.25% trypsin-EDTA in PBS (calcium and magnesium ions free). Cell morphology was checked under Nikon TE2000S Inverted Microscope (Tokyo, Japan) with phase contrast. Number and viability of cells were estimated by trypan blue exclusion test using Automatic Cell Counter TC20TM (Biorad Laboratories, Hercules, CA, USA). All assays were performed in triplicates in three independent experiments.

2.3. Cytotoxicity (NR and XTT) assays

Cytotoxicity of α-mangostin was estimated by neutral red uptake (NR) and XTT reduction assays allowing determination of cellular membrane integrity and mitochondria condition, respectively. Cells were seeded in a flat, clear bottom 96-well culture plate in three replicates at a density of 1×10^4 cells/well and allowed to attach for 24 h. Then the cells were treated with α-mangostin (2.5–40 µM) for 48 h. After exposure to the drug, NR assay or XTT reduction assay was performed as earlier described (Uram et al., 2017a).

2.4. Proliferation assay

Proliferation of α-mangostin-treated cells was monitored using the CyQUANT GR Cell Proliferation Assay Kit. Cells were seeded in a flat, clear bottom 96-well plate at a density of 5×10^3 and incubated for 24 h to attach. Then the cells were treated with 5–20 µM α-mangostin solutions (200 µl/well) for 72 h, followed by centrifugation (5 min, 700 g) and gentle culture medium removal. Afterwards the plate was frozen at −80 °C and thawed (repeated twice), 200 µl/well of CyQUANT GR dye/cell-lysis buffer, prepared according to manufacturer's protocol was added, followed by incubation on a shaker for 5 min and fluorescence measurement at 480/520 nm with Tecan Infinite M200 PRO Multimode Microplate Reader (TECAN Group Ltd., Switzerland).

2.5. Cell adhesion assay

To evaluate adhesiveness of cells treated with α-mangostin, the crystal violet assay was performed. Cells were seeded in a 96-well clear plate at a density of 1×10^4 (BJ and U-118 MG) and 2×10^4 (SCC-15) cells/well, and allowed to attach for 24 h. Following attachment, cells were incubated with 5–20 µM α-mangostin solutions for 48 h, and crystal violet assay was performed as described by Uram et al. (2013).

2.6. Cell migration assay

α-Mangostin influence on cell migration was estimated using the scratch assay, known also as wound healing assay. Cells were seeded into a 24-well plate at a density of 1×10^5 (for BJ and U-118 MG) and 2×10^5 (for SCC-15) cells/well in 600 µl culture medium and incubated for 24 h to attach and reach confluence. All subsequent steps were carried out as previously described (Uram et al., 2017b). To inhibit cells proliferation and avoid false results, decrease of the FBS concentration in culture medium up to 2% was performed (Liang et al., 2007; Uram et al., 2017b). The influence of lowering FBS concentration to 2% on

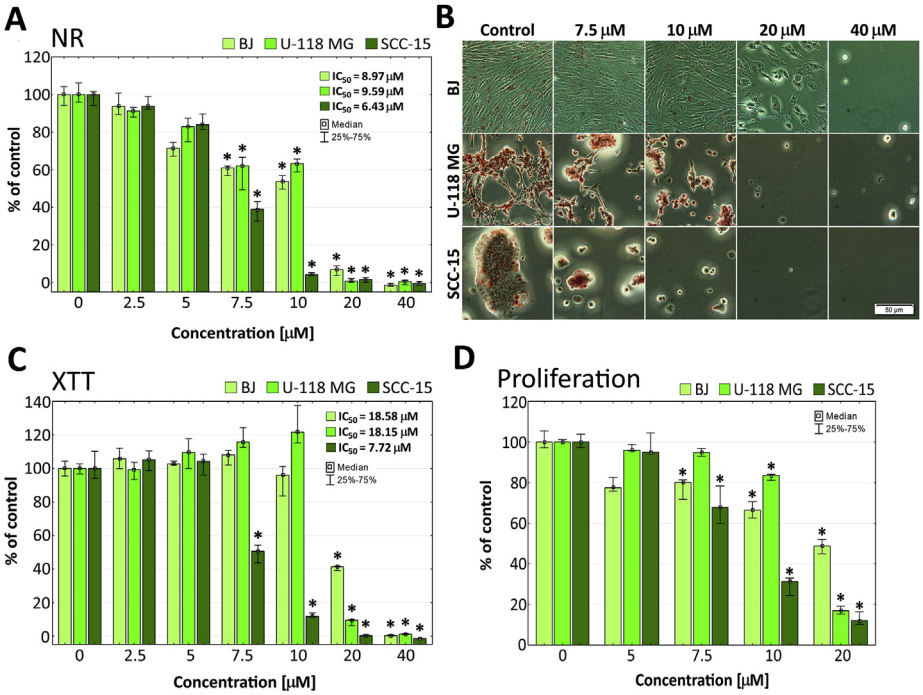

Fig. 2. Viability of BJ, U-118 MG and SCC-15 cells after 48 h treatment with α-mangostin at different concentrations, determined by neutral red uptake (A) and XTT reduction (C) assays. (D) Cancer (SCC-15 and U-118 MG) and normal (BJ) cells proliferation after 72 h incubation with α-mangostin in the range of 5–20 µM concentrations. Results, presented as medians of triplicate assays in three independent experiments, are expressed as % of non-treated controls. The whiskers are lower (25%) and upper (75%) quartile ranges. *P ≤ 0.05; Kruskal-Wallis test (against non-treated control). (B) Cell morphology and neutral red accumulation after α-mangostin treatment and 1 h incubation with neutral red dye. Red vesicles are lysosomes containing dye. Numbers indicate a micromolar concentration of α-mangostin. Images were collected with Olympus IX-83 microscope with contrast phase (scale bar = 50 µm).

cell proliferation was tested and proliferation inhibition confirmed.

2.7. Determination of intracellular ATP level

Estimation of intracellular ATP level (reflecting cell energy metabolism condition) in α-mangostin-treated cells was carried out using CellTiterGlo® Luminescent Cell assay. Cells were plated in a flat, clear bottom 96-well plates at a density of 1×10^4/well and treated with 5–20 µM α-mangostin solutions (100 µl/well) for 48 h. The CellTiter-Glo® Reagent was prepared accordingly to manufacturer's protocol and added 100 µl/well, followed by 10 min incubation on plate shaker. Luminescence was measured in Tecan Infinite M200 PRO microplate reader and adjusted relatively to the number of cells per well (the number of cells was determined by fluorescence measurement after DAPI staining).

2.8. Apoptosis assay

Apo-ONE® Homogenous Caspase-3/7 Assay was performed to verify whether α-mangostin would induce programmed cell death in tested cells. The assay allows to measure activity of caspase-3 and -7, two executive caspases involved in a late stage of apoptosis (Elmore, 2007). To perform an assay cells were seeded in a flat, clear bottom 96-well microplate (1×10^4/well) and treated with α-mangostin under conditions described above. After treatment, Apo-ONE® Caspase-3/7 Reagent was prepared according to manufacturer's protocol and added in a 1:1 vol ratio followed by 1.5 h incubation on a plate shaker. Fluorescence was read at 495/525 nm with Tecan Infinite M200 PRO Multimode Microplate Reader (TECAN Group Ltd., Switzerland), adjusted in relation to the number of cells per well (the number of cells was determined by fluorescence measurement after DAPI staining).

2.9. Toxicity to Caenorhabditis elegans, a nematode parasite model

C. elegans was maintained as previously described (Wińska et al., 2005). The effect of α-mangostin or mebendazole (the latter used as a positive control) on *C. elegans* population growth was determined according to Simpkin and Coles (1981), with the chlorhexidine pre-washing step omitted, by comparing the population levels reached in the control and test wells after 7 days of incubation at 20 °C. Tests were done in 12-well plates, with two wells used for each experimental group. Mebendazole was used in a parallel test as a positive control.

2.10. Statistical analysis

Due to the lack of normal distribution in the experimental groups, statistical analysis was performed using the non-parametric Kruskal-Wallis test to estimate the differences between the α-mangostin-treated cells and non-treated control in each cell lines, P ≤ 0.05 was considered as statistically significant. Calculations were performed using Statistica 12 (StatSoft). In addition, IC_{50} values were calculated based on results of the cytotoxicity assays (NR and XTT) using MS Excel. Medians of viability (%) were plotted against α-mangostin concentration (µM), followed by transforming the X axis to logarithmic. Using logarithmic regression, $y = a*\ln(x) + b$ equation was obtained and used to calculate the α-mangostin concentration corresponding to the cells viability decrease by 50%. The results describing reduction of *C. elegans* population are presented as LC_{50} values being means ± S.E.M., followed by the number of independent experiments (N) in parentheses.

3. Results

3.1. Cytotoxicity and cells proliferation

The biological effect of α-mangostin on normal (BJ) and cancer cells (U-118 MG and SCC-15) was estimated with two viability assays: neutral red uptake (NR) and reduction of tetrazolium salts (XTT). NR is one of the most sensitive assays, which relies on the uptake and retention of neutral red dye within lysosome compartments of the viable cells. XTT in turn, evaluates the reducing properties of *trans*-plasma membrane electron transport including the activities of mitochondrial oxidoreductases (Repetto et al., 2008; Uram et al., 2017a). Additionally, α-mangostin influence on cells proliferation after 72 h treatment was measured with the CyQUANT GR Cell Proliferation Assay Kit, which delivers CyQUANT GR dye that binds to DNA of intact cells and, after excitation at 480 nm, emits green fluorescence proportional to the cell number.

α-Mangostin revealed concentration- and cell-type-dependent

effect, in both toxicity and proliferation assays, as shown in Fig. 2.

The strongest effect of α-mangostin, monitored by the NR assay, was observed in squamous carcinoma cells, with significant decrease of their viability to about 40% at 7.5 μM concentration, then reducing it to zero at the highest concentrations. Activity of α-mangostin against U-118 MG and BJ cells was lower, with cell viability at 7.5 and 10 μM concentration being around 60%, and total viability reduction observed only at 20 and 40 μM concentrations (Fig. 2A). This effect was also visible during microscopic observations, presented in Fig. 2B. As the concentration of α-mangostin increased, accumulation of neutral red in lysosomes decreased and the cell morphology changed, followed by cells shrinkage and loss of adhesion. At 20 μM concentration only normal BJ cells were alive but at 40 μM concentration almost all cells lost their adhesion (Fig. 2B). With the use of the XTT assay similar toxicity pattern was demonstrated of α-mangostin against SCC-15 cells, with glioma and fibroblast cells showing weaker response (Fig. 2C). The highest sensitivity of SCC-15 cells to the drug, demonstrated by both NR and XTT assays, is reflected also by the IC_{50} values (insets in Fig. 2A and C).

Due to high toxicity and lack of viable cells, 40 μM concentration of α-mangostin was omitted in further studies.

The effect of α-mangostin on proliferation of investigated cells was closely correlated with its toxicity pattern (Fig. 2C). Stronger inhibition of proliferation was observed for SCC-15 cells (reduction to 12% at 7.5–20 μM drug) than glioma cells (2.5-fold weaker at 10 μM drug) or fibroblasts (reduction to 49% at 20 μM drug).

3.2. Cellular motility

Cellular motility is a cell movement from one location to another, with associated consumption of energy, constituting a very important parameter of the cancer metastasis process. Cell motility phenomenon relies on adhesion and migration of a cell, resulting from interactions of adhesion receptors on the cell surface with immobile constituents of extracellular matrix or on the surface of other cells (Soloviev et al., 2006).

Adhesion of cancer (SCC-15 and U-118 MG) and normal (BJ) cells after incubation with α-mangostin was assessed with crystal violet dye that stains DNA in the nuclei of intact adherent cells. Squamous carcinoma cells were more susceptible to the adhesion loss than glioma and fibroblast cells. Results presented in Fig. 3A, show significantly stronger decrease of adhesion of SCC-15 than fibroblasts and glioma cells under influence of α-mangostin.

At the highest concentration all tested cells lost their adhesion. Microscopic observations (Fig. 3B), in accord with results of measurement demonstrated the number of adherent cells to decrease with increasing α-mangostin concentration; in particular, this was evident for 10 μM concentration applied with SCC-15 and BJ cells.

The scratch assay is a common method for evaluation of cell migration *in vitro* (Liang et al., 2009), allowing reveal reorganization of the actin cytoskeleton and mimic to some extent migration of cells *in vivo*. In our experiments migration of cancer cells SCC-15 and U-118 MG was stopped only at 10 μM of α-mangostin, whereas migration of fibroblasts was distinctly more sensitive to the drug (decrease to the 12.7% of the control at 5 μM α-mangostin; Fig. 4A and B).

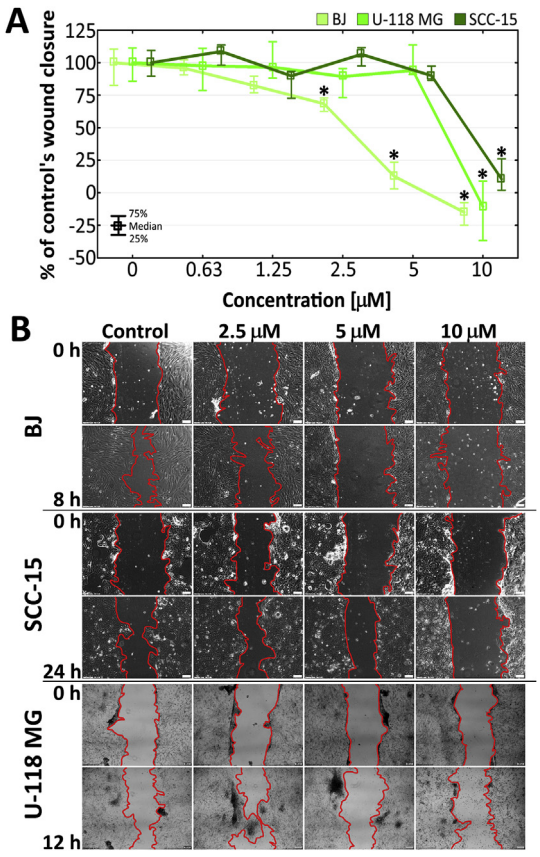

Fig. 4. (A) Cancer (SCC-15 and U-118 MG) and normal (BJ) cells migration after incubation with α-mangostin at the range of 0.63–10 μM concentrations estimated with scratch assay. Results are presented as medians and whiskers are lower (25%) and upper (75%) quartile ranges. *P ≤ 0.05, Kruskal-Wallis test (against non-treated control). (B) Representative images of scratch assay of BJ, SCC-15 and U-118 MG cells treated with α-mangostin. Images were obtained using inverted phase contrast microscope (10 × objective for BJ and SCC-15, scale bar = 100 μm; 4 × objective for U-118 MG, scale bar = 200 μm).

3.3. Apoptosis and ATP level changes

In order to determine pro-apoptotic activity of α-mangostin and its influence on intracellular ATP level in the studied cells, the Apo-ONE® Homogenous Caspase-3/7 (Promega) and CellTiterGlo® Luminescent Cell (Promega) assays were applied. The results are shown as a

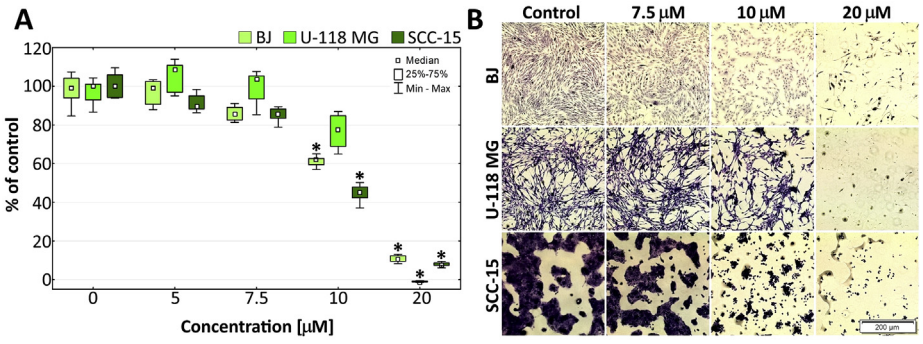

Fig. 3. Adhesiveness of BJ, U-118 MG and SCC-15 cells after 48 h incubation with α-mangostin at different concentrations obtained with crystal violet assay. A) Results are medians of triplicate assays of three independent experiments expressed as a % of non-treated controls. The whiskers are lower (25%) and upper (75%) quartile ranges. *P ≤ 0.05, Kruskal-Wallis test (against non-treated control). B) Cells morphology and adhesion to the bottom of 96-well plate after 48 h α-mangostin treatment and after 30 min incubation with crystal violet. Numbers indicate a micromolar concentration of α-mangostin. Images collected with Olympus IX-83 microscope with contrast phase. Violet signal: crystal violet, scale bar = 200 μm.

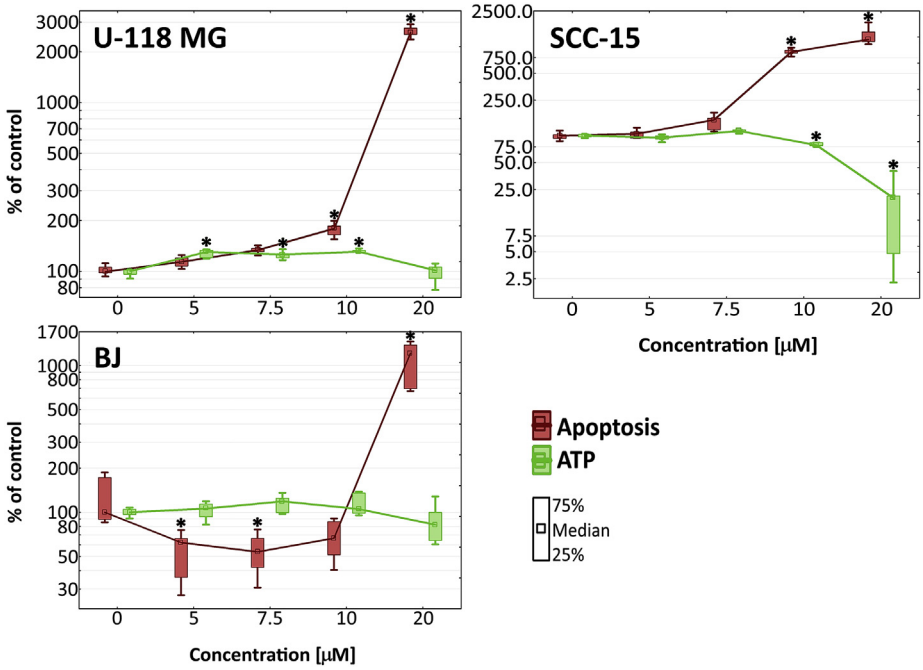

Fig. 5. Changes of caspase-3/7 activity and intracellular ATP level in BJ, U-118 MG and SCC-15 cells after 48 h treatment with 5–20 μM concentration range of α-mangostin, measured with Apo-ONE® Homogenous Caspase-3/7 assay and CellTiterGlo® Luminescent Cell assay, respectively. Results are medians of triplicate assays from three independent experiments expressed as a % of non-treated controls and presented in logarithmic graph. The whiskers are lower (25%) and upper (75%) quartile ranges. *P ≤ 0.05, Kruskal-Wallis test (against non-treated control).

relationship between the intracellular ATP level and executioner caspases activity in each cell line (Fig. 5).

α-Mangostin induced apoptosis in all the tested cell lines, with lower concentrations affecting cancer than normal cells. While a significant increase of caspases activity in SCC-15 and U-118 MG cells was apparent already at 10 μM α-mangostin, the corresponding effect in fibroblasts required 20 μM of drug. At 10 μM α-mangostin caspase-3/7 activity in squamous carcinoma cells was 5-fold higher than in glioma cells (865% and 180% of control, respectively). Interestingly, in fibroblasts at non-toxic concentrations a significant decrease of caspse-3/7 activity was observed.

When activity of caspases in SCC-15 cells has been raising, intracellular ATP level was undergoing reduction to 80%, and then to 12%. Different effect was seen in U-118 MG cells, where at the non-toxic concentrations of the drug, activity of caspases was not growing but ATP level significantly increased to 130% and then returned to control level at the highest drug concentration. In case of fibroblasts, no changes in the intracellular ATP level were observed at the range of studied concentrations.

3.4. Toxicity to C. elegans

The nematode *Caenorhabditis elegans*, a multicellular organism widely recognized as a model for basic biological and medical research, is also used to model a live animal in anti-cancer drug screening (Kobet et al., 2014). In the present study it was used to model parasitic nematodes, in order to test a potential antiparasitic effect of α-mangostin. The results revealed α-mangostin to cause reduction of growth of *C. elegans* population with the LC_{50} value of 3.8 ± 0.5 μM (5). Of note is that mebendazole, tested in parallel experiments, showed slightly lower activity, reflected by the LC_{50} value of 4.0 ± 0.5 μM (10), the latter in accord with the finding of 1.2 μM concentration of this drug being the minimum detectable dose against *C. elegans* (Simpkin and Coles, 1981).

4. Discussion

α-Mangostin shows strong pharmacological effects in a variety cancer models, including breast, prostate, lung, colon, pancreatic cancer and leukemia, both *in vitro* and *in vivo* (Akao et al., 2008; Cai et al., 2016; Ibrahim et al., 2016). Cai et al. (2016) revealed that α-mangostin inhibits cell proliferation in four hepatocellular carcinoma (HCC) cell lines in a dose- and time-dependent manner, with the IC_{50} values in the range of 10 μM, by inducing the G0/G1 phase cell cycle arrest. Anti-proliferative effect of α-mangostin was demonstrated also by Matsumoto et al. (2005) with human colon cancer cells (DLD-1), where the drug caused cell-cycle arrest in the G1 phase and subsequent induction of apoptosis *via* the intrinsic pathway resulting in nuclear condensation and fragmentation. The same author described studies on four human leukemia cell lines (HL60, K562, NB4 and U937) and reported cell growth inhibition and apoptosis induction at 5–10 μM concentrations of α-mangostin after 24–72 h incubation (Matsumoto et al., 2003).

The presented results are in line with reports from other researchers. The strongest cytotoxic effect was seen in squamous carcinoma cells with the IC_{50} equal 6.43 μM (NR assay) and total viability reduction at concentrations ≥ 10 μM after 48 h treatment. The toxic effect of α-mangostin in SCC-15 cells caused the disruption of the cell membrane integrity and mitochondria functions. Similar toxic effect against human skin cancer cells was observed for human oral squamous carcinoma cells (HSC-2, HSC-3 and HSC-4 cell lines). The IC_{50} values determined after 24 h treatment were 8–10 μM (Kwak et al., 2016) and for human melanoma cell lines, SK-MEL-2 and SK-MEL-30 after 48 h of incubation with α-mangostin, the IC_{50} values were 8.14 μM and 7.78 μM, respectively (Xia et al., 2016). Likewise, for human melanoma cells SK-MEL-28, the IC_{50}, determined after 48 h treatment, was 5.92 μM (Wang et al., 2011). Also Kaomongkolgit et al. (2011) found that α-mangostin at 3 μg mL^{-1}(7.32 μM) concentration after 48 h exposure, displayed moderate cytotoxicity against head and neck squamous carcinoma cell lines (HN-22, HN-30, and HN-31 cells) with inhibition rates of 45%–60%.

Glioma and fibroblast cells showed a weaker response in both tests, as confirmed by the IC_{50} values, which in the XTT assay for U-118 MG were 2-fold higher than for SCC-15 cells (18.15 μM against 7.72 μM), and a significant decrease of cell viability was seen at concentrations above 20 μM. Moreover, α-mangostin-mediated-toxicity in glioma and fibroblasts was mostly achieved by destroying cell membrane. Stronger effect of α-mangostin against two glioblastoma cell lines has been revealed by Chao et al. (2011), who obtained the IC_{50} values 6.4 μM for GBM8401 and 7.3 μM for DBTRG-05MG after 48 h treatment using WST-1 assay.

Anticancer activity of α-mangostin was also manifested by inhibition of cell proliferation. After 72 h treatment with α-mangostin, SCC-15 cells displayed significant reduction of proliferation at concentrations ≥7.5 μM. However, U-118 MG cells showed a lower sensitivity than SCC-15 (83% against 31% at 10 μM), with BJ cells exhibiting the weakest response.

Cytotoxic effect of α-mangostin also affected cells motility. This parameter was assessed by crystal violet and scratch assay, which determine cells adhesion and migration, respectively. Cell adhesion plays an essential role in stimulating signals that regulate cell differentiation, cell cycle, cell migration and cell survival. Dysregulation of these cellular processes is involved in initiation and/or progression of various diseases including cancer metastasis. The cell adhesion plays a pivotal role in the driving force production of the cell migration (Zhong et al., 2012). Cell adhesiveness is generally reduced in human cancers and decreases in line with their increasing "metastatic potential". Tumor cells are characterized by changes in adhesion to ECM (extracellular matrix) due to possessed alterations in the expression and pattern of plasma-membrane protein complexes (Ahmad Khalili and Ahmad, 2015; Uram et al., 2017b).

Some research groups have studied anti-metastatic potential of α-mangostin. In the research conducted by Zhang et al. (2018) α-mangostin inhibited migration of A549 cells in a dose-dependent manner. At 5 μM concentration, cellular migration was found to be inhibited by almost 33% and in the presence of 10 μM α-mangostin, migration was inhibited by 60%. It has been proven that α-mangostin displayed anti-metastatic effects also in human skin cancer cell lines, melanoma and squamous cell carcinoma. Beninati et al. (2014) observed a marked reduction (by 70%) of the adhesion of human melanoma cells (A375) and the invasion decrease by 38% and 28% in SK-MEL-28 and A375 cells, respectively after treatment with 15 μM α-mangostin. According to Wang et al. (2012), α-mangostin inhibited motility, adhesion, migration and invasion of human squamous carcinoma (A-431) and human melanoma (SK-MEL-28) cells after 48-h treatment. The migration inhibitory effect was found to be concentration-dependent and was the most marked for the concentration of 1.25 μg/ml (3.05 μM) for A-431 (migration reduced to 6%) and 2.5 μg/ml (6.1 μM) for SK-MEL-28 (migration reduced to 23%). The adhesive capability decreased to around 55% and to 61% for A-431 and SK-MEL-28 cells, respectively.

In our research, α-mangostin showed the strongest effect of reducing cellular adhesion in squamous carcinoma cells. This cell line demonstrated 60% loss of adhesion at 10 μM concentration of α-mangostin while glioma cells did not reveal significant adhesion decrease at the same concentration. Moreover, at toxic α-mangostin concentrations, migration of each tested cell line was reduced to about zero, however at non-toxic concentrations (< 10 μM) ability to migrate was affected only in normal cells. Referring to cytotoxicity results, at 10 and 20 μM concentrations of α-mangostin, all tested cells remained dead, so the adhesion and migration decrease is likely due to the toxic action of the compound, therefore it will not have the anti-metastatic potential. Such effect would be suspected if the reduction of cancer cells adhesion and/or migration occurred at non-toxic concentrations.

α-Mangostin potential to induce apoptosis has been documented by numerous studies. Zhang et al. (2018) demonstrated that drug treatment caused a dose-dependent induction of apoptosis, associated by an increased Bax/Bcl-2 ratio in human lung cancer cell (A549). According to Wang et al. (2011), α-mangostin induced apoptosis in human melanoma SK-MEL-28 cell line, due to caspase activation and mitochondrial membrane pathway disruption, revealed by 25-fold increase in caspase-3 activity and 9-fold decrease in mitochondrial membrane potential when compared to untreated cells. In accord, α-mangostin induced mitochondrial-dependent apoptosis in human hepatoma SK-Hep-1 cells (Hsieh et al., 2013), and in human leukemia HL60 cells (Matsumoto et al., 2004), with activation of caspase-9 and -3 but not caspase-8. Parameters of mitochondrial dysfunctions such as swelling, loss of membrane potential, decrease in intracellular ATP, ROS accumulation and cytochrome *c*/AIF release, were observed within 1 or 2 h after the treatment, indicating that α-mangostin preferentially targets mitochondria in the early phase. There is also an evidence of Chao et al. (2011) that α-mangostin in 2.5–10 μM concentrations does not induce apoptotic cell death in glioblastoma cells (GBM8401 and DBTRG-05MG cell lines) after 48 h of incubation, but autophagy with formation of acidic vesicular organelles (AVOs) and autophagic vacuoles.

In our research, α-mangostin induced apoptosis both in cancer and normal cells, but in squamous carcinoma cells this process has started earlier, with caspase 3 and 7 activities 5-fold higher than in glioblastoma cells. In addition, induction of apoptosis in SCC-15 cells was accompanied by ATP decrease. Pradelli et al. (2014) established the loss of energy production during apoptosis, orchestrated by caspases, to be involved in the dismantling of the dying cell. Interestingly, U-118 MG cells at non-toxic concentrations of α-mangostin displayed increase of ATP level, presumably providing energy for pro-apoptotic proteins synthesis. In contrast, fibroblasts showed no changes of ATP level in the drug-treated cells. In this context it should be mentioned that Pradelli et al. (2014) demonstrated the decrease of cellular ATP level during apoptosis in a caspase-dependent manner, as a consequence of a caspase-dependent inhibition of glycolysis.

Certain selectivity of α-mangostin, showing stronger toxicity toward tumor squamous carcinoma than glioblastoma and normal cells, according with previous observations of cell type-dependent drug activity and related potential for human skin cancer and leukemia treatment (Kaomongkolgit et al., 2011; Matsumoto et al., 2003). Moreover, it is noteworthy that α-mangostin preferentially targeted cancer cells over non-cancerous cells, indicating some potential as a chemopreventive or selective anticancer agent (Shan et al., 2011).

Of particular interest is anti-nematode activity of α-mangostin, especially as the drug is similarly toxic toward *C. elegans* as mebendazole, a known anthelmintic drug (McKellar and Scott, 1990; Simpkin and Coles, 1981), and rather more toxic than certain other anthelmintics, including albendazole (Hu et al., 2013; Sant'anna et al., 2013), ivermectin, nitazoxanide and pyrantel (Hu et al., 2013). Of note is also that α-mangostin lacked activity or showed only low activity against several other nematode species (Keiser et al., 2012). Thus, further parallel studies of antiparasitic and anticancer properties of α-mangostin and its analogues are warranted, aimed at potential shared target (s) (Dorosti et al., 2014).

5. Conclusions

α-Mangostin, a xanthone derivative from the pericarp of the mangosteen, with a wide range of biological activity (Ibrahim et al., 2016), displayed at concentrations lower than 10 μM cytotoxic activity, manifested by cell viability decrease, inhibition of proliferation, induction of apoptosis and reduction of adhesion. The toxicity, causing cell membrane disruption and mitochondria impairment, showed certain selectivity, being somewhat stronger with tumor squamous carcinoma than glioblastoma and normal cells. Of interest, α-mangostin demonstrates, beside antitumor also anti-nematode activity, suggesting further studies in search of mechanism(s) of both activities.

CRediT author statement

Joanna Markowicz: Conceptualization, Methodology, Formal Analysis, Investigation, Writing-Original Draft, Writing-Review & Editing, Visualization, Project Administration

Łukasz Uram: Methodology, Formal Analysis, Investigation, Resources, Writing-Review & Editing

Justyna Sobich: Methodology, Formal Analysis, Investigation

Laura Mangiardi: Conceptualization

Piotr Maj: Methodology

Wojciech Rode: Conceptualization, Resources, Writing-Original

Draft, Writing-Review & Editing

Acknowledgments

This work was supported by grants 2014/13/D/NZ3/02825 and 2016/21/B/NZ1/00288 from the National Science Centre, Poland. Stimulating discussions and cooperation from COST Action CM1407 are acknowledged.

References

Ahmad Khalili, A., Ahmad, M.R., 2015. A review of cell adhesion studies for biomedical and biological applications. Int. J. Mol. Sci. 16, 18149–18184. https://doi.org/10.3390/ijms160818149.

Akao, Y., Nakagawa, Y., Iinuma, M., Nozawa, Y., 2008. Anti-cancer effects of xanthones from pericarps of mangosteen. Int. J. Mol. Sci. 9, 355–370.

Artal-Sanz, M., de Jong, L., Tavernarakis, N., 2006. Caenorhabditis elegans: a versatile platform for drug discovery. Biotechnol. J. 1, 1405–1418. https://doi.org/10.1002/biot.200600176.

Beninati, S., Oliverio, S., Cordella, M., Rossi, S., Senatore, C., Liguori, I., Lentini, A., Piredda, L., Tabolacci, C., 2014. Inhibition of cell proliferation, migration and invasion of B16-F10 melanoma cells by α-mangostin. Biochem. Biophys. Res. Commun. 450, 1512–1517. https://doi.org/10.1016/j.bbrc.2014.07.031.

Bürglin, T.R., Lobos, E., Blaxter, M.L., 1998. Caenorhabditis elegans as a model for parasitic nematodes. Int. J. Parasitol. 28, 395–411.

Cai, N., Xie, S.-J., Qiu, D.-B., Jia, C.-C., Du, C., Liu, W., Chen, J.-J., Zhang, Q., 2016. Potential effects of α-mangostin in the prevention and treatment of hepatocellular carcinoma. J. Funct. Foods 26, 309–318. https://doi.org/10.1016/j.jff.2016.08.014.

Chao, A.-C., Hsu, Y.-L., Liu, C.-K., Kuo, P.-L., 2011. α-Mangostin, a dietary xanthone, induces autophagic cell death by activating the AMP-activated protein kinase pathway in glioblastoma cells. J. Agric. Food Chem. 59, 2086–2096. https://doi.org/10.1021/jf1042757.

Dorosti, Z., Yousefi, M., Sharafi, S.M., Darani, H.Y., 2014. Mutual action of anticancer and antiparasitic drugs: are there any shared targets? Future Oncol. 10, 2529–2539. https://doi.org/10.2217/fon.14.65.

Elmore, S., 2007. Apoptosis: a review of programmed cell death. Toxicol. Pathol. 35, 495–516. https://doi.org/10.1080/01926230701320337.

Fei, X., Jo, M., Lee, B., Han, S.-B., Lee, K., Jung, J.-K., Seo, S.-Y., Kwak, Y.-S., 2014. Synthesis of xanthone derivatives based on α-mangostin and their biological evaluation for anti-cancer agents. Bioorg. Med. Chem. Lett 24, 2062–2065. https://doi.org/10.1016/j.bmcl.2014.03.047.

Geary, T.G., 2012. Are new anthelmintics needed to eliminate human helminthiases? Curr. Opin. Infect. Dis. 25, 709–717. https://doi.org/10.1097/QCO.0b013e328359f04a.

Hotez, P.J., Brindley, P.J., Bethony, J.M., King, C.H., Pearce, E.J., Jacobson, J., 2008. Helminth infections: the great neglected tropical diseases. J. Clin. Investig. 118, 1311–1321. https://doi.org/10.1172/JCI34261.

Hsieh, S.-C., Huang, M.-H., Cheng, C.-W., Hung, J.-H., Yang, S.-F., Hsieh, Y.-H., 2013. α-Mangostin induces mitochondrial dependent apoptosis in human hepatoma SK-Hep-1 cells through inhibition of p38 MAPK pathway. Apoptosis 18, 1548–1560. https://doi.org/10.1007/s10495-013-0888-5.

Hu, Y., Ellis, B.L., Yiu, Y.Y., Miller, M.M., Urban, J.F., Shi, L.Z., Aroian, R.V., 2013. An extensive comparison of the effect of anthelmintic classes on diverse nematodes. PLoS One 8, e70702. https://doi.org/10.1371/journal.pone.0070702.

Ibrahim, M.Y., Hashim, N.M., Mariod, A.A., Mohan, S., Abdulla, M.A., Abdelwahab, S.I., Arbab, I.A., 2016. α-Mangostin from Garcinia mangostana Linn: an updated review of its pharmacological properties. Arabian J. Chem. 9, 317–329. https://doi.org/10.1016/j.arabjc.2014.02.011.

Johnson, J.J., Petiwala, S.M., Syed, D.N., Rasmussen, J.T., Adhami, V.M., Siddiqui, I.A., Kohl, A.M., Mukhtar, H., 2012. α-Mangostin, a xanthone from mangosteen fruit, promotes cell cycle arrest in prostate cancer and decreases xenograft tumor growth. Carcinogenesis 33, 413–419. https://doi.org/10.1093/carcin/bgr291.

Kaomongkolgit, R., Chaisomboon, N., Pavasant, P., 2011. Apoptotic effect of alpha-mangostin on head and neck squamous carcinoma cells. Arch. Oral Biol. 56, 483–490. https://doi.org/10.1016/j.archoralbio.2010.10.023.

Keiser, J., Vargas, M., Winter, R., 2012. Anthelminthic properties of mangostin and mangostin diacetate. Parasitol. Int. 61, 369–371. https://doi.org/10.1016/j.parint.2012.01.004.

Klinkert, M.Q., Heussler, V., 2006. The use of anticancer drugs in antiparasitic chemotherapy. Mini Rev. Med. Chem. 6, 131–143. https://doi.org/10.2174/138955706775475939.

Kobet, R.A., Pan, X., Zhang, B., Pak, S.C., Asch, A.S., Lee, M.-H., 2014. Caenorhabditis elegans: a model system for anti-cancer drug discovery and therapeutic target identification. Biomol Ther (Seoul) 22, 371–383. https://doi.org/10.4062/biomolther.2014.084.

Kwak, H.-H., Kim, I.-R., Kim, H.-J., Park, B.-S., Yu, S.-B., 2016. α -mangostin induces apoptosis and cell cycle arrest in oral squamous cell carcinoma cell. Evid. Based Complement Altern. Med. 2016 1–10. https://doi.org/10.1155/2016/5352412.

Kyriakakis, E., Markaki, M., Tavernarakis, N., 2015. Caenorhabditis elegans as a model for cancer research. Mol. Cell. Oncol. 2, e975027. https://doi.org/10.4161/23723556.2014.975027.

LEE, H.N., JANG, H.Y., KIM, H.J., SHIN, S.A., CHOO, G.S., PARK, Y.S., KIM, S.K., JUNG, J.Y., 2016. Antitumor and apoptosis-inducing effects of α-mangostin extracted from the pericarp of the mangosteen fruit (Garcinia mangostana L.) in YD-15 tongue mucoepidermoid carcinoma cells. Int. J. Mol. Med. 37, 939–948. https://doi.org/10.3892/ijmm.2016.2517.

Liang, C.-C., Park, A.Y., Guan, J.-L., 2007. *In vitro* scratch assay: a convenient and inexpensive method for analysis of cell migration *in vitro*. Nat. Protoc. 2, 329–333. https://doi.org/10.1038/nprot.2007.30.

Liang, M., Yang, H., Fu, J., 2009. Nimesulide inhibits IFN-gamma-induced programmed death-1-ligand 1 surface expression in breast cancer cells by COX-2 and PGE2 independent mechanisms. Cancer Lett. 276, 47–52. https://doi.org/10.1016/j.canlet.2008.10.028.

Matsumoto, K., Akao, Y., Kobayashi, E., Ohguchi, K., Ito, T., Tanaka, T., Iinuma, M., Nozawa, Y., 2003. Induction of apoptosis by xanthones from mangosteen in human leukemia cell lines. J. Nat. Prod. 66, 1124–1127. https://doi.org/10.1021/np020546u.

Matsumoto, K., Akao, Y., Ohguchi, K., Ito, T., Tanaka, T., Iinuma, M., Nozawa, Y., 2005. Xanthones induce cell-cycle arrest and apoptosis in human colon cancer DLD-1 cells. Bioorg. Med. Chem. 13, 6064–6069. https://doi.org/10.1016/j.bmc.2005.06.065.

Matsumoto, K., Akao, Y., Yi, H., Ohguchi, K., Ito, T., Tanaka, T., Kobayashi, E., Iinuma, M., Nozawa, Y., 2004. Preferential target is mitochondria in alpha-mangostin-induced apoptosis in human leukemia HL60 cells. Bioorg. Med. Chem. 12, 5799–5806. https://doi.org/10.1016/j.bmc.2004.08.034.

McKellar, Q.A., Scott, E.W., 1990. The benzimidazole anthelmintic agents–a review. J. Vet. Pharmacol. Ther. 13, 223–247.

Ostrom, Q.T., Bauchet, L., Davis, F.G., Deltour, I., Fisher, J.L., Langer, C.E., Pekmezci, M., Schwartzbaum, J.A., Turner, M.C., Walsh, K.M., Wrensch, M.R., Barnholtz-Sloan, J.S., 2014. The epidemiology of glioma in adults: a "state of the science" review. Neuro Oncol. 16, 896–913. https://doi.org/10.1093/neuonc/nou087.

Ovalle-Magallanes, B., Eugenio-Pérez, D., Pedraza-Chaverri, J., 2017. Medicinal properties of mangosteen (Garcinia mangostana L.): a comprehensive update. Food Chem. Toxicol. 109, 102–122. https://doi.org/10.1016/j.fct.2017.08.021.

Pradelli, L.A., Villa, E., Zunino, B., Marchetti, S., Ricci, J.-E., 2014. Glucose metabolism is inhibited by caspases upon the induction of apoptosis. Cell Death Dis. 5, e1406. https://doi.org/10.1038/cddis.2014.371.

Repetto, G., del Peso, A., Zurita, J.L., 2008. Neutral red uptake assay for the estimation of cell viability/cytotoxicity. Nat. Protoc. 3, 1125–1131. https://doi.org/10.1038/nprot.2008.75.

Sant'anna, V., Vommaro, R.C., de Souza, W., 2013. Caenorhabditis elegans as a model for the screening of anthelminthic compounds: ultrastructural study of the effects of albendazole. Exp. Parasitol. 135, 1–8. https://doi.org/10.1016/j.exppara.2013.05.011.

Shan, T., Cui, X., Li, W., Lin, W., Lu, H., Li, Y., Chen, X., Wu, T., 2014. α-Mangostin suppresses human gastric adenocarcinoma cells in vitro via blockade of Stat3 signaling pathway. Acta Pharmacol. Sin. 35, 1065–1073. https://doi.org/10.1038/aps.2014.43.

Shan, T., Ma, Q., Guo, K., Liu, J., Li, W., Wang, F., Wu, E., 2011. Xanthones from mangosteen extracts as natural chemopreventive agents: potential anticancer drugs. Curr. Mol. Med. 11, 666–677.

Simpkin, K.G., Coles, G.C., 1981. The use of Caenorhabditis elegans for anthelmintic screening. J. Chem. Technol. Biotechnol. 31, 66–69. https://doi.org/10.1002/jctb.503310110.

Soloviev, D.A., Pluskota, E., Plow, E.F., 2006. Cell adhesion and migration assays. Methods Mol. Med. 129, 267–278. https://doi.org/10.1385/1-59745-213-0:267.

Sutherland, I.A., Leathwick, D.M., 2011. Anthelmintic resistance in nematode parasites of cattle: a global issue? Trends Parasitol. 27, 176–181. https://doi.org/10.1016/j.pt.2010.11.008.

Uram, Ł., Szuster, M., Filipowicz, A., Zaręba, M., Wałajtys-Rode, E., Wołowiec, S., 2017a. Cellular uptake of glucoheptoamidated poly(amidoamine) PAMAM G3 dendrimer with amide-conjugated biotin, a potential carrier of anticancer drugs. Bioorg. Med. Chem. 25, 706–713. https://doi.org/10.1016/j.bmc.2016.11.047.

Uram, Ł., Szuster, M., Gargasz, K., Filipowicz, A., Wałajtys-Rode, E., Wołowiec, S., 2013. In vitro cytotoxicity of the ternary PAMAM G3-pyridoxal-biotin bioconjugate. Int. J. Nanomed. 8, 4707–4720. https://doi.org/10.2147/IJN.S53254.

Uram, Ł., Szuster, M., Misiorek, M., Filipowicz, A., Wołowiec, S., Wałajtys-Rode, E., 2017b. The effect of G3 PAMAM dendrimer conjugated with B-group vitamins on cell morphology, motility and ATP level in normal and cancer cells. Eur. J. Pharm. Sci. 102, 275–283. https://doi.org/10.1016/j.ejps.2017.03.022.

Wang, J.J., Sanderson, B.J.S., Zhang, W., 2012. Significant anti-invasive activities of α-mangostin from the mangosteen pericarp on two human skin cancer cell lines. Anticancer Res. 32, 3805–3816.

Wang, J.J., Sanderson, B.J.S., Zhang, W., 2011. Cytotoxic effect of xanthones from pericarp of the tropical fruit mangosteen (Garcinia mangostana Linn.) on human melanoma cells. Food Chem. Toxicol. 49, 2385–2391. https://doi.org/10.1016/j.fct.2011.06.051.

Wińska, P., Gołos, B., Cieśla, J., Zieliński, Z., Fraczyk, T., Wałajtys-Rode, E., Rode, W., 2005. Developmental arrest in Caenorhabditis elegans dauer larvae causes high expression of enzymes involved in thymidylate biosynthesis, similar to that found in Trichinella muscle larvae. Parasitology 131, 247–254.

Won, Y.-S., Lee, J.-H., Kwon, S.-J., Kim, J.-Y., Park, K.-H., Lee, M.-K., Seo, K.-I., 2014. α-Mangostin-induced apoptosis is mediated by estrogen receptor α in human breast cancer cells. Food Chem. Toxicol. 66, 158–165. https://doi.org/10.1016/j.fct.2014.01.040.

Xia, Y., Li, Y., Westover, K.D., Sun, J., Chen, H., Zhang, J., Fisher, D.E., 2016. Inhibition of cell proliferation in an NRAS mutant melanoma cell line by combining sorafenib and α-mangostin. PLoS One 11, e0155217. https://doi.org/10.1371/journal.pone.0155217.

Yokoyama, T., Kitakami, R., Mizuguchi, M., 2019. Discovery of a new class of MTH1 inhibitor by X-ray crystallographic screening. Eur. J. Med. Chem. 167, 153–160. https://doi.org/10.1016/j.ejmech.2019.02.011.

Zhang, C., Yu, G., Shen, Y., 2018. The naturally occurring xanthone α-mangostin induces ROS-mediated cytotoxicity in non-small scale lung cancer cells. Saudi J. Biol. Sci. 25, 1090–1095. https://doi.org/10.1016/j.sjbs.2017.03.005.

Zhang, K., Gu, Q., Yang, K., Ming, X., Wang, J., 2017. Anticarcinogenic effects of α-mangostin: a review. Planta Med. 83, 188–202. https://doi.org/10.1055/s-0042-119651.

Zhong, Y., He, S., Ji, B., 2012. Mechanics in mechanosensitivity of cell adhesion and its roles in cell migration. Int. J. Comput. Mater. Sci. Eng. 1, 1250032. https://doi.org/10.1142/S2047684112500327.

molecules

MDPI

Article

Alvaxanthone, a Thymidylate Synthase Inhibitor with Nematocidal and Tumoricidal Activities

Piotr Maj [1,2], Mattia Mori [3], Justyna Sobich [1], Joanna Markowicz [4], Łukasz Uram [4], Zbigniew Zieliński [1], Deborah Quaglio [5], Andrea Calcaterra [5], Ylenia Cau [3], Bruno Botta [5] and Wojciech Rode [1,*]

1 Nencki Institute of Experimental Biology, 3 Pasteur Street, 02-093 Warsaw, Poland; p.maj@nencki.edu.pl (P.M.); j.sobich@nencki.edu.pl (J.S.); z.zielinski@nencki.edu.pl (Z.Z.)
2 Department of Pharmacology, University of Oxford, Mansfield Road, Oxford OX1 3QT, UK
3 Department of Biotechnology, Chemistry and Pharmacy, Department of Excellence 2018-2022, via Aldo Moro 2, 53100 Siena, Italy; m.mattia79@gmail.com (M.M.); cau.ylenia@gmail.com (Y.C.)
4 Faculty of Chemistry, Rzeszów University of Technology, 6 Powstańców Warszawy Ave, 35-959 Rzeszów, Poland; jmarkowicz@stud.prz.edu.pl (J.M.); luram@prz.edu.pl (Ł.U.)
5 Department of Chemistry and Technology of Drugs, Department of Excellence 2018–2022, Sapienza University of Rome, Piazzale Aldo Moro 5, 00185 Rome, Italy; deborah.quaglio@uniroma1.it (D.Q.); andrea.calcaterra@uniroma1.it (A.C.); bruno.botta@uniroma1.it (B.B.)
* Correspondence: w.rode@nencki.edu.pl; Tel.: +48-608-351-155; Fax: +48-22-822-5342

Academic Editor: Athina Geronikaki
Received: 3 May 2020; Accepted: 19 June 2020; Published: 23 June 2020

Abstract: With the aim to identify novel inhibitors of parasitic nematode thymidylate synthase (TS), we screened in silico an in-house library of natural compounds, taking advantage of a model of nematode TS three-dimensional (3D) structure and choosing candidate compounds potentially capable of enzyme binding/inhibition. Selected compounds were tested as (i) inhibitors of the reaction catalyzed by TSs of different species, (ii) agents toxic to a nematode parasite model (*C. elegans* grown in vitro), (iii) inhibitors of normal human cell growth, and (iv) antitumor agents affecting human tumor cells grown in vitro. The results pointed to alvaxanthone as a relatively strong TS inhibitor that causes *C. elegans* population growth reduction with nematocidal potency similar to the anthelmintic drug mebendazole. Alvaxanthone also demonstrated an antiproliferative effect in tumor cells, associated with a selective toxicity against mitochondria observed in cancer cells compared to normal cells.

Keywords: thymidylate synthase; inhibitor; nematocidal activity; cytotoxicity; xanthones

1. Introduction

Thymidylate synthase (TS; EC 2.1.1.45) catalyzes the reductive methylation of deoxyuridine monophosphate (dUMP) by $N^{5,10}$-methylenetetrahydrofolate (meTHF) to generate thymidylate (dTMP) and dihydrofolate. Being the sole de novo source of dTMP in animal cells [1], the enzyme is consequently a target of antitumor, antiviral, antifungal, and antiprotozoan chemotherapy [2–9].

Parasitic nematodes belong to the most common infectious agents, and the majority of infections affect developing countries [10–12]. In our previous studies, we were interested in *Trichinella spiralis*, which is responsible in both developing and developed countries for a serious disease, i.e., trichinellosis [13], and a free-living nematode *Caenorhabditis elegans*, which is often used as a model organism in parasitological studies [14–16]. Of particular interest was a high TS-specific activity present throughout the developmental cycles of the two nematode species, including their developmentally arrested forms (lacking cell proliferation and thus expected to show TS activity either low or none

at all), including *T. spiralis* infective muscle larvae [16–19] and *C. elegans* dauer larvae [17], the latter corresponding to developmentally arrested infective larvae of parasitic nematodes [14]. It pointed to the high TS level as a result of an unusual cell cycle regulation, leading to a long-term cell cycle arrest, in the developmentally arrested larvae (discussed in Reference [17,18]). Although TS protein in those larvae is probably catalytically irrelevant (no DNA synthesis), it may play a regulatory role in view of the enzyme's certain non-catalytic activities, including capacity to bind mRNA (its own and some others) and inhibit translation, with potential regulation of several cellular genes [19,20], as well as an oncogene-like activity [21]. Thus, in view of the latter, a possibility to selectively interfere with nematode TS catalytic/non-catalytic activities could be applied not only in an attempt to kill a parasite but also to study the physiological significance of the high expression of TS in nematodes' cells, particularly in their developmentally arrested larvae.

The present study was aimed at seeking new TS inhibitors within the in-house library of natural compounds and their derivatives (around 1000 compounds) organized and maintained by the group of Professor Bruno Botta of Sapienza University of Rome. Of particular interest was a possibility of inhibition of parasitic nematode TS. Thanks to the availability of a model nematode TS X-ray crystallographic structure, candidate compounds potentially capable of enzyme binding/inhibition were identified by means of a structure-based virtual screening of the above library. In an attempt to make the best use of the results of the screen and considering a strong conservation of the enzyme protein [5], the selected compounds, confirmed to be TS inhibitors, were tested not only as antinematode but also as antitumor agents. Therefore, the tested properties included (i) potential to inhibit the reaction catalyzed by TSs of different specific origin, (ii) toxicity to a nematode parasite model (*C. elegans* grown in vitro), (iii) potential to inhibit normal human cell growth, and (iv) antitumor activity affecting human tumor cells grown in vitro.

2. Results

2.1. Chemical Library and Virtual Screening

The in-house library of natural product contains around 1000 small molecules isolated, purified, and characterized mostly from plants used in the traditional medicine of South America countries, as well as a number of chemical derivatives. The library owns a significant chemical diversity and was already used as source of hit and lead compounds in previous drug discovery projects [22–27]. To pursue the aim of identifying potential TS inhibitors, here, 865 compounds from the library were screened against the crystallographic structure of *C. elegans* TS in complex with 2′-deoxyuridine-5′-monophosphate (dUMP) and the small molecule inhibitor Tomudex (PDB ID: 4IQQ). Docking simulations were carried out with FRED (OpenEye scientific software) on the Tomudex binding site, after removing the coordinates of Tomudex and co-crystallized water molecules from the receptor structure. Docking results were then sorted according to the FRED score, which is calculated by the Chemgauss4 function, while the shortlist of compounds to select for biological studies was finalized by a combination of score, visual inspection, and chemical diversity. This operation led to the selection of 20 natural compounds as putative TS inhibitors (Table 1).

Table 1. Assessment of the IC_{50} values describing inhibition of thymidylate synthases (TSs) of different origin by compounds selected by the 3D structure-based virtual search of the in-house library of natural compounds (Table 1, compounds **1**–**20**) and obtained from that library, and by α-mangostin (Table 1, compound **21**), a close structural analogue of alvaxanthone, included in the study after learning inhibitory properties of the latter and purchased from a commercial source.

Compound (No.)	Structure	IC_{50} [μM] Assessment (% Remaining Activity) [a]			
		mTS	**hTS**	***Ce*TS**	***Ts*TS**
Curcumin (**1**)	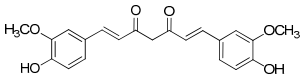	>50(83) <500(37)	>50(86) <500(20)	>50(84) <500(30)	>500(73)
Aloin (**2**)	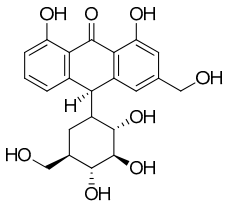	>1000(95)	>100(94) <1000(49)	>100(83) <1000(36)	>1000(93)
Chlorogenic acid (**3**)	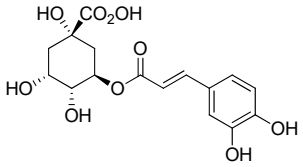	>1000(83)	>1000(76)	>1000(82)	>1000(94)
Phloretin (**4**)	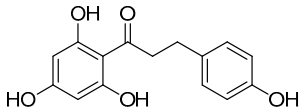	>100(78) <1000(45)	>100(86) <1000(31)	>100(82) <1000(48)	>1000(61)
Sophoronol (**5**)	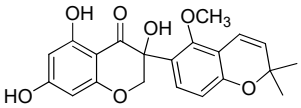	>100(75) <1000(10)	>100(75) <1000(8)	>100(77) <1000(8)	>100(74) <1000(35)
Bixin (**6**)	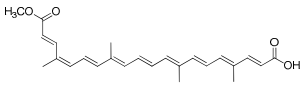	>667(73)	(667)NI [b]	>67(93) <667(46)	>67(76) <667(47)
Myricetin-4′-OAc (**7**)	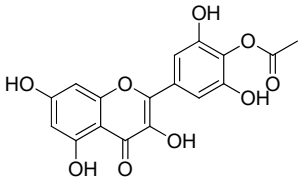	>100(61) <1000(49)	>100(56) >1000(31)	>100(69) <1000(28)	>1000(66)
Agnuside (**8**)	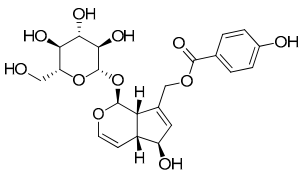	>1000(72)	>100(90) <1000(47)	>100(100) <1000(36)	>1000(63)
Clusiacitran A (**9**)	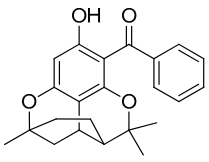	>1000(62)	>100(89) <1000(47)	>100(88) <1000(44)	>1000(95)

Table 1. *Cont.*

Compound (No.)	Structure	IC_{50} [μM] Assessment (% Remaining Activity) [a]			
		mTS	**hTS**	***Ce*TS**	***Ts*TS**
Jatrowediol (**10**)	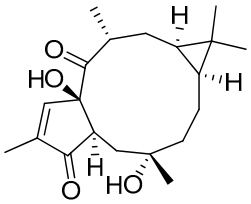	>1000(80)	>100(100) <1000(43)	>1000(77)	>1000(95)
6-Chromane-*O*-7-flavanone (**11**)	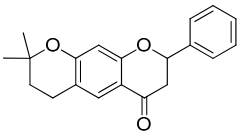	>100(91) <1000(10)	>10(100) <100(37)	>10(100) <100(24)	>1000(85)
Alnusin (**12**)	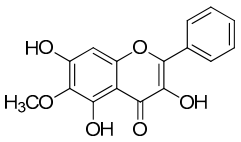	(1000)NI [b]	>100(85) <1000(30)	>1000(80)	(1000)NI [b]
Leucosceptoside A (**13**)	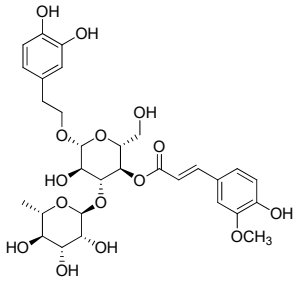	>1000(77)	>1000(66)	>1000(83)	(1000)NI [b]
(±)-7-Hydro-xy-8-C-prenyl flavanone (Ovaliflavanone B) (**14**)	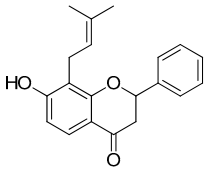	>100(71) <1000(2)	>100(74) <1000(7)	>100(65) <1000(3)	>100(90) <1000(25)
Alvaxanthone (**15**)	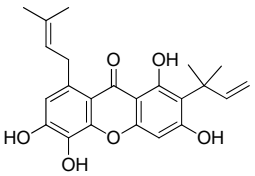	>10(79) <100(40)	<10(39)	>10(85) <100(18)	>10(98) <100(47) >10 [†](97) <100 [†](14)
1,3-OH-2-OMe-Xanthone (**16**)	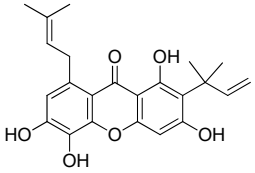	>100(67) <1000(32)	>100(54) <1000(27)	>1000(65)	>100(92) <1000(23) >100 [†](82) <1000 [†](32)
Rheediaxanthone B (**17**)	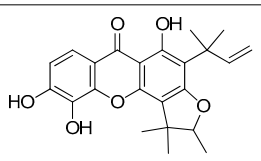	>10 [†](56) <100 [†](2)	>10 [†](59 <100 [†](5)	>10 [†](59) <100 [†](14)	>10 [†](68) <100 [†](40)

Table 1. *Cont.*

Compound (No.)	Structure	IC_{50} [μM] Assessment (% Remaining Activity) [a]			
		mTS	**hTS**	***Ce*TS**	***Ts*TS**
Rheediaxanthone C (**18**)	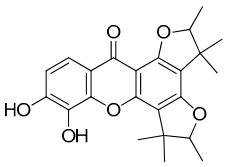	>10 †(77) <100 †(39)	>100 †(57)	>100 †(71)	>100 †(73)
1-OH-7-OMe-Xanthone (**19**)	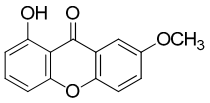	>1000 † (94)	>1000 † (100)	>1000 † (81)	>1000 † (89)
2-OMe-Xanthone (**20**)	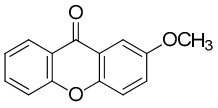	>1000 † (84)	>1000 † (88)	>1000 † (95)	>1000 † (92)
α-Mangostin (**21**)	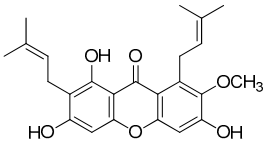	>10 †(75) <100 †(5)	>10 †(89) <100 †(19)	>10 †(79) <100 †(27)	>100 †(85)

[a] Inhibition by each compound was tested at three concentrations in the enzyme-catalyzed reaction run with 20 μM deoxyuridine monophosphate (dUMP) and either 250 μM or 50† μM methylenetetrahydrofolate (meTHF) in the reaction mixture. The remaining activity (%) at an indicated concentration is shown in parentheses following that concentration. [b] No inhibition. The highest obtained concentration of a compound (reported in parentheses) showed no inhibition of the activity of a specific TS variant. † The reaction run at 20 μM dUMP and 50 μM meTHF in the reaction mixture.

2.2. Predicted Properties of Compounds From the In-House Library

The majority of compounds are likely to exhibit favorable ADME/tox properties. Apart from agnuside and leucospectoside A, all remaining compounds follow the Lipinski Rule of 5 [28] with either one or no violations. Similarly, agnuside and leucospectoside A are consistently among compounds with the most violations of other sets of medchem rules, e.g., Veber rules [29], "Traffic Lights" [30], "BOILED-Egg" [31], Egan rules [32], and Muegge rules [33]. Of note, some of the compounds are marked as likely promiscuous binders or aggregators due to matching Pan-assay interference compounds (PAINS) PAINS filters [34] or identity/high similarity to compounds present in the Aggregator Advisor database [35]. Curcumin is the only compound both explicitly listed as a known aggregator and matching PAINS filters, in accord with multiple reports of false positive results caused by curcumin in biological assays [36]. Some of the remaining xanthone derivatives, e.g., alvaxanthone, rheediaxanthone B, and rheediaxanthone C, match PAINS filters and are at least 70% similar to compounds known to act via aggregation. Therefore, more thorough future assays, especially ones focusing on enzyme activity in vitro, should involve measures testing for aggregation and promiscuous binding, e.g., dynamic light scattering (DLS) DLS measurements or activity assays with unrelated enzymes [37].

2.3. TS Inhibition

The molecular docking campaign resulted in 20 compounds (Table 1, compounds **1**–**20**) suggested as potentially selective inhibitors of nematode TS. Their activity against four enzyme preparations, corresponding to two mammalian (human and mouse, hTS and mTS, respectively) and two nematode species (*T. spiralis* and *C. elegans*, *Ts*TS and *Ce*Ts, respectively) was assessed by testing inhibition by each compound at three concentrations, i.e., 10, 100, and 1000 μM (unless low solubility did not allow to reach the highest concentration), of the enzyme-catalyzed reaction run with 20 μM dUMP and either 250 μM or 50 μM meTHF in the reaction mixture. The results pointed to alvaxanthone (Table 1, compound **15**) as the strongest inhibitor, showing the IC_{50} values with different enzyme preparation

studied ranging from below 10 μM to around 100 μM, with further strong inhibitors in this group being rheediaxanthone B and rheediaxanthone C (Table 1, compounds **17** and **18**, respectively) but only for mTS. Other compounds inhibited TS by at least one order of magnitude weaker. Further comparison of inhibition by alvaxanthone of *Ts*TS and hTS, with 20 μM dUMP and 50 μM meTHF in the reaction mixture, showed the IC_{50} values of 41.9 ± 8.1 μM (3) and 6.3 ± 1.6 μM (3), respectively. Furthermore, initial results showed time-dependent inhibition, suggesting its slow-binding character [38]. Inhibition by rheediaxanthone B of *Ts*TS, *Ce*TS, hTS, and mTS, tested under the above conditions, showed the IC_{50} values of 50.8 μM, 11.4 μM, 17.9 μM, and 14.3 μM, respectively (the experiments have not been repeated). Compared to alvaxanthone, also α-mangostin, another xanthone derivative, characterized by a high structural similarity to alvaxanthone and demonstrated previously to inhibit *C. elegans* population growth [39], was not a rather strong inhibitor of TS (Table 1, compound **21**).

2.4. Toxicity to C. elegans

Alvaxanthone was found to be also a relatively strong inhibitor of *C. elegans*, which is considered as a model of parasitic nematodes [14], causing reduction of growth of the nematode population with LC_{50} of 4.60 ± 0.57 μM (4). The latter value was similar to those previously found [39] for the above mentioned α-mangostin (3.8 μM) and the well-known antiparasitic drug mebendazole (4.0 μM), pointing to a potential antiparasitic activity of alvaxanthone.

Considering the inhibitory activities of alvaxanthone (Table 1, compound **15**) against both TS and the nematode population growth, several structurally similar compounds were selected, including 1,3-OH-2-OMe-xanthone, rheediaxanthone B and C, 1-OH-7-OMe-xanthone, and 2-OMe-xanthone (Table 1, compounds **16**–**20**), to be tested against *C. elegans*. Only rheediaxanthone B and 2-OMe-xanthone were active, showing LC_{50} values of 16.0 ± 10.2 μM (2) and 33.8 ± 2.1 μM (2), respectively, with the remaining derivatives demonstrating weaker effects by at least one order of magnitude.

2.5. Cytotoxicity

The same group of xanthones, including alvaxanthone, 1,3-OH-2-OMe-xanthone, rheediaxanthone B and C, 1-OH-7-OMe-xanthone, and 2-OMe-xanthone, underwent cytotoxicity tests. The compounds varied significantly in both toxicity and selectivity (Table 2). While the strongest toxicity was exerted by rheediaxanthone B and C and alvaxanthone, only alvaxanthone and rheediaxanthone B caused stronger inhibition of cancer (glioma cells U-118 MG) than normal (human fibroblasts-BJ) cells (Table 2). Therefore, these two compounds were selected for further studies.

Table 2. Cytotoxicity of alvaxanthone and several other xanthones determined by the neutral red assay.

Compound (No.)	IC_{50} (μM) [a]		
	BJ	U-118 MG	SCC-15
Alvaxanthone (**15**)	15.76	13.07	17.66
1,3-OH-2-OMe-xanthone (**16**)	>40	>40	>40
Rheediaxanthone B (**17**)	5.5	4.75	9.2
Rheediaxanthone C (**18**)	5.95	18.27	11.04
1-OH-7-OMe-Xanthone (**19**)	>40	40	>40
2-OMe-Xanthone (**20**)	>40	>40	>40

[a] Calculated by plotting the median cell viability (% of control) values against compound concentrations (μM), followed by abscissa transformation to the logarithmic form. The logarithmic regression led to the y = aln(x) + b equation, allowing to calculate the IC_{50} value.

Biological effect of alvaxanthone and rheediaxanthone B on normal (BJ) and cancer cells (U-118 MG and SCC-15) was estimated using two viability assays, the neutral red uptake (NR) and tetrazolium salts reduction (XTT) assays. The results of three independent triplicate assays are presented in Figure 1.

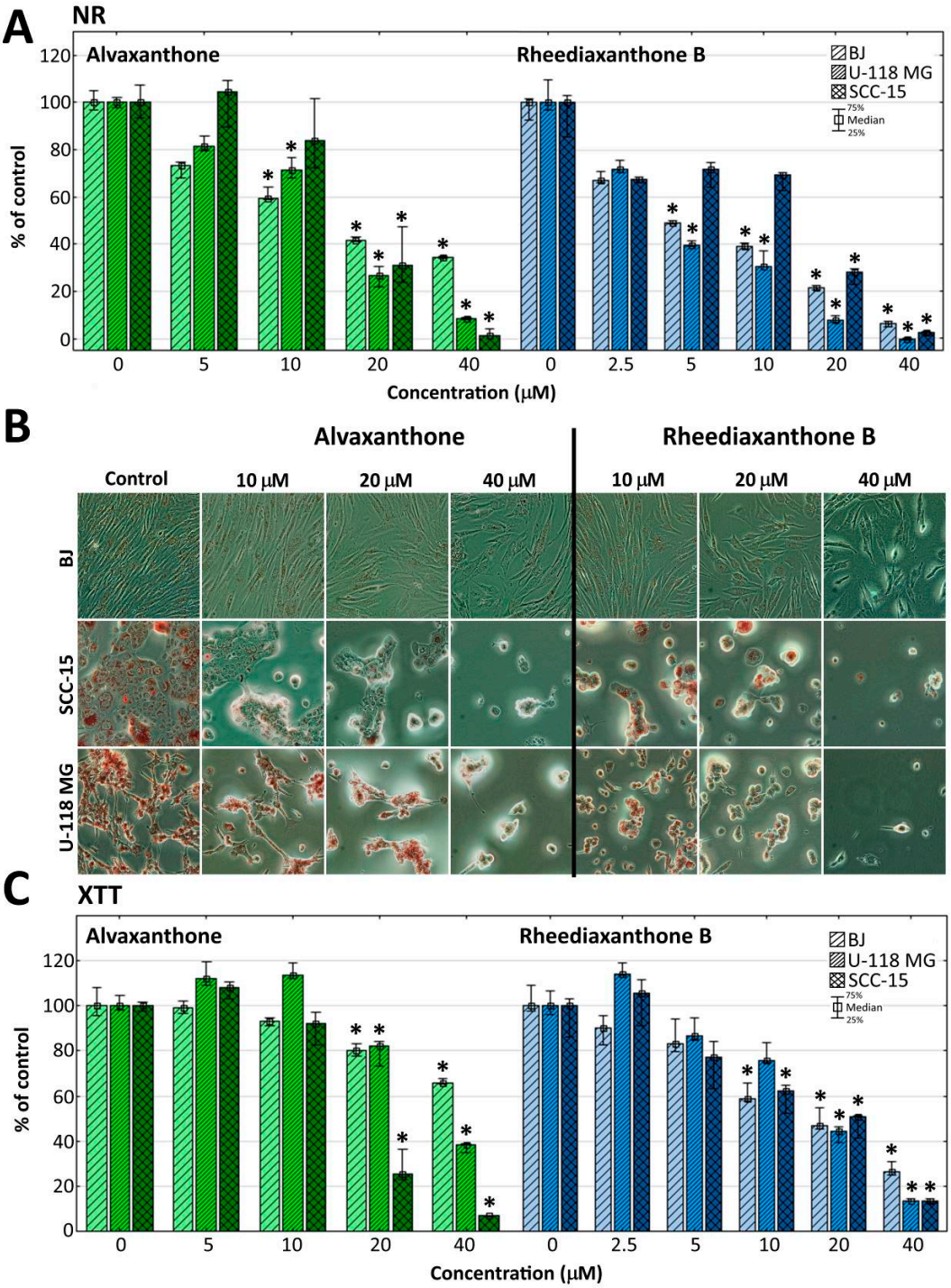

Figure 1. Viability of BJ, U-118 MG and SCC-15 cells after 48 h treatment with alvaxanthone or rheediaxanthone B, estimated by NR (**A**) and XTT (**C**) assays. Each bar represents the median of a population of 9 results, obtained in consequence of three independent experiments, each done in triplicate. The whiskers are the lower (25%) and upper (75%) quartile ranges. The results significantly different from control (in a view of the Kruskal–Wallis test) are marked * ($p \leq 0.05$). (**B**) Cell morphology and neutral red accumulation following 48 h alvaxanthone or rheediaxanthone B treatment and 1 h incubation with neutral red. Red vesicles are lysosomes containing the dye.

Both assays revealed concentration- and cell type-dependent toxicity of each of the two compounds. Tested by the more sensitive NR assay, rheediaxanthone B was slightly more toxic (IC_{50} < 10 μM,

compared to alvaxanthone (15 μM < IC_{50} < 18 μM), none of them showing a significant selectivity against cancer cells. At the highest concentration of 40 μM, cancer cells were distinctly more susceptible than normal cells to alvaxanthone (viability decreased to 10% with U-118 MG, and 1.5% with SCC-15 cells, vs. 35% with fibroblasts). On the other hand, activity of mitochondrial dehydrogenases and oxidoreductases, tested by the XTT assay, provided information about the condition of mitochondrial metabolism and indicated selectivity of alvaxanthone against both SCC-15 and U-118 MG cells (compared to BJ fibroblasts 5.3-fold and 2.7-fold more sensitive, respectively; Figure 1). Thus, alvaxanthone may be damaging mitochondria and impairing their metabolism exerting one of possible mechanisms active in destroying cancer cells [40]. Changes of cell morphology in dependence on increasing alvaxanthone and rheediaxanthone B concentration were also recorded. While the glioma and squamous carcinoma cells formed clusters, lost their adhesion, shrank, and accumulated less NR dye, normal fibroblasts preserved rather normal shapes but the amount of the neutral red dye and confluence of cells decreased. In addition, a lower number of BJ cells was detected (Figure 1B).

A possible cytotoxic mechanism of alvaxanthone can be hypothesized, relying in glioma and fibroblasts on cellular and lysosomal membrane disruption rather than mitochondrial function impairment, as indicated by lower viability of both U-118 MG and BJ cells observed in the NR than XTT assay at the highest alvaxanthone concentration. A different toxic pattern was observed in squamous carcinoma cells, manifested by similar cell viability levels at the whole range of alvaxanthone concentrations and equal IC_{50} values observed with both assays (IC_{50} = 17 μM), indicating both cell membrane damage and mitochondrial dysfunction. These results suggest also that alvaxanthone impact on mitochondrial metabolism was in SCC-15 cells stronger compared to the other cell lines. In accord, Hou et al. [41] showed the IC_{50} values estimated for human oral squamous carcinoma cells (HSC-2 cell line) and normal human gingival fibroblasts (HGF) after 24 h incubation to be almost equal (22 μM and 25 μM, respectively).

2.6. Proliferation

The influence of alvaxanthone and rheediaxanthone B on cell proliferation (Figure 2) was assessed by quantitative measurement of the total cellular DNA content, proportional to the cell number [42].

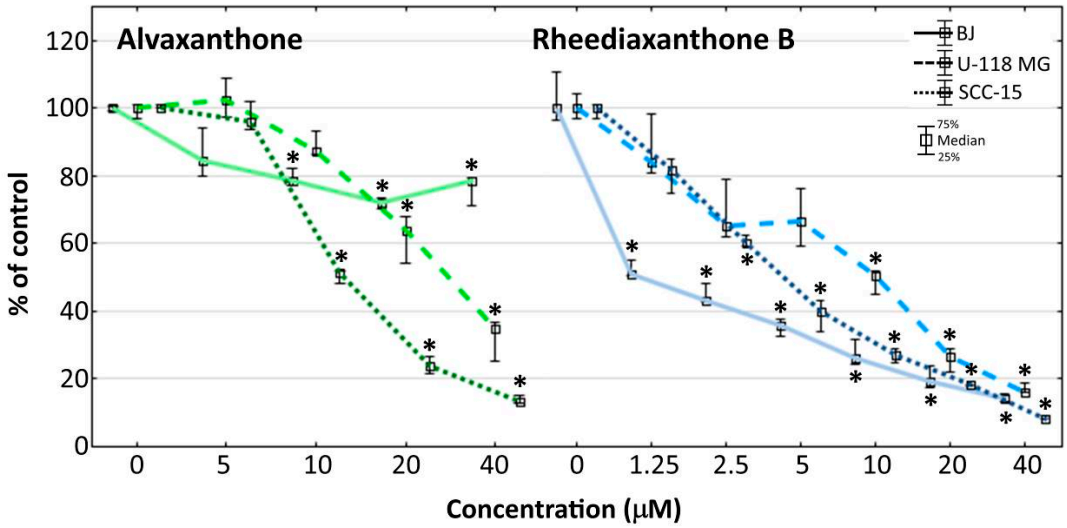

Figure 2. Proliferation of cancer (U-118 MG and SCC-15) and normal (BJ) cells after 72 h incubation with 5–40 μM alvaxanthone or 1.25–40 μM rheediaxanthone B, determined with the CyQUANT GR Cell Proliferation Assay Kit. Median results are presented of three independent experiments, each performed in triplicate. The whiskers are lower (25%) and upper (75%) quartile ranges. The results significantly different from control (in view of the Kruskal–Wallis test) are indicated * ($p \leq 0.05$). Images collected with Olympus IX-83 microscope with contrast phase (scale bar = 100 μm).

Alvaxanthone was a somewhat stronger inhibitor of the cancer (glioma and squamous carcinoma) than normal (BJ fibroblasts) cell proliferation, the effect noticeable only at concentrations above 10 μM, with the inhibition at 40 μM alvaxanthone being by 5.8- and 2.3-fold weaker with normal (BJ) than cancer (SCC-15 and U-118 MG, respectively) cells (Figure 2). Rheediaxanthone B, being apparently a stronger proliferation inhibitor than alvaxanthone, shows also similar selectivity but at a lower concentration range (up to some 2 μM; Figure 2).

2.7. Adhesion

Cancer metastasis, resulting from an impairment of adhesion between cancer cells and the extracellular matrix may cause cell migration from a primary tumor into distant parts of an organism [43]. The cristal violet assay was used to examine alvaxanthone and rheediaxanthone B ability to influence cellular adhesion. The results indicate alvaxanthone significantly reduces adhesion of normal fibroblasts and squamous carcinoma cells, compared with glioma cells, at lower (20 μM vs. 40 μM) concentration (Figure 3).

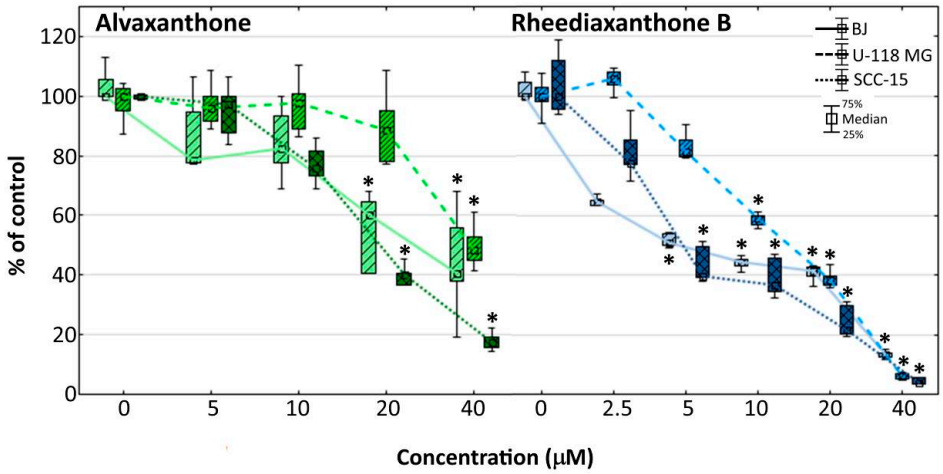

Figure 3. Influence of alvaxanthone or rheediaxanthone B on BJ, U-118 MG, and SCC-15 cells adhesion after 48-h treatment. The crystal violet assay was used. Results are medians of triplicate assays of three independent experiments expressed as a % of non-treated controls. The whiskers are lower (25%) and upper (75%) quartile ranges. * $p \leq 0.05$, Kruskal–Wallis test (against non-treated control).

The effect of rheediaxanthone B was apparent at lower concentrations (at 5 μM with BJ and SCC-15, and 10 μM with U-118 MG cells; Figure 3). The results are consistent with those of the NR cytotoxicity assay (Figure 1), showing similar profile of the toxic effect with respect to the cell lines and drug concentrations affecting their growth, pointing to the decrease of cell adhesion to be caused by each of the two prenylated xanthones as a result of the compound's toxic action, without increasing the probability of metastasis during therapy. Additional information provides Figure 4, presenting changes of the intracellular ATP level in treated cells. With both compounds at concentrations causing decreased cell adhesion, considerably depleted ATP levels were apparent that probably reduced cells capacity to move and migrate. Thus, considering potential chemotherapeutic application, the tested compounds should not be expected to increase migration of cancer cells to other parts of an organ or organism or lead to metastasis processes.

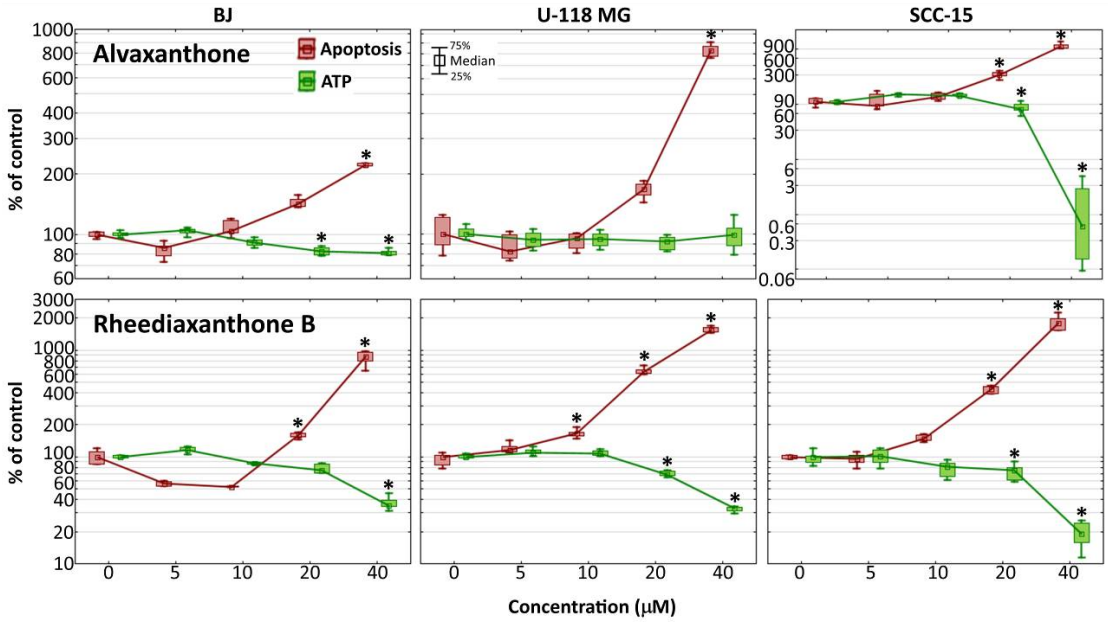

Figure 4. Changes of caspase-3/7 activities and intracellular ATP level in BJ, U-118 MG, and SCC-15 cells after 48-h incubation with 5–40 μM alvaxanthone or rheediaxanthone B. Median results are presented of three independent experiments, each performed in triplicate. The whiskers are lower (25%) and upper (75%) quartile ranges. The results significantly different from control (in view of the Kruskal–Wallis test) are indicated as * ($p \leq 0.05$).

2.8. Caspase-3/7 and ATP Level

The Apo-ONE® Homogenous Caspase-3/7 Assay provides a measurement of the executioner caspases 3/7 activation, characteristic for apoptosis induced via both the intrinsic and extrinsic pathway [44]. It was used to determine apoptosis induction in cells by alvaxanthone and rheediaxanthone B. In each of the three cell lines, compared to the respective non-treated control, treatment with each of the two compounds for 48 h led to a significant activation of the caspases 3/7 (by 2- to 10-fold for alvaxanthone and 8- to 18-fold for rheediaxanthone B), the effect being stronger in cancer than normal cells (Figure 4).

As induction of apoptosis has been previously suggested to cause a caspase-dependent fall of ATP levels [45,46], the CellTiterGlo® Luminescent Cell Assay was performed to determine changes in ATP level. After incubation with alvaxanthone, the level of ATP in glioma cells remained unaltered; in normal fibroblasts, it showed only a slight decrease, and, in SCC-15, it was dramatically reduced. On the other hand, rheediaxanthone B caused a reduction of ATP level down to around 30% in glioma cells and fibroblasts, and to 20% in squamous carcinoma cells (Figure 4). In general, with increasing Caspase-3/7 activity the ATP level was decreasing, in accord with the results of Reference [46]. However, contrary to the latter, Oropesa et al., demonstrated that, during apoptosis in alvaxanthone-treated glioblastoma cells, the level of ATP was unchanged or even increased during early phases of apoptosis, despite caspase 3 and 7 undergoing activation [47].

2.9. Predicted Binding Mode of Alvaxanthone and Rheediaxanthone B

The possible binding mode of the most interesting TS inhibitors identified by virtual screening and in vitro tests, i.e., alvaxanthone and rheediaxanthone B, was investigated by molecular docking against human and *C. elegans* TS. Compared to the virtual screening settings, here, we stored a larger number of binding poses of each compound to enrich our analysis with statistical significance. Overall, both compounds proved to bind within the TS catalytic site, in close proximity and in stacking conformation to the co-crystallized dUMP cofactor. Notably, both compounds adopted a very similar binding mode against the catalytic site of TS from both human and *C. elegans*, which is not surprising

according to the high degree of sequence and structural identity between TS from the two species [48]. Besides stacking to dUMP, the major anchor point is the side chain of Asp220 (in *C. elegans* Ts) or Asp 218 (in human TS), which is H-bonded to a hydroxyl group connected to the xanthone ring (Figure 5). Similar to docking poses, also docking scores highlighted that both alvaxanthone and rheediaxanthone B bind with comparable affinity to each protein (chemgauss4 score for alvaxanthone: −8.60 (*C. elegans*) and −8.91 (human); rheediaxanthone: −8.10 (*C. elegans*) and −8.50 (human)). These theoretical results are in agreement with experimental data above and may facilitate the design of TS inhibitors with improved features.

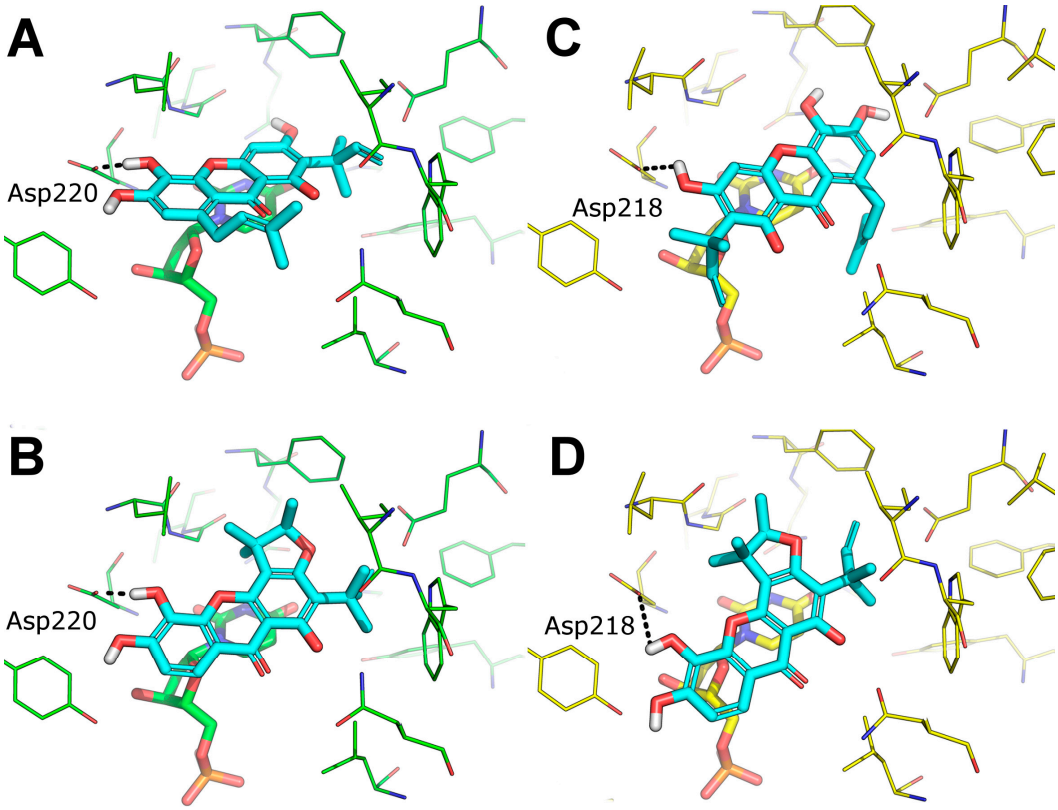

Figure 5. Predicted binding mode of alvaxanthone and rheediaxanthone against TS. (**A**,**B**) docking pose of alvaxanthone (**A**) and rheediaxanthone (**B**) against the catalytic site of TS from *C. elegans*, PDB ID 4IQQ (green lines). (**C**,**D**) docking pose of alvaxanthone (**C**) and rheediaxanthone (**D**) against the catalytic site of TS from homo sapiens PDB ID 5X5D (yellow lines). TS inhibitors are shown as cyan lines. dUMP is shown as sticks and colored as the protein. H-bonds are showed as black dashed lines. Only residues within 5 Å from the docked ligands are shown.

3. Discussion

The present results highlight two natural compounds selected by virtual screening of an in-house library of natural products and their derivatives as inhibitors of the reaction catalyzed by TS of different species. The most potent enzyme inhibitors are between xanthone derivatives, with alvaxanthone inhibiting stronger than rheediaxanthone B and the latter stronger than rheediaxanthone C. Similarly, another commercially available compound, α-mangostin (Table 1, compound **21**), which is a close analogue of alvaxanthone [39], is as potent inhibitor as the latter (Table 1). Comparison of the xanthone group (Table 1, compounds **15**–**21**) with regard to the inhibitory potential allows a rough identification of the structural requirements, including hydroxyls at the positions 1, 3, and 6, and hydrophobic substituents at the positions 2 and 8.

The xanthone derivatives capable of inhibition of TS-catalyzed reaction, including alvaxanthone, α-mangostin, and rheediaxanthone B, are toxic for *C. elegans* and mammalian cells. However,

rheediaxanthone C that inhibits the enzyme does not show toxicity for the worm. Besides, 2-OMe-xanthone, lacking an apparent TS inhibitor activity, is toxic only for *C. elegans* (Tables 1 and 2 [39]). Thus, it remains to be established whether TS is the target in both the organismal (*C. elegans*) and cell-based model systems.

Of particular interest is nematocidal activity of alvaxanthone, which proved to be toxic for *C. elegans* to a similar extent as the well-known reference anthelmintic drug mebendazole [49,50] and α-mangostin [39]. While the lack of selective toxicity against the nematode worms versus human cells does not point to alvaxanthone as a potential chemotherapeutic drug to combat human nematode parasites, it does not preclude its potential application against plant nematode parasites. Besides, it may be treated as a leading compound to be modified in search of a selective chemotherapeutic drug. Furthermore, as the compound is also a TS inhibitor, it may be used as a tool in further studies of the physiological significance of the high expression of TS in nematodes' cells (see Introduction).

Alvaxanthone has been previously demonstrated to show antimicrobial [51,52], antifungal [53], and cytotoxic [41,53] activities. To the best of our knowledge, there are no records on the biological activity of rheediaxanthone B and rheediaxanthone C. The present results show alvaxanthone, rheediaxanthone B and rheediaxanthone C to be cytotoxic. Compared to alvaxanthone, the cytotoxic and antiproliferative effects of rheediaxanthone B were slightly stronger and associated with lowered adhesion and elevated activities of the executioner caspases (Figures 1–4). While in glioblastoma and fibroblast cells alvaxanthone toxicity was based mostly on disturbing lysosomal membranes or alterations in cellular membrane, in the SCC-15 cells, it was associated with both cell membrane and mitochondrial metabolism changes. Of particular interest is an antiproliferative effect of alvaxanthone in tumor cells, associated by a selective toxicity against mitochondria observed in cancer cells and cell death via the more desirable apoptosis pathway. Of note is also that in view of lowered adhesion being caused by each of two compounds toxicity (Figures 1 and 3), neither alvaxanthone nor rheediaxanthone B appear to increase the probability of metastasis. Overall, these natural products share common pharmacophoric features and stand as a promising starting point for the design of further generation of TS inhibitors inspired by natural sources.

4. Materials and Methods

4.1. Materials

The compounds selected to be tested were obtained from the in-house library of natural compounds organized and maintained by the group of Professor *Bruno Botta* of Sapienza University of Rome. In total, 865 compounds that composed the in-house library of natural products at the time of the study were screened in silico by molecular docking simulations. We used the above-mentioned library as a source of natural compounds endowed with high structural and chemical diversity, with the aim to identify novel chemotypes of TS inhibitors. α-Mangostin (**21**) was purchased from Sigma-Aldrich (St. Louis, MO, USA). Standard samples of compounds **1**, **2**, **3**, **4**, **6**, and **9** were purchased from Sigma-Aldrich (St. Louis, MO, USA) and compared with the corresponding samples from the library. The compounds tested with cell cultures were prepared from stock solutions in corresponding cell culture media by adjusting the DMSO concentration to ≤ 0.05% (showing no significant effect on treated cells).

4.2. Computational Methods

The in-house library of natural products available at the Department of Chemistry and Technology of Drugs of Sapienza University of Rome (Prof. Bruno Botta) was computationally screened against the crystallographic structure of C. elegans TS in complex with dUMP and a small molecule inhibitor (PDB ID: 4IQQ) through molecular docking simulations. Docking was carried out with the FRED program from OpenEye [54,55], using the default settings and the highest docking resolution. Ligand conformational analysis was carried out with OMEGA from OpenEye [56,57], storing up to

600 conformers for each ligand. In docking against the human form of TS, the PDB ID: 5X5D (TS in complex with dUMP) was used [58]. Receptor structures were prepared with the make_receptor utility of FRED. In virtual screening, only the top-scoring pose of each ligand was stored and analyzed, while, in docking alvaxanthone and rheediaxanthone B, up to 20 docking poses were stored. Druglikeness and ADME/tox properties of the compounds were assessed using freely available online tools: FAF-Drugs4 [59], SwissADME [60], and Aggregator Advisor [35].

4.3. Chemistry

Standard samples of compounds **1**, **2**, **3**, **4**, **6**, **8**, and **9** were purchased from Sigma-Aldrich (St. Louis, MO, USA) and compared with the corresponding samples from the library. Samples of compounds **1**, **2**, **3**, **4**, **6**, **8**, and **9** from the library resulted to be spectroscopically and chromatographically identical to the commercial samples.

Compound **5** showed NMR spectra identical to those reported in the literature [61–63]. Compound **7** showed NMR spectra in accordance with those reported in the literature [64].

NMR spectra identical to those reported in the literature were observed also for compounds **10** [65], **11** [66], **12** [67], **13** [68], **14** [69,70], **15** [71], **16** [72,73], **17** [74], **18** [74], **19** [75], and **20** [75].

4.4. TS preparation

The recombinant human, rat, mouse, *T. spiralis* and *C. elegans* TS proteins were produced, purified and separated into phosphorylated and non-phosphorylated fraction, as previously described [20]. TS activity was monitored, following tritium release from [5-^{3}H]dUMP, and its inhibition studied as earlier reported [76]. At concentrations ≤10% DMSO (used to dissolve compounds to be tested) did not affect the reaction rate.

4.5. Determination of Toxicity to C. elegans, a Nematode Parasite Model

C. elegans was maintained as previously described [17]. The effect of the compounds studied on *C. elegans* population growth was determined as earlier presented [39].

4.6. Cell Culture Studies

Human glioblastoma cells U-118 MG (ATCC® HTB-15), human squamous carcinoma cells SCC-15 (ATCC® CRL-1623), and normal human skin fibroblasts (ATCC® CRL-2522) were grown, their morphology checked, and number and viability estimated as earlier presented [39].

Influence of selected compounds on cells was tested by performing the cytotoxicity (NR and XTT) assays, proliferation assay, cell adhesion assay, cell migration assay, determination of intracellular ATP level, and apoptosis assay as previously reported [39].

4.7. Statistical Analysis

This was performed using the nonparametric Kruskal-Wallis test to estimate the differences between the compounds-treated cells and non-treated control in each cell lines. $p \leq 0.05$ was considered as statistically significant. Calculations were performed using Statistica 12 (StatSoft, Tulsa, OK, USA). The results describing TS inhibition and reduction of *C. elegans* population are presented as means ± S.E.M., or means ± % difference between the mean and each of two results, followed by the number of experiments (N) in parentheses.

Author Contributions: Conceptualization analytical studies, B.B. and W.R.; investigation, P.M., M.M., Y.C., J.S., J.M., Ł.U. and Z.Z.; resources and, D.Q., A.C. and Y.C.; writing—original draft preparation, W.R., Ł.U., M.M. and B.B. All authors have read and agreed to the published version of the manuscript.

Funding: This research was funded by the National Science Center, Poland, grants no. 2016/21/B/NZ1/00288 and 2014/13/D/NZ3/02825.

Acknowledgments: Cooperation resulting in the present paper developed as part of the COST Action CM1407. The studies presented here are parts of the doctoral dissertations of Piotr Maj (ORCID: 0000-0002-9832-2344), Joanna Markowicz (ORCID: 0000-0002-0263-2621) and Justyna Sobich (ORCID: 0000-0001-5075-0879). The authors wish to thank the OpenEye Free Academic Licencing Programme for providing a free academic licence for molecular modeling and chemoinformatics software.

Conflicts of Interest: The authors declare no conflict of interest.

References

1. Rode, W. Specificity of Thymidylate Synthase Inactivation by 4,5-Bisubstituted DUMP Analogues. *Acta Biochim. Pol.* **1993**, *40*, 363–368. [CrossRef] [PubMed]
2. Georgopapadakou, N.H.; Walsh, T.J. Antifungal Agents: Chemotherapeutic Targets and Immunologic Strategies. *Antimicrob. Agents Chemother.* **1996**, *40*, 279–291. [CrossRef]
3. Rathod, P.K. Antimalarial Agents Directed at Thymidylate Synthase. *J. Pharm. Pharmacol.* **1997**, *49*, 65–69. [CrossRef]
4. Takemura, Y.; Jackman, A.L. Folate-Based Thymidylate Synthase Inhibitors in Cancer Chemotherapy. *Anti-Cancer Drugs* **1997**, *8*, 3–16. [CrossRef] [PubMed]
5. Costi, M.P.; Ferrari, S.; Venturelli, A.; Calò, S.; Tondi, D.; Barlocco, D. Thymidylate Synthase Structure, Function and Implication in Drug Discovery. *Curr. Med. Chem.* **2005**, *12*, 2241–2258. [CrossRef]
6. Gmeiner, W.H. Novel Chemical Strategies for Thymidylate Synthase Inhibition. *Curr. Med. Chem.* **2005**, *12*, 191–202. [CrossRef]
7. Singh, P.; Bhardwaj, A. Mechanism of Action of Key Enzymes Associated with Cancer Propagation and Their Inhibition by Various Chemotherapeutic Agents. *Mini-Rev. Med. Chem.* **2008**, *8*, 388–398. [CrossRef]
8. Jarmuła, A.; Frączyk, T.; Cieplak, P.; Rode, W. Mechanism of Influence of Phosphorylation on Serine 124 on a Decrease of Catalytic Activity of Human Thymidylate Synthase. *Bioorg. Med. Chem.* **2010**, *18*, 3361–3370. [CrossRef]
9. Taddia, L.; D'Arca, D.; Ferrari, S.; Marraccini, C.; Severi, L.; Ponterini, G.; Assaraf, Y.G.; Marverti, G.; Costi, M.P. Inside the Biochemical Pathways of Thymidylate Synthase Perturbed by Anticancer Drugs: Novel Strategies to Overcome Cancer Chemoresistance. *Drug Resist. Updat.* **2015**, *23*, 20–54. [CrossRef]
10. Pacifico, P. Nematodes: Worms of the World. *MLO: Med. Lab. Obs.* **2001**, *33*, 24–31.
11. Hotez, P.J.; Brindley, P.J.; Bethony, J.M.; King, C.H.; Pearce, E.J.; Jacobson, J. Helminth Infections: The Great Neglected Tropical Diseases. *J. Clin. Investig.* **2008**, *118*, 1311–1321. [CrossRef] [PubMed]
12. L'Ollivier, C.; Piarroux, R. Diagnosis of Human Nematode Infections. *Expert Rev. Anti-Infect. Ther.* **2013**, *11*, 1363–1376. [CrossRef]
13. Murrell, K.D.; Pozio, E. Trichinellosis: The Zoonosis That Won't Go Quietly. *Int. J. Parasitol.* **2000**, *30*, 1339–1349. [CrossRef]
14. Bürglin, T.R.; Lobos, E.; Blaxter, M.L. Caenorhabditis Elegans as a Model for Parasitic Nematodes. *Int. J. Parasitol.* **1998**, *28*, 395–411. [CrossRef]
15. Burns, A.R.; Luciani, G.M.; Musso, G.; Bagg, R.; Yeo, M.; Zhang, Y.; Rajendran, L.; Glavin, J.; Hunter, R.; Redman, E.; et al. Caenorhabditis Elegans Is a Useful Model for Anthelmintic Discovery. *Nat. Commun.* **2015**, *6*, 7485. [CrossRef]
16. Chaweeborisuit, P.; Suriyonplengsaeng, C.; Suphamungmee, W.; Sobhon, P.; Meemon, K. Nematicidal Effect of Plumbagin on *Caenorhabditis elegans*: A Model for Testing a Nematicidal Drug. *Z. Naturforsch. C J. Biosci.* **2016**, *71*, 121–131. [CrossRef] [PubMed]
17. Wińska, P.; Gołos, B.; Cieśla, J.; Zieliński, Z.; Fraczyk, T.; Wałajtys-Rode, E.; Rode, W. Developmental Arrest in *Caenorhabditis elegans* Dauer Larvae Causes High Expression of Enzymes Involved in Thymidylate Biosynthesis, Similar to That Found in *Trichinella* Muscle Larvae. *Parasitology* **2005**, *131*, 247–254. [CrossRef]
18. Rode, W.; Dabrowska, M.; Zieliński, Z.; Gołos, B.; Wranicz, M.; Felczak, K.; Kulikowski, T. *Trichinella spiralis* and *Trichinella pseudospiralis*: Developmental Patterns of Enzymes Involved in Thymidylate Biosynthesis and Pyrimidine Salvage. *Parasitology* **2000**, *120*, 593–600. [CrossRef]
19. Parsels, L.; Chu, E. The Role of Translational Control of the Cell Cycle. *Cancer J. Sci. Am.* **1998**, *4*, 287–295.
20. Frączyk, T.; Ruman, T.; Wilk, P.; Palmowski, P.; Rogowska-Wrzesinska, A.; Cieśla, J.; Zieliński, Z.; Nizioł, J.; Jarmuła, A.; Maj, P.; et al. Properties of Phosphorylated Thymidylate Synthase. *Biochim. Biophys. Acta* **2015**, *1854*, 1922–1934. [CrossRef]

21. Rahman, L.; Voeller, D.; Rahman, M.; Lipkowitz, S.; Allegra, C.; Barrett, J.C.; Kaye, F.J.; Zajac-Kaye, M. Thymidylate Synthase as an Oncogene: A Novel Role for an Essential DNA Synthesis Enzyme. *Cancer Cell* **2004**, *5*, 341–351. [CrossRef]
22. Casciaro, B.; Calcaterra, A.; Cappiello, F.; Mori, M.; Loffredo, M.R.; Ghirga, F.; Mangoni, M.L.; Botta, B.; Quaglio, D. Nigritanine as a new potential antimicrobial alkaloid for the treatment of Staphylococcus aureus-induced infections. *Toxins* **2019**, *11*, 511. [CrossRef] [PubMed]
23. Mori, M.; Tottone, L.; Quaglio, D.; Zhdanovskaya, N.; Ingallina, C.; Fusto, M.; Ghirga, F.; Peruzzi, G.; Crestoni, M.E.; Simeoni, F.; et al. Identification of a novel chalcone derivative that inhibits Notch signaling in T-cell acute lymphoblastic leukemia. *Sci. Rep.* **2017**, *7*, 2213. [CrossRef] [PubMed]
24. Infante, P.; Alfonsi, R.; Ingallina, C.; Quaglio, D.; Ghirga, F.; D'Acquarica, I.; Bernardi, F.; Di Magno, L.; Canettieri, G.; Screpanti, I.; et al. Inhibition of Hedgehog-dependent tumors and cancer stem cells by a newly identified naturally occurring chemotype. *Cell Death Dis.* **2016**, *7*, e2376. [CrossRef] [PubMed]
25. Infante, P.; Mori, M.; Alfonsi, R.; Ghirga, F.; Aiello, F.; Toscano, S.; Ingallina, C.; Siler, M.; Cucchi, D.; Po, A.; et al. Gli1/DNA interaction is a druggable target for Hedgehog-dependent tumors. *EMBO J.* **2015**, *34*, 200–217. [CrossRef]
26. Cevatemre, B.; Erkisa, M.; Aztopal, N.; Karakas, D.; Alper, P.; Tsimplouli, C.; Sereti, E.; Dimas, K.; Armutak, E.I.I.; Gurevin, E.G.G.; et al. A promising natural product, pristimerin, results in cytotoxicity against breast cancer stem cells in vitro and xenografts in vivo through apoptosis and an incomplete autopaghy in breast cancer. *Pharmacol. Res.* **2018**, *129*, 500–514. [CrossRef]
27. Cevatemre, B.; Botta, B.; Mori, M.; Berardozzi, S.; Ingallina, C.; Ulukaya, E. The plant-derived triterpenoid tingenin B is a potent anticancer agent due to its cytotoxic activity on cancer stem cells of breast cancer in vitro. *Chem. Biol. Interact.* **2016**, *260*, 248–255. [CrossRef]
28. Lipinski, C.A.; Lombardo, F.; Dominy, B.W.; Feeney, P.J. Experimental and Computational Approaches to Estimate Solubility and Permeability in Drug Discovery and Development Settings. *Adv. Drug Deliv. Rev.* **2001**, *46*, 3–26. [CrossRef]
29. Veber, D.F.; Johnson, S.R.; Cheng, H.-Y.; Smith, B.R.; Ward, K.W.; Kopple, K.D. Molecular Properties that Influence the Oral Bioavailability of Drug Candidates. *J. Med. Chem.* **2002**, *45*, 2615–2623. [CrossRef]
30. Lobell, M.; Hendrix, M.; Hinzen, B.; Keldenich, J.; Meier, H.; Schmeck, C.; Schohe-Loop, R.; Wunberg, T.; Hillisch, A. In Silico ADMET Traffic Lights as a Tool for the Prioritization of HTS Hits. *ChemMedChem* **2006**, *1*, 1229–1236. [CrossRef]
31. Daina, A.; Zoete, V. A BOILED-Egg to Predict Gastrointestinal Absorption and Brain Penetration of Small Molecules. *ChemMedChem* **2016**, *11*, 1117–1121. [CrossRef] [PubMed]
32. Egan, W.J.; Merz, K.M.; Baldwin, J.J. Prediction of Drug Absorption Using Multivariate Statistics. *J. Med. Chem.* **2000**, *43*, 3867–3877. [CrossRef] [PubMed]
33. Muegge, I.; Heald, S.L.; Brittelli, D. Simple Selection Criteria for Drug-like Chemical Matter. *J. Med. Chem.* **2001**, *44*, 1841–1846. [CrossRef]
34. Baell, J.B.; Holloway, G.A. New Substructure Filters for Removal of Pan Assay Interference Compounds (PAINS) from Screening Libraries and for Their Exclusion in Bioassays. *J. Med. Chem.* **2010**, *53*, 2719–2740. [CrossRef] [PubMed]
35. Irwin, J.J.; Duan, D.; Torosyan, H.; Doak, A.K.; Ziebart, K.T.; Sterling, T.; Tumanian, G.; Shoichet, B.K. An Aggregation Advisor for Ligand Discovery. *J. Med. Chem.* **2015**, *58*, 7076–7087. [CrossRef]
36. Nelson, K.M.; Dahlin, J.L.; Bisson, J.; Graham, J.; Pauli, G.F.; Walters, M.A. The Essential Medicinal Chemistry of Curcumin. *J. Med. Chem.* **2017**, *60*, 1620–1637. [CrossRef]
37. Shoichet, B.K. Screening in a Spirit Haunted World. *Drug Discov. Today* **2006**, *11*, 607–615. [CrossRef]
38. Morrison, J.F. The slow-binding and slow, tight-binding inhibition of enzyme-catalysed reactions. *Trends Biochem. Sci.* **1982**, *7*, 102–105. [CrossRef]
39. Markowicz, J.; Uram, Ł.; Sobich, J.; Mangiardi, L.; Maj, P.; Rode, W. Antitumor and Anti-Nematode Activities of α-Mangostin. *Eur. J. Pharmacol.* **2019**, *863*, 172678. [CrossRef]
40. Rozanov, D.; Cheltsov, A.; Nilsen, A.; Boniface, C.; Forquer, I.; Korkola, J.; Gray, J.; Tyner, J.; Tognon, C.E.; Mills, G.B.; et al. Targeting Mitochondria in Cancer Therapy Could Provide a Basis for the Selective Anti-Cancer Activity. *PLoS ONE* **2019**, *14*, e0205623. [CrossRef]
41. Hou, A.-J.; Fukai, T.; Shimazaki, M.; Sakagami, H.; Sun, H.-D.; Nomura, T. Benzophenones and Xanthones with Isoprenoid Groups from Cudrania Cochinchinensis. *J. Nat. Prod.* **2001**, *64*, 65–70. [CrossRef] [PubMed]

42. Romar, G.A.; Kupper, T.S.; Divito, S.J. Research Techniques Made Simple: Techniques to Assess Cell Proliferation. *J. Investig. Dermatol.* **2016**, *136*, e1–e7. [CrossRef]
43. Abduljauwad, S.N.; Ahmed, H.-R. Enhancing Cancer Cell Adhesion with Clay Nanoparticles for Countering Metastasis. *Sci. Rep.* **2019**, *9*, 1–12. [CrossRef] [PubMed]
44. Elmore, S. Apoptosis: A Review of Programmed Cell Death. *Toxicol. Pathol.* **2007**, *35*, 495–516. [CrossRef] [PubMed]
45. Waterhouse, N.J.; Goldstein, J.C.; von Ahsen, O.; Schuler, M.; Newmeyer, D.D.; Green, D.R. Cytochrome c Maintains Mitochondrial Transmembrane Potential and ATP Generation after Outer Mitochondrial Membrane Permeabilization during the Apoptotic Process. *J. Cell Biol.* **2001**, *153*, 319–328. [CrossRef]
46. Pradelli, L.A.; Villa, E.; Zunino, B.; Marchetti, S.; Ricci, J.-E. Glucose Metabolism Is Inhibited by Caspases upon the Induction of Apoptosis. *Cell Death Dis.* **2014**, *5*, e1406. [CrossRef]
47. Oropesa, M.; de la Mata, M.; Maraver, J.G.; Cordero, M.D.; Cotán, D.; Rodríguez-Hernández, A.; Domínguez-Moñino, I.; de Miguel, M.; Navas, P.; Sánchez-Alcázar, J.A. Apoptotic Microtubule Network Organization and Maintenance Depend on High Cellular ATP Levels and Energized Mitochondria. *Apoptosis* **2011**, *16*, 404–424. [CrossRef]
48. Jarmuła, A.; Wilk, P.; Maj, P.; Ludwiczak, J.; Dowierciał, A.; Banaszak, K.; Rypniewski, W.; Cieśla, J.; Dąbrowska, M.; Frączyk, T.; et al. Crystal Structures of Nematode (Parasitic *T. spiralis* and Free Living *C. elegans*), Compared to Mammalian, Thymidylate Synthases (TS). Molecular Docking and Molecular Dynamics Simulations in Search for Nematode-Specific Inhibitors of TS. *J. Mol. Graph. Model.* **2017**, *77*, 33–50. [CrossRef]
49. McKellar, Q.A.; Scott, E.W. The Benzimidazole Anthelmintic Agents-a Review. *J. Vet. Pharmacol. Ther.* **1990**, *13*, 223–247. [CrossRef]
50. Simpkin, K.G.; Coles, G.C. The Use of *Caenorhabditis elegans* for Anthelmintic Screening. *J. Chem. Technol. Biotechnol.* **1981**, *31*, 66–69. [CrossRef]
51. Fukai, T.; Oku, Y.; Hou, A.J.; Yonekawa, M.; Terada, S. Antimicrobial activity of hydrophobic xanthones from *Cudrania cochinchinensis* against *Bacillus subtilis* and methicillin-resistant *Staphylococcus aureus*. *Chem. Biodivers.* **2004**, *1*, 1385–1390. [CrossRef] [PubMed]
52. Fukai, T.; Oku, Y.; Hou, A.J.; Yonekawa, M.; Terada, S. Antimicrobial Activity of Isoprenoid-Substituted Xanthones from *Cudrania Cochinchinensis* against Vancomycin-Resistant Enterococci. *Phytomedicine* **2005**, *12*, 510–513. [CrossRef]
53. Wang, Y.-H.; Hou, A.-J.; Zhu, G.-F.; Chen, D.-F.; Sun, H.-D. Cytotoxic and Antifungal Isoprenylated Xanthones and Flavonoids from Cudrania Fruticosa. *Planta Med.* **2005**, *71*, 273–274. [CrossRef] [PubMed]
54. McGann, M. FRED Pose Prediction and Virtual Screening Accuracy. *J. Chem. Inf. Model.* **2011**, *51*, 578–596. [CrossRef] [PubMed]
55. FRED 3.0.1 OpenEye Scientific Software, Santa Fe, NM. Available online: http://www.eyesopen.com (accessed on 21 June 2020).
56. OMEGA 3.0.1.2: OpenEye Scientific Software, Santa Fe, NM. Available online: http://www.eyesopen.com (accessed on 21 June 2020).
57. Hawkins, P.C.D.; Skillman, A.G.; Warren, G.L.; Ellingson, B.A.; Stahl, M.T. Conformer Generation with OMEGA: Algorithm and Validation Using High Quality Structures from the Protein Databank and Cambridge Structural Database. *J. Chem. Inf. Model.* **2010**, *50*, 572–584. [CrossRef]
58. Chen, D.; Jansson, A.; Sim, D.; Larsson, A.; Nordlund, P. Structural analyses of human thymidylate synthase reveal a site that may control conformational switching between active and inactive states. *J. Biol. Chem.* **2017**, *292*, 13449–13458. [CrossRef]
59. Lagorce, D.; Bouslama, L.; Becot, J.; Miteva, M.A.; Villoutreix, B.O. FAF-Drugs4: Free ADME-Tox Filtering Computations for Chemical Biology and Early Stages Drug Discovery. *Bioinformatics* **2017**, *33*, 3658–3660. [CrossRef]
60. Daina, A.; Michielin, O.; Zoete, V. SwissADME: A Free Web Tool to Evaluate Pharmacokinetics, Drug-Likeness and Medicinal Chemistry Friendliness of Small Molecules. *Sci. Rep.* **2017**, *7*, 42717. [CrossRef]
61. Kim, C.-K.; Ebizuka, Y.; Sankawa, U. Two new isoflavonoids from *Echinosophora koreensis* Nakai and the structure revision of sophoronol. *Chem. Pharm. Bull.* **1989**, *37*, 2879–2881. [CrossRef]

62. Delle Monache, F.; Delle Monache, G.; Marini-Bettolo, G.B.; Albuquerque, M.F.D.; Mello, F.D.; Lima, O.G.D. Flavonoids of *Sophora tomentosa* (Leguminosae). II. Isosophoranone, a new diprenylated isoflavanone. *Gazz. Chim. Ital.* **1977**, *107*, 189–192. [CrossRef]
63. Delle Monache, F.; Delle Monache, G.; Marini-Bettolo, G.B.; Albuquerque, M.F.D.; Mello, F.D.; Lima, O.G.D. Flavonoids of *Sophora tomentosa* (Leguminosae). I. sophoronol, a new 3-hydroxyflavanone. *Gazz. Chim. Ital.* **1976**, *106*, 935–945.
64. Khan, I.U.; Ansari, W.H. flavonol glycosides from *Callitris Glauca*. *Phytochemistry* **1987**, *26*, 1221–1222. [CrossRef]
65. Brum, R.L.; Cavalheiro, A.J.; Delle Monache, F.; Vencato, I. Jatrowediol, a Lathyrane Diterpene from *Jatropha weddelliana*. *J. Braz. Chem. Soc.* **2001**, *12*, 259–262. [CrossRef]
66. Delle Monache, F.; De Lima, O.G.; De Mello, J.F.; Delle Monache, G.; Marini Bettolo, G.B. Chroman- and cromene-chalcones from Cordoin and Isocordoin. *Gazz. Chim. Ital.* **1973**, *103*, 779–784.
67. Asakawa, Y. Chemical Constituents of *Alnus sieboldiana* (BETULACEAE) II. The Isolation and Structure of Flavonoids and Stilbenes. *Bull. Chem. Soc. Jpn.* **1971**, *44*, 2761–2766. [CrossRef]
68. Akcos, Y.; Ezer, N.; Çalis, I.; Demirdamar, R.; Tel, B.C. Polyphenolic Compounds of Sideritis lycia and Their Anti-Inflammatory Activity. *Pharm. Biol.* **1999**, *37*, 118–122. [CrossRef]
69. Fukai, T.; Wang, Q.H.; Inami, R.; Nomura, T. Structures of Prenylated Dihydrochalcone, Gancaonin J and Homoisoflavonone, Gancaonin K from *Glycyrrhiza pallidiflora*. *Heterocycles* **1990**, *31*, 643–650. [CrossRef]
70. Ágnes, K. Természetes eredetű, potenciálisan biológiailag aktív O- és Cprenilezett flavanonok szintézise. Ph.D. Thesis, University of Debrecen, Debrecen, Hungary, Debrecen, 2007. Available online: https://adoc.tips/termeszetes-eredet-potencialisan-biologiailag-aktiv-o-es-c-p.html (accessed on 21 June 2020).
71. Wolfrom, M.L.; Komitsky, F.; Mundell, P.M. Osage Orange Pigments. XVI. The Structure of Alvaxanthone. *J. Org. Chem.* **1965**, *30*, 1088–1091. [CrossRef]
72. Morales Moisela, M.M.; Brel, O.; Bourdy, G.; de La Cruz, M.G.; Castro Dionicio, I.Y.; Carraz, M.; Jullian, V. Xanthones from *Hypericum laricifolium* Juss., and their antiproliferative activity against HEP3B cells. *Rev. Soc. Quím. Perú* **2018**, *84*, 428–435.
73. Delle Monache, F.; Marquina, M.; Delle Monache, G.; Marini Bettolo, G.B.; Alves De lima, R. Xanthones, xanthonolignoids and other constituents of the roots of *Vismia guaramirangae*. *Phytochemistry* **1983**, *22*, 227–232. [CrossRef]
74. Delle Monache, F.; Botta, B.; Nicoletti, M.; de Barros Coêlho, J.S.; de Andrade Lyra, F.D. Three new xanthones and macluraxanthone from Rheedia benthamiana PI. Triana (Guttiferae). *J. Chem. Soc. Perkin Trans.* **1981**, *1*, 484–488. [CrossRef]
75. Rui, D.; Chen, X.; Li, Z.; Tang, L. Chemical Constituents of Hypericum petiolulatum. *Chem. Nat. Compd.* **2017**, *53*, 457–462. [CrossRef]
76. Rode, W.; Kulikowski, T.; Kedzierska, B.; Shugar, D. Studies on the Interaction with Thymidylate Synthase of Analogues of 2′-Deoxyuridine-5′-Phosphate and 5-Fluoro-2′-Deoxyuridine-5′-Phosphate with Modified Phosphate Groups. *Biochem. Pharmacol.* **1987**, *36*, 203–210. [CrossRef]

Sample Availability: Samples of the compounds might be available upon request. the compounds … … are available from.

International Journal of
Molecular Sciences

MDPI

Article

Biotin Transport-Targeting Polysaccharide-Modified PAMAM G3 Dendrimer as System Delivering α-Mangostin into Cancer Cells and *C. elegans* Worms

Joanna Markowicz [1,*], Łukasz Uram [1], Stanisław Wołowiec [2] and Wojciech Rode [3,*]

[1] Faculty of Chemistry, Rzeszow University of Technology, 6 Powstancow Warszawy Ave., 35-959 Rzeszow, Poland; luram@prz.edu.pl
[2] Medical College, Rzeszow University, 1a Warzywna Str., 35-310 Rzeszow, Poland; swolowiec@ur.edu.pl
[3] Nencki Institute of Experimental Biology, 3 Pasteur Street, 02-093 Warsaw, Poland
* Correspondence: jmarkowicz@stud.prz.edu.pl (J.M.); w.rode@nencki.edu.pl (W.R.)

Abstract: The natural xanthone α-mangostin (αM) exhibits a wide range of pharmacological activities, including antineoplastic and anti-nematode properties, but low water solubility and poor selectivity of the drug prevent its potential clinical use. Therefore, the targeted third-generation poly(amidoamine) dendrimer (PAMAM G3) delivery system was proposed, based on hyperbranched polymer showing good solubility, high biocompatibility and low immunogenicity. A multifunctional nanocarrier was prepared by attaching αM to the surface amine groups of dendrimer via amide bond in the ratio 5 ($G3^{2B12gh5M}$) or 17 ($G3^{2B10gh17M}$) residues per one dendrimer molecule. Twelve or ten remaining amine groups were modified by conjugation with D-glucoheptono-1,4-lactone (gh) to block the amine groups, and two biotin (B) residues as targeting moieties. The biological activity of the obtained conjugates was studied in vitro on glioma U-118 MG and squamous cell carcinoma SCC-15 cancer cells compared to normal fibroblasts (BJ), and in vivo on a model organism *Caenorhabditis elegans*. Dendrimer vehicle $G3^{2B12gh}$ at concentrations up to 20 μM showed no anti-proliferative effect against tested cell lines, with a feeble cytotoxicity of the highest concentration seen only with SCC-15 cells. The attachment of αM to the vehicle significantly increased cytotoxic effect of the drug, even by 4- and 25-fold for $G3^{2B12gh5M}$ and $G3^{2B10gh17M}$, respectively. A stronger inhibition of cells viability and influence on other metabolic parameters (proliferation, adhesion, ATP level and Caspase-3/7 activity) was observed for $G3^{2B10gh17M}$ than for $G3^{2B12gh5M}$. Both bioconjugates were internalized efficiently into the cells. Similarly, the attachment of αM to the dendrimer vehicle increased its toxicity for *C. elegans*. Thus, the proposed α-mangostin delivery system allowed the drug to be more effective in the dendrimer-bound as compared to free state against both cultured the cancer cells and model organism, suggesting that this treatment is promising for anticancer as well as anti-nematode chemotherapy.

Keywords: α-mangostin; poly(amidoamine) dendrimer; targeted drug delivery; biotin targeting; glioblastoma multiforme; squamous cell carcinoma; antiparasitic therapy

Citation: Markowicz, J.; Uram, Ł.; Wołowiec, S.; Rode, W. Biotin Transport-Targeting Polysaccharide-Modified PAMAM G3 Dendrimer as System Delivering α-Mangostin into Cancer Cells and *C. elegans* Worms. *Int. J. Mol. Sci.* **2021**, *22*, 12925. https://doi.org/10.3390/ijms222312925

Academic Editor: Angela Stefanachi

Received: 25 October 2021
Accepted: 26 November 2021
Published: 29 November 2021

1. Introduction

The isoprenylated xanthone α-mangostin (αM) was firstly isolated from the pericarp of mangosteen tree (*Garcinia mangostana* L., *Clusiaceae*) that has long been used in traditional medicine in Southeast Asia to treat inflammation, ulcer, skin infection, and wounds [1]. Nowadays, numerous in vitro and in vivo studies have proved that mangostins possess diverse pharmacological activities, such as antioxidant, anti-inflammatory, antibacterial, antifungal, antimalarial, anticancer and anthelmintic [2–5].

Considering the potential pharmacological application of αM, it is significantly limited by its low water solubility (2.03×10^{-4} mg/L at 25 °C) [6], a major obstacle in achieving maximum drug bioavailability and accumulation in the target organs. The latter, together

with insufficient target selectivity in the human body, resulted in the fact that αM has not been approved for clinical use.

One strategy increasing the concentration of biologically active substances in target locations and cells is to take advantage of a drug delivery agent [7], e.g., to bind a drug with nanoparticles, in order to improve its physicochemical properties and transport. Among the αM delivery systems tested so far, nanolipids, nanopolymers, nanomicelles, nanoliposomes, nanoemulsion, nanofibers and metal nanoparticles have been studied [8], e.g., αM-loaded fibroin nanoparticles (FNPs) crosslinked with EDC or PEI, compared to the free αM, confirmed the crosslinked FNPs to increase the drug's solubility by about 3-fold [9], as well as to offer sustained drug release and reduced hematotoxicity. Anticancer studies of these nanoparticles with Caco-2 colorectal and MCF-7 breast adenocarcinoma cell lines showed αM to cause apoptosis with cytotoxicity exceeding that of free drug. Additionally, cyclodextrin-based hyperbranched polymer nanoparticles (CDNPs) were used [10] to solubilize αM encapsulated in the CD cavity. They assumed that release of αM in the slow mode is essential for its retention until the cancerous region is reached. Samprasit et al. [11] used αM-loaded mucoadhesive nanoparticles as colon-targeted drug delivery. They proved that chitosan and thiolated chitosan nanoparticles crosslinked by genipin (GP) and modified by Eudragit® L100 increased αM loading limited the release of the drug in the upper gastrointestinal tract, and enhanced its delivery to the colon.

The vast majority of the proposed carriers encapsulate αM; moreover, there are many potential carriers that allow binding it via covalent bonds and significantly increase the stability of such a system. An interesting example presents poly(amidoamine) dendrimers (PAMAM) that are spheroidal or ellipsoidal three-dimensional polymers with the peripheral functional groups and internal cavities. PAMAM dendrimers may be favorably used in drug delivery due to their hydrophilic, biocompatible, and non-immunogenic nature [12], having been applied as targeting drug or gene delivery systems and as diagnostic agents. Drugs or biologically active molecules can be encapsulated in the interior space of dendrimers, attracted by electrostatic interactions or linked via surface groups [13], but covalently attached drugs, e.g., methotrexate, are more stable compared to non-covalent drugs [14]. Additionally, polyvalency of PAMAMs has a potential role in intracellular targeted drug delivery by surface modification [13]. Especially in anticancer therapy, drug targeting is important in order to maximize the therapeutic potential in tumor area with minimizing side effects in normal tissues [15]. The PAMAM dendrimers present the platform for surface modification with numerous ligand moieties that can improve active targeting to the cancer cells and increase tumor specificity with minimum systemic toxicity [12]. Examples of such ligands include monoclonal antibodies, polypeptides, antibody–drug conjugates, nucleic acids and signal transduction inhibitors [16]. Additionally, vitamins, such as folic acid and biotin, are promising molecules targeting nanoparticles and potential drugs conjugates into cancer cells overexpressing folate and biotin receptors, respectively, e.g., breast, ovarian, lung, and colon cancer cells [17–19]. Notably, biotinylated dendrimers have been demonstrated to be absorbed into cells stronger than non-biotinylated [20,21].

The aim of this study was to design, synthesize, characterize, and investigate the biological, anti-cancer activity of biotin-targeted, polysaccharide modified PAMAM G3 dendrimers substituted covalently by αM ($G3^{2B12gh5M}$ and $G3^{2B10gh17M}$, differing by the substitution level) against human grade IV glioma U-118 MG cells, human squamous cell carcinoma (SCC-15), compared to normal human fibroblasts (BJ), with the three cell lines found previously to accumulate biotin [22]. The effects of the above-mentioned conjugates or their vehicle ($G3^{2B12gh}$) on viability, proliferation, adhesion, apoptosis, as well as the intracellular ATP level were determined. Cellular accumulation and localization of fluorescently labeled analogues were also evaluated. Additionally, the in vivo toxicity of dendrimer conjugates and αM was tested with model nematode *Caenorhabditis elegans*, which has been used extensively in toxicological studies of many nanoparticles and as a model organism providing insights into cancer cells metabolism, also allowing to assess the anti-parasitic activity.

2. Materials and Methods

2.1. Reagents

α-Mangostin (αM, purity ≥ 98% (HPLC)) was purchased from Aktin Chemicals, Inc. (Chengdu, China). Ethylenediamine, methyl acrylate, D-glucoheptono-1,4-lactone (GHL), biotin *N*-hydroxysuccinimide ester (NHS-Biotin), 4-nitrophenyl chloroformate (NPCF), 2-Chloro-1-methylpyridinium iodide (Mukaiyama reagent), 4-dimethylaminopyridine (DMAP), 6-[fluorescein-5(6)-carboxamido]hexanoic acid (FCH), dimethyl sulfoxide (dmso) and other reagents used in syntheses were obtained from Merck KGaA (Darmstadt, Germany). Spectra/Por® 3 RC dialysis membrane (cellulose, MW_{cutoff}–3.5 kD) was provided by Carl Roth GmbH & Co. KG (Karlsruhe, Germany).

Human glioblastoma (U-118 MG, ATCC® HTB-15), human squamous cell carcinoma (SCC-15, ATCC® CRL-1623), and human normal fibroblast (BJ, ATCC® CRL-2522) cell lines were purchased from the American Type Culture Collection (ATCC, Manassas, VA, USA). Dulbecco's Modified Eagle's Media (DMEM and DMEM/ F-12), Eagle's Minimum Essential Medium (EMEM), and fetal bovine serum (FBS) were obtained from Corning Inc. (New York, NY, USA). Penicillin and streptomycin solution, phosphate-buffered saline (PBS) with and without magnesium and calcium ions, and DAPI (4′,6-diamidino-2-phenylindole, dihydrochloride), Hoechst 33342, and MitoTracker™ Deep Red FM were provided by Thermo Fisher Scientific Inc. (Waltham, MA, USA). Trypsin-EDTA solution, hydrocortisone, 0.33% neutral red solution (3-amino-m-dimethylamino-2-methyl-phenazine hydrochloride), XTT sodium salt (2,3-bis[2-methoxy-4-nitro-5-sulfophenyl]-2H-tetrazolium-5-carboxanilide inner salt), phenazinemethosulfate (PMS), crystal violet, 0.4% trypan blue solution, dimethylsulfoxide (dmso) for molecular biology, 5-Fluoro-2′-deoxy-uridine (FUdR), and other chemicals and buffers were purchased from Merck KGaA (Darmstadt, Germany). CellTiter-Glo® Luminescent Cell Viability Assay and Apo-ONE® Homogenous Caspase-3/7 Assay were obtained from Promega Corporation (Madison, WI, USA). Cell cultures dishes and materials were from Corning Incorporated (Corning, NY, USA), Greiner (Kremsmünster, Austria), or Nunc (Roskilde, Denmark). All reagents used for *C. elegans* culture and synchronization were supplied by Sigma-Aldrich (Saint Louis, MO, USA) or Carl Roth GmbH & Co., KG (Karlsruhe, Germany).

2.2. Chemical Syntheses and Purification Methods

2.2.1. PAMAM G3 Conjugation with Biotin

PAMAM G3 dendrimer was synthesized starting from an ethylenediamine core by repeatable two-step procedure according to Tomalia's protocol [23] and stored as 20.1 mM solution in methanol for further use. Then PAMAM G3, after prior methanol evaporation, was substituted with two equivalents of biotin by stepwise addition of 99 mg (290 μmoles) of solid NHS-Biotin to 695 mg of G3 (145 μmoles) dissolved in 4 mL of dmso with vigorous stirring. The solution was left at 50 °C for 4 h, then transferred into dialytic tube (cellulose, MW_{cutoff} = 3.5 kD) and dialyzed for 3 days against water (7 × 3 L). Afterwards, the solvent was removed by vacuum rotary evaporation and dried under high vacuum overnight. The product was identified by ^{1}H NMR spectroscopy as G3 substituted with average two residues of amide-bonded biotin $G3^{2B}$, as described before [24,25]. The isolated yield of the product was 47% (501 mg; 68 μmoles; MW_{calc} = 7362 g mol^{-1}).

2.2.2. Activation of α-Mangostin with NPCF and Attachment to $G3^{2B}$

α-Mangostin (αM) was activated with 4-nitrophenyl chloroformate (NPCF; 10% molar excess), which further provided one carbon linker between hydroxyl group of αM and amino group of PAMAM G3. Thus, 223.3 mg (544 μmoles) of αM was dissolved in 25 mL of chloroform, then 120.6 mg (598 μmoles) of NPCF was added in portions as solid with vigorous stirring. To this solution, 146.6 mg (1200 μmoles) of 4-dimethylaminopyridine (DMAP) was added and the mixture was heated under reflux for 4 h. Then, chloroform was removed by vacuum rotary evaporation and remained solid dried under high vacuum. The solid product, α-mangostin 4-nitrophenylcarbonate (αM-NPC) was dissolved in 10 mL

dmso to obtain 54.4 mM stock solution. This solution (6 mL, 326.4 μmoles of αM-NPC, 143 mg of αM) was added dropwise into 162 mg of $G3^{2B}$ (22 μmoles) in 1.6 mL dmso to obtain highly substituted conjugate [A]. In another synthesis process, stock solution of αM-NPC (2 mL, 109 μmoles) was added to 22 μmoles of $G3^{2B}$ in 1.6 mL dmso [B]. In both cases, the mixtures were heated at 50 °C for 3 h, then dialyzed and isolated solids were dried in vacuo. Yields: 273.2 mg, 91.4% for [A], identified by ^{1}H NMR spectroscopy as $G3^{2B17M}$ and 188.7 mg, 90% for [B], identified by ^{1}H NMR spectroscopy as $G3^{2B5M}$. Long-lasting dialysis of synthesized conjugates, especially $G3^{2B17M}$ (4 days, 12 times 5 L of receiving water), resulted in loss of low-substituted fraction of $G3^{2BxM}$ (x < 5). During the dialytic process, immediate precipitation of highly substituted derivatives was observed. The solids inside dialytic tubes were irritated throughout dialysis in order to remove solid-entrapped low molecular weight DMAP, *p*-nitrophenol, dmso, and other reagents. The products [A] and [B] were further converted by reaction with GHL (vide infra).

2.2.3. $G3^{2B}$ and $G3^{2BM}$ Supplementation with D-Glucoheptono-1,4-lactone

To the solutions of $G3^{2B17M}$ and $G3^{2B5M}$ obtained in the previous step according to protocol [A] and [B] (ca 20 μmoles each), in 5 mL dmso, 264 μmoles of solid GHL (54.9 mg) were added in portions with vigorous stirring. The mixtures were left for 16 h at 50 °C. Thereafter, purification was performed according to the procedure described earlier (3 days of dialysis followed by 24 h drying under high vacuum).

The steps of synthesis of dendrimer PAMAM G3 conjugates with α-mangostin, biotin and D-glucoheptono-1,4-lactone is presented in the Scheme 1.

The obtained conjugates were characterized by the ^{1}H NMR (Figures 1 and 2), and 2-D ^{1}H-^{1}H COSY spectroscopy in dmso-d_6 (Figure S1), which revealed the level of PAMAM $G3^{2B}$ substitution by αM and gh residues: $G3^{2B12gh}$, $G3^{2B12gh5M}$, and $G3^{2B10gh17M}$, with the isolated yield 94.5% (20.8 μmoles, MW_{calc} = 9859 g mol^{-1}), 86% (19 μmoles, MW_{calc} = 11,660 g mol^{-1}), and 91% (20 μmoles, MW_{calc} = 16,896 g mol^{-1}), respectively.

Analytical Data

^{1}H NMR (dmso-d_6; for atom numbering see Scheme 1): chemical shift [ppm] (intensity, multiplicity, assignment):

α-Mangostin (Figure 1A): 13.72 ([1H], s, $1'^{M}$); 11.01 ([1H], bs, $3'^{M}$); 10.82 ([1H], bs, $6'^{M}$); 6.80 ([1H], s, 5^{M}); 6.34 ([1H], s, 4^{M}); 5.16 ([2H], t overlapped, $12,17^{M}$); 4.01 ([2H], d, 11^{M}); 3.70 ([3H], s, $7'^{M}$); 3.34 (s, HDO); 3.21 ([2H], d, 16^{M}); 1.70 ([12H], m, $14,15,19,20^{M}$).

$G3^{2B12gh5M}$ (Figure 1B): 7.10 ([5H], s, NH(carbamate)); 6.51 ([5H], s, 5^{M}); 6.26 ([5H], s, 4^{M}); 5.17 ([10H], t overlapped, $12,17^{M}$); 3.95 ([10H], m, 11^{M}); 3.68 ([15H], s, $7'^{M}$); 1.69 ([60H], overlapped s, $14,15,19,20^{M}$); PAMAM G3 CH_2 broad resonances: 3.12, 2.64, 2.42, 2.19 [484H]; PAMAM G3 NH: 8.0 ppm, [73H]; Biotin resonances: 6.43 ([4H], bs, 10^{B} and 11^{B}); 4.31 and 4.14 ([2H] and [2H], 8^{B} and 9^{B}); 2.04 ([4H], 2^{B}); 1.49–1.22 ([12H], 3^{B},4^{B},5^{B}); gh resonances: 3.87 and 3.58–3.36 ([84H], s and m, CH^{gh}).

$G3^{2B10gh17M}$ (Fig 1C): 6.65 ([17H], s, 5^{M}); 6.29 ([17H], s, 4^{M}); 5.16 ([34H], t overlapped, $12,17^{M}$); 3.99 ([34H]; d, 11^{M}); 3.70 ([51H], s, $7'^{M}$); 3.19 ([34H], d, 16^{M}); 1.70 ([204H], four overlapped singlets, $14,15,19,20^{M}$); PAMAM G3 CH_2 broad resonances: 3.14–2.20 [484H]; PAMAM G3 NH: 8.02 ppm, [60H]; biotin resonances: 6.51 and 6.44 ([4H], s and s, 10^{B} and 11^{B}); 4.31 and 4.13 ([4H], s and s, 8^{B} and 9^{B}); 2.06 ([4H], 2^{B}); 1.51–1.28 ([12H], 3^{B},4^{B},5^{B}); gh resonances: 3.87 and 3.59–3.37 ([70H], s and m, CH^{gh}).

$G3^{2B12gh}$ (Figure 2A): 6.47 ([4H], d, $10,11^{B}$); 4.36 (overlapped singlets, OH^{gh}); 3.66 ([84H], m, CH^{gh}); 1.39 ([12H], m, $3,4,5^{B}$); PAMAM G3 CH_2 broad resonances: 3.10, 2.63, 2.41, 2.19 [480H]; PAMAM G3 NH broad resonance is centered at 8.00 ppm, [78H].

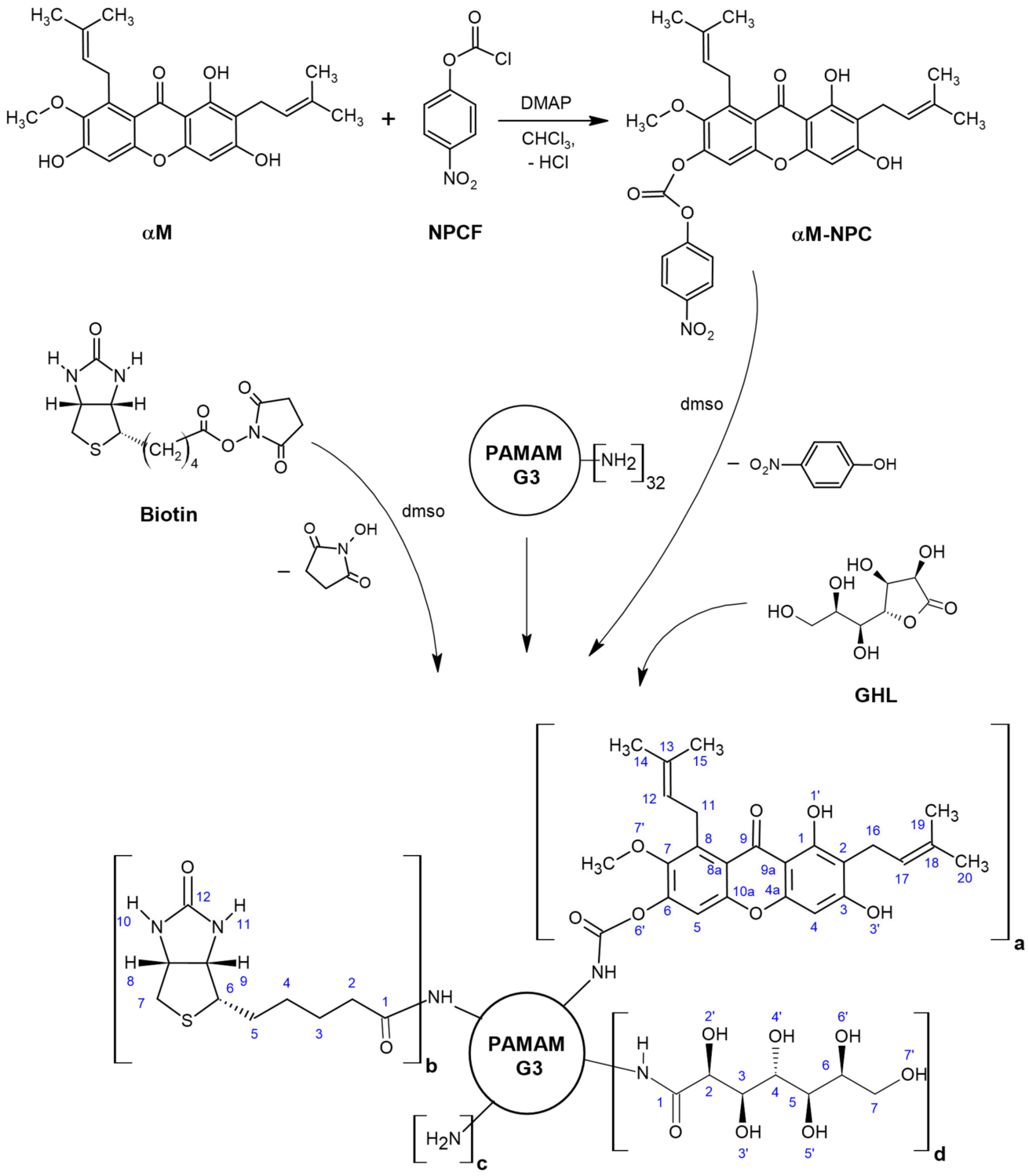

Scheme 1. The scheme of synthesis of dendrimer PAMAM G3 conjugates with αmangostin, biotin and D-glucoheptono-1,4-lactone attached via amide bond. The following conjugates were obtained: $G3^{2B12gh5M}$ (a = 5, b = 2, c = 13, d = 12), $G3^{2B10gh17M}$ (a = 17, b = 2, c = 3, d = 10), and $G3^{2B12gh}$ (a = 0, b = 2, c = 18, d = 12). Abbreviations: NPCF—4-nitrophenyl chloroformate, αM-NPC—p-nitrophenyl) carbonate derivative of αM, DMAP—4-dimethylaminopyridine.

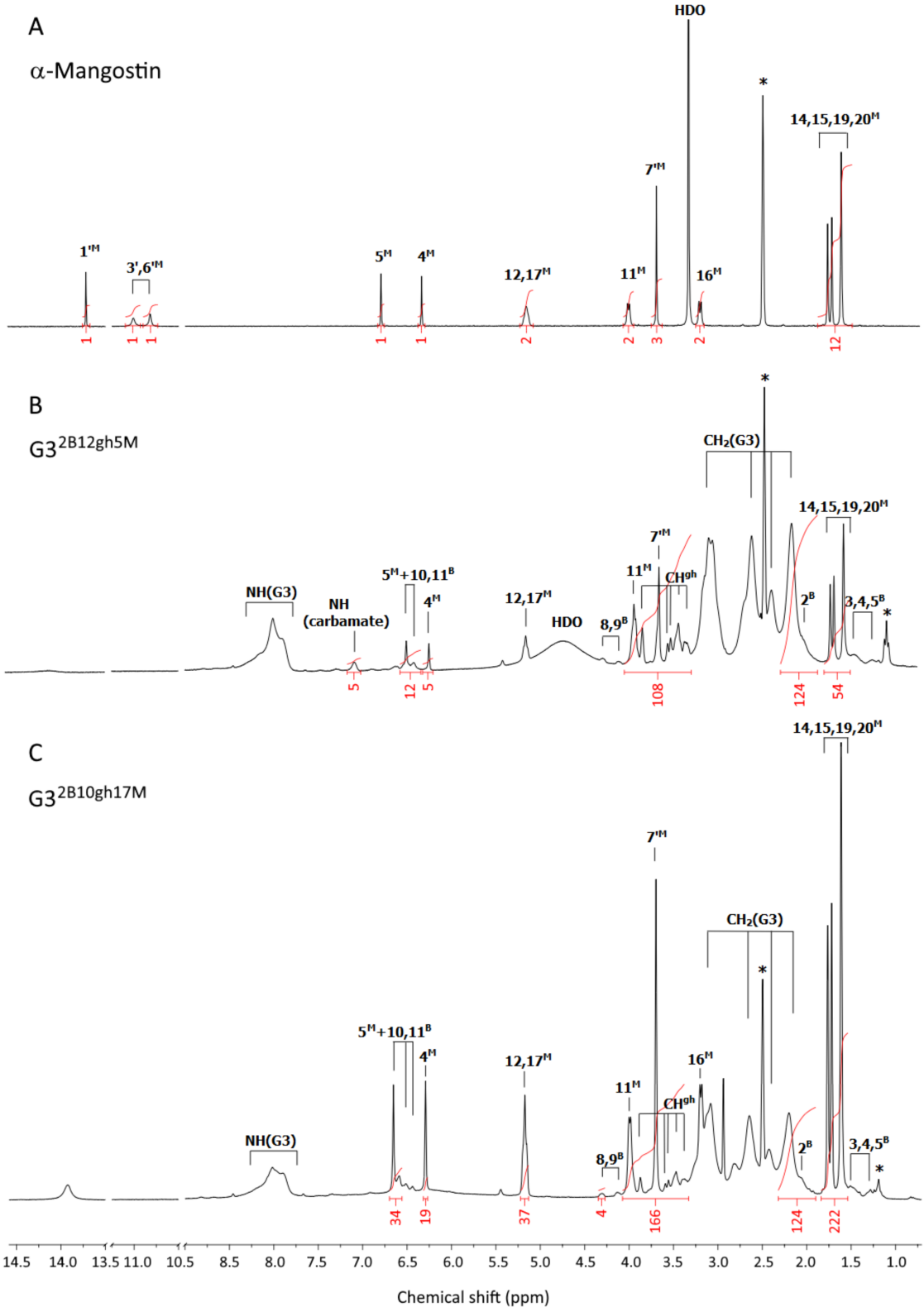

Figure 1. The ^{1}H-NMR spectra of α-mangostin (**A**), G3^{2B12gh5M} (**B**), and G3^{2B10gh17M} (**C**) conjugates in dmso-d$_6$. The residual solvent peak at 2.5 and impurity resonances are marked with asterisks *. The PAMAM G3 core dendrimer resonances are labeled as CH_2(G3) and NH(G3) in spectrum B and C. The resonances of α-mangostin, biotin, and glucoheptoamide are labeled by locants with ^{M}, ^{B}, and ^{gh} upper indexes, respectively, according to the atom numbering in Scheme 1.

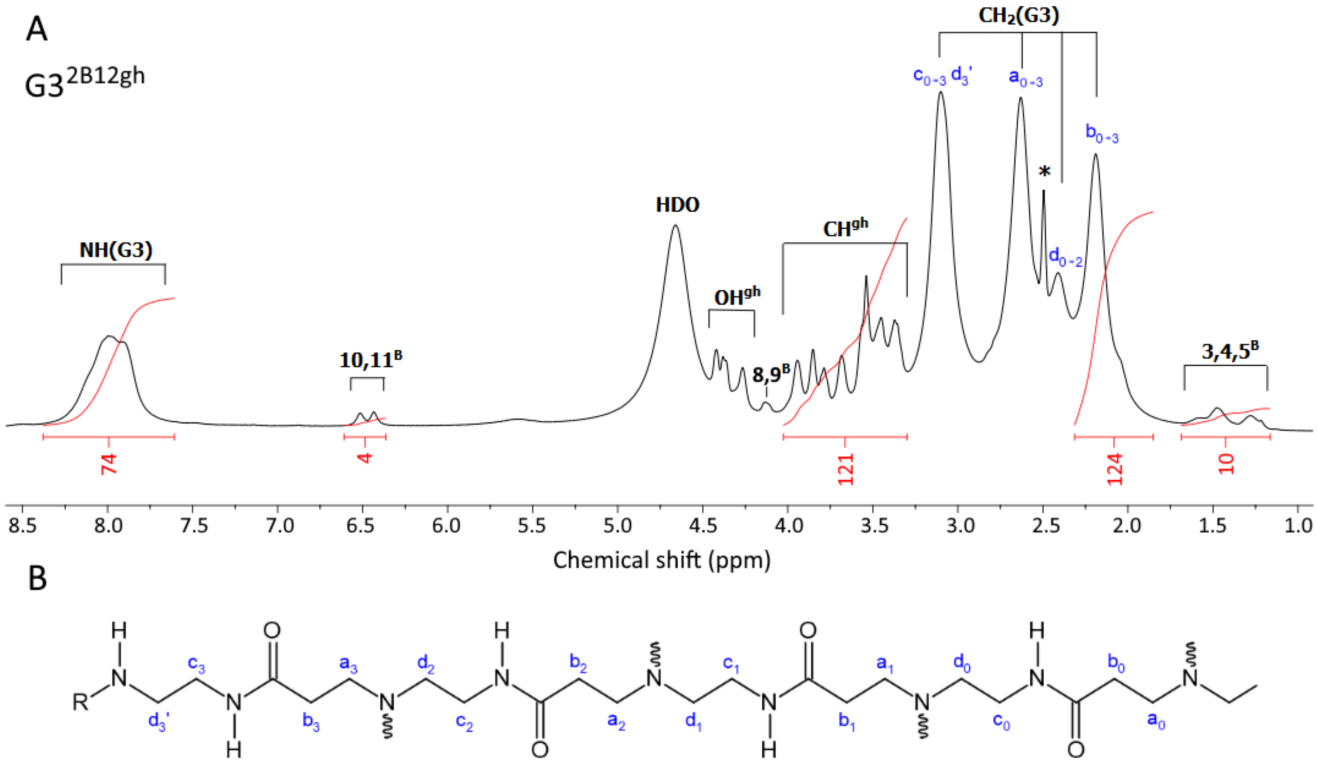

Figure 2. (**A**) The ^{1}H-NMR spectrum of G3^{2B12gh} vehicle in dmso-d$_6$. The PAMAM G3 core dendrimer resonances are labeled as CH_2(G3) and NH(G3). The resonances of biotin and D-glucoheptoamide residues are labeled with locants with ^{B} and ^{gh}. The residual solvent peak is labeled with an asterisk *. For atom numbering, see Scheme 1. (**B**) The selected chain of the PAMAM G3 dendrimer core with carbon atom numbering. Branch points at ternary nitrogen atoms are marked with wavy lines. R = H, biotin or gh residues.

2.2.4. Fluorescent Labeling of the Conjugates

Fluorescently labeled analogues of G3^{2B12gh5M} and G3^{2B10gh17M} were synthesized by attachment of one equivalent of 6-[fluorescein-5(6)-carboxamido]hexanoic acid (FCH) via an ester bond. The carboxyl groups of FCH were activated by Mukaiyama reagent (2-Chloro-1-methylpyridinium iodide). Specifically, 9.0 mg (18 µmoles) of solid FCH was dissolved in 1 mL of dmso with vigorous stirring and protection from light. Then, 6.2 mg (27 µmoles) of Mukaiyama reagent and 6.6 mg (54 µmoles) of DMAP were added with stirring and the mixture was heated at 45 °C for 0.5 h. The activated FCH was divided into two parts and added dropwise to 0.8 mL (7.1 µmoles) of G3^{2B12gh5M} and 2 mL (7.8 µmoles) of G3^{2B10gh17M} in dmso in equimolar amount. Both reaction mixtures were kept on the heating block at 45 °C overnight followed by purification as before. The ^{1}H NMR spectra in dmso-d$_6$ were taken and confirmed the attachment of one equivalent of FCH to the dendrimer conjugates. The isolated yield for G3^{2B12gh5MF} was 59% (4.19 µmoles, MW_{calc} = 12,150 g mol^{-1}) and for G3^{2B10gh17MF} was 53% (4.1 µmoles, MW_{calc} = 17,386 g mol^{-1}). These fluorescent-labeled compounds were used for cellular internalization studies by CLSM.

2.3. NMR Spectroscopy

The 1D ^{1}H and ^{13}C NMR spectra and 2D ^{1}H-^{1}H correlations spectroscopy (COSY), ^{1}H-^{13}C heteronuclear single quantum correlation (HSQC), and heteronuclear multiple bond correlation (HMBC) spectra were recorded in dmso-d$_6$ using Bruker 300 MHz instrument (Rheinstetten, Germany) at College of Natural Sciences, University of Rzeszów.

2.4. Conjugate Size and ζ Potential Measurements

Size and ζ potential of G3^{2B12gh}, G3^{2B12gh5M}, and G3^{2B10gh17M} conjugates were measured using the dynamic light scattering technique at pH 5 (0.05 M acetate buffer) and

in water using the Zetasizer Nano instrument (Malvern, UK) for 1 mg/mL samples (0.7–1.0 mM solutions).

2.5. Biological Studies

2.5.1. Cell Cultures

Human glioblastoma cells (U-118 MG, doubling time—37 h) were grown in DMEM, human squamous carcinoma cells (SCC-15, doubling time—48 h) were cultured in DMEM F-12 supplemented with hydrocortisone (400 ng/mL), and normal human skin fibroblasts (BJ, doubling time—1.9 day) were cultured in EMEM. Culture media were supplemented with heat-inactivated 10% FBS and 100 U/mL penicillin and 1% streptomycin solution. All cell lines were cultured at 37 °C in a humidified atmosphere of 95% air with 5% CO_2. Growth media were changed every 2–3 days and cells were passaged at 80–85% confluence with 0.25% trypsin-0.03% EDTA in PBS (calcium and magnesium ions free). Cell morphology was observed with Nikon TE2000S Inverted Microscope (Tokyo, Japan) with phase contrast. Viability and cell density were estimated by trypan blue exclusion test using Automatic Cell Counter TC20TM (BioRad Laboratories, Hercules, CA, USA). All assays were performed in triplicates in three independent experiments. The working solutions of synthesized dendrimer conjugates were prepared from stock solutions in a corresponding cell culture media by adjusting the dmso concentration to 0.05–0.2% (depending on the type of conjugate), which had no effect on treated cells. Control samples with non-treated cells in complete culture medium with adjusted dmso concentration were included in all assays.

2.5.2. Cytotoxicity (NR and XTT Assays)

The cytotoxicity of PAMAM G3 conjugates with αM ($G3^{2B12gh5M}$ or $G3^{2B10gh17M}$) and the $G3^{2B12gh}$ vehicle was assessed with neutral red uptake (NR) assay and XTT reduction assay. Cells were seeded in flat, clear bottom 96-well culture plates in triplicate (100 µL cell suspension/well) at a density of 1×10^4 cells/well and allowed to attach for 24 h. Then, cells were incubated with working solutions of dendrimer conjugates and vehicle in complete culture medium for 48 h. After that, the NR assay and XTT reduction assay were performed as described in Uram et al. [20]. Additionally, to present cells morphology and the level of accumulation of neutral red dye in lysosomes, microscopic images were collected with a Delta Optical IB-100 microscope with contrast phase under 200× magnification.

2.5.3. Fluorescently Labeled $G3^{2B12gh5M}$ or $G3^{2B10gh17M}$ Cellular Accumulation and Distribution

Cellular accumulation as well as colocalization with nuclei and mitochondria of fluorescently labeled dendrimer conjugates were analyzed using confocal microscopy. Cells were seeded into an 8-well Lab-tek™ Chambered Coverglass (Nunc, Denmark) with a borosilicate glass bottom at a density of 7×10^4 cells/well in 400 µL and placed in an incubator for 24 h. Then, BJ, U118 MG or SCC-15 cells were incubated with non-toxic concentrations of FCH-labeled $G3^{2B12gh5M}$ (1 µM concentration) and $G3^{2B10gh17M}$ (0.1 µM concentration) conjugates, respectively, for 4 or 48 h. After incubation, the dendrimer solution was replaced with an 8 µM Hoechst 33,342 and 50 nM MitoTracker Deep Red FM mixture in growth medium without FBS and incubated at 37 °C for 15 min. Following nuclei and mitochondria staining, cells were washed with PBS (three times) and fixed with 3.7% formaldehyde in PBS. The images were collected in three channels with a confocal microscope (Olympus Fluoview FV10i, Tokyo, Japan) at 361/497 nm for Hoechst, 491/515 nm for FCH, and 644/665 nm for MitoTracker. Images were collected using an objective with water immersion, under a total magnification of 240×. The obtained images had an optical section thickness of app. 1.2 µm. Image analysis was performed with the ImageJ software.

2.5.4. Apoptosis and Intracellular ATP Level

The activity of caspase-3 and -7, the apoptosis marker, was measured to check the ability of the synthesized compounds to induce apoptosis in studied cells. In addition, the intracellular ATP level was assessed. For both parameters, commercially available kits Apo-ONE® Homogenous Caspase-3/7 Assay (Promega) and CellTiter-Glo® Luminescent Cell Viability Assay (Promega) were used. Cells were plated at a density of 1×10^4 per well into a flat, black bottom 96-microplates for apoptosis assay and into a clear 96-microplate for ATP level assay. After 24 h of incubation, cells were treated with the $G3^{2B12gh5M}$ or $G3^{2B10gh17M}$ solutions (100 µL/well) for a further 48 h. Both assays were carried out as described by Uram et al. [26], who used Hoechst 33342 staining to determine the number of cells.

2.5.5. Proliferation

Cell proliferation was estimated using DAPI staining. The 5×10^3 cells/well were seeded into a flat, clear bottom 96-well plates and incubated for 24 h at 37 °C to attach. After removing the growth media, cells were treated with working solutions of $G3^{2B12gh5M}$ or $G3^{2B10gh17M}$ conjugates for 72 h in increasing concentrations. In the next step, plates were centrifuged (5 min, 700 g) and the medium was gently removed. The assay was performed according to Uram et al. [26].

2.5.6. Adhesion

Evaluation of cell adhesion was performed with crystal violet (CV) assay. Cells were seeded into a 96-well clear bottom plates at a density of 1×10^4 cells/well and left 24 h at 37 °C to attach. Afterwards, cells were incubated with working solutions of studied compounds for 48 h and the subsequent operations were carried out as described in Markowicz et al. [5]. Images of the studied cells stained with crystal violet were collected with a Delta Optical IB-100 microscope with contrast phase, with a 10× objective magnification.

2.5.7. Toxicity to Caenorhabditis Elegans and the Worm Survival Analysis

The model organism *Caenorhabditis elegans* was used to estimate in vivo activity of the synthesized dendrimer conjugates and α-mangostin alone in the multicellular system. The wild type *C. elegans* strain N2, variety Bristol, was cultured at 20 °C on NGM agar plates with *E. coli* OP50 lawn as a food source [27]. Survival assay was based on the protocol by Bischof et al. [28] and was adapted to a 96-well plate. Worms at L4 stage were used in the assay and obtained from eggs by prior synchronization of all-stages-nematode population by treatment with hypochlorite. The obtained eggs were left in M9 buffer overnight at room temperature for hatching. The next day, nematodes at L1 stage were transferred to NGM plates with bacterial lawn and grown at 20 °C until the L4 stage (approx. 44 h). After that, the L4 worms were washed twice with distilled water and centrifuged at 250 g followed by resuspension in complete S medium ([29] and centrifugation. Then, the density of nematode suspension was estimated according to Scanlan et al. [30]. Nematodes were suspended in complete S medium supplemented with E. coli OP50 (1:1000), 0.08% cholesterol (5 mg/mL in Et-OH), 1% penicillin-streptomycin, 1% nystatin, and 100 mM FUdR (in final concentration 200 µM) to obtain 20 nematodes in 50 µL transferred to each well. FUdR was added to sterilize nematodes. The working solutions of tested compounds were prepared in the complete S medium with dmso (adjusted to 0.1%, 0.36%, and 0.41% for αM, $G3^{2B12gh5M}$, and $G3^{2B10gh17M}$, respectively) and pipetted (50 µL/well) to a 96-well plate with previously seeded worms. Then, worms were incubated at 20 °C for 7 days. Every day live (moving and curling) and dead nematodes were counted under an inverted microscope. Additionally, images of some morphological changes in nematodes after incubation with $G3^{2B12gh5M}$ were collected using Delta Optical IB-100 microscope under 10× and 20× magnification. The assay was performed in triplicates in three independent experiments.

2.5.8. Statistical Analysis

Due to the lack of a normal distribution of the data in the experimental groups, the non-parametric Kruskal–Wallis test was used to evaluate the differences between dendrimer-treated cells and non-treated control in each cell line. To determine the statistically significant differences between $G3^{2B12gh5M}$ and $G3^{2B10gh17M}$ treated groups, a Mann–Whitney U test was performed. $p \leq 0.05$ was considered statistically significant. The survival curves of *C. elegans* were presented in a plot of the Kaplan–Meier estimator. Statistically significant differences (with $p \leq 0.05$) between treated and non-treated control groups were indicated using Gehan's Wilcoxon test. All analyses and calculations were performed using Statistica 13.3 software (StatSoft Poland, Cracow).

3. Results and Discussion

3.1. Dendrimer Conjugates Synthesis and Characterization

The bioavailability of α-mangostin (αM) is low due to its poor solubility in aqueous solutions, below 0.5 μM at ambient temperature. On the other hand, it has been evidenced that αM shows a wide range of pharmacological activities, including anticancer, antioxidant, anti-inflammatory [31], and antibacterial [32]. In vitro and in vivo studies on various cancer models have proven that the anticancer activity of αM is manifested by, i.a., inhibition of cell proliferation, induction of apoptosis [33,34], and inhibition of metastasis [35]. In order to overcome limitations of αM, we performed several attempts to functionalize it by attachment it to PAMAM dendrimers, which are known to act both as solubilizers for hydrophobic drug molecules and as macromolecular carriers for covalently attached (pro)drugs [36]. Thus, we have used poly(amidoamine) dendrimer of the third generation, G3, as macromolecular carrier, and attempted to bind αM via short link provided by *p*-nitrophenyl chloroformate (NPCF). αM was functionalized with NPCF to obtain *p*-nitrophenylcarbonate derivative, αM-NPC which was further used to bind it to terminal primary amine groups of G3. Although we were able to isolate G3-αM with NPCF-derived carbonyl linker, the water solubility of obtained derivatives was too low to progress with biological tests. Therefore, we converted G3-αM conjugates into more soluble compounds by reaction of remained primary amine groups with D-glucoheptono-1,4-lactone (GHL) to obtain amide-attached polyhydroxyalkyl chains. Two G3-αM derivatives were prepared (Scheme 1) differing by αM substitution levels amounting on average to 17 and 5 residues per dendrimer molecule. These were additionally furnished with two equivalents of amide-attached biotin per dendrimer molecule and exhaustively or semi-exhaustively glucoheptoamidated with GHL. The macromolecular G3 substrate was equipped with 2 biotin to obtain $G3^{2B}$ as before, reacted with αM-NPC, and further converted with excess of GHL, as described before [24]. Additionally, in order to obtain the control carrier, void of αM, G3 substrate was substituted with two biotin residues per dendrimer molecule and further glucoheptoamidated with excess of GHL to obtain $G3^{2B12gh}$. The conjugates were well soluble in dmso and characterized by NMR spectroscopy in this solvent, while molecular size was determined by DLS measurements in diluted aqueous solutions.

The ^{1}H NMR spectra of the final products, $G3^{2B12gh5M}$ and $G3^{2B10gh17M}$, are presented in Figure 1B,C. For comparison, the ^{1}H-NMR spectrum of αM in dmso-d_6 was recorded (Figure 1A) and ^{1}H resonances were assigned in accordance with literature data [37,38]. Common features of the ^{1}H NMR spectra were the PAMAM G3 core methylene proton (a,b,c,d) resonances within 2.19–3.10 ppm region, while protons of amide groups gave broad signal at 8.0 ppm (NH(G3)). In the case of biotin, resonances of aliphatic chain protons (2^B and $3,4,5^B$), ureido ring protons ($10,11^B$), and thiophane ring protons ($8,9^B$) were separated from gh and G3 core resonances (Figure 1B,C). The resonances of gh C-H protons were observed in the 3.3–3.9 ppm region.

For both dendrimer conjugates $G3^{2B12gh5M}$ and $G3^{2B10gh17M}$, the characteristic resonances of αM in the ^{1}H NMR spectra are observed (Figure 1): partially overlapped singlets within 1.61–1.77 ppm from protons of four methyl groups, and methoxy group proton singlet resonance at 3.70 ppm. Although prenyl methylene proton (11 and 16) doublets remain non-equivalent in both $G3^{2B12gh5M}$ and $G3^{2B10gh17M}$, the 11-H doublet was found

at 3.99 ppm (for $G3^{2B10gh17M}$) and at 3.95 (for $G3^{2B12gh5M}$). The 12 and 17-H triplets are overlapped at 5.16 ppm for αM, $G3^{2B12gh5M}$, and $G3^{2B10gh17M}$.

The resonances of two αM aromatic protons in both conjugated spectra are considerably shifted upfield, due to the shielding effect of the hyperbranched dendrimer with additional polyhydroxyalkylamide chains. The larger shift of 5^{M} resonance in both conjugates related to αM (0.30 ppm upfield) in comparison with the 4^{M} signal (0.08 ppm upfiled) were observed. The ^{1}H and ^{13}C resonances of αM in $G3^{2B12gh5M}$ and $G3^{2B10gh17M}$ were assigned based on 2-D ^{1}H-^{1}H COSY (Figure S1) and heteronuclear ^{1}H-^{13}C HSQC and HMBC experiments (for combined HSQC/HMBC map see Figure S2) and are listed in Table S1.

The considerable shift of H5 proton resonance (0.30 ppm upfield) together with 4.4 ppm downfield shift of C6 and 1.5 ppm upfield shift of C7 resonance in relation to αM alone spectra in dmso-d_6 strongly suggest that 6′ oxygen is involved in carbamide linker. In such a bonding mode, both prenyl proton multiplets remain unshifted in the conjugates.

We were not able to isolate an αM-NPC intermediate single crystal to verify unambiguously which hydroxyl group was substituted with *para*-nitrophenylcarbonate and further involved in a bonding with dendrimer.

Additionally, $G3^{2B12gh}$ conjugate was synthesized to examine the vehicle cytotoxicity. All of these conjugates were extensively purified by dialysis against water, in order to remove low molecular reagents or side products, such as *p*-nitrophenol and DMAP, and dried under high vacuum. The ^{1}H NMR spectrum of $G3^{2B12gh}$ conjugate is shown in Figure 2A. The ^{1}H resonances were assigned based on COSY spectrum as described before [24]. The number of attached residues of αM, biotin and gh was estimated based upon the integral intensity of ^{1}H resonances in relation to the reference intensity of $b_{0\text{-}3}$ protons resonance from the dendrimer core, namely [120H].

Because no free amine groups of G3 were readily available in $G3^{2B10gh17M}$, all conjugates were single-labeled with fluorescein using FCH, which was activated with Mukaiyama reagent and attached to gh hydroxyl groups via ester bond. The average 1:1 stoichiometry was confirmed by ^{1}H NMR spectra (not shown) in $G3^{2B12gh5MF}$ and $G3^{2B10gh17MF}$.

3.2. Size and Zeta Potential of Conjugates

Unlike PAMAM G3, the $G3^{2B12gh}$ derivative has smaller dynamic diameter in water, which increases upon acidification of the solution to pH 5 about four times (Figure 3; for numbers, see Table 1) due to protonation of internal tertiary amine groups, as observed before within a series of $G3^{gh}$ derivatives [39]. The highest value of diameter was observed already for half-substituted $G3^{16gh}$, namely 4.60 nm (averaged by volume) or 3.80 nm (averaged by number); the biotin-containing conjugate $G3^{2B12gh}$ has a comparable size.

Although we have prepared two relatively well water-soluble αM conjugates, namely $G3^{2B12gh5M}$ and $G3^{2B10gh17M}$, in contrary to non-glucoheptoamidated semiproducts, the size measurements of aqueous solutions evidenced high association of each $G3^{2B12gh5M}$ and $G3^{2B10gh17M}$. DLS measurements indicated the number-averaged size for $G3^{2B12gh5M}$, amounting to 1262 nm with major contribution from large size particles (d(V) = 1367 > d(N)). These associates were destabilized at pH 5, resulting in a decrease of particle size within the <200,100> nm region. The $G3^{2B10gh17M}$ conjugate did not show an additional association in neutral aqueous solution, and finally, the size of particles was within <230,100> nm regardless of the pH (7 or 5). Nonetheless, both conjugates showed major contribution of larger associates in acidic solution, which is illustrated by d(V) > d(N) in Figure 3B.

The values of the zeta potential are positive for all conjugates studied (Figure 4). The vehicle $G3^{2B12gh}$ has a ζ of circa 11 mV, the same as the $G3^{16gh}$ studied in a regular series of derivatives [39]. αM-containing conjugates showed the same ζ, circa 22 mV, which is twice that for the vehicle itself, despite the 10-fold size difference between $G3^{2B12gh5M}$ and $G3^{2B10gh17M}$ in water. On the other hand, the potential increased considerably upon a two log increase of hydrogen cation concentration, presumably due to protonation of core PAMAM and considerable increase of cationic charge of nanoparticles of the conjugates. For the size-dependent biological behavior of conjugates vide infra.

Table 1. Size and zeta potential values ± standard deviation determined by DLS analysis.

Compound	Size [nm]				Zeta Potential [mV]	
	pH 7		pH 5		pH 7	pH 5
	d(V)	d(N)	d(V)	d(N)		
$G3^{2B12gh}$	1.0 ± 0.24	0.9 ± 0.22	4.5 ± 0.14	3.8 ± 0.18	11.1 ± 2.89	17.4 ± 1.87
$G3^{2B12gh5M}$	1367 ± 245.7	1262 ± 196.4	178.3 ± 5.73	113.8 ± 7.34	22.7 ± 1.01	37.5 ± 2.32
$G3^{2B10gh17M}$	149 ± 33.9	111 ± 14.1	230.6 ± 12.4	130.8 ± 12.25	22.1 ± 0.61	39.5 ± 3.67

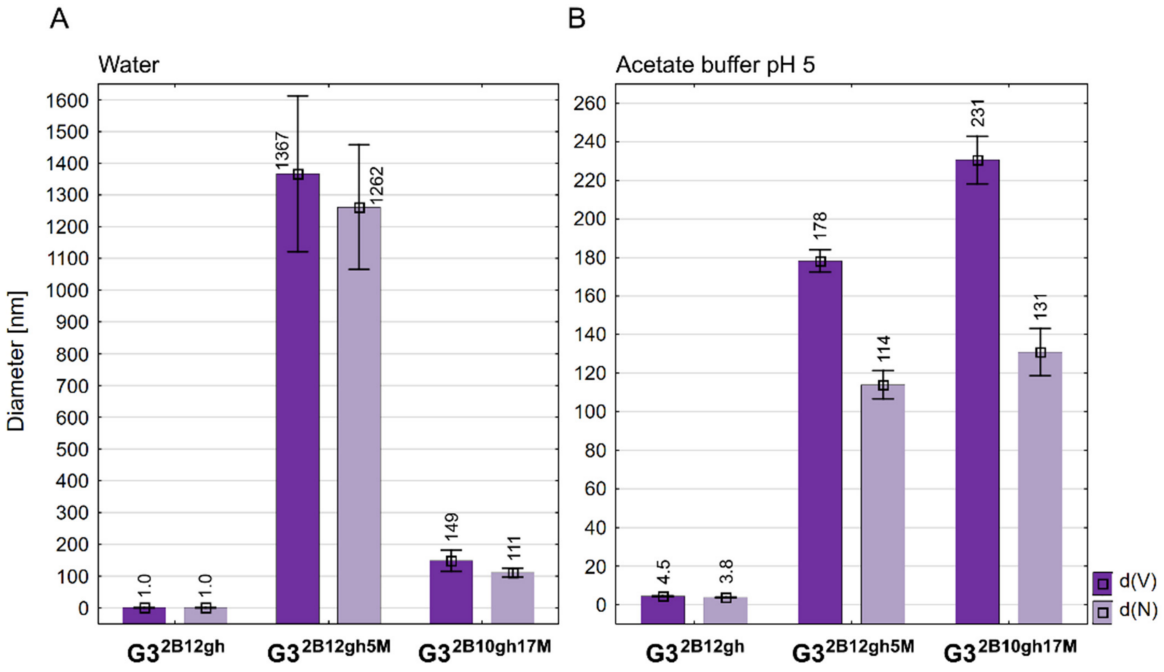

Figure 3. Diameter of conjugates averaged by volume (d(V)) and by number of molecules (d(N)) measured in water (**A**) and in acetate buffer pH 5 (**B**). Data are presented as mean ± standard deviation with mean values marked above the columns.

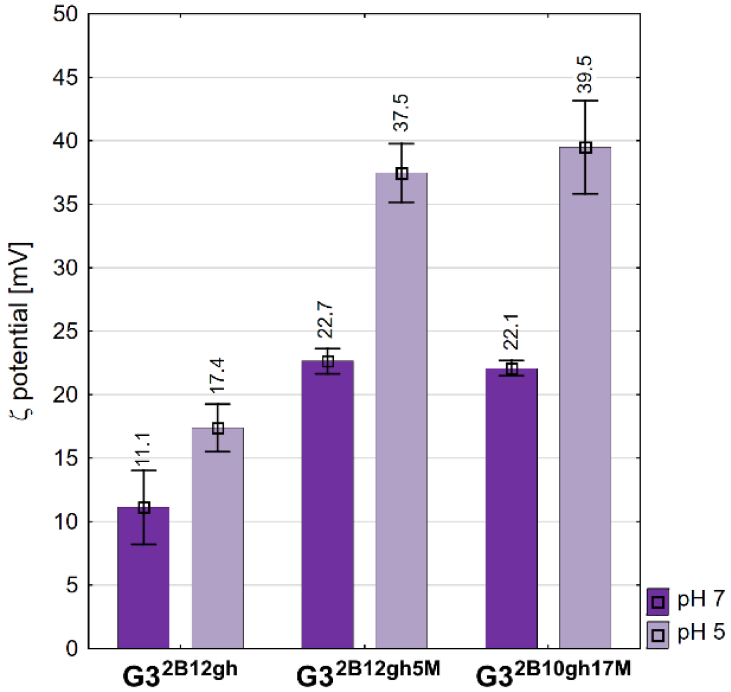

Figure 4. Zeta potential values of conjugates measured in water and acetate buffer pH 5. Data are presented as mean ± standard deviation with mean values marked above the columns.

3.3. Cytotoxicity

The main goal of this study was to design an efficient αM delivery vehicle, based on the biotinylated and glucoheptoamidated (gh) PAMAM G3 dendrimer, increasing the drug's toxicity against cancer cells and *C. elegans*. While substitution by biotin was supposed to increase the intracellular accumulation of the conjugates, modification by gh residues was expected to reduce the toxicity of the surface groups of the αM carrier (PAMAM G3 dendrimer).

The results of the NR assay (Figure 5) revealed that both studied αM conjugates were active at low, micromolar concentrations, with the effect depending on the level of dendrimer substitution by the drug. Thus, $G3^{2B10gh17M}$ killed all cells more efficiently than $G3^{2B12gh5M}$. Surprisingly, normal cells were as sensitive as SCC-15 cells, with glioma cells being less sensitive. The results were confirmed by microscopic analysis. At toxic or higher concentrations, the studied compounds cells formed aggregates, shrank, lost their adhesion, and absorbed a lower amount of neutral red dye (Figure 5B).

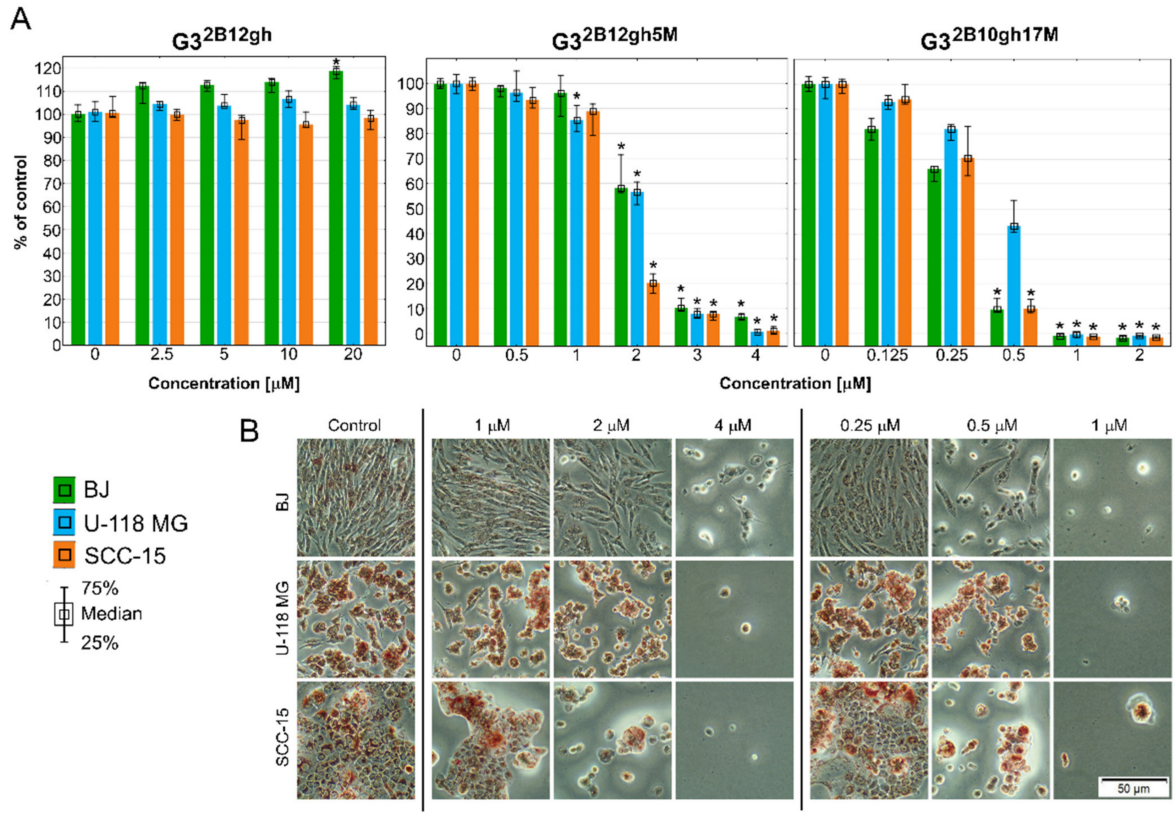

Figure 5. Cytotoxicity of $G3^{2B12gh5M}$, $G3^{2B10gh17M}$, and the control vehicle $G3^{2B12gh}$ against human cells: normal fibroblasts (BJ), glioma cells (U-118 MG), and squamous carcinoma cells (SCC-15) after 48 h of incubation estimated with an NR assay. (**A**) Cell viability expressed as medians of a percent against non-treated control (control expressed as 100%). The whiskers are the lower (25%) and upper (75%) quartile ranges. * $p \leq 0.05$; Kruskal–Wallis test (against non-treated control). (**B**) Morphology of the cells incubated with chosen concentrations of $G3^{2B12gh5M}$ and $G3^{2B10gh17M}$. Red signal on microscopic images represents a neutral red dye.

The results of XTT assay, detecting mainly mitochondria damages, showed a weaker response than those of NR test (Figure 6). Of note is that despite the effect of the $G3^{2B12gh5M}$ compound, compared to that of $G3^{2B10gh17M}$ compound, the former seems to be a better candidate for the destruction of neoplastic cells, in view of a strong toxicity of the latter towards normal human fibroblasts (Figure 6, Table 2).

The results of the NR and XTT assays allowed to determine the half maximal inhibitory concentration IC_{50} values, demonstrating both drug conjugates to lack cytotoxic selectivity against BJ vs. squamous carcinoma SCC-15/glioma U-118 MG cells (Table 2, Figures 5 and 6).

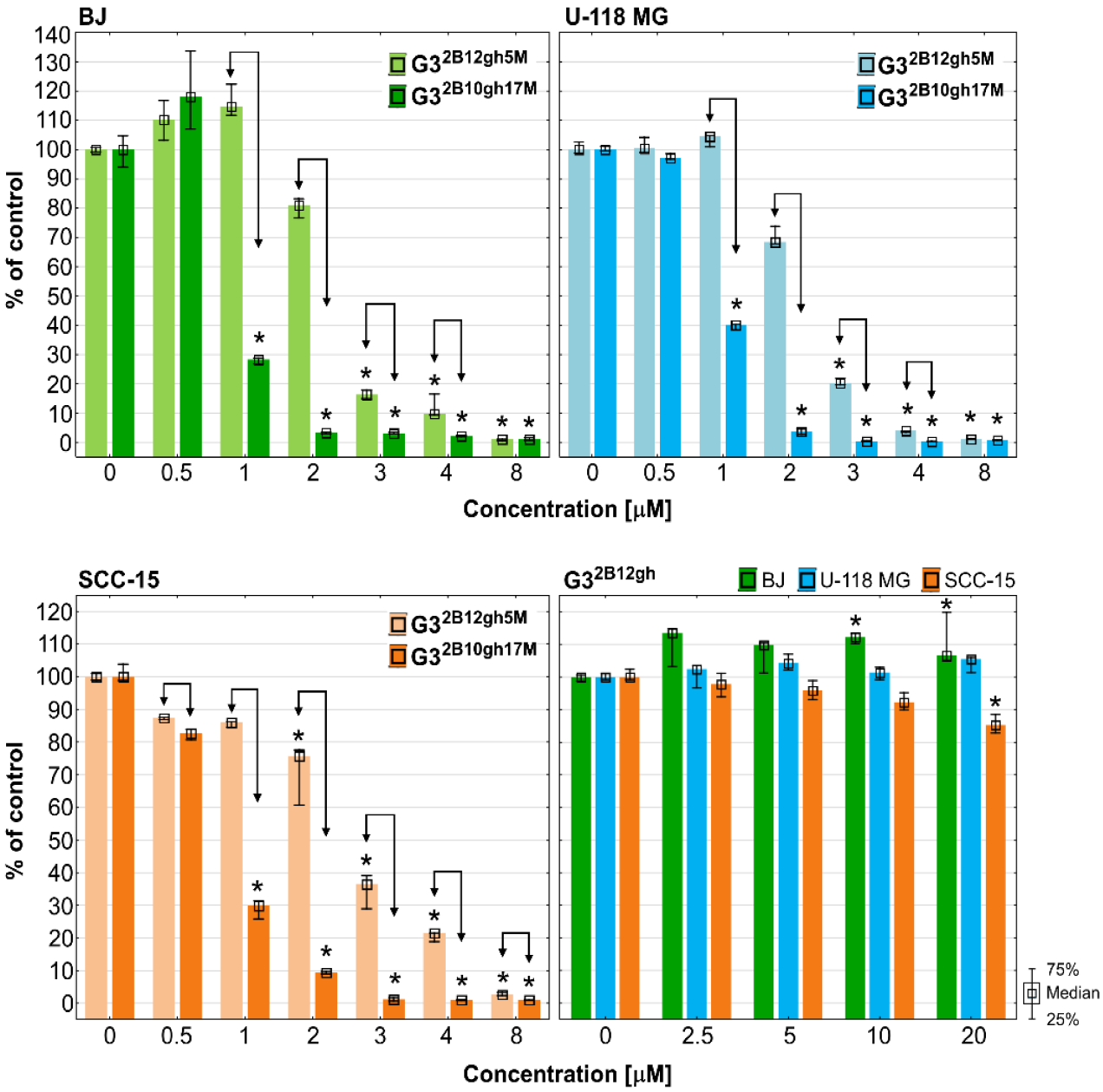

Figure 6. The results of XTT assay performed on BJ, U-118 MG and SCC-15 cells after 48 h of incubation with $G3^{2B12gh5M}$ and $G3^{2B10gh17M}$ conjugates and the control vehicle $G3^{2B12gh}$. Cells viability expressed as medians of a percent against non-treated control (control expressed as 100%). The whiskers are lower (25%) and upper (75%) quartile ranges. * $p \leq 0.05$; Kruskal–Wallis test (against non-treated control), ↕ $p \leq 0.05$; Mann–Whitney *U* test (the $G3^{2B12gh5M}$-treated group against the $G3^{2B10gh17M}$-treated group).

Of note is that with the control dendrimer vehicle $G3^{2B12gh}$, void of αM, at concentrations up to 20 μM (the highest allowed in view of dmso in the dendrimer preparation) following 48 h of treatment, a feeble cytotoxicity of the highest concentration was seen only for SCC-15 cells with the XTT assay (Figures 5 and 6). These results are in agreement with our earlier results, indicating that a similar G3 PAMAM dendrimer substituted with 16 gh residues was non-toxic up to 100 μM [39]. It confirms that biotinylated and partially glucoheptoamidated PAMAM G3 dendrimer is useful as a drug nanocarrier. The conjugation of αM with non-toxic dendrimeric carrier ($G3^{2B12gh}$) resulted in the drug's toxicity increase, as compared to that of the free αM [5]. The increase of toxicity was dependent on the level of substitution of the carrier by the drug, observed not only against SCC-15 cells (about 4.5- or 21-fold), but also for U-118 MG (about 5.2- or 25-fold) and BJ cells (4.5- or 11.5-fold for $G3^{2B12gh5M}$ and $G3^{2B10gh17M}$, respectively). It

should be noted that the conjugate with five residues of αM enhanced its toxicity on average by ca. 5-fold, which may be related to the polyvalency or multivalency phenomenon [40]. Of interest is that the conjugate with 17 residues enhanced αM activity by about 21–25-fold in cancer cells but by only 11.5-fold in normal cells. This suggests that addition of more xanthone residues increase its activity in cancer cells with simultaneous moderation of this effect in normal cells, resulting in an apparent enhancing of antineoplastic efficacy [41].

Table 2. The half maximal inhibitory concentration (IC_{50}) values determined following 48 h of treatment of BJ, U-118 MG, or SCC-15 cells with $G3^{2B12gh5M}$ or $G3^{2B10gh17M}$.

IC_{50} [μM] NR Assay			
	BJ	U-118 MG	SCC-15
$G3^{2B12gh5M}$	2	1.83	1.41
$G3^{2B10gh17M}$	0.28	0.39	0.31
α-Mangostin[1]	8.97	9.59	6.43
IC_{50} [μM] XTT Assay			
	BJ	U-118 MG	SCC-15
$G3^{2B12gh5M}$	2.37	2.05	2.52
$G3^{2B10gh17M}$	0.78	1.01	0.85
α-Mangostin [1]	18.58	18.15	7.72

[1] IC_{50} values for α-mangostin quoted from our earlier work [5].

It should also be mentioned that U-118 MG cells, compared to the remaining cell lines, did not present higher sensitivity to the drug bound to both biotinylated vehicles, which was unexpected considering that glioma cells tend to overexpress biotin receptors and in consequence demonstrate increased biotin uptake [42,43].

3.4. Cellular Accumulation and Distribution of Fluorescently Labeled $G3^{2B12gh5M}$ or $G3^{2B10gh17M}$

Drug vehicles, including dendrimers, may change cellular uptake and accumulation of delivered substances. Based on our earlier experience [22] and considering higher cellular uptake of biotinylated vs. non-biotinylated dendrimers [20,21] the glucoheptoamidated dendrimers used in this study were substituted with two biotin residues per dendrimer molecule, in order to enhance their accumulation and, in consequence, also αM accumulation in the studied cancer cells. It should be added that an increased uptake of biotinylated dendrimer-drug conjugates by cancer cells could be expected, in view of biotin receptors and transporters being frequently overexpressed by such cells [19].

Cellular uptake, accumulation and toxicity are dependent on molecule size, charge and charge-related zeta potential of nanoparticles. Increased cytotoxicity of nanoparticles in non-phagocytic cells correlates with their small size [44]. At physiological pH, $G3^{2B12gh5M}$ and $G3^{2B10gh17M}$ conjugates indicated high association with diameter determined by DLS, equal to about 1300 nm for $G3^{2B12gh5M}$ and 130 nm for $G3^{2B10gh17M}$ compared to an αM-free carrier (about 1 nm diameter). Probably for this reason, microscopic observations of cells after 4 h of incubation with both FCH-labeled $G3^{2B12gh5M}$ and $G3^{2B10gh17M}$ revealed no visible fluorescence signal inside them. Only 48 h of incubation of fluorescently labeled $G3^{2B12gh5M}$ or $G3^{2B10gh17M}$ indicated that both compounds were taken up by all cell lines with the highest accumulation in normal human fibroblasts, while in cancer cells, their amount was significantly lower (Figure 7). This phenomenon may be due to the ability of fibroblasts to more efficiently uptake biotin compared to other cells as we described [22]. It is also possible that the stronger accumulation of studied compound in these cells may be a result of their ability to non-professional phagocytosis or phagocytosis [45,46]. The formation of associates by αM conjugates resulted not only in slower uptake of these nanoparticles—the toxicity was also caused by the presence of αM itself rather than by the interaction of positively charged dendrimer vehicles and negatively charged cell membranes. Microscopic observations revealed that absorbed conjugates remained in endocytic vesicles, with only

a small part of the dendrimer present in the cytoplasm of the cells. It is known that αM induces caspase-3 and -9 activation causes swelling, loss of membrane potential (delta psi), decrease in intracellular ATP, ROS accumulation, and cytochrome c/AIF release in human leukemia HL60 cells [47] and also provokes the release of cytochrome C, increase of Bax, decrease of Bcl-2, and activation of caspase-9/caspase-3 cascade in cervical cancer cells [33]. Therefore, mitochondria seem to be a natural goal for the anticancer activity of αM. In this study, both conjugates penetrated into mitochondria of SCC-15 cells and normal fibroblasts, but very poorly into mitochondria of glioma U-118 MG cells (Figure 7), suggesting a reason of glioblastoma cells being resistant to αM conjugates (see Figures 5 and 6).

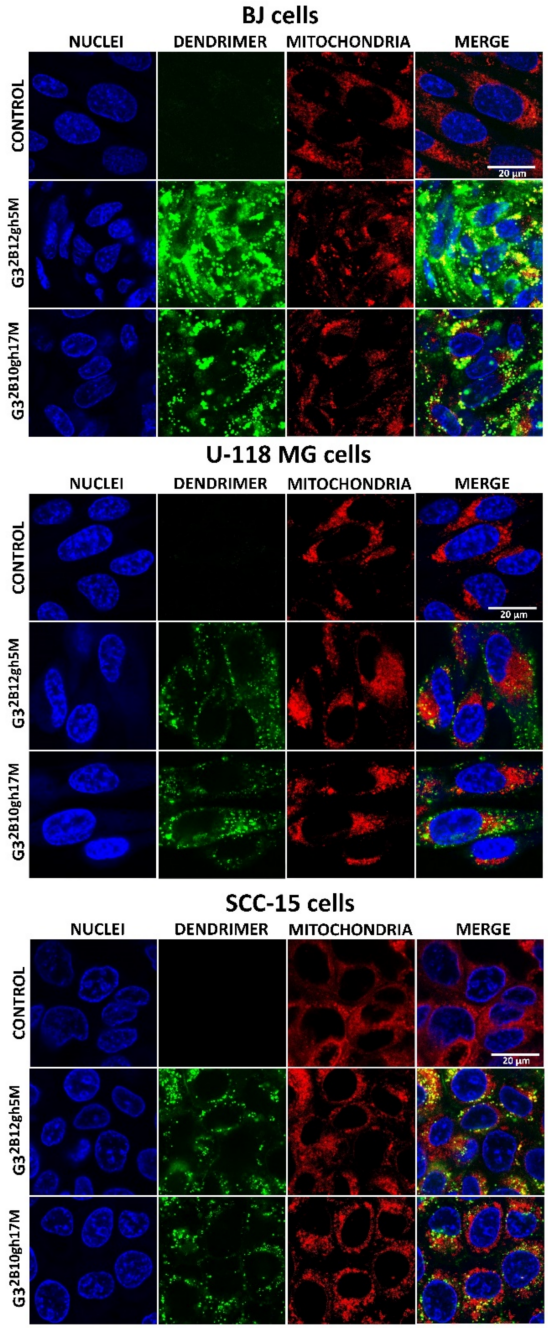

Figure 7. Images obtained with confocal microscopy presenting cellular accumulation and localization of fluorescently labeled $G3^{2B12gh5M}$ or $G3^{2B10gh17M}$ conjugates after 48 h of incubation with 1 µM or 0.1 µM non-toxic concentrations. Green signal: FCH-labeled dendrimer, blue signal: cell nuclei stained with Hoechst 33342, red signal: MitoTracker Deep Red FM labeled mitochondria, yellow signal: colocalization of FCH labeled dendrimer and MitoTracker labeled mitochondria. Scale bar is equal 20 µm.

3.5. Caspase-3/7 and Intracellular ATP Level

Another sign of advanced cytotoxicity is the entry of cells into the programmed pathway of death, apoptosis. Regardless of whether this is an extrinsic or intrinsic mechanism, executive caspases (caspase 3,6,7) are produced to proteolytically degrade components of damaged or malfunctioning cells [48]. In this experiment, the potential of dendrimer conjugates with 5 or 17 residues of αM to induce apoptosis in cancer cells compared to normal cells was studied. In addition, the intracellular ATP level was also estimated. The results are shown in Figure 8 as a relationship between the activity of executioner caspases and intracellular ATP level in studied cell lines. Both conjugates $G3^{2B12gh5M}$ and $G3^{2B10gh17M}$ significantly increased activity of caspase-3/7 in all tested cell lines at concentrations higher than IC_{50}. The most active was the conjugate with 17 residues of αM, inducing Cas-3/7 activity growth with a concentration of 0.5 μM, while the conjugate with 5 αM residues induced this effect with a concentration of 3 μM.

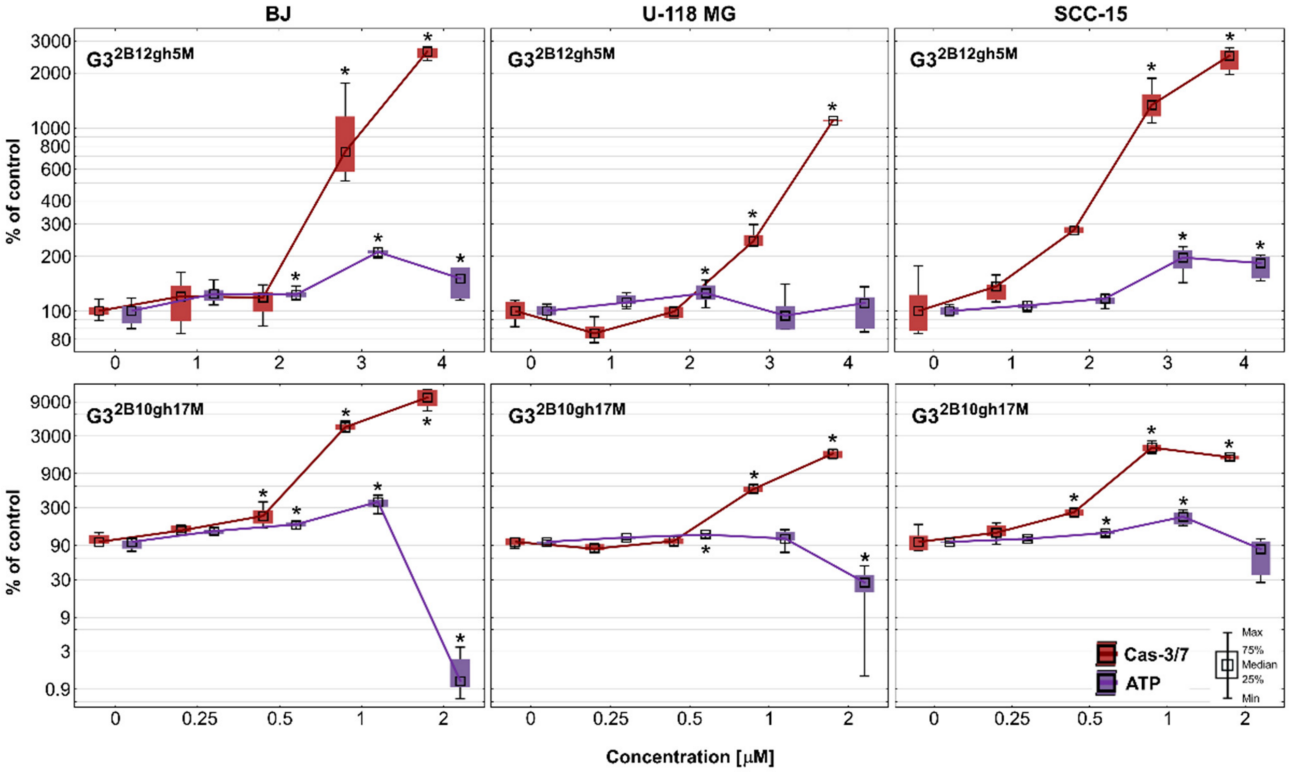

Figure 8. Activity of caspase-3/7 and intracellular ATP level in BJ, U-118 MG, and SCC-15 cells after 48 h of incubation with $G3^{2B12gh5M}$ (1–4 μM) and $G3^{2B10gh17M}$ (0.25–2 μM) conjugates. The results from three independent experiments are medians expressed as a percentage of non-treated control, where data for caspase-3/7 level are marked in red, while data for ATP level are marked in violet. Boxes represent the first (25%) and third (75%) quartile; whiskers are the minimum and maximum range. * $p \leq 0.05$, Kruskal–Wallis test (against non-treated control).

As the cytotoxicity of αM significantly increases upon the conjugation with the dendrimer, the same effect is observed for apoptosis. In our earlier studies [5], αM alone induced apoptosis from 10 μM in cancer and from 20 μM concentration in normal cells. Thus, lower concentrations of αM affected cancer than normal cells. Two other similar xanthones, namely alvaxanthone and rheediaxanthone B, induced higher activity of caspases-3/7 in cancer cell lines comparing to normal cells [49]. For αM conjugated with PAMAM G3 dendrimer, this effect was not seen—the most sensitive were fibroblasts. Referring to non-treated control, at the highest concentration of $G3^{2B12gh5M}$, there was a 11-, 25- and 26-fold increase in caspases activity in U-118 MG, SCC-15, and BJ cells, respectively. In case of $G3^{2B10gh17M}$, there was 17-fold growth in glioblastoma cells and 21-fold growth in the SCC-15 cell line, while fibroblasts obtained a 104-fold increase of caspases activity.

This result may be due to the presence of biotin in conjugates and its higher uptake by fibroblasts compared to remaining cancer cells, as previously observed by Uram et al. [22]. The results of the accumulation studies of fluorescently labeled $G3^{2B12gh5M}$ and $G3^{2B10gh17M}$ conjugates are consistent with this, demonstrating higher uptake of biotinylated conjugates by fibroblasts (Figure 7). On the other hand, the lowest level of caspases activity in glioblastoma cells may be caused by their intrinsic mechanisms of decreased apoptosis, which makes GBM resistant to apoptosis inhibitors [50] and causes the propensity of astrocytic glioma to necrosis [51]. Considering this fact, the obtained statistically significant induction of apoptosis by αM dendrimer conjugates at low concentrations makes them interesting in the context of anticancer properties.

Since ATP plays a key role in the decision of cell death fate and the ATP-dependent nature of apoptosis [48,52], intracellular ATP level after 48 h of incubation with $G3^{2B12gh5M}$ and $G3^{2B10gh17M}$ was assessed. After treatment with 1–3 μM $G3^{2B12gh5M}$, the ATP amount has grown to 195% in SCC-15 cells and to 210% in BJ cells, and then, at the highest concentration, this was 183% and 150%, respectively. In the case of U-118 MG cells, the level of ATP remained mostly unchanged. In the same range of concentrations, activity of caspases has grown significantly in all three cell lines. Meanwhile, incubation of both cancer and normal cells with $G3^{2B10gh17M}$ led to an increase in ATP level at 1 μM, followed by a reduction at 2 μM concentration. The biggest rise and fall of ATP level was observed in fibroblasts (363% and 1.2% of control), while in SCC-15 cells it was 225% and 80%. In glioblastoma cells, the ATP level increased only to 112%, but then decreased to 27%. These ATP changes were accompanied by growth in caspases-3/7 activity in all tested cells, alike for $G3^{2B12gh5M}$. As a high level of intracellular ATP often favors apoptosis [52], and caspases 3 and 7 are activated in the advanced stage of this process, it can be concluded that the studied conjugates induced ATP-dependent apoptosis in a concentration-dependent manner. However, considering the fact that various forms of cell death (autophagy, apoptosis, and necrosis) can be induced simultaneously or successively and that low level of ATP often promotes necrosis [52], the tested conjugates at highly toxic concentrations (4 μM of $G3^{2B12gh5M}$ and 2 μM of $G3^{2B10gh17M}$) could also induce necrosis in both cancer and normal cells. A similar effect was observed by Uram et al. [53] in studies regarding biotinylated dendrimer PAMAM G3 conjugated with celecoxib and Fmoc-L-Leucine (G3-BCL). In fibroblasts, the apoptotic pathway was dominant up to 2 μM of G3-BCL conjugate with a constant ATP supply, while at 4 μM concentration, a significant increase of late apoptosis/necrosis was observed with simultaneous extensive depletion of ATP level. The same pattern of cell death fate was revealed in glioblastoma cells but still with a high level of ATP observed at 4 μM of G3-BCL.

3.6. Proliferation

It is known that αM exhibits a strong anti-proliferative effect in human colon HCT116 carcinoma cells with inhibition of the activity of DNA topoisomerases I and II, and blockade of the cell cycle in the G2/M phase [54], and also in human breast cancer T47D cells [55] and several others [56]. $G3^{2B12gh5M}$ inhibited BJ and SCC-15 cell proliferation from 2 μM concentration and U-118 MG glioma cells from 3 μM, while at higher concentrations cell proliferation was lower than 20% and close to zero. A stronger effect was observed in case of $G3^{2B10gh17M}$, which significantly suppressed proliferation from 1 μM concentration for BJ and U-118 MG or even 0.5 μM for SCC-15 cells. Moreover, activity of conjugate with 17 αM residues was always stronger than $G3^{2B12gh5M}$. It is worth noting that the control dendrimer vehicle $G3^{2B12gh}$ at concentrations up to 20 μM showed no anti-proliferative effect against tested cell lines and even increased the proliferation of fibroblasts by 40% (Figure 9).

Comparing this effect with the toxicity results, it can be concluded that the anti-proliferative effect coincides with the toxicity pattern (Figures 5 and 6). It is also visible that conjugation of αM with PAMAM G3 dendrimers enhanced its antiproliferative effect since our previous studies showed activity of αM alone against BJ, U-118 MG and SCC-15 cells in range of 7.5–20 μM concentrations [5]. Finally, the use of the biotinylated carrier for 5 αM residues led to a reduction of cell proliferation about three-fold, while $G3^{2B10gh17M}$ inhibited

cell divisions by 7-, 15-, and 10-fold in BJ, U-118 MG, and SCC-15 cells, respectively, compared to αM alone. This phenomenon may be the result of multi/polyvalency effect or higher amount of αM accumulation inside the studied cells and showed that the studied compounds may play an important role as new anticancer agents.

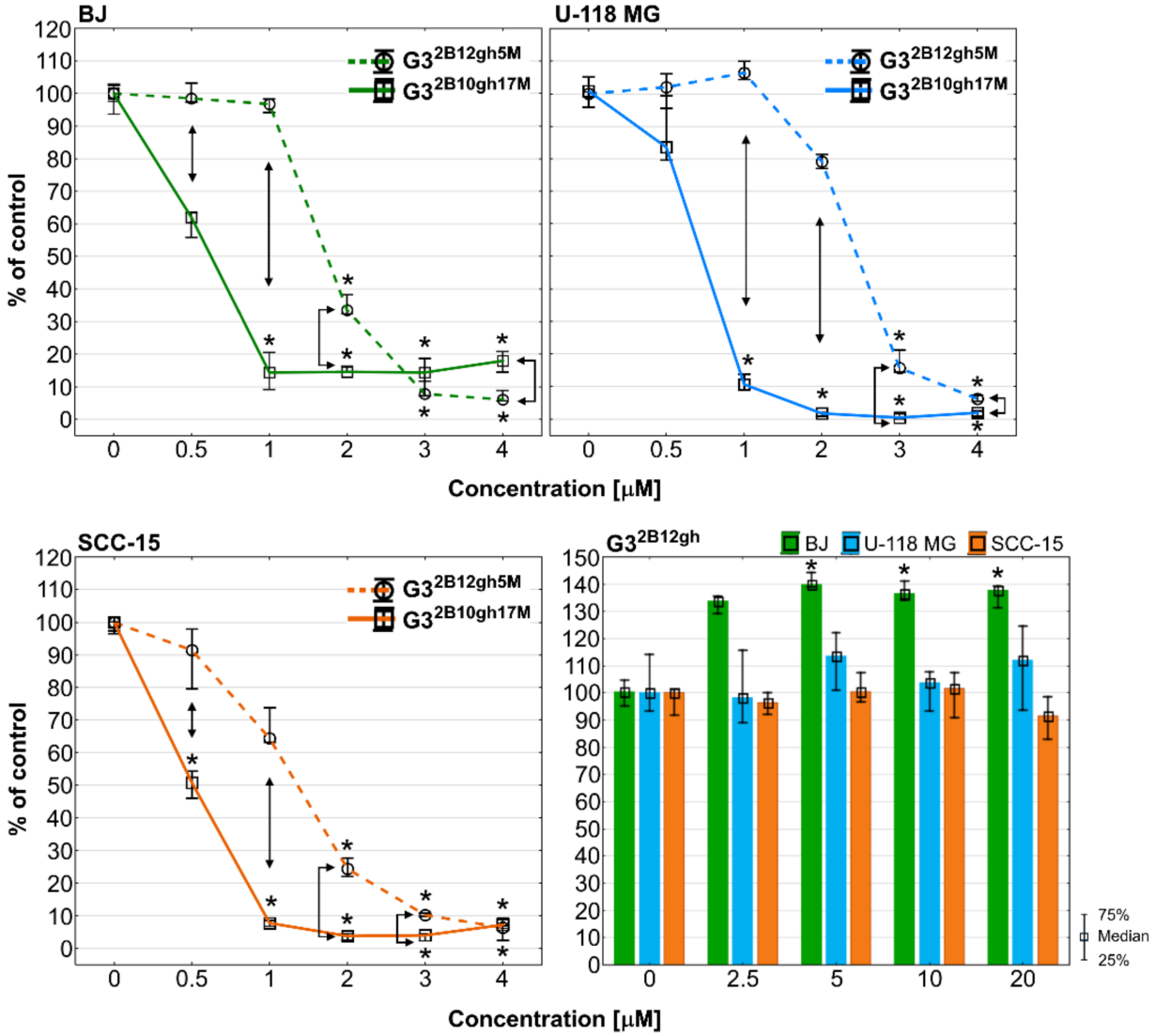

Figure 9. Anti-proliferative action of $G3^{2B12gh5M}$ and $G3^{2B10gh17M}$ on BJ, U-118 MG, and SCC-15 cells after 72 h of incubation, determined with Hoechst staining. Results are from three independent experiments, performed in triplicates and presented as medians (percentage of non-treated control). Whiskers indicate the lower (25%) and upper (75%) quartile ranges. * $p \leq 0.05$, Kruskal–Wallis test (against non-treated control). ↕ $p \leq 0.05$; Mann–Whitney *U* test (the $G3^{2B12gh5M}$-treated group against the $G3^{2B10gh17M}$-treated group).

3.7. Adhesion

Among the ten hallmarks of cancer development and progression, there is the activation of invasion and metastatic processes [57]. Malignant cells during migration adhere to extracellular matrix (ECM) proteins, providing a path to the new metastasis site [58,59]. As cell-to-cell and cell-to-ECM adhesion plays a very important role in tumor metastasis, the molecules with anti-adhesion properties may contribute to suppress the cancer expansion to other tissues. The ability of αM dendrimer conjugates to affect cells adhesion was evaluated by the assay with crystal violet dye, which stains DNA of intact adherent cells. The obtained results are presented in Figure 10.

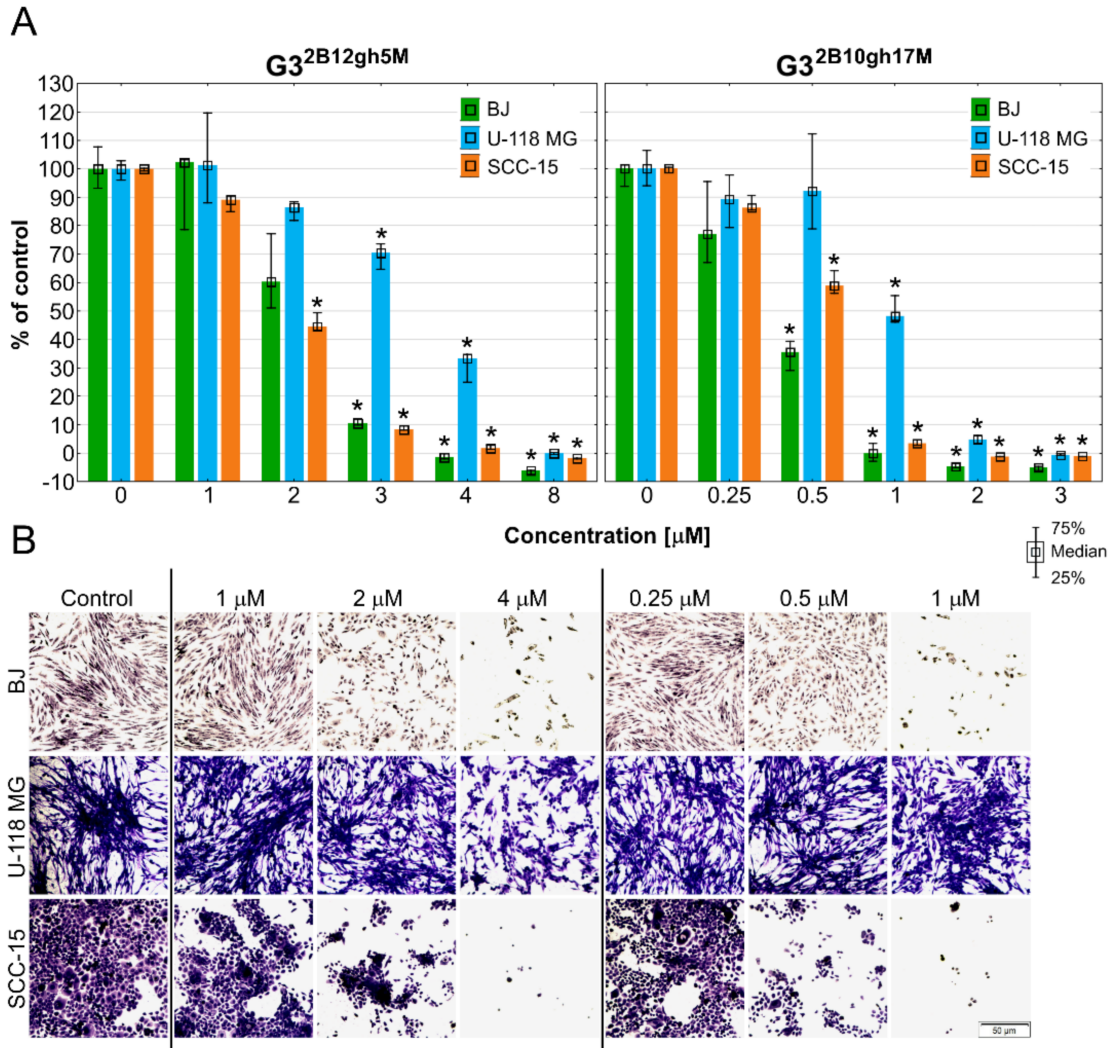

Figure 10. The ability of BJ, U-118 MG, and SCC-15 cells to adhere determined by crystal violet assay after 48 h of treatment with $G3^{2B12gh5M}$ or $G3^{2B10gh17M}$ at different concentrations. (**A**) Results are medians with first (25%) and third (75%) quartile obtained in three independent experiments and expressed as a percentage of non-treated control. * $p \leq 0.05$, Kruskal-Wallis test (against control group). (**B**) Cells attached to the bottom of 96-well plate and stained with crystal violet after 48 h of incubation with studied dendrimer conjugates. Violet signal represents a crystal violet dye inside the cells. Scale bar = 50 μm.

The SCC-15 cells were the most susceptible to loss of adhesion after incubation with $G3^{2B12gh5M}$, having 45% of attached cells at 2 μM and 1.7% at 4 μM concentration. Fibroblasts and glioblastoma cells achieved a statistically significant decrease of adhesion at 3 μM of $G3^{2B12gh5M}$, but the difference between these two cell lines was 60% in favor of U-118 MG cells. PAMAM G3 dendrimer with 17 residues of αM influenced cells attachment stronger, significantly decreasing adhesion of BJ and SCC-15 cells from 0.5 μM concentration. For this conjugate, U-118 MG cells were also the least affected, having 48% of adherent cells at 1 μM, which is 12 times more than for BJ and SCC-15 cells. These results are in line with the microscopic observations shown in the Figure 10B, which present the number of adherent cells stained with crystal violet dye after incubation with tested conjugates in selected concentrations. U-118 MG cells retained relatively high adhesiveness even after treatment with conjugates at concentrations higher than the IC_{50} values. Similar results were obtained for αM and other xanthones [5,49]. In these studies, the adhesion of squamous carcinoma cells was slightly more disturbed compared to fibroblasts, while the weakest effect was observed in glioblastoma cells. Considering the cytotoxicity of the tested conjugates, the $G3^{2B12gh5M}$ conjugate seems to be more potent in anti-adhesion properties in squamous cell carcinoma treatment. In case of GBM, extracranial metastases are extremely rare,

affecting 0.4–0.5% of all patients with GBM [60], but in the last decade, clinical reported cases of extraneural dissemination have become more frequent [61]. In addition, GBM is suggested to disseminate not only via cerebrospinal fluid, but also through bloodstream and lymphatic vessels. Therefore, the ability of $G3^{2B10gh17M}$ to reduce adhesion of U-118 MG cells by 52% at 1 μM concentration is noteworthy.

3.8. Toxicity to C. elegans and the Effect on the Worm Survival

Caenorhabditis elegans nematode was used as a model organism to examine in vivo effect of synthesized αM dendrimer conjugates on multicellular system. It has been shown that *C. elegans* is valuable animal model for studies on toxicity and biocompatibility of various nanoparticles [62,63]. Synchronized population of L4 stage-worms was incubated for 7 days in the medium (see Section 2.5.7) containing different concentrations of αM, $G3^{2B12gh5M}$ and $G3^{2B10gh17M}$, as well as $G3^{2B12gh}$ (control vehicle). The results are presented in Figure 11 as survival curves determined by the Kaplan–Meier method.

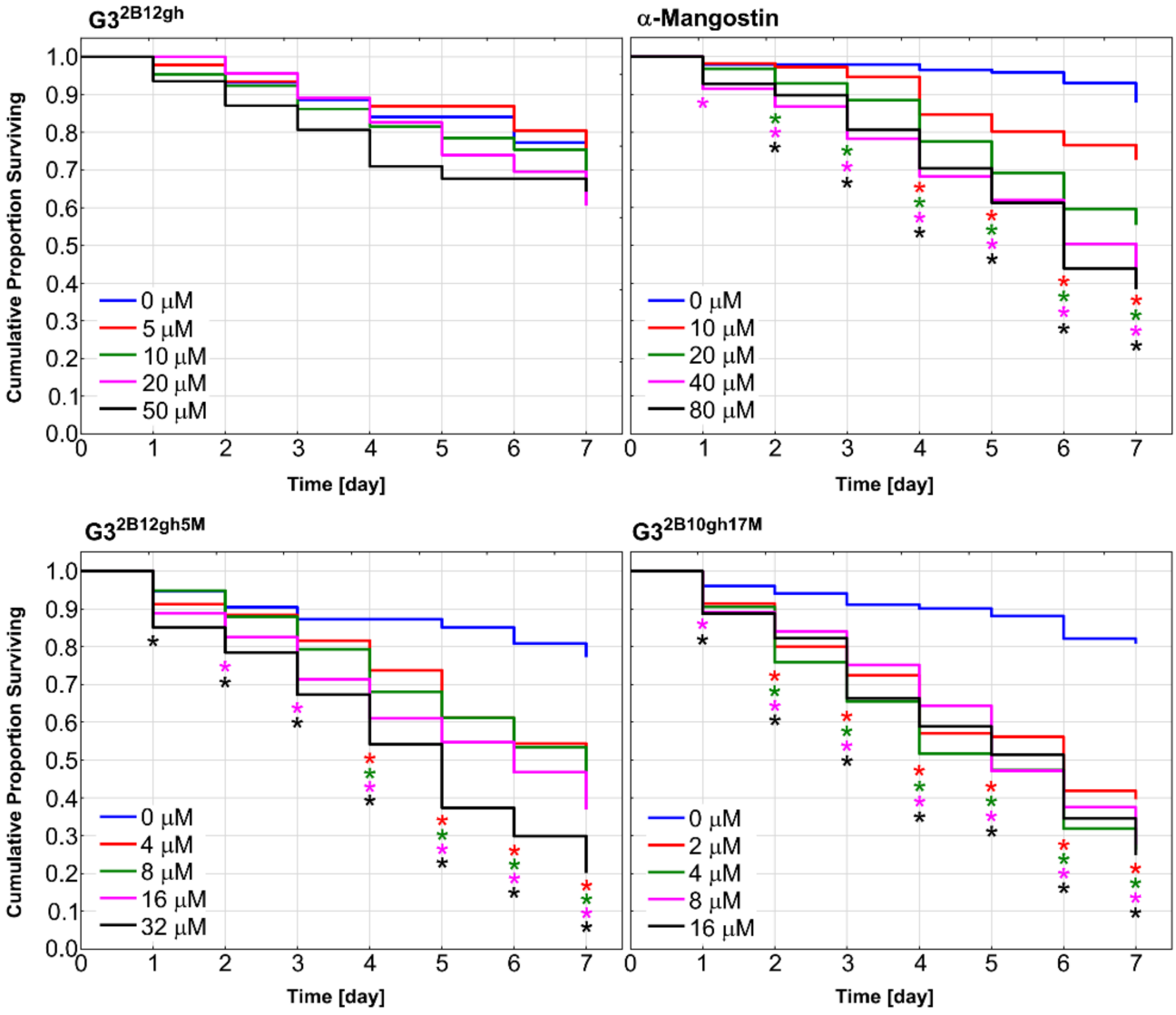

Figure 11. Kaplan–Meier survival curves of *C. elegans* after 7 days of incubation with α-mangostin, $G3^{2B12gh5M}$, $G3^{2B10gh17M}$, and $G3^{2B12gh}$ vehicle at different concentrations. Results are presented as cumulative proportion surviving. Statistically significant differences against non-treated control obtained in Gehan's Wilcoxon test are marked with asterisks ($p \leq 0.05$) in the colors corresponding to the tested concentrations.

Similar to the results of the in vitro studies, attachment of αM to dendrimer vehicle increased its toxicity against *C. elegans* organism, but to a slightly lesser extent. The concentrations in which the proportion of live nematodes was 0.4 after 7 days of incubation were 40 µM of αM, 16 µM of $G3^{2B12gh5M}$, and 2 µM of $G3^{2B10gh17M}$ (Figure 11), pointing to the activity of $G3^{2B12gh5M}$ and $G3^{2B10gh17M}$, compared to free αM, being 2.5- and 20-fold stronger, respectively.

Based on the survival curves after 7 days of incubation, the LC_{50} values were also calculated for αM, $G3^{2B12gh5M}$, $G3^{2B10gh17M}$, and control vehicle $G3^{2B12gh}$ (Table 3, Figure 12), the latter showing a moderate toxicity level [64].

Table 3. The LC_{50} values against *C. elegans* for free and dendrimer-bound αM, and a control dendrimer vehicle, determined following 7 days of incubation with αM, $G3^{2B12gh5M}$, $G3^{2B10gh17M}$, or $G3^{2B12gh}$ presented as medians and the first and third quartile. The LC_{50} values were determined using an online calculator (AAT Bioquest, Inc. Quest Graph™ IC_{50} Calculator. Retrieved from https://www.aatbio.com/tools/ic50-calculator (accessed on 14 October 2021).

	LC50 [µM]	1st Quartile	3rd Quartile
$G3^{2B12gh}$	49.88	40.58	57.98
α-Mangostin	18.74	18.64	20.23
$G3^{2B12gh5M}$	7.87	4.95	8.09
$G3^{2B10gh17M}$	1.38	1.03	1.42

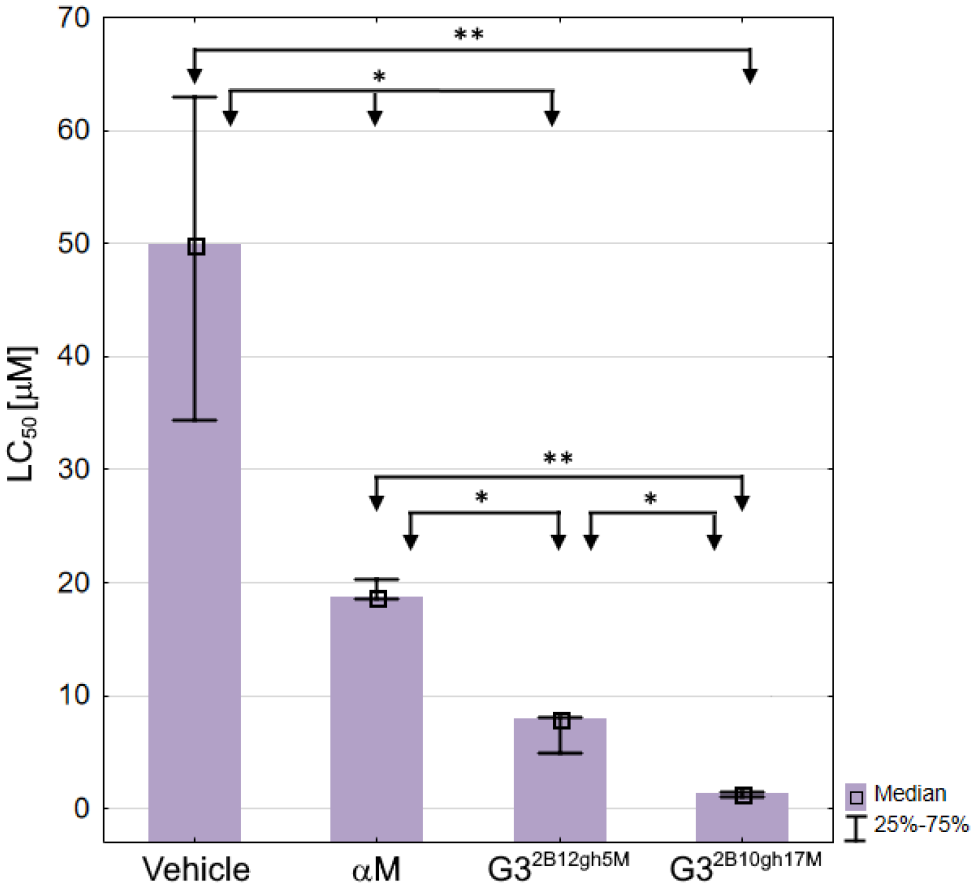

Figure 12. The LC_{50} values against *C. elegans* for αM, dendrimer vehicle $G3^{2B12gh}$ and $G3^{2B12gh5M}$ or $G3^{2B10gh17M}$ conjugates presented as medians with the first and third quartile. Statistically significant differences estimated by the Kruskal–Wallis test are marked with ** and by U Mann–Whitney test with * $p \leq 0.05$.

As expected, each of the $G3^{2B12gh5M}$ and $G3^{2B10gh17M}$ conjugates was more toxic than the $G3^{2B12gh}$ control vehicle (by 6.3- and 36-fold, respectively) or free αM, with the activities of $G3^{2B12gh5M}$ and $G3^{2B10gh17M}$, compared to free αM, being stronger by 2.4- and 13.6-fold, respectively (Table 3).

The present results obtained for free αM, tested against the L4 stage nematodes (Table 3), differ from those obtained earlier in toxicity assay performed by a different method and against a mixed *C. elegans* population [5]. The LC_{50} value for αM was found 3.8 ± 0.5 μM, thus the nematode at L4 stage (LC_{50} = 18.74) appears distinctly less sensitive to the drug than the other developmental forms.

The toxic effects of αM and its conjugates with biotinylated PAMAM G3 dendrimer was accompanied by morphological and locomotion changes of the treated nematodes. Already after 24 h of incubation with the highest concentrations of $G3^{2B12gh5M}$ and $G3^{2B10gh17M}$, slower and vibrating movements were observed. As the toxic effect progressed, the wavy motion declined, leading to straightening and stiffening of the *C. elegans* worm, until it became motionless. Moreover, the creases of the cuticula and degradation of this tissue were seen (Figure 13).

It should be noted that the increase of αM toxicity, resulting from the drug binding with the dendrimer molecules in $G3^{2B12gh5M}$ and further enhancement in consequence of the higher level of dendrimer substitution by αM in $G3^{2B10gh17M}$, was similar when tested in vivo with *C. elegans* (by 14-fold in terms of the LC_{50} values; Table 3) and in vitro with cells (by 9–32-fold considering the IC_{50} values; Table 2). Thus, the free drug and its dendrimer-bound forms appear to interact with cells and the model organism following a common mechanism. Further studies are needed to follow the dendrimer-bound αM uptake by *C.elegans* and compare it with that documented for certain other nanomolecules [65–67], such a study being impeded by a certain level of the worm autofluorescence.

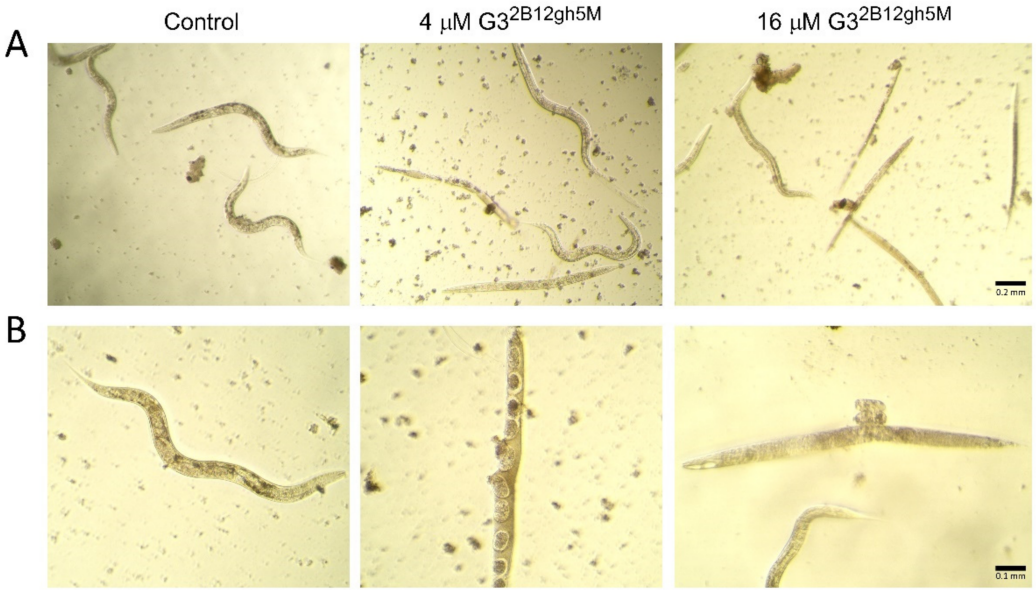

Figure 13. Morphology of *C. elegans* nematodes after 7 days of incubation with $G3^{2B12gh5M}$ dendrimer at a concentration of 4 and 16 μM in comparison to the control group representative, presented under 10× (**A**) and 20× (**B**) objective magnification.

4. Conclusions

Since α-mangostin is considered a useful agent in anticancer therapy, it seems necessary to try to increase its solubility, efficacy and selectivity by finding a suitable carrier for it. In this study, we showed that non-toxic, third-generation glucoheptoamidated and biotinylated poly(amidoamine) dendrimers can provide an excellent carrier for αM, making its cytotoxic, antiproliferative, and anti-adhesive properties more visible at significantly

lower concentrations. Additionally, it gives the opportunity to avoid side effects associated with a too high concentration of αM in therapy. At the same time, the mechanism of action of the described conjugates remains characteristic for αM itself (pro-apoptotic effect and changes in ATP levels related to the mitochondrial pathway). This means that despite the lack of selectivity against neoplastic cells, the studied conjugates may be a valuable tool in the local therapy of glioblastoma and squamous cell carcinoma. It is worth to underline that the dendrimer vehicle at concentrations up to 20 μM showed no anti-proliferative effect against tested cell lines, with a feeble cytotoxicity of the highest concentration seen only with squamous carcinoma cells. The present results indicate that the proposed αM delivery system allows the drug to be more effective in the dendrimer-bound than in the free state against both cultured cancer cells and the model organism, suggesting that this treatment is promising for anticancer as well as anti-nematode chemotherapy.

Supplementary Materials: The following are available online at https://www.mdpi.com/article/10.3390/ijms222312925/s1.

Author Contributions: Conceptualization, J.M., Ł.U. and W.R.; methodology, Ł.U. and S.W.; software, J.M.; validation, J.M., Ł.U. and S.W.; formal analysis, Ł.U. and W.R.; investigation, J.M., Ł.U. and S.W.; resources, Ł.U., S.W. and W.R.; data curation, J.M., Ł.U. and S.W.; writing—original draft preparation, J.M., Ł.U. and S.W.; writing—review and editing, J.M., Ł.U., S.W. and W.R.; visualization, J.M. and Ł.U.; supervision, Ł.U., S.W. and W.R.; project administration, J.M. and Ł.U.; funding acquisition, Ł.U. and W.R. All authors have read and agreed to the published version of the manuscript.

Funding: This research was funded by the National Science Center, Poland, grant no. 2016/21/B/NZ1/00288.

Institutional Review Board Statement: Not applicable.

Informed Consent Statement: Not applicable.

Data Availability Statement: Data supporting the reported results are available on request from the corresponding author.

Acknowledgments: The kind support by Agata Wawrzyniak from the Rzeszow University to enable us to use the confocal microscope to perform measurements is gratefully acknowledged.

Conflicts of Interest: The authors declare no conflict of interest.

References

1. Wang, M.-H.; Zhang, K.-J.; Gu, Q.-L.; Bi, X.-L.; Wang, J.-X. Pharmacology of Mangostins and Their Derivatives: A Comprehensive Review. *Chin. J. Nat. Med.* **2017**, *15*, 81–93. [CrossRef]
2. Akao, Y.; Nakagawa, Y.; Nozawa, Y. Anti-Cancer Effects of Xanthones from Pericarps of Mangosteen. *Int. J. Mol. Sci.* **2008**, *9*, 355–370. [CrossRef] [PubMed]
3. Araújo, J.; Fernandes, C.; Pinto, M.; Tiritan, M.E. Chiral Derivatives of Xanthones with Antimicrobial Activity. *Molecules* **2019**, *24*, 314. [CrossRef] [PubMed]
4. Feng, Z.; Lu, X.; Gan, L.; Zhang, Q.; Lin, L. Xanthones, A Promising Anti-Inflammatory Scaffold: Structure, Activity, and Drug Likeness Analysis. *Molecules* **2020**, *25*, 598. [CrossRef]
5. Markowicz, J.; Uram, Ł.; Sobich, J.; Mangiardi, L.; Maj, P.; Rode, W. Antitumor and Anti-Nematode Activities of α-Mangostin. *Eur. J. Pharmacol.* **2019**, *863*, 172678. [CrossRef]
6. PubChem Alpha-Mangostin. Available online: https://pubchem.ncbi.nlm.nih.gov/compound/5281650 (accessed on 13 August 2021).
7. Patra, J.K.; Das, G.; Fraceto, L.F.; Campos, E.V.R.; Rodriguez-Torres, M.d.P.; Acosta-Torres, L.S.; Diaz-Torres, L.A.; Grillo, R.; Swamy, M.K.; Sharma, S.; et al. Nano Based Drug Delivery Systems: Recent Developments and Future Prospects. *J. Nanobiotechnol.* **2018**, *16*, 71. [CrossRef]
8. Wathoni, N.; Rusdin, A.; Motoyama, K.; Joni, I.M.; Lesmana, R.; Muchtaridi, M. Nanoparticle Drug Delivery Systems for Alpha-Mangostin. *Nanotechnol. Sci. Appl.* **2020**, *13*, 23–36. [CrossRef]
9. Pham, D.T.; Saelim, N.; Tiyaboonchai, W. Alpha Mangostin Loaded Crosslinked Silk Fibroin-Based Nanoparticles for Cancer Chemotherapy. *Colloids Surf. B Biointerfaces* **2019**, *181*, 705–713. [CrossRef]
10. Doan, V.T.H.; Takano, S.; Doan, N.A.T.; Nguyen, P.T.M.; Nguyen, V.A.T.; Pham, H.T.T.; Nakazawa, K.; Fujii, S.; Sakurai, K. Anticancer Efficacy of Cyclodextrin-Based Hyperbranched Polymer Nanoparticles Containing Alpha-Mangostin. *Polym. J.* **2021**, *53*, 481–492. [CrossRef]

11. Samprasit, W.; Opanasopit, P.; Chamsai, B. Mucoadhesive Chitosan and Thiolated Chitosan Nanoparticles Containing Alpha Mangostin for Possible Colon-Targeted Delivery. *Pharm. Dev. Technol.* **2021**, *26*, 362–372. [CrossRef]
12. Chis, A.A.; Dobrea, C.; Morgovan, C.; Arseniu, A.M.; Rus, L.L.; Butuca, A.; Juncan, A.M.; Totan, M.; Vonica-Tincu, A.L.; Cormos, G.; et al. Applications and Limitations of Dendrimers in Biomedicine. *Molecules* **2020**, *25*, 3982. [CrossRef]
13. Kharwade, R.; More, S.; Warokar, A.; Agrawal, P.; Mahajan, N. Starburst Pamam Dendrimers: Synthetic Approaches, Surface Modifications, and Biomedical Applications. *Arab. J. Chem.* **2020**, *13*, 6009–6039. [CrossRef]
14. Patri, A.K.; Kukowska-Latallo, J.F.; Baker, J.R. Targeted Drug Delivery with Dendrimers: Comparison of the Release Kinetics of Covalently Conjugated Drug and Non-Covalent Drug Inclusion Complex. *Adv. Drug Deliv. Rev.* **2005**, *57*, 2203–2214. [CrossRef]
15. Sandoval-Yañez, C.; Castro Rodriguez, C. Dendrimers: Amazing Platforms for Bioactive Molecule Delivery Systems. *Materials* **2020**, *13*, 570. [CrossRef]
16. Zhong, L.; Li, Y.; Xiong, L.; Wang, W.; Wu, M.; Yuan, T.; Yang, W.; Tian, C.; Miao, Z.; Wang, T.; et al. Small Molecules in Targeted Cancer Therapy: Advances, Challenges, and Future Perspectives. *Signal Transduct. Target* **2021**, *6*, 1–48. [CrossRef]
17. Lin, H.-M.; Lin, H.-Y.; Chan, M.-H. Preparation, Characterization, and in Vitro Evaluation of Folate-Modified Mesoporous Bioactive Glass for Targeted Anticancer Drug Carriers. *J. Mater. Chem. B* **2013**, *1*, 6147–6156. [CrossRef]
18. Perumal, D.; Golla, M.; Pillai, K.S.; Raj, G.; PK, A.K.; Varghese, R. Biotin-Decorated NIR-Absorbing Nanosheets for Targeted Photodynamic Cancer Therapy. *Org. Biomol. Chem.* **2021**, *19*, 2804–2810. [CrossRef]
19. Ren, W.X.; Han, J.; Uhm, S.; Jang, Y.J.; Kang, C.; Kim, J.-H.; Kim, J.S. Recent Development of Biotin Conjugation in Biological Imaging, Sensing, and Target Delivery. *Chem. Commun.* **2015**, *51*, 10403–10418. [CrossRef]
20. Uram, Ł.; Szuster, M.; Filipowicz, A.; Zaręba, M.; Wałajtys-Rode, E.; Wołowiec, S. Cellular Uptake of Glucoheptoamidated Poly(Amidoamine) PAMAM G3 Dendrimer with Amide-Conjugated Biotin, a Potential Carrier of Anticancer Drugs. *Bioorg. Med. Chem.* **2017**, *25*, 706–713. [CrossRef]
21. Yang, W.; Cheng, Y.; Xu, T.; Wang, X.; Wen, L. Targeting Cancer Cells with Biotin–Dendrimer Conjugates. *Eur. J. Med. Chem.* **2009**, *44*, 862–868. [CrossRef]
22. Uram, Ł.; Filipowicz, A.; Misiorek, M.; Pieńkowska, N.; Markowicz, J.; Wałajtys-Rode, E.; Wołowiec, S. Biotinylated PAMAM G3 Dendrimer Conjugated with Celecoxib and/or Fmoc-l-Leucine and Its Cytotoxicity for Normal and Cancer Human Cell Lines. *Eur. J. Pharm. Sci.* **2018**, *124*, 1–9. [CrossRef]
23. Tomalia, D.A.; Baker, H.; Dewald, J.; Hall, M.; Kallos, G.; Martin, S.; Roeck, J.; Ryder, J.; Smith, P. A New Class of Polymers: Starburst-Dendritic Macromolecules. *Polym. J.* **1985**, *17*, 117–132. [CrossRef]
24. Kaczorowska, A.; Malinga-Drozd, M.; Kałas, W.; Kopaczyńska, M.; Wołowiec, S.; Borowska, K. Biotin-Containing Third Generation Glucoheptoamidated Polyamidoamine Dendrimer for 5-Aminolevulinic Acid Delivery System. *Int. J. Mol. Sci.* **2021**, *22*, 1982. [CrossRef]
25. Wróbel, K.; Wołowiec, S. Low Generation Polyamidoamine Dendrimers (PAMAM) and Biotin-PAMAM Conjugate—The Detailed Structural Studies by 1H and 13C Nuclear Magnetic Resonance Spectroscopy. *Eur. J. Clin. Exp. Med.* **2020**, *18*, 281–285. [CrossRef]
26. Uram, Ł.; Markowicz, J.; Misiorek, M.; Filipowicz-Rachwał, A.; Wołowiec, S.; Wałajtys-Rode, E. Celecoxib Substituted Biotinylated Poly(Amidoamine) G3 Dendrimer as Potential Treatment for Temozolomide Resistant Glioma Therapy and Anti-Nematode Agent. *Eur. J. Pharm. Sci.* **2020**, *152*, 105439. [CrossRef]
27. Stiernagle, T. *Maintenance of C. elegans*; WormBook: Online, 2006. [CrossRef]
28. Bischof, L.J.; Huffman, D.L.; Aroian, R.V. Assays for Toxicity Studies in C. Elegans with Bt Crystal Proteins. In *C. elegans: Methods and Applications*; da Strange, K., Ed.; Methods in Molecular Biology; Humana Press: Totowa, NJ, USA, 2006; pp. 139–154, ISBN 978-1-59745-151-2.
29. Lewis, J.; Fleming, J. Basic Culture Methods. *Methods Cell Biol.* **1995**, *48*, 3–29.
30. Scanlan, L.; Lund, S.; Coskun, S.; Hanna, S.; Johnson, M.; Sims, C.; Brignoni, K.; Lapasset, P.; Elliott, J.; Nelson, B. Counting Caenorhabditis Elegans: Protocol Optimization and Applications for Population Growth and Toxicity Studies in Liquid Medium. *Sci. Rep.* **2018**, *8*, 904. [CrossRef]
31. Herrera-Aco, D.R.; Medina-Campos, O.N.; Pedraza-Chaverri, J.; Sciutto-Conde, E.; Rosas-Salgado, G.; Fragoso-González, G. Alpha-Mangostin: Anti-Inflammatory and Antioxidant Effects on Established Collagen-Induced Arthritis in DBA/1J Mice. *Food Chem. Toxicol.* **2019**, *124*, 300–315. [CrossRef]
32. Sivaranjani, M.; Leskinen, K.; Aravindraja, C.; Saavalainen, P.; Pandian, S.K.; Skurnik, M.; Ravi, A.V. Deciphering the Antibacterial Mode of Action of Alpha-Mangostin on Staphylococcus Epidermidis RP62A Through an Integrated Transcriptomic and Proteomic Approach. *Front. Microbiol.* **2019**, *10*, 150. [CrossRef]
33. Lee, C.-H.; Ying, T.-H.; Chiou, H.-L.; Hsieh, S.-C.; Wen, S.-H.; Chou, R.-H.; Hsieh, Y.-H. Alpha-Mangostin Induces Apoptosis through Activation of Reactive Oxygen Species and ASK1/P38 Signaling Pathway in Cervical Cancer Cells. *Oncotarget* **2017**, *8*, 47425–47439. [CrossRef] [PubMed]
34. Won, Y.-S.; Lee, J.-H.; Kwon, S.-J.; Kim, J.-Y.; Park, K.-H.; Lee, M.-K.; Seo, K.-I. α-Mangostin-Induced Apoptosis Is Mediated by Estrogen Receptor α in Human Breast Cancer Cells. *Food Chem. Toxicol.* **2014**, *66*, 158–165. [CrossRef] [PubMed]
35. Wang, J.J.; Sanderson, B.J.S.; Zhang, W. Significant Anti-Invasive Activities of α-Mangostin from the Mangosteen Pericarp on Two Human Skin Cancer Cell Lines. *Anticancer Res.* **2012**, *32*, 3805–3816.

36. Tripathi, P.K.; Tripathi, S. 6—Dendrimers for Anticancer Drug Delivery. In *Pharmaceutical Applications of Dendrimers*; Chauhan, A., Kulhari, H., Eds.; Micro and Nano Technologies; Elsevier: Amsterdam, The Netherlands, 2020; pp. 131–150, ISBN 978-0-12-814527-2.
37. Ahmad, M.; Yamin, B.M.; Lazim, A.M. Preliminary study on dispersion of α-Mangostin in Pnipam microgel system. *Malays. J. Anal. Sci.* **2012**, *16*, 256–261.
38. Buravlev, E.V.; Shevchenko, O.G.; Anisimov, A.A.; Suponitsky, K.Y. Novel Mannich Bases of α- and γ-Mangostins: Synthesis and Evaluation of Antioxidant and Membrane-Protective Activity. *Eur. J. Med. Chem.* **2018**, *152*, 10–20. [CrossRef] [PubMed]
39. Czerniecka-Kubicka, A.; Tutka, P.; Pyda, M.; Walczak, M.; Uram, Ł.; Misiorek, M.; Chmiel, E.; Wołowiec, S. Stepwise Glucoheptoamidation of Poly(Amidoamine) Dendrimer G3 to Tune Physicochemical Properties of the Potential Drug Carrier: In Vitro Tests for Cytisine Conjugates. *Pharmaceutics* **2020**, *12*, 473. [CrossRef]
40. Santos, A.; Veiga, F.; Figueiras, A. Dendrimers as Pharmaceutical Excipients: Synthesis, Properties, Toxicity and Biomedical Applications. *Materials* **2020**, *13*, 65. [CrossRef]
41. Luong, D.; Kesharwani, P.; Deshmukh, R.; Mohd Amin, M.C.I.; Gupta, U.; Greish, K.; Iyer, A.K. PEGylated PAMAM Dendrimers: Enhancing Efficacy and Mitigating Toxicity for Effective Anticancer Drug and Gene Delivery. *Acta Biomater.* **2016**, *43*, 14–29. [CrossRef]
42. Miranda-Gonçalves, V.; Honavar, M.; Pinheiro, C.; Martinho, O.; Pires, M.M.; Pinheiro, C.; Cordeiro, M.; Bebiano, G.; Costa, P.; Palmeirim, I.; et al. Monocarboxylate Transporters (MCTs) in Gliomas: Expression and Exploitation as Therapeutic Targets. *Neuro-oncology* **2013**, *15*, 172–188. [CrossRef]
43. Russell-Jones, G.; McTavish, K.; McEwan, J.; Rice, J.; Nowotnik, D. Vitamin-Mediated Targeting as a Potential Mechanism to Increase Drug Uptake by Tumours. *J. Inorg. Biochem.* **2004**, *98*, 1625–1633. [CrossRef]
44. Fröhlich, E. The Role of Surface Charge in Cellular Uptake and Cytotoxicity of Medical Nanoparticles. *Int. J. Nanomed.* **2012**, *7*, 5577–5591. [CrossRef]
45. Seeberg, J.C.; Loibl, M.; Moser, F.; Schwegler, M.; Büttner-Herold, M.; Daniel, C.; Engel, F.B.; Hartmann, A.; Schlötzer-Schrehardt, U.; Goppelt-Struebe, M.; et al. Non-Professional Phagocytosis: A General Feature of Normal Tissue Cells. *Sci. Rep.* **2019**, *9*, 11875. [CrossRef]
46. Swanson, J.A. Shaping Cups into Phagosomes and Macropinosomes. *Nat. Rev. Mol. Cell. Biol.* **2008**, *9*, 639–649. [CrossRef]
47. Matsumoto, K.; Akao, Y.; Yi, H.; Ohguchi, K.; Ito, T.; Tanaka, T.; Kobayashi, E.; Iinuma, M.; Nozawa, Y. Preferential Target Is Mitochondria in α-Mangostin-Induced Apoptosis in Human Leukemia HL60 Cells. *Bioorg. Med. Chem.* **2004**, *12*, 5799–5806. [CrossRef]
48. D'Arcy, M.S. Cell Death: A Review of the Major Forms of Apoptosis, Necrosis and Autophagy. *Cell Biol. Int.* **2019**, *43*, 582–592. [CrossRef]
49. Maj, P.; Mori, M.; Sobich, J.; Markowicz, J.; Uram, Ł.; Zieliński, Z.; Quaglio, D.; Calcaterra, A.; Cau, Y.; Botta, B.; et al. Alvaxanthone, a Thymidylate Synthase Inhibitor with Nematocidal and Tumoricidal Activities. *Molecules* **2020**, *25*, 2894. [CrossRef]
50. Valdés-Rives, S.A.; Casique-Aguirre, D.; Germán-Castelán, L.; Velasco-Velázquez, M.A.; González-Arenas, A. Apoptotic Signaling Pathways in Glioblastoma and Therapeutic Implications. *BioMed Res. Int.* **2017**, *2017*, 7403747. [CrossRef]
51. Furnari, F.B.; Fenton, T.; Bachoo, R.M.; Mukasa, A.; Stommel, J.M.; Stegh, A.; Hahn, W.C.; Ligon, K.L.; Louis, D.N.; Brennan, C.; et al. Malignant Astrocytic Glioma: Genetics, Biology, and Paths to Treatment. *Genes Dev.* **2007**, *21*, 2683–2710. [CrossRef]
52. Chen, Q.; Kang, J.; Fu, C. The Independence of and Associations among Apoptosis, Autophagy, and Necrosis. *Signal Transduct. Target Ther.* **2018**, *3*, 18. [CrossRef]
53. Uram, Ł.; Misiorek, M.; Pichla, M.; Filipowicz-Rachwał, A.; Markowicz, J.; Wołowiec, S.; Wałajtys-Rode, E. The Effect of Biotinylated PAMAM G3 Dendrimers Conjugated with COX-2 Inhibitor (Celecoxib) and PPARγ Agonist (Fmoc-L-Leucine) on Human Normal Fibroblasts, Immortalized Keratinocytes and Glioma Cells in Vitro. *Molecules* **2019**, *24*, 3801. [CrossRef]
54. Mizushina, Y.; Kuriyama, I.; Nakahara, T.; Kawashima, Y.; Yoshida, H. Inhibitory Effects of α-Mangostin on Mammalian DNA Polymerase, Topoisomerase, and Human Cancer Cell Proliferation. *Food Chem. Toxicol.* **2013**, *59*, 793–800. [CrossRef]
55. Kritsanawong, S.; Innajak, S.; Imoto, M.; Watanapokasin, R. Antiproliferative and Apoptosis Induction of α-Mangostin in T47D Breast Cancer Cells. *Int. J. Oncol.* **2016**, *48*, 2155–2165. [CrossRef] [PubMed]
56. Ibrahim, M.Y.; Hashim, N.M.; Mariod, A.A.; Mohan, S.; Abdulla, M.A.; Abdelwahab, S.I.; Arbab, I.A. α-Mangostin from Garcinia Mangostana Linn: An Updated Review of Its Pharmacological Properties. *Arab. J. Chem.* **2016**, *9*, 317–329. [CrossRef]
57. Sasahira, T.; Kirita, T. Hallmarks of Cancer-Related Newly Prognostic Factors of Oral Squamous Cell Carcinoma. *Int. J. Mol. Sci.* **2018**, *19*, 2413. [CrossRef] [PubMed]
58. Gkretsi, V.; Stylianopoulos, T. Cell Adhesion and Matrix Stiffness: Coordinating Cancer Cell Invasion and Metastasis. *Front. Oncol.* **2018**, *8*, 145. [CrossRef]
59. Wu, X.-X.; Yue, G.G.-L.; Dong, J.-R.; Lam, C.W.-K.; Wong, C.-K.; Qiu, M.-H.; Lau, C.B.-S. Actein Inhibits the Proliferation and Adhesion of Human Breast Cancer Cells and Suppresses Migration in Vivo. *Front. Pharmacol.* **2018**, *9*, 1466. [CrossRef]
60. Da Cunha, M.L.V.; Maldaun, M.V.C. Metastasis from Glioblastoma Multiforme: A Meta-Analysis. *Rev. Assoc. Med. Bras.* **2019**, *65*, 424–433. [CrossRef]
61. Hoffman, H.A.; Li, C.H.; Everson, R.G.; Strunck, J.L.; Yong, W.H.; Lu, D.C. Primary Lung Metastasis of Glioblastoma Multiforme with Epidural Spinal Metastasis: Case Report. *J. Clin. Neurosci.* **2017**, *41*, 97–99. [CrossRef]

62. Wu, T.; Xu, H.; Liang, X.; Tang, M. Caenorhabditis Elegans as a Complete Model Organism for Biosafety Assessments of Nanoparticles. *Chemosphere* **2019**, *221*, 708–726. [CrossRef]
63. Zhao, X.; Wan, Q.; Fu, X.; Meng, X.; Ou, X.; Zhong, R.; Zhou, Q.; Liu, M. Toxicity Evaluation of One-Dimensional Nanoparticles Using Caenorhabditis Elegans: A Comparative Study of Halloysite Nanotubes and Chitin Nanocrystals. *ACS Sustain. Chem. Eng.* **2019**, *7*, 18965–18975. [CrossRef]
64. Walczynska, M.; Jakubowski, W.; Wasiak, T.; Kadziola, K.; Bartoszek, N.; Kotarba, S.; Siatkowska, M.; Komorowski, P.; Walkowiak, B. Toxicity of Silver Nanoparticles, Multiwalled Carbon Nanotubes, and Dendrimers Assessed with Multicellular Organism Caenorhabditis Elegans. *Toxicol. Mech. Methods* **2018**, *28*, 432–439. [CrossRef]
65. Meyer, J.N.; Lord, C.A.; Yang, X.Y.; Turner, E.A.; Badireddy, A.R.; Marinakos, S.M.; Chilkoti, A.; Wiesner, M.R.; Auffan, M. Intracellular Uptake and Associated Toxicity of Silver Nanoparticles in Caenorhabditis Elegans. *Aquat. Toxicol.* **2010**, *100*, 140–150. [CrossRef]
66. Hu, C.-C.; Wu, G.-H.; Hua, T.-E.; Wagner, O.I.; Yen, T.-J. Uptake of TiO2 Nanoparticles into C. Elegans Neurons Negatively Affects Axonal Growth and Worm Locomotion Behavior. *ACS Appl. Mater. Interfaces* **2018**, *10*, 8485–8495. [CrossRef]
67. Cagno, S.; Brede, D.A.; Nuyts, G.; Vanmeert, F.; Pacureanu, A.; Tucoulou, R.; Cloetens, P.; Falkenberg, G.; Janssens, K.; Salbu, B.; et al. Combined Computed Nanotomography and Nanoscopic X-Ray Fluorescence Imaging of Cobalt Nanoparticles in Caenorhabditis Elegans. *Anal. Chem.* **2017**, *89*, 11435–11442. [CrossRef]

Supplementary materials: Biotin Transport-Targeting Polysaccharide-Modified PAMAM G3 Dendrimer as System Delivering alpha-Mangostin into Cancer Cells and *C. elegans* Worms

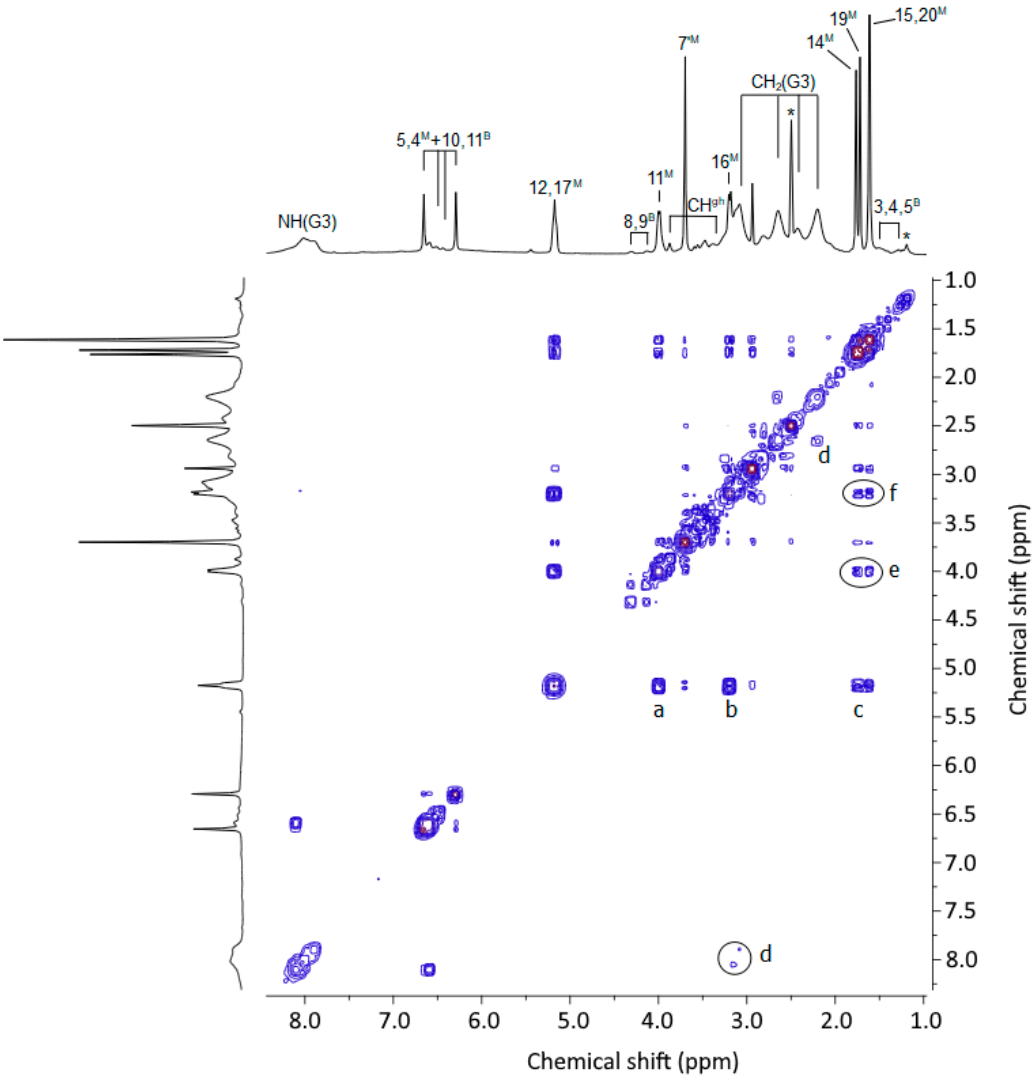

Figure S1. COSY spectrum for $G3^{2B10gh17M}$ in dmso-d_6. The relevant cross-peaks are labeled as follow: a - 12H/11H; b - 17H/16H; c – group of scalar coupling peaks between 14H, 15H, 19H, 20H (methyl group singlets) with 12H, 17H (overlapped methylene triplets); e - 14H,15H/11H; f - 19H,20H/16H; d – group of internal PAMAM G3 cross-peaks (not specified; for detailed assignment see [39].

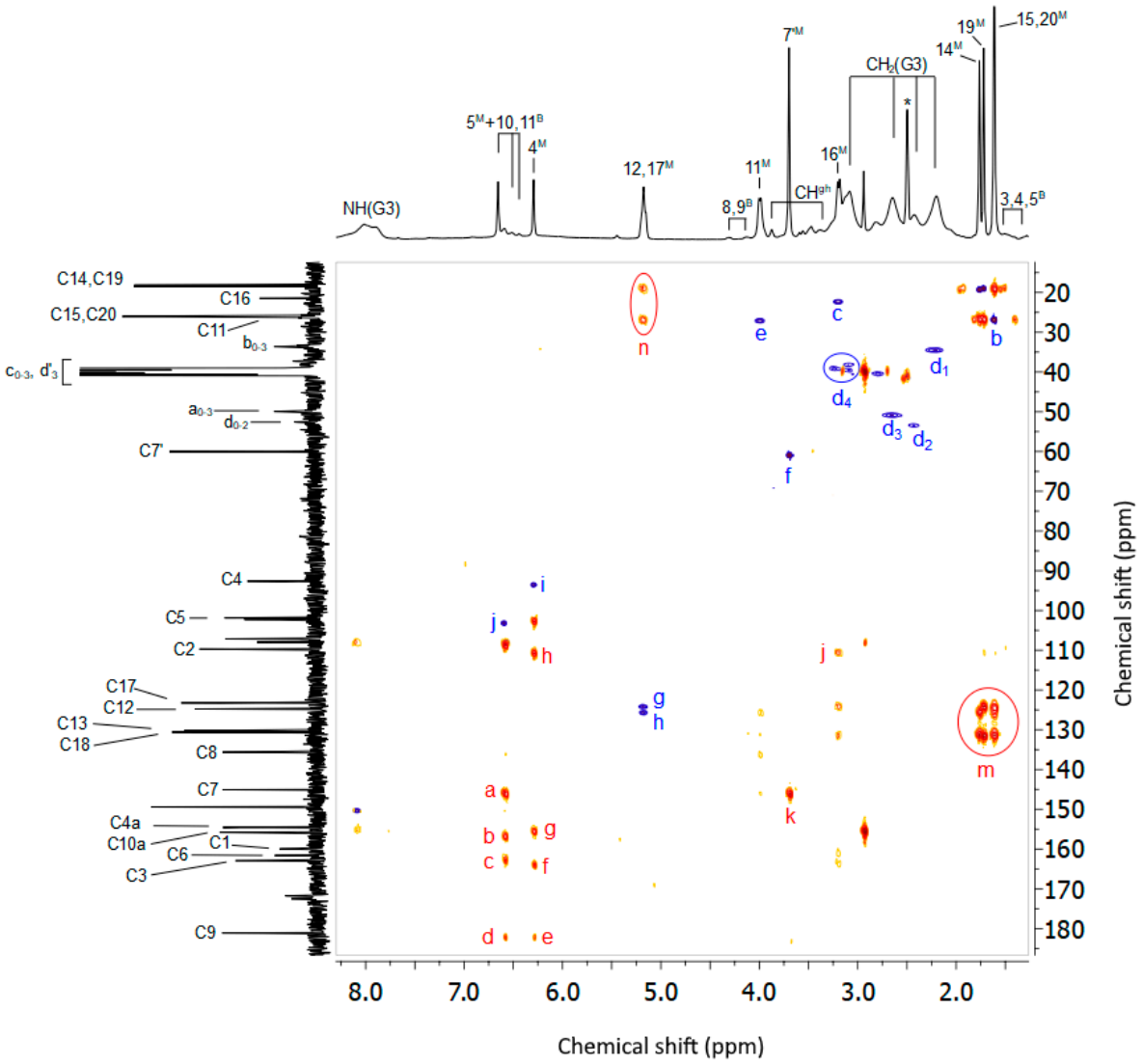

Figure S2. Combined HSQC/HMBC map for G3^{2B10gh17M} in dmso-d$_6$. One-bond correlation peaks are shown and labeled in blue, while longer distance ^{1}H-^{13}C cross-peaks obtained in HMBC experiment are drawn and labeled in red-yellow scale. The following unambiguous HSQC peaks for internal G3 are: d_1 – $b_{0\text{-}3}$; d_2 – $d_{0\text{-}2}$; d_3 – $a_{0\text{-}3}$; d_4 – $c_{0\text{-}3}$,$d_{3'}$, while series of M residues HMBC are: a – H14,H19/C14,C19; b – H15,H20/C15,C20; c – H16/C16; e – H11/C11; f – H7′/C7′; g,h – H12,H17/C12,C17; i – H4/C4; ; j – H5/C5. The relevant HMBC peaks are as follows: a – H5/C7; b – H5/C10a; c – H5/C6; d – H5/C9; e – H4/C9; f – H4/C3; g – H4/C4a; h – H4/C2, j – H16/C2; k – H7′/C7, m – H14,H15/C12,C13 and H19,H20/C17,C18; n – H12,H17/C14,C15,C19,C20.

Table S1. The ^{1}H and ^{13}C resonance assignments for α-mangostin in $G3^{2B10gh17M}$

Locant (Scheme 1)	Chemical shift	
	^{13}C	^{1}H
1	160.0	-
2	109.7	-
3	162.9	-
4	92.6	6.29 [1H], s
4a	154.5	-
9a	154.9	-
9	181.2	-
8a	108.0	-
10a	155.8	-
5	101.9	6.65 [1H], s
6	161.6	-
7	145.1	-
7′	60.2	3.69 [3H], s
8	135.6	-
11	26.2	3.99 [2H], d
12	124.8	5.17 [1H], t
13	130.2	-
14	18.4	1.75 [3H], s
15	26.1	1.61[3H], s
16	21.6	3.19
17	123.3	5.17 [1H], t
18	130.6	-
19	18.2	1.72 [3H], s
20	26.0	1.61[3H], s

pharmaceutics

Article

Synthesis and Properties of α-Mangostin and Vadimezan Conjugates with Glucoheptoamidated and Biotinylated 3rd Generation Poly(amidoamine) Dendrimer, and Conjugation Effect on Their Anticancer and Anti-Nematode Activities

Joanna Markowicz [1,*], Stanisław Wołowiec [2], Wojciech Rode [3] and Łukasz Uram [1]

[1] Faculty of Chemistry, Rzeszów University of Technology, 6 Powstancow Warszawy Ave, 35-959 Rzeszów, Poland; luram@prz.edu.pl
[2] Medical College, Rzeszów University, 1a Warzywna Str., 35-310 Rzeszów, Poland; swolowiec@ur.edu.pl
[3] Nencki Institute of Experimental Biology, 3 Pasteur Street, 02-093 Warsaw, Poland; w.rode@nencki.edu.pl
* Correspondence: jmarkowicz@stud.prz.edu.pl

Abstract: α-Mangostin and vadimezan are widely studied potential anticancer agents. Their biological activities may be improved by covalent bonding by amide or ester bonds with the third generation poly(amidoamine) (PAMAM) dendrimer, substituted with α-D-glucoheptono-1,4-lactone and biotin. Thus, conjugates of either ester- (**G3^{gh4B5V}**) or amide-linked (**G3^{2B12gh5V}**) vadimezan, and equivalents of α-mangostin (**G3^{gh2B5M}** and **G3^{2B12gh5M}**, respectively), were synthesized, characterized and tested in vitro against cancer cells: U-118 MG glioma, SCC-15 squamous carcinoma, and BJ normal human fibroblasts growth, as well as against *C. elegans* development. α-Mangostin cytotoxicity, stronger than that of Vadimezan, was increased (by 2.5–9-fold) by conjugation with the PAMAM dendrimer (with the amide-linking being slightly more effective), and the strongest effect was observed with SCC-15 cells. Similar enhancement of toxicity resulting from the drug conjugation was observed with *C. elegans*. Vadimezan (up to 200 μM), as well as both its dendrimer conjugates, was not toxic against both the studied cells and nematodes. It showed an antiproliferative effect against cancer cells at concentrations ≥100 μM. This effect was significantly enhanced after conjugation of the drug with the dendrimer via the amide, but not the ester bond, with **G3^{2B12gh5V}** inhibiting the proliferation of SCC-15 and U-118 MG cells at concentrations ≥4 and ≥12 μM, respectively, without a visible effect in normal BJ cells. Thus, the drug delivery system based on the PAMAM G3 dendrimer containing amide bonds, partially-blocked amino groups on the surface, larger particle diameter and higher zeta potential can be a useful tool to improve the biological properties of transported drug molecules.

Keywords: α-mangostin conjugate; vadimezan conjugate; PAMAM G3 dendrimer; cytotoxicity; proliferation; glioblastoma; squamous cell carcinoma; human fibroblasts; *Caenorhabditis elegans*

Citation: Markowicz, J.; Wołowiec, S.; Rode, W.; Uram, Ł. Synthesis and Properties of α-Mangostin and Vadimezan Conjugates with Glucoheptoamidated and Biotinylated 3rd Generation Poly(amidoamine) Dendrimer, and Conjugation Effect on Their Anticancer and Anti-Nematode Activities. *Pharmaceutics* **2022**, *14*, 606. https://doi.org/10.3390/pharmaceutics14030606

Academic Editors: Kristiina Huttunen and Magdalena Markowicz-Piasecka

Received: 8 February 2022
Accepted: 7 March 2022
Published: 10 March 2022

1. Introduction

Many natural and synthetic compounds with anticancer potential are not active enough in terms of bioavailability and full exploitation of their biological properties. Xanthones, presenting examples of such compounds, are polyphenolic heterocyclic compounds that can be isolated from mangosteen rind or semi/fully synthesized [1]. α-Mangostin (αM), the main representative of the xanthones family, exhibits anticancer activity through various molecular mechanisms, the most important of which are the induction of mitochondria-mediated apoptosis and the inhibition of proliferation, migration, invasion, and angiogenesis [2–6]. These activities were confirmed with in vitro and in vivo models of brain [7], pancreatic [8], liver [9], cervical [10], prostate [11] and colorectal [12] cancers. Recently, αM co-administered with doxorubicin was reported to be effective in reducing cell stemness in luminal breast cancer [13].

Another xanthone, vadimezan (5,6-dimethylxanthenone-4-acetic acid, DMXAA, ASA404), is an analogue of flavone acetic acid, considered one of the most promising antivascular agents. Direct and indirect mechanisms of action have been proposed for Vadimezan (V). A direct mechanism of V action includes the induction of apoptosis in endothelial cells, which causes hemorrhagic necrosis and ischemia in tumor tissues and, consequently, a specific and irreversible destruction of established tumor vasculatures, resulting in the complete blockade of tumor blood flow. Indirect mechanisms of V action include activation of the innate immune system, which stimulates production of inflammatory cytokines (such as TNF and IL-6), activation of NFκB and p38 (MAPK), production of nitric oxide, and reduction of tumor energetics and membrane turnover [14,15]. Later, the molecular target of V was discovered—the stimulator-of-interferon-genes (STING) protein that plays a central role in the innate immune system response. Although due to the satisfying results of in vivo studies, V has undergone several clinical trials as a single agent or in combination with taxanes, as well as in the context of carboplatin-based chemotherapy, the results of phase III clinical trials were disappointing [16]. One of the reasons for the lack of efficacy is the specificity of V to stimulate only murine STING protein but not the human STING [17]. Despite the failure of V to act as a STING agonist, attempts are made to re-develop V alone or in combination with properly targeted delivery systems. Liu et al. [18] introduced the hSTING mutant, $STING^{S162A/G230I/Q266I}$, to reignite STING activity in Merkel cell carcinoma (MCC), where it is completely silenced. Since this hSTING mutant is highly sensitive to V, the delivery of $STING^{S162A/G230I/Q266I}$ to MCC cells and treatment with V stimulated downstream antitumor cytokine production, T cell migration, and T cell activation in vitro. Boron difluoride dipyrromethene (BODIPY)-vadimezan conjugate was synthesized and enwrapped in mPEG-PPDA polymer brushes to obtain a highly-efficient type I photosensitizer for photodynamic therapy of hypoxic-and-metastatic tumors [19].

The employment of drug nanocarriers can improve water solubility and biodistribution of a drug transported in an organism. An ideal nanocarrier should present certain features, among which the most important are hydrophilicity, biocompatibility, and non-immunogenicity. Furthermore, it should be easy to conjugate or encapsulate the transported drug, as well as a proper ligand or targeting moiety, which can direct the drug to selected tissues and cells compartments [20]. Poly(amidoamine) (PAMAM) dendrimers meet the above-mentioned requirements. They are three-dimensional and hyperbranched polymers, attractive for drug delivery purposes [21,22]. Due to their spherical shape and easy-to-modify surface amine groups, they allow for the sustained release of the drug. This effect can be achieved by selecting an appropriate linkage between drug and nanocarrier. The use of different types of drug linkages can result in different drug release sites and rates. The mechanism of drug release may involve enzymatic or pH-dependent hydrolysis. Amide and ester bonds are most commonly used for the conjugation of small drugs to polymers, whereas other linkages, for example, disulfide bonds, have also been demonstrated. Amide bonds are generally stable towards various reaction conditions (acidic and basic), high temperature, and the presence of other chemicals. Additionally, they are the least reactive and their degradation is very slow as the amide bond is stabilized by the partial double bond [23]. However, Luo et al. [24] proved that in a multifunctional enveloped nanocarrier with PEG-PLL(DMA) (poly(ethylene glycol)-blocked-2,3-dimethylmaleic anhydride-modified poly(L-lysine) on its surface, the hydrolysis of amide linkages between amines and DMA occurred at acidic pH, while at physiological pH, amide bonds remained stable. The main enzymes responsible for amide hydrolysis are serine and cysteine hydrolases [25]. Ester linkages are generally easy to hydrolyze and the esterases play a major role in their enzymatic degradation. Furthermore, esterase hydrolysis represents an interesting potential strategy for targeted therapy of cancers that overexpress esterases, or which express esterases with different specificities [26,27]. Kurtoglu et al. compared ibuprofen release profiles from ester- and amide-bonded conjugates of the PAMAM G4 dendrimer and found

that while the hydrolysis of ester bonds was pH-dependent, the amide conjugates were very stable at all pH buffers, suggesting the drug release to be caused by enzymatic cleavage [28].

We have previously used biotinylated and glucoheptoamidated 3rd generation poly(amidoamine) dendrimer (PAMAM G3) to covalently attach αM by amide bond (**G3^{12gh2B5M}**) [29] and demonstrated that drug coupling with the non-toxic vehicle significantly increased its cytotoxicity and improved other biological activities, such as pro-apoptotic and anti-proliferative in vitro, as well as nematocidal in vivo. The goal of this paper was the design, synthesis and characterization of three biotinylated and glucoheptoamidated PAMAM G3 dendrimer conjugates: (i) with ester-linked αM (**G3^{gh2B5M}**), (ii) with ester-linked V (**G3^{gh4B5V}**) and (iii) with amide-linked V (**G3^{12gh2B5V}**) and investigation of the influence of their size, zeta potential, and the type of chemical bond between drugs and carrier on their biological activity in vivo and in vitro. Biotin was used as a targeting agent, in view of certain cancer cells having been demonstrated to overexpress biotin receptors and transporters [30]. Moreover, biotinylation of PAMAM dendrimers significantly increases cellular uptake and accumulation of these nanoparticles compared to non-biotinylated ones [31–34]. Biotinylation allows also PAMAM dendrimers to cross the blood-brain barrier more effectively, which is essential in the treatment of central nervous system tumors, for example, gliomas [35]. Glucoheptoamidation was performed to increase the conjugate solubility and block the amine groups present on the dendrimer surface that are responsible for the cytotoxicity of the native PAMAM G3 dendrimers [36]. The NMR and DLS analyses of the obtained conjugates were performed. The anti-cancer activity of conjugates was studied on human grade IV glioma cells (U-118 MG), human squamous carcinoma cells (SCC-15), compared to normal human fibroblasts (BJ). *Caenorhabditis elegans* nematode, widely used in nano-sciences to study genotoxicity, neurotoxicity and impact on reproduction [37], was used to study nematocidal activity in vivo.

2. Materials and Methods

2.1. Reagents

α-Mangostin (αM, purity ≥ 98% (HPLC)) was purchased from Aktin Chemicals, Inc. (Chengdu, China) and vadimezan (V, DMXAA, purity > 98%) was obtained from DC Chemicals (Shanghai, China). Ethylenediamine, methyl acrylate, D-glucoheptono-1,4-lactone (GHL), succinic anhydride (SucAnh), 2-chloro-1-methylpyridinium iodide (Mukaiyama reagent), 4-dimethylaminopyridine (DMAP), biotin, dimethyl sulfoxide (DMSO) and other reagents used in chemical syntheses were provided by Merck KGaA (Darmstadt, Germany). Spectra/Por® 3 RC dialysis membrane (cellulose, MW_{cutoff} = 3.5 kDa) was purchased in Carl Roth GmbH & Co. KG (Karlsruhe, Germany).

2.2. Biochemical Reagents, Cell Lines and Materials

Human cancer cell lines: glioblastoma (U-118 MG) and squamous cell carcinoma (SCC-15), human normal fibroblast cell line (BJ), Eagle's Minimum Essential Medium (EMEM) and fetal bovine serum (FBS) used for supplementation of this medium were obtained from the American Type Culture Collection (ATCC, Manassas, VA, USA). Dulbecco's Modified Eagle's Media (DMEM and DMEM/F-12) and fetal bovine serum (FBS) were purchased from Corning Inc. (New York, NY, USA). Penicillin and streptomycin solution, phosphate-buffered saline (PBS) with and without magnesium and calcium ions, and Hoechst 33,342 were provided by Thermo Fisher Scientific Inc. (Waltham, MA, USA). Trypsin-EDTA solution, hydrocortisone, 0.33% neutral red solution, XTT sodium salt, phenazinemethosulfate (PMS), 0.4% trypan blue solution, dimethylsulfoxide (DMSO) for molecular biology, 5-Fluoro-2'-deoxy-uridine (FUdR), and other chemicals and buffers were purchased from Merck KGaA (Darmstadt, Germany). Cell culture dishes and materials were from Corning Inc. (New York, NY, USA), Greiner (Kremsmünster, Austria), or Nunc (Roskilde, Denmark). All reagents used to culture and synchronize *C. elegans* nematodes were supplied by Sigma-Aldrich (Saint Louis, MO, USA) or Carl Roth GmbH & Co. KG (Karlsruhe, Germany).

2.3. Syntheses of Dendrimer Conjugates with Ester-Bonded Biotin and α-Mangostin or Vadimezan

2.3.1. Synthesis of Fully Glucoheptoamidated PAMAM G3

PAMAM G3 dendrimer was obtained according to Tomalia's protocol [38] and was converted into fully glucoheptoamidated derivative $G3^{32gh}$ by reaction with an excess of α-D-glucoheptono-1,4-lactone (GHL) in DMSO (Scheme 1A) as described earlier [39] on a scale of 95 μmoles. Thus, the PAMAM G3 (661 mg, 95.6 μmoles) was dissolved in 5 mL of DMSO. To this solution a two-fold excess of GHL (1273 mg, 6118 μmoles) was added in portions with vigorous stirring. The mixture was heated at 50 °C for 12 h, transferred to a dialytic bag and dialyzed for 3 days against water. Water was removed by vacuum rotary evaporation and a solid residue was dried overnight under high vacuum (2 mbars). The final product (**$G3^{gh}$**) was obtained in 35.4% yield (459 mg, 33.83 μmoles, MW = 13,568 g mol^{-1}). This compound was then used as a core dendrimer to attach covalently biotin and α-mangostin or vadimezan via ester bonds. Five μmoles of **$G3^{gh}$** were used as stock solution (12.7 mM in water) for biological studies to evaluate the cytotoxicity of the dendrimeric nanocarrier.

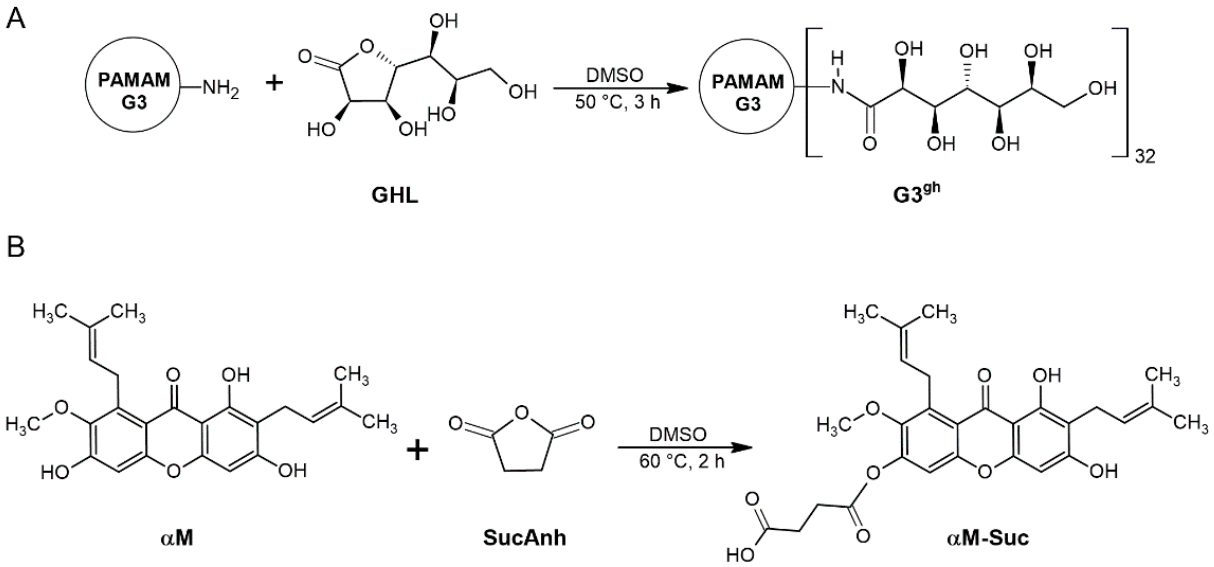

Scheme 1. The conversion of (**A**) PAMAM G3 dendrimer into fully glucoheptoamidated derivative **$G3^{gh}$** and (**B**) α-mangostin into carboxy-terminated derivative αM-Suc using succinic anhydride.

2.3.2. Synthesis of Biotinylated $G3^{gh}$—α-Mangostin Conjugate

The α-mangostin (αM) was converted into a 6-succinate derivative with succinic anhydride (Scheme 1B) as it was performed previously [39].

46.3 mg (112 μmoles) of αM was dissolved in 2 mL of DMSO and then succinic anhydride (17 mg, 168 μmoles) was added. The solution was heated at 60 °C for 2 h and used later to conjugate αM to dendrimer as follows: to the $G3^{gh}$ dendrimer (300 mg, 22 μmoles) solution in 2 mL of DMSO, 11 mg of biotin (44 μmoles) was added followed by dropwise addition of αM-Suc in DMSO. Then, DMAP (57.2 mg, 468 μmoles) and Mukaiyama reagent (59.8 mg, 234 μmoles) were added and the mixture was heated at 50 °C for 18 h. Afterwards, the solution was transferred into a dialytic tube (cellulose, MW_{cutoff} = 3.5 kDa) and dialyzed for 3 days against water (six times 3 L). Water was removed by rotary evaporation and remained solid was dried under high vacuum for 12 h. 201 mg of final product was obtained and dissolved in 2.5 mL of DMSO-d_6. The product was identified by ^{1}H-NMR spectroscopy as **$G3^{gh2B5M}$** and stored as a stock solution of 4.9 mM concentration. The isolated yield of the product was 55.5% (12.2 μmoles, MW_{calc} = 16,451 g mol^{-1}).

Analytical data:

^{1}H NMR (DMSO-d_6): chemical shift [ppm] (intensity, multiplicity, assignment): **$G3^{gh2B5M}$** (for atom numbering see Scheme 2, for spectrum see Figure 1B): 13.73 ([5H], s,

1′^{M}); 6.79 ([5H], s, 5^{M}); 6.34 ([5H], s, 4^{M}); 5.15 ([10H], overlapped t, 12^{M}, 17^{M}); 3.99 ([10H], m, 11^{M}); 3.69 ([15H], s, 7′^{M}); 3.19 ([10H], 16^{M}); 1.69 ([60H], overlapped s, 14^{M}, 15^{M}, 19^{M}, 20^{M}); PAMAM G3 resonances: 7.93 ([60+32H], m, NH(G3)); 3.13-2.20 ([484H], CH_2(G3)); biotin resonances: 6.48 and 6.40 ([4H], s and s, 10^{B} and 11^{B}); 4.29 and 4.12 ([4H], s and s, 8^{B} and 9^{B}); glucoheptoamide OH resonances: 5.62, 5.07-4.16 (overlapped s, OH^{gh}); CH_2 resonances: 3.94 ([32H], bm, 2^{gh}); 3.86 ([32H], bm, 4^{gh}); 3. 69 (m, 3^{gh} overlapped with 7′^{M}); 3.60-3.30 ([128H], overlapped s and m, 5-7^{gh}). For detailed peak assignments see COSY spectrum (Figure S1, Supplementary materials), HSQC/HMBC combined spectra (Figure S2), and Table S1.

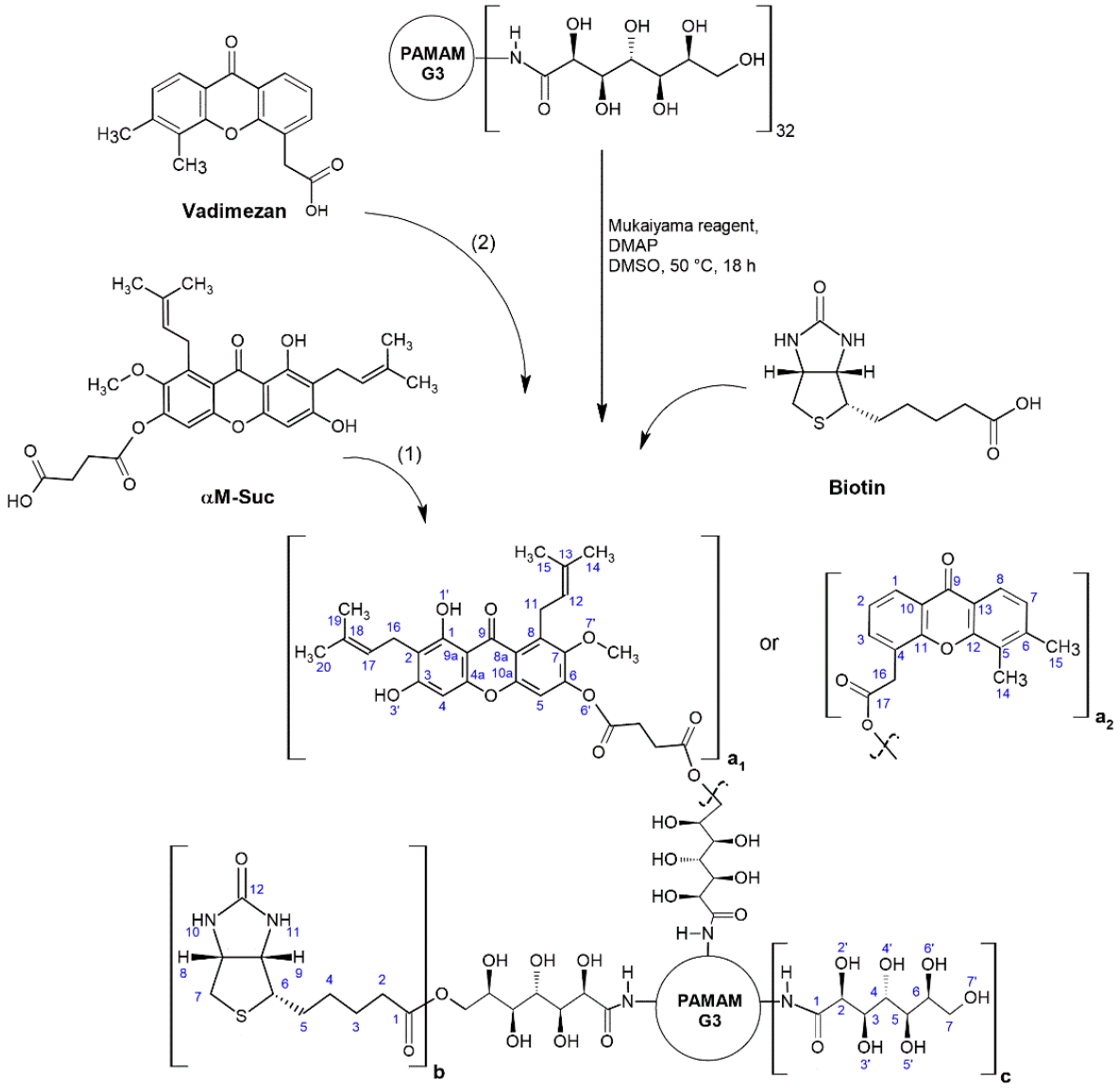

Scheme 2. Synthesis of PAMAM G3^{gh} dendrimer conjugates with α-mangostin (1) or vadimezan (2), and biotin attached via ester bond: (1) **G3^{gh2B5M}** (a_1 = 5, a_2 = 0, b = 2, c = 25), (2) **G3^{gh4B5V}** (a_1 = 0, a_2 = 5, b = 4, c = 23).

2.3.3. Synthesis of Biotinylated G3^{gh}—Vadimezan Conjugate

The **G3^{gh}** dendrimer (172 mg, 12.7 μmoles) was dissolved in 3 mL of DMSO. In this solution, vadimezan (20.0 mg, 76 μmoles) and biotin (18.6 mg, 76 μmoles) were dissolved. Then DMAP (74.4 mg, 608 μmoles) was added followed by stepwise addition of Mukaiyama reagent (77.8 mg, 304 μmoles) into solution and heated at 50 °C for 18 h. The mixture was placed in a dialytic bag (cellulose, MW_{cutoff} = 3.5 kDa) and dialyzed against water

for 4 days (8 times 3L). Water was evaporated at 50 °C and remaining solid (71 mg) was dissolved in 650 µL DMSO-d_6. The ^{1}H NMR spectrum was taken at room temperature and the average stoichiometry of conjugate was determined based on integral integration of biotin (B) and vadimezan (V) resonances versus G3^{gh} reference resonances (vide infra), as **G3^{gh4B5V}**. The concentration of **G3^{gh4B5V}** in DMSO-d_6 was 6.9 mM. The isolated yield of the product was 35% (71 mg, 4.5 µmoles, MW_{calc} = 15,795 g mol^{-1}).

Analytical data:

^{1}H NMR (DMSO-d_6): chemical shift [ppm] (intensity, multiplicity, assignment): **G3^{gh4B5V}** (for atom numbering see Scheme 2, for spectrum see Figure 2B): 8.20-7.72 ([75H], m, NH(G3)+1,8,3^V); 7.38 and 7.26 ([10H], overlapped t and d, 2^V and 7^V); 2.37 ([30H], overlapped, 14^V,15^V); biotin resonances: 6.46 and 6.40 ([4H] and [4H], overlapped s, 10^B and 11^B); 4.31 and 4.13 ([4H] and [4H], 8^B and 9^B); 2.82 and 2.78 ([4H] and [4H], 6^B and 7^B); 2.05 ([8H], 2^B); 1.56-1.29 ([24H], overlapped m, 3^B, 4^B, 5^B); gh O<u>H</u> resonances: 5.60 ([32H], s, 2′^{gh}); 4.86 ([32H], s, 3′^{gh}); 4.54-4.43 ([128H], m, 4′-7′^{gh}); gh CH_2 resonances: 3.94 ([32H], bs, 2^{gh}); 3.85 ([32H], bs, 4^{gh}); 3.69 ([32H], bs, 3^{gh}); 3.58-3.43 ([128H], m, 5^{gh}, 6^{gh}, 7^{gh}); PAMAM G3 CH_2 broad resonances: 3.13-2.19 ([484H], CH_2(G3)).

For detailed peak assignments see COSY spectrum (Figure S3), HSQC/HMBC combined spectra (Figure S4), and Table S1. For comparison the vadimezan spectrum (Figure 2A) was recorded and the resonances were assigned based on 2-D COSY and HSQC/ HMBC spectra: 8.09 ([1H], d, 1^V); 7.92 ([1H], d, 8^V); 7.79 ([1H], d, 3^V); 7.41 ([1H], t, 2^V); 7.30 ([1H], d, 7^V); 3.98 ([2H], s, 16^V); 2.41 ([6H], overlapped s, 14,15^V).

2.4. Syntheses of Dendrimer Conjugates with Amide-Bonded Biotin, GHL and α-Mangostin or Vadimezan

The detailed synthetic pathway of biotinylated and half-glucoheptoamidated dendrimer PAMAM G3 with α-mangostin (**G3^{2B12gh5M}**) and its chemical characterization were described previously [29].

Synthesis of Biotinylated and Half-Glucoheptoamidated G3 with Vadimezan

Vadimezan (53 mg, 188 µmoles) and biotin (23 mg, 94 µmoles) were dissolved in 4 mL of DMSO. To this solution 51.7 mg (423 µmoles) of DMAP and 72 mg (282 µmoles) of Mukaiyama reagent were added, stirred until completely dissolved, and left at room temperature for 1 h. This mixture was added dropwise to a PAMAM G3 dendrimer (216 mg, 31.3 µmoles) solution in 2 mL of DMSO, followed by heating at 50 °C for 18 h. The reaction mixture was worked-up by dialysis, evaporation of solvent, and drying under high vacuum as before. The obtained solid was slightly soluble in DMSO. The ^{1}H-NMR analysis allowed us to identify the product as G3^{2B5V} and the isolated yield was 35.5% (87 mg, 11.1 µmoles, MW_{calc} = 7810 g mol^{-1}). Finally, glucoheptoamidation of the remaining amine groups was performed by reaction of G3^{2B5V} with GHL (Scheme 3). Thus, to G3^{2B5V} solution (87 mg, 11.1 µmoles) in 2.25 mL of DMSO-d_6, GHL (28 mg, 133.6 µmoles) was added stepwise with vigorous stirring at RT. The product became soluble in DMSO. The ^{1}H-NMR measurement was performed and allowed the determination of average stoichiometry of the conjugate as **G3^{2B12gh5V}**. Based on a calculated average molecular weight (MW_{calc} = 11,306 g mol^{-1}) the stock solution of this conjugate was estimated as 3.3 mM.

Analytical data:

^{1}H NMR (DMSO-d_6): chemical shift [ppm] (intensity, multiplicity, assignment): **G3^{2B12gh5V}** (for atom numbering see Scheme 3, for spectrum see Figure 2C): 8.20-7.69 ([73H], m, NH(G3)+1,8,3^V); 7.33 ([10H], overlapped t and d, 2^V and 7^V); biotin resonances: 6.46 and 6.40 ([2H] and [2H], overlapped s, 10^B and 11^B); 2.05 ([4H], 2^B); 1.61-1.29 ([12H], 3^B, 4^B, 5^B); gh O<u>H</u> resonances: 4.43-4.28 ([36H], m, 2′-4′^{gh}); gh CH_2 resonances: 3.87-3.71 ([36H], m, 2-4^{gh}); 3.58-3.37 ([48H], m, 5-7^{gh}); PAMAM G3 CH_2 broad resonances: 3.09-2.20 ([484H], CH_2(G3)).

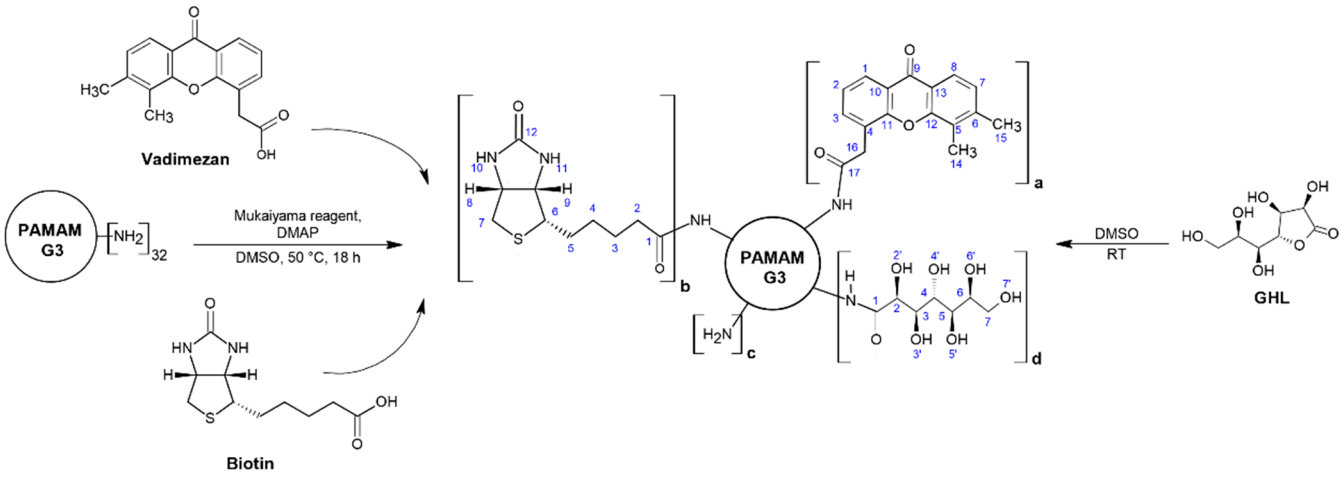

Scheme 3. Synthesis pathway of PAMAM G3 dendrimer substituted with vadimezan, biotin and α-D-glucoheptono-1,4-lactone attached via amide bond: $G3^{2B12gh5V}$ (a = 5, b = 2, c = 13, d = 12).

2.5. NMR Spectroscopy

The 1-D ^{1}H and ^{13}C NMR spectra and 2-D ^{1}H-^{1}H correlations spectroscopy (COSY), ^{1}H-^{13}C heteronuclear single quantum correlation (HSQC), and heteronuclear multiple bond correlation (HMBC) spectra were obtained with Bruker 300 MHz instrument (Rheinstetten, Germany) at the University of Rzeszow (College of Natural Sciences).

2.6. Conjugates Size and ζ Potential Measurements

ζ potential and size of $G3^{gh2B5M}$, $G3^{12gh2B5M}$, $G3^{gh4B5V}$ and $G3^{12gh2B5V}$ were estimated with the dynamic light scattering technique at pH 5 (0.05 M acetate buffer) and pH 7 (water) using the Zetasizer Nano instrument (Malvern, UK). Measurements were performed for 1 mg/mL samples (0.06–0.1 mM solutions).

2.7. Biological Studies

2.7.1. Cell Cultures

Human cancer cell lines: U-118 MG (glioblastoma multiforme, grade IV) and SCC-15 (squamous cell carcinoma) were grown in DMEM and DMEM/F-12 with hydrocortisone (400 ng/mL), respectively. Normal human skin fibroblasts (BJ) were cultured in EMEM. Growth media were supplemented with heat-inactivated 10% FBS and 100 U/mL penicillin and 1% streptomycin solution. Cells were cultured at 37 °C in a humidified 95% air/5% CO_2 with growth media changed every 2–3 days. Cells were passaged at 75%–85% confluence using 0.25% trypsin–0.03% EDTA in PBS (calcium and magnesium ions free). The morphology of cells was observed under a Nikon TE2000S Inverted Microscope with phase contrast (Tokyo, Japan). The number and viability of cells were estimated by a trypan blue exclusion test using an Automatic Cell Counter TC20 (BioRad Laboratories, Hercules, CA, USA) or a Neubauer chamber. All assays were performed in triplicates in three independent experiments. The working solutions of the synthesized dendrimer conjugates and the drugs alone were prepared from stock solutions in cell culture media with an adjusted concentration of DMSO. Control samples with non-treated cells in a complete culture medium with adjusted DMSO concentration were included in all biological tests.

2.7.2. Cytotoxicity

The cytotoxicity of αM, V, and their conjugates with PAMAM G3 modified dendrimer ($G3^{gh2B5M}$, $G3^{2B12gh5M}$, $G3^{gh4B5V}$ and $G3^{2B12gh5V}$) was examined with neutral red (NR) uptake assay or XTT reduction assay. BJ, U-118 MG and SCC-15 cells were seeded in flat, clear bottom 96-well plates in triplicate (100 µL of cell suspension/well) at a density of 1×10^4 cells/well and left for 24 h to attach. Then, culture medium was removed and cells were incubated in 37 °C with 100 µL of working solutions of αM, V, $G3^{gh2B5M}$, $G3^{2B12gh5M}$,

G3^{gh4B5V} or **G3^{2B12gh5V}** for 48 h. After that, NR or XTT assays were performed as earlier described [31].

2.7.3. Proliferation

Cells proliferation was estimated using Hoechst 33,342 staining. BJ, U-118 MG and SCC-15 cells at a density of 5×10^3/well were seeded into 96-well plates and incubated for 24 h at 37 °C to attach. Then, following the culture medium removal, cells were incubated with 100 µL of working solutions of the studied drugs or dendrimer conjugates for 72 h. Afterwards, plates were centrifuged (5 min, 700 g) and the working solutions of studied compounds removed. Cells were fixed in 3.7% formaldehyde solution in PBS for 10 min at room temperature and again centrifuged followed by staining with 1 µg/mL Hoechst 33,342 solution in PBS (100 µL, 1 h). The fluorescence signal was measured using Tecan Infinite M200 PRO Multimode Microplate Reader (TECAN Group Ltd., Männedorf, Switzerland) at 350/461 nm.

2.7.4. Toxicity to *Caenorhabditis elegans* and the Worm Survival Analysis

Caenorhabditis elegans nematodes (wild type strain N2, variety Bristol) were cultured at 20 °C on NGM agar plates with *E. coli* OP50 lawn as a food source [40]. Worm survival analysis was performed as described in [29].

2.7.5. Statistical Analysis

In order to estimate the differences between treated cells and non-treated control groups, statistical analysis was performed using the non-parametric Kruskal-Wallis test due to the lack of a normal distribution of the data. To determine the statistically significant differences between the ester conjugate-treated group (**G3^{gh2B5M}** or **G3^{gh4B5V}**) against the amide conjugate-treated group (**G3^{2B12gh5M}** or **G3^{2B12gh5V}**), a Mann–Whitney U test was applied ($p \leq 0.05$ was considered statistically significant). The survival curves of *C. elegans* nematodes were presented in a plot of the Kaplan–Meier estimator. Gehan's Wilcoxon test was used to assess statistically significant differences (with $p \leq 0.05$) between treated and non-treated control nematodes. All analyses and calculations were performed with Statistica 13.3 software (StatSoft Poland, Cracow).

3. Results and Discussion

3.1. Syntheses and Characterization of Dendrimer Conjugates

The PAMAM G3 dendrimer was converted by exhaustive glucoheptoamidation with GHL as described before [39] to obtain **G3^{gh}** (Scheme 1A). This 2 nm sized dendrimer was then used as a core to attach αM or V and biotin (B). The αM was modified by ester attachment of succinyl linker (αM-Suc) via 6-O (Scheme 1B) as was determined before [39]. At the step of conjugate formation, the carboxyl groups of αM-Suc or V, and B were activated efficiently with Mukaiyama reagent (2-chloro-1-methylpyridinium iodide) in the presence of 4-(dimethylamino)pyridine (DMAP), enabling further reaction with the **G3^{gh}** core hydroxyl groups. Mukaiyama reagent is commonly used for synthesis of esters, lactones, amides and ketenes, causing activation of hydroxyl groups of carboxylic acids and alcohols [41]. The products were isolated by extensive removal of low molecular reagents and side-products by dialysis and were characterized by NMR spectroscopy and DLS. The synthesis pathway and conjugate formula with atom numbering are presented in Scheme 2.

The ^{1}H NMR spectrum of **G3^{gh}** dendrimer conjugated with αM and biotin via ester bonds is presented in Figure 1B compared to αM alone (Figure 1A) (both measurements were performed in DMSO-d_6).

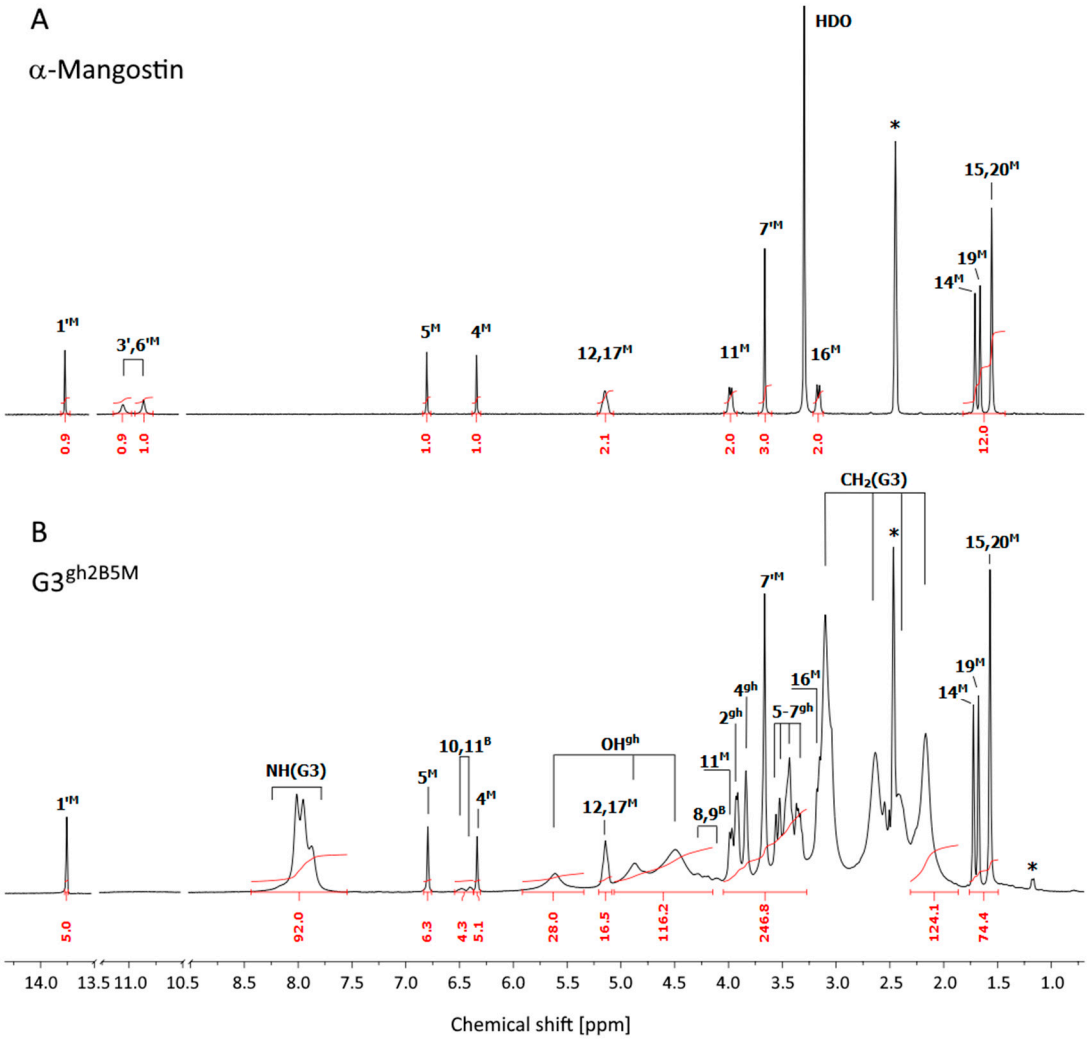

Figure 1. The ^{1}H NMR spectra of α-mangostin (**A**) and G3^{gh2B5M} conjugate (**B**) in DMSO-d$_6$. The residual solvent peak at 2.5 ppm and impurity resonances are marked with asterisks *. The PAMAM G3 core dendrimer resonances are labeled as CH_2(G3) and NH(G3) in spectrum B. The resonances of α-mangostin, biotin, and glucoheptoamide are labeled by locants with ^{M}, ^{B}, and ^{gh} upper indexes, respectively, according to the atom numbering in Scheme 2. The 1A spectrum was taken from [29].

Additional 2-D COSY, HSQC and HMBC measurements were performed (Figures S1 and S2) and allowed for detailed assignments of ^{1}H and ^{13}C resonances (Table S1). The number of attached residues of αM and B to **G3^{gh}** dendrimer was estimated based upon the integral intensity of αM aromatic protons (5^{M} at 6.79 ppm and 4^{M} at 6.34 ppm) and one free hydroxyl proton (1′^{M} at 13.73 ppm) resonances, and B resonances (10^{B} and 11^{B} at 6.48 and 6.40 ppm) in relation to the reference intensity of b$_{0-3}$ protons resonance from the dendrimer core, namely [120H] (for detailed assignment of protons from internal PAMAM G3 arms see Figure 2 in [29]). The averaged final product was identified as G3^{gh2B5M}. In its ^{1}H-NMR spectrum, the characteristic resonances of αM protons are observed and retained the same chemical shifts as resonances of protons recorded in αM alone. Proton resonances from 3′^{M} and 6′^{M} hydroxyl groups were not detected, while singlet resonance at 13.73 ppm corresponding to the third hydroxyl group proton (1′^{M}) was found. It suggests that either of the 3′^{M} and 6′^{M} protons participate in bonding to **G3^{gh}** dendrimer.

The ^{1}H NMR spectrum of **G3^{gh}** conjugated with vadimezan and biotin is shown in Figure 2B in comparison with vadimezan (Figure 2A) (both in DMSO-d$_6$), while detailed NMR spectral assignments were performed by 2-D COSY, HSQC, and HMBC measure-

ments as presented in Figure S3 (COSY) and Figure S4 (combined heteronuclear ^{1}H-^{13}C HSQC/HMBC) with Table S1.

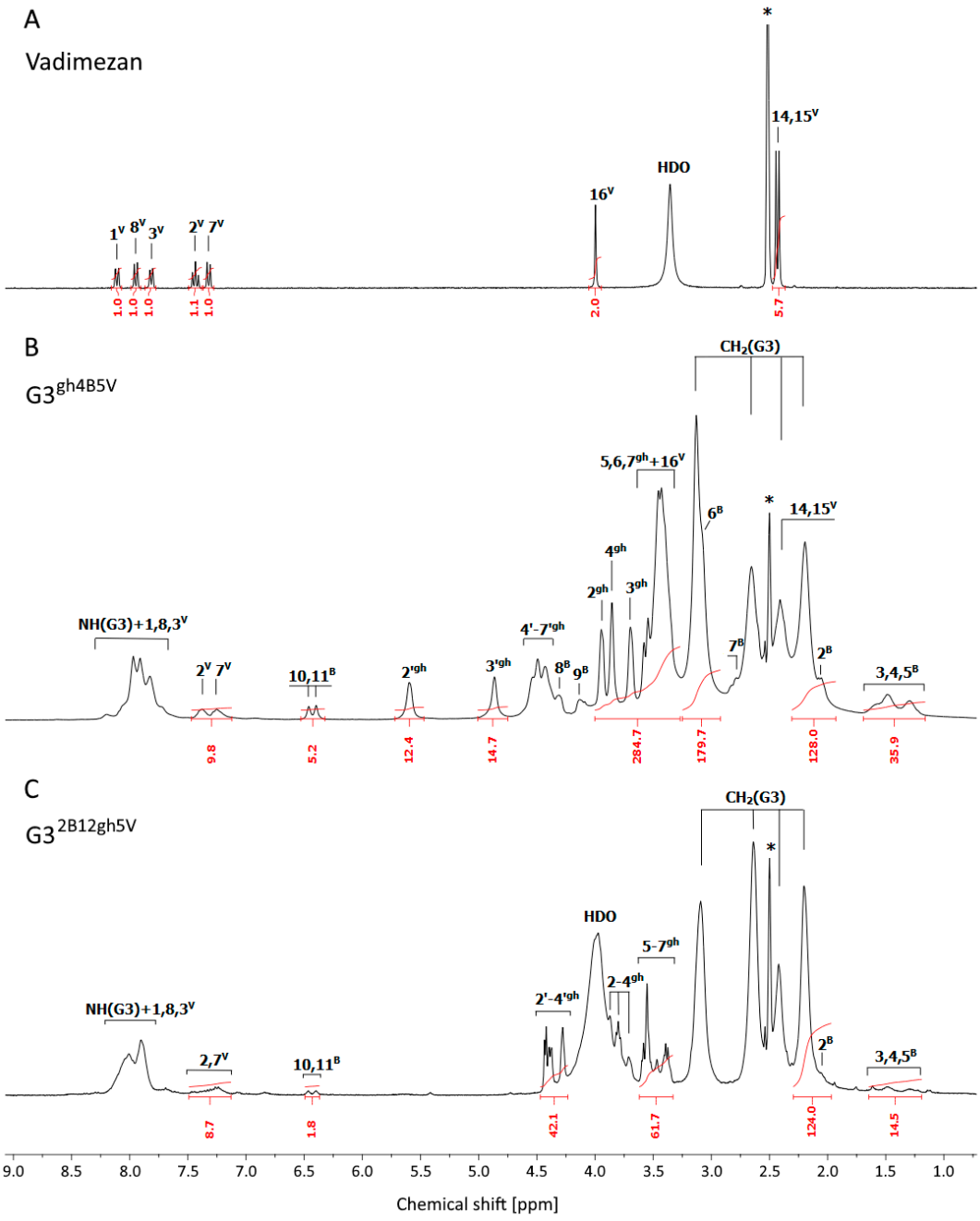

Figure 2. The ^{1}H NMR spectra of vadimezan (**A**), **G3^{gh4B5V}** (**B**) and **G3^{2B12gh5V}** (**C**) conjugates in DMSO-d_6. The residual solvent peak at 2.5 ppm is marked with asterisks *. The PAMAM G3 core dendrimer resonances are labeled as CH_2(G3) and NH(G3) in spectrum B and C. The resonances of vadimezan, biotin, and glucoheptoamide are labeled by locants with ^{V}, ^{B}, and ^{gh} upper indexes, respectively, according to the atom numbering in Schemes 2 and 3.

The stoichiometry of conjugate was determined by a comparison of integral intensity of V aromatic proton resonances (2^{V} and 7^{V}) at 7.50–7.15 ppm, and B resonances (10^{B} and 11^{B} at 6.50–6.35 ppm) versus CH_2($b_{0\text{-}3}$) PAMAM G3 core resonance centered at 2.20 ppm ([120H]); additional intensity comes from 4 biotin CH_2 multiplet identified in COSY (Figure S3, cross-peak q). The average conjugate was identified as **G3^{gh4B5V}**. Only 2^{V} and 7^{V} aromatic protons resonances were recorded as isolated signals, while the remaining signals

of vadimezan protons are overlapped by resonances of dendrimer and gh protons. 2-D COSY, HSQC and HMBC measurements allowed for detailed assignment of each signal. It is worth noting that within glucoheptoamide residues the CH resonances were identified unambiguously (in COSY cross-peak j is between 2^{gh} and 3^{gh}), while scalar couplings within hydroxymethylene groups HO-C-H were observed (cross-peaks e, f, h, and g in COSY experiment, see Figure S3), which enabled to combine vicinal OH and H in gh residues (Table S1).

PAMAM G3 dendrimer conjugate with amide-bonded vadimezan, biotin, and GHL was synthesized to compare its activity with that of the αM dendrimer conjugate (**G3^{2B12gh5M}**) obtained and described earlier [29]. As in the synthesis of the ester conjugates described above, Mukaiyama reagent was also used in the synthesis of the amide conjugate with V. In this procedure, native PAMAM G3 was used as a conjugate core. In the presence of Mukaiyama reagent and DMAP, amine groups from the dendrimer surface were able to react with carboxyl groups of V and B. The intermediate product, isolated by dialysis and characterized by NMR spectroscopy, was identified as G3^{2B5V} and further converted into half-glucoheptoamidated derivative by the substitution of half of the remaining amine groups with GHL. The synthesis pathway and conjugate formula with atom numbering are presented in Scheme 3. The ^{1}H NMR spectrum of the conjugate in DMSO-d_6 is shown in Figure 2C. The stoichiometry of the conjugate was estimated in the same way as described above for ester-bonded vadimezan conjugate and allowed us to identify product as **G3^{2B12gh5V}**.

The conjugates were obtained in rather low yield (<55%) due to compromising it against the high purity reached by extensive dialysis.

3.2. Size and ζ Potential of Dendrimer Conjugates

DLS measurements were performed to determine the size and zeta potential of the synthesized conjugates. Obtained values are collected in Table 1 and illustrated in Figures S5 and S6.

Table 1. Size of conjugates averaged by volume (d(V)) and by number of molecules (d(N)) and zeta potential values ± standard deviation determined by DLS analysis.

Compound	Size [nm]				Zeta Potential [mV]	
	pH 7		pH 5		pH 7	pH 5
	d(V)	d(N)	d(V)	d(N)		
G3^{gh}	1.7 ± 0.44	1.5 ± 0.51	4.3 ± 0.34	3.6 ± 0.32	4.5 ± 0.58	5.3 ± 0.81
G3^{gh2B5M}	155.1 ± 3.46	113 ± 5.89	212.7 ± 4.29	144.5 ± 6.49	10 ± 0.39	24.9 ± 1.78
G3^{2B12gh5M} [29]	1367 ± 245.7	1262 ± 196.4	178.3 ± 5.73	113.8 ± 7.34	22.7 ± 1.01	37.5 ± 2.32
G3^{gh4B5V}	3.7 ± 0.23	2.9 ± 0.56	4.9 ± 0.14	4.2 ± 0.18	7.6 ± 4.35	6.2 ± 0.81
G3^{2B12gh5V}	1166 ± 153	970.4 ± 81.6	1090 ± 39.2	924.4 ± 39	22.8 ± 0.69	33.4 ± 2.82

The dynamic diameter of **G3^{gh}** in an aqueous solution is 1.5 nm (averaged by number) or 1.7 nm (averaged by volume), which is nearly two-fold smaller than diameter of the native PAMAM G3. In the acidic environment (pH 5) the diameter of **G3^{gh}** increases to 3.6 nm (d(N)) or 4.3 nm (d(V)) upon protonation of internal tertiary amine groups, which was observed earlier for the series of G3 substituted with variable amount of gh residues [42]. Slightly higher dynamic diameter of **G3^{gh4B5V}** conjugate, equal 2.9 nm (by number) or 3.7 nm (by volume) in water and 4.2 nm (d(N)) or 4.9 nm (d(V)) in pH 5, indicates that this conjugate is dispersed at unimolecular level. The other conjugates were associated both in pH 7 and pH 5, with the strongest effect observed for **G3^{2B12gh5M}** and **G3^{2B12gh5V}**. The molecules of the ester conjugate G3^{gh2B5M} also associate but particle size is 10 times smaller than that of the amide **G3^{2B12gh5M}** analogue. However, the particle size of **G3^{2B12gh5M}** was reduced by seven times upon a pH decrease from 7 to 5. This effect can be attributed to the presence of ca. 12 free amine groups in the **G3^{2B12gh5M}** conjugate which are readily to protonate, while amine groups in ester conjugate are fully glucoheptoamidated.

All studied conjugates have positive zeta potential. For conjugates with small molecular size, **G3^{gh}** and **G3^{gh4B5V}** zeta potential values are <10 mV and increase with the conjugates diameter up to 33.4 mV and 37.5 mV for **G3^{2B12gh5V}** and **G3^{2B12gh5M}**, respectively. It is also worth noting that amide conjugates, **G3^{2B12gh5M}** and **G3^{2B12gh5V}** have comparable zeta potential and particle size but they differ in biological activity (vide infra). Due to the fact that the cell membrane is negatively charged, nanoparticles with positive net charge have a greater ability to enter and penetrate cells [43].

3.3. Cytotoxicity

The NR and XTT assays revealed that vadimezan (V) after 48 h incubation showed no cytotoxic effect against any studied cell line (BJ, SCC-15 and U-118 MG) up to 200 μM concentration (Table 2). Vadimezan is a Vascular Disrupting Agent (VDA) whose anticancer action, based mainly on an irreversible destruction of established tumor vessels and tumor blood flow arrest, has been observed mainly in the endothelial cells where it induced apoptosis [14]. However, the present results do not indicate V to lower viability of cells, including epithelial cancer cells (SCC-15). Our results are consistent with other, pointing to the drug's selective toxicity against vascular endothelial cells. Using the MTT assay, Zhang et al. [44] showed that V did not disturb the mitochondrial metabolism of any of ten cell lines (Ishikawa, A549, Bewo, HeLa, Siha, MCF-7, HL-60, BEL-7402, NCI-460, BGC-823) after 48 h incubation. Lv et al. [45] also found free V (up to 35.4 μM) to be non-toxic to breast carcinoma MCF-7 cells, lung carcinoma A549 cells and mouse embryo fibroblast NIH/3T3 cells after 48 h treatment. Only human vein umbilical cell (HUVEC) growth was demonstrated to undergo inhibition by vadimezan (IC_{50} > 20 μM) [44]. On the other hand, the delivery of nanoparticles (mPEG-*b*-PHEA) conjugated with V and encapsulated with DOX resulted in cytotoxicity to both tumorous and nontumorous cells. Furthermore, those nanoparticles equipped with V and DOX showed a similar inhibition of cells proliferation to free DOX [45].

Table 2. The half maximal inhibitory concentration (IC_{50}) values estimated with NR and XTT assay after 48 h incubation of BJ, U-118 MG and SCC-15 cells with αM or V, each used either as a free drug or the dendrimer conjugate. The IC_{50} values were calculated with AAT Bioquest IC_{50} calculator [46].

	IC_{50} [μM] NR Assay		
	BJ	**U-118 MG**	**SCC-15**
α-mangostin [2]	8.97	9.59	6.43
G3^{gh2B5M}	2.02	2.52	1.7
G3^{2B12gh5M} [29]	2	1.83	1.41
Vadimezan	>>200	>>200	>>200
G3^{gh4B5V}	>>24	>>24	>>24
G3^{2B12gh5V}	>>12	>>12	>>12
	IC_{50} [μM] XTT Assay		
	BJ	**U-118 MG**	**SCC-15**
α-mangostin [2]	18.58	18.15	7.72
G3^{gh2B5M}	3.36	4.14	3.02
G3^{2B12gh5M} [29]	2.37	2.05	2.52
Vadimezan	>>200	>>200	>200
G3^{gh4B5V}	>>24	>>24	>>24
G3^{2B12gh5V}	>>12	>>12	>>12

The anticancer activity of xanthones depends on the type, number, and position of the attached functional groups in their skeleton [47]. Anticancer activity of αM seems to depend on the presence of two isoprenyl groups localized on 2-nd and 8-th carbon in xanthenone ring [29], not present in vadimezan. Castanheiro et al. [48] showed that the introduction of the prenyl group to the 1-hydroxyxanthone markedly increased its anticancer activity against the MCF-7 cell line, in accordance with the presence of prenyl groups being associated with an improvement of potency and selectivity of xanthones [49].

At present, prenylated xanthones are the most valued xanthones, in view of their promising properties as active and selective anticancer agents [47].

The present results reflect an attempt to increase the anti-tumor activity of V and αM by covalent binding the drugs to biotinylated PAMAM G3 dendrimers, demonstrated previously to be effective in this respect [50]. Cytotoxicity assays revealed that vadimezan attached to biotinylated and glucoheptoamidated PAMAMs did not exert any significant inhibitory activity (up to 24 μM $G3^{gh4B5V}$ or 12 μM $G3^{2B12gh5V}$ after 48 h incubation (Table 2, Figures 3 and 4). It should be added that the latter observation provided additional evidence that the applied V vehicles do not show biological activity (*cf.* Figure S7 for $\mathbf{G3^{gh}}$ and [29] for $\mathbf{G3^{2B12gh}}$. Of note is (Figures 3 and 4) that 4–12 μM $G3^{2B12gh5V}$ lowered SCC-15 cell viability down to 80% (apparent only in the XTT assay) and 2–12 μM $G3^{gh4B5V}$ increased BJ cell viability by 25–40% (apparent only in the NR assay). This effect might be caused by changes in cell proliferation rate, as discussed below.

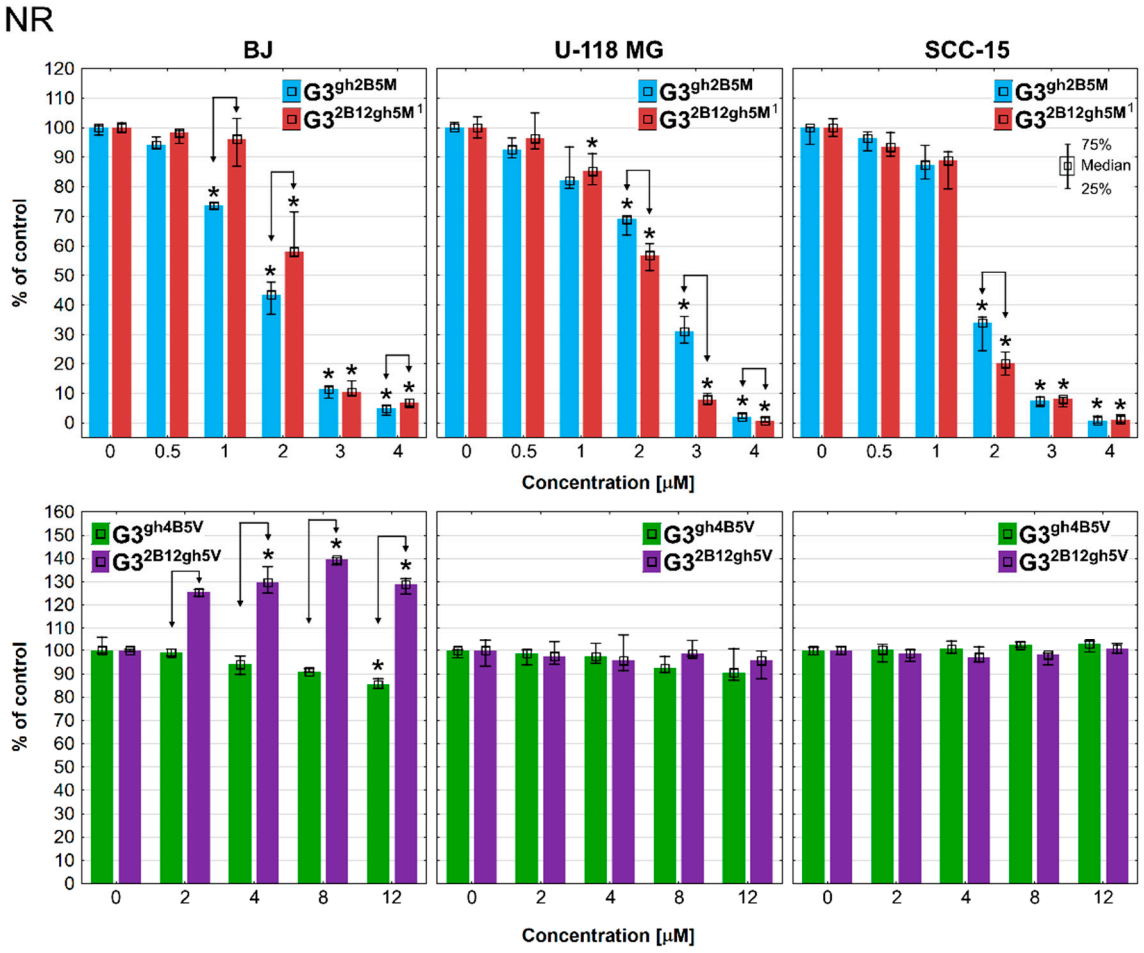

Figure 3. Cytotoxic effect of dendrimers conjugated via ester or amide bond with αM ($G3^{gh2B5M}$ and $G3^{2B12gh5M}$) and V ($G3^{gh4B5V}$ and $G3^{2B12gh5V}$) after 48 h of incubation with normal fibroblasts (BJ), glioblastoma cells (U-118 MG), and squamous carcinoma cells (SCC-15), estimated with the NR assay. Cell viability (expressed as percent of the non-treated control) medians are plotted. The whiskers are lower (25%) and upper (75%) quartile ranges. * $p \leq 0.05$; Kruskal-Wallis test (against non-treated control), $\updownarrow$ $p \leq 0.05$; Mann-Whitney U test (ester against amide-attached drug-conjugate). [1] Data for $G3^{2B12gh5M}$ were reproduced from [29].

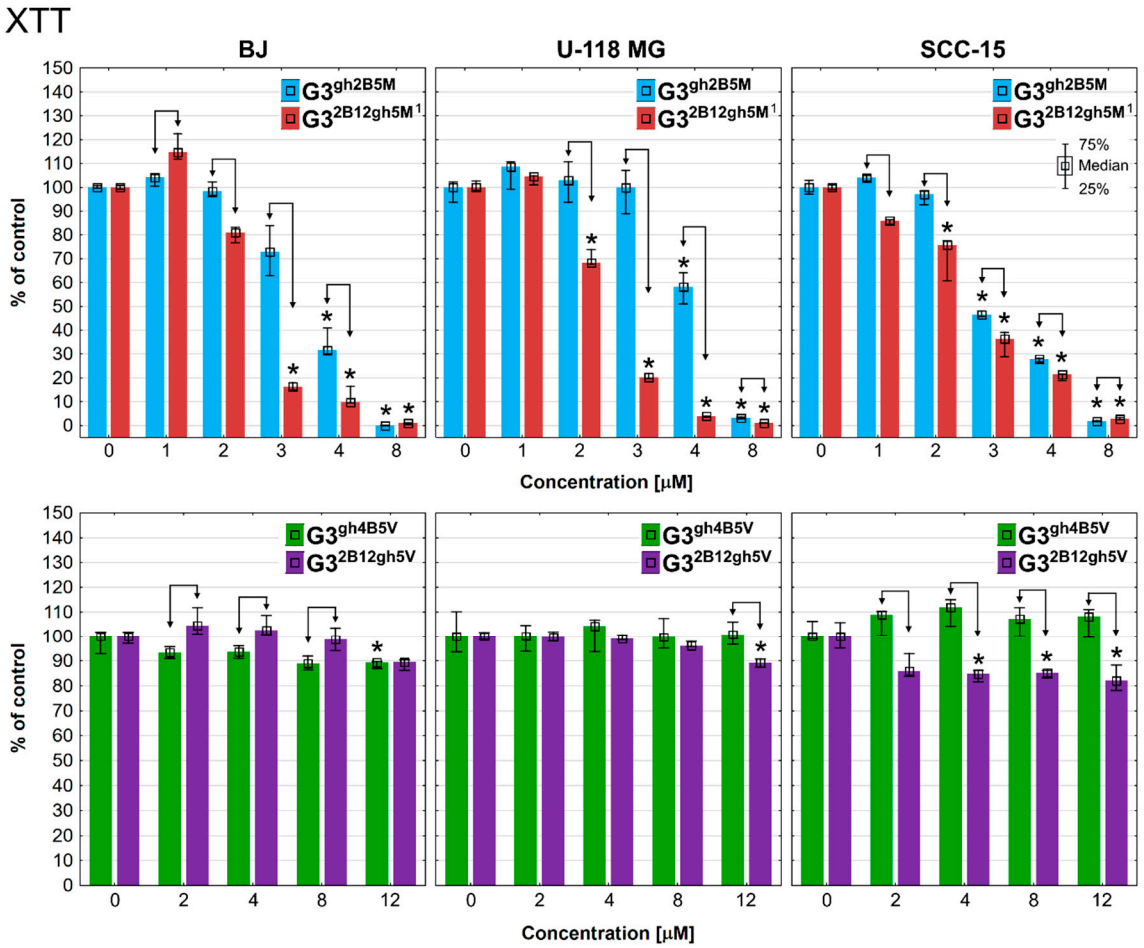

Figure 4. Viability of normal fibroblasts (BJ), glioblastoma cells (U-118 MG) and squamous carcinoma cells (SCC-15) after 48 h of incubation with $G3^{gh2B5M}$, $G3^{2B12gh5M}$, $G3^{gh4B5V}$ and $G3^{2B12gh5V}$, assessed by XTT assay. Cells viability (expressed as percent of the non-treated control) medians are plotted. The whiskers are lower (25%) and upper (75%) quartile ranges. * $p \leq 0.05$; Kruskal-Wallis test (against non-treated control), $\updownarrow$ $p \leq 0.05$; Mann-Whitney U test (ester- against amide-attached drug-conjugate). [1] Data for $G3^{2B12gh5M}$ were reproduced from [29].

The activity of αM increased significantly after attaching it to the studied carriers. The action of conjugate $G3^{2B12gh5M}$ was slightly stronger than $G3^{gh2B5M}$ with an IC_{50} of approx. 1.4–2 μM (NR assay) and 2–2.5 μM (XTT assay) for all studied cell lines. The largest differences were observed in glioma cells, where $G3^{2B12gh5M}$ acted two-fold stronger than $G3^{gh2B5M}$. Moreover, the strongest effect of both conjugates was still observed in SCC-15 cells (Table 2, Figures 3 and 4).

The greater effect of an αM-amide conjugated dendrimer may result from the fact that it has free amino groups responsible for the cytotoxic effect. As it was presented in Section 3.2. the zeta potential of the $G3^{2B12gh5M}$ conjugate was higher than that of $G3^{gh2B5M}$. It could be the reason of a higher activity of the former, since dendrimers with higher zeta potential and surface charge indicate higher cytotoxicity also in consequence of more efficient cellular uptake [51,52]. An important issue is the mechanism of possible enzymatic degradation of amide or ester bonds in conjugates with the participation of lysosomal or other intracellular enzymes and the consequent release of attached drugs. Kurtoglu et al. have shown that PAMAM dendrimer–ibuprofen conjugates with ester or amide linkers differ in the degree of drug release. Amide and ester-linked conjugates were very stable after 48 h of incubation in buffer. The ester-linked conjugates showed pH-dependent release and the extent of release varied with pH from 3% (pH 5) to 38% (pH 8.5) within a 10-day studied period. Moreover, direct amide- and ester-linked conjugates did

not release ibuprofen enzymatically in cathepsin B buffer and diluted human plasma [28]. This means that the incubation time of both tested dendrimers ($\mathbf{G3^{2B12gh5M}}$ and $\mathbf{G3^{gh2B5M}}$) with cells in FBS containing medium was too short to observe significant differences in the release of αM from the conjugates. This was also confirmed by the results of our previous studies concerning the release of doxorubicin conjugated through amide linker to glucoheptoamidated PAMAM G3 dendrimer [39]. Although ester bonds are generally easy to hydrolyze (such as carboxylate ester bond), some ester structures, such as alkyl esters, hydrolyze very slowly, even in the presence of esterase [27]. This could be the reason of weaker activity of dendrimeric conjugates with ester-bonded αM. Quintana et al. [53] and Thomas et al. [54] used, as a model drug, methotrexate (MTX), having two available functional groups for conjugation, carboxylic and amine, in order to examine the effect of the type of chemical bond on the conjugate activity. MTX conjugated to acetamide-functionalized G5 PAMAM dendrimer through ester bond was found four times more active than free MTX, whereas MTX conjugated via amide bonds to the same dendrimer was less active compared to free MTX. However, in this case, changing the binding site of the drug molecule may induce changes in its activity.

An important factor influencing the toxicity of nanoparticles is the efficiency and the pathway they enter cells that depends on their size and charge. All studied conjugates indicated positive charge on their surface. The smallest conjugates ($\mathbf{G3^{gh}}$ and $\mathbf{G3^{gh4B5V}}$) can probably enter cells through passive uptake, while slightly larger compound $\mathbf{G3^{gh2B5M}}$ (ca. 113 nm diameter) via clathrin-mediated endocytosis. In the case of $\mathbf{G3^{2B12gh5M}}$ and $\mathbf{G3^{2B12gh5V}}$ conjugates, the most possible route of internalization seems to be phagocytosis and/or micropinocytosis (associates diameter ca. 1000–1300 nm) [55]. This phenomenon requires further research.

3.4. Proliferation

There are no clear examples of the antiproliferative activity of vadimezan in the available literature, which suggests that such properties were not observed at therapeutic concentrations. One paper showed that the combination of tCoa-NGR fusion proteins with V suppressed the growth and proliferation of B16-F10 melanoma tumors in C57/BL6 mice [56]. In our studies, V inhibited the proliferation of cancer SCC-15 cells from 100 μM concentration and U-118 MG glioma cells from 200 μM, but not normal cells (Figure 5). PAMAM G3 dendrimer, biotinylated and partially glucoheptoamidated with V bound via amide linker ($\mathbf{G3^{2B12gh5V}}$), enhanced its anti-proliferative activity by as much as 50-fold. This construct distinctly limited proliferation of SCC-15 and U-118 MG cells when applied at concentrations 2 and 12 μM, respectively. This effect apparently was related to the decrease of mitochondrial efficiency observed at 4–12 μM $\mathbf{G3^{2B12gh5V}}$ in SCC-15 and U-118 MG cells(Figure 4). Of note is that in normal BJ cells $\mathbf{G3^{2B12gh5V}}$ rather promoted cell proliferation at 8 and 12 μM concentrations (Figure 5), suggesting $\mathbf{G3^{2B12gh}}$ vehicle to be responsible for this effect, as it significantly increased fibroblasts growth at the 5–20 μM range of concentrations [29]. No effect was observed with the conjugate containing the ester linkage ($\mathbf{G3^{gh4B5V}}$), despite the fact that the 20 μM $\mathbf{G3^{gh}}$ vehicle itself showed a weak anti-proliferative effect against SCC-15 cells (Figure S7, part C). The size and zeta potential of the studied conjugates may be important factors influencing their properties, as the $\mathbf{G3^{2B12gh5V}}$, compared to $\mathbf{G3^{gh4B5V}}$ conjugate, showed higher activity and formed associations with diameter at pH 7 being about 300-fold larger (about 1000–1200 nm vs. 2.90–3.7 nm). Thus, it may increase the polyvalence of conjugates, which is responsible for their increased activity [57]. The size of the molecule and the presence of free amino groups on the $\mathbf{G3^{2B12gh5V}}$ surface corresponded to its 3-fold higher zeta potential, responsible for a stronger toxicity of dendrimers [51]. However, it seems that this was a rather minor effect, since this phenomenon was not seen in normal BJ fibroblasts (BJ cells are more sensitive to high surface charge of dendrimers than SCC-15 cancer cells [58]).

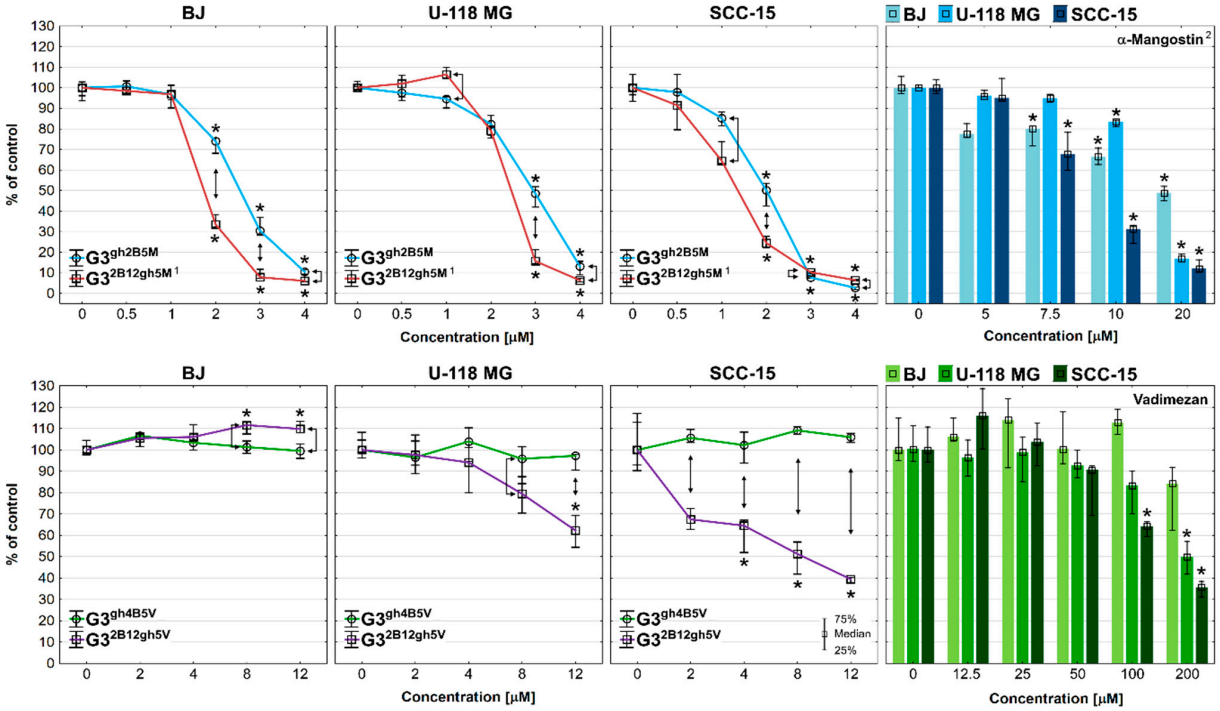

Figure 5. Anti-proliferative effect of $G3^{gh2B5M}$, $G3^{2B12gh5M}$, $G3^{gh4B5V}$, $G3^{2B12gh5V}$, αM, and V on BJ, U-118 MG, and SCC-15 cells after 72 h of incubation, determined with Hoechst 33,342 staining. Medians of the fluorescence signal (expressed as percent of the non-treated control), indicating the cell number in a well, are plotted. The whiskers indicate lower (25%) and upper (75%) quartile ranges. * $p \leq 0.05$; Kruskal-Wallis test (against non-treated control), ↕ $p \leq 0.05$; Mann-Whitney U test (ester against amide-attached drug-conjugate). [1,2] Data for $G3^{2B12gh5M}$ conjugate and αM were reproduced from [2,29], respectively.

Unlike vadimezan, αM is a well-known anti-proliferative agent. The inhibition of cell proliferation induced by αM led to G1-phase arrest and S-phase suppression in MDA-MB231 human breast cancer cells with altering the expression of cell-cycle-related molecules, such as $p21^{cip1}$, CHEK2, cyclins, CDKs, and PCNA [59]. The G0/G1 phase arrest and the G1 arrest caused by αM was also observed in four hepatocellular carcinoma (HCC) cell lines [9] and human oral squamous carcinoma cells (OSCC) [60], respectively. In our study, the proliferation of cancer cells (U-118 MG and SCC-15) and normal BJ fibroblasts was studied after 72 h of incubation with each of the xanthones (αM and V) and their dendrimer conjugates. The results are presented in Figure 5 and demonstrate anti-proliferative activity of αM in the concentration range of 7.5–20 μM [2]. The strongest inhibition of proliferation was observed for SCC-15 cells (reduction to 12% at 20 μM), slightly weaker for glioma cells (reduction to 17% at 20 μM) and the weakest for normal fibroblasts (reduction to 49% at 20 μM).

Conjugation of biotinylated dendrimers with 5 residues of αM enhanced its anti-proliferative activity against both cancer and normal cell lines, with the $G3^{gh2B5M}$ ester conjugate acting slightly weaker (over 3-fold enhancement) than the $G3^{2B12gh5M}$ amide conjugate (over 5-fold enhancement). The proliferation of SCC-15 cells underwent the strongest inhibition by these two αM conjugates (almost no viable cells at 3 and 4 μM, respectively). The latter effect was less pronounced in the case of normal cells (30% viable cells at 3 μM $G3^{gh2B5M}$ and 34% viable cells at 2 μM $G3^{2B12gh5M}$), with glioblastoma cells being the least sensitive (49% and 16% at 3 μM $G3^{gh2B5M}$ and $G3^{2B12gh5M}$, respectively). The most significant difference in suppression of cell growth elicited by αM ester or amide conjugates was observed with fibroblasts (74% and 33% viable cells at 2 μM $G3^{gh2B5M}$ and $G3^{2B12gh5M}$, respectively).

3.5. Toxicity against C. elegans and the Effect on the Worm Survival

Biological activities of αM and V, used as free compounds or their dendrimer conjugates, were also evaluated with a model nematode, *Caenorhabditis elegans*, a cost-effective and powerful model widely used for screening of bioactive compounds prior to be tested with higher animals [37]. *C. elegans* has been previously used in studies on the toxicity of drug-loaded nanoparticles, such as glibenclamide-loaded PVM/MA (poly(methylvinyl ether-co-maleic anhydride)) nanoparticles for oral delivery purposes [61], insulin-loaded PPA (PEG-polu(anhydride) conjugate) nanoparticles with the ability to mucus permeation for the oral administration of insulin [62], and the toxicity of bare nanoparticles, for example, zinc oxide nanoparticles (ZnO-NPs) [63] and gold nanoparticles (AuNPs) [64].

We used synchronized population of L4-stage nematodes to examine survivability and general toxicity after 7 days of incubation with free αM or V, and with their dendrimer conjugates: $G3^{gh2B5M}$, $G3^{2B12gh5M}$, $G3^{gh4B5V}$, $G3^{2B12gh5V}$ at different concentration ranges. The results of worms' survival are shown in Figure 6 and in Table 3 (LC_{50} values).

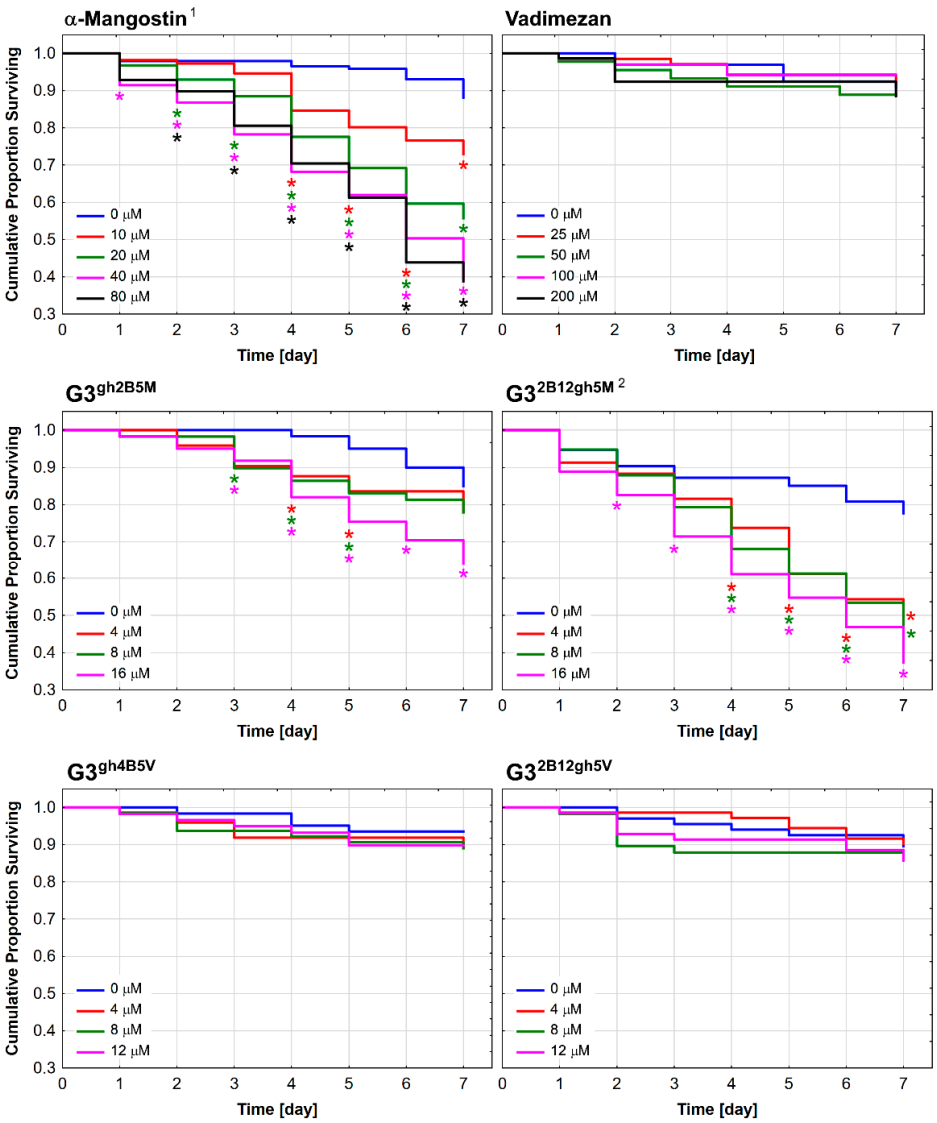

Figure 6. The Kaplan-Meier survival curves of *C. elegans* after 7 days of incubation with αM, V, $G3^{gh2B5M}$, $G3^{2B12gh5M}$, $G3^{gh4B5V}$ or $G3^{2B12gh5V}$. Results are presented as cumulative proportion surviving. Statistically significant differences against dmso-treated control obtained in Gehan's Wilcoxon test are marked with asterisks * ($p \leq 0.05$) in the colours corresponding to the tested concentrations. [1,2] Data for αM and $G3^{2B12gh5M}$ conjugate were reproduced from [2,29], respectively.

Table 3. The half maximal lethal concentration (LC_{50}) values estimated after 7 days incubation of *C. elegans* nematodes with free αM and V, or their dendrimer conjugates. Data are presented as medians with the first and third quartile. Presented values were calculated with AAT Bioquest IC_{50} calculator [46].

	LC_{50} [μM]	1st Quartile	3rd Quartile
α-Mangostin [2]	18.74	18.64	20.23
$G3^{gh2B5M}$	>16	>16	>16
$G3^{2B12gh5M}$ [29]	7.87	4.95	8.09
Vadimezan	>>200	>>200	>>200
$G3^{gh4B5V}$	>>24	>>24	>>24′
$G3^{2B12gh5V}$	>>12	>>12	>>12

Free V exhibited no toxicity against *C. elegans* up to 200 μM concentration with a cumulative proportion surviving equal to 90%. The conjugation of V to the dendrimer by either ester or amide bonds also did not increase its toxicity. On the other hand, αM caused a toxic effect with the LC_{50} value, the minimum being over 10 times higher than that of V (comparing LC_{50} values). This confirms that the presence of prenyl residues in αM structure has a significant influence on its toxicity in vivo. Substitution of αM with biotinylated and glucoheptoamidated dendrimers via ester linker ($G3^{gh2B5M}$) increased its toxicity only by 20%, while conjugate with amide-bonded αM ($G3^{2B12gh5M}$) was more active by 140% comparing to free αM (Table 3). Additionally, $G3^{gh2B5M}$ conjugate showed two-fold weaker activity than $G3^{2B12gh5M}$ in the worm.

4. Conclusions

Similar toxicity profiles of the tested conjugates in vitro and in vivo allow us to conclude that the main factors influencing the differences in the activity of evaluated agents were: differences in the value of the zeta potential and the size of the nanoparticles, as well as the presence of various linkers (amide or ester). The results clearly show that conjugates containing amide bonds, partially-blocked amino groups on the surface, larger particle diameters and higher zeta potentials could be a more effective tool for therapy for cancer and nematode infections. Considering the vadimezan mechanism of action, based on its selective effect on blood vessel cells in the tumor environment, conjugates with vadimezan are still valuable research objects. An antiproliferative effect of $G3^{2B12gh5V}$ in vitro against cancer, but not normal cells, is also interesting. Therefore, the proposed drug delivery system based on the PAMAM G3 dendrimer with partially-blocked amine groups on the surface can be a useful tool to improve the biological properties of transported drug molecules. Further studies on the in vivo model with implanted and perfused tumors are necessary.

Supplementary Materials: The following supporting information can be downloaded at: https://www.mdpi.com/article/10.3390/pharmaceutics14030606/s1, Figure S1: The ^{1}H-^{1}H COSY spectrum of $G3^{gh2B5M}$ in DMSO-d_6; Figure S2: The HSQC/HMBC combined spectra for $G3^{gh2B5M}$ in DMSO-d_6; Figure S3: The ^{1}H-^{1}H COSY spectrum of $G3^{gh4B5V}$ in DMSO-d_6; Figure S4: The HSQC/HMBC combined spectra for $G3^{gh4B5V}$ in DMSO-d_6; Figure S5: Diameter of conjugates averaged by volume (d(V)) and by number of molecules (d(N)) measured in water (A) and in acetate buffer pH 5 (B); Figure S6: Zeta potential of conjugates measured in water (pH 7) and acetate buffer (pH 5); Figure S7: Cytotoxicity of $G3^{gh}$ vehicle estimated with NR (A) and XTT (B) assay after 48 h incubation with normal fibroblasts (BJ), glioblastoma cells (U-118 MG) and squamous carcinoma cells (SCC-15); Table S1: The ^{1}H and ^{13}C resonance assignments of the $G3^{gh4B5V}$, V, $G3^{gh2B5M}$ and αM based on COSY and HSQC/HMBC spectra in DMSO-d_6.

Author Contributions: Conceptualization, J.M., W.R. and Ł.U.; methodology, S.W. and Ł.U.; software, J.M.; validation, J.M., S.W. and Ł.U.; formal analysis, W.R. and Ł.U.; investigation, J.M., S.W. and Ł.U.; resources, S.W., W.R. and Ł.U.; data curation, J.M., S.W. and Ł.U.; writing—original draft preparation, J.M., S.W. and Ł.U.; writing—review and editing, J.M., S.W., W.R. and Ł.U.; visualization,

J.M.; supervision, S.W., W.R. and Ł.U.; project administration, J.M. and Ł.U.; funding acquisition, W.R. and Ł.U. All authors have read and agreed to the published version of the manuscript.

Funding: Supported by the National Science Center, Poland, grant no. 2016/21/B/NZ1/00288.

Institutional Review Board Statement: Not applicable.

Informed Consent Statement: Not applicable.

Data Availability Statement: Data supporting the reported results are available on request from the corresponding author.

Acknowledgments: The kind support by Małgorzata Walczak from the Rzeszów University of Technology to enable us to perform DLS measurements is gratefully acknowledged.

Conflicts of Interest: The authors declare no conflict of interest.

References

1. Ho, L.Y.; Lim, Y.Y.; Tan, C.P.; Siow, L.F. Comparison of physicochemical properties and aqueous solubility of xanthone prepared via oil-in-water emulsion and complex coacervation techniques. *Int. J. Food Prop.* **2018**, *21*, 784–798. [CrossRef]
2. Markowicz, J.; Uram, Ł.; Sobich, J.; Mangiardi, L.; Maj, P.; Rode, W. Antitumor and anti-nematode activities of α-mangostin. *Eur. J. Pharmacol.* **2019**, *863*, 172678. [CrossRef] [PubMed]
3. Aukkanimart, R.; Boonmars, T.; Sriraj, P.; Sripan, P.; Songsri, J.; Ratanasuwan, P.; Laummaunwai, P.; Boueroy, P.; Khueangchaingkhwang, S.; Pumhirunroj, B.; et al. In Vitro and in Vivo Inhibitory Effects of α-Mangostin on Cholangiocarcinoma Cells and Allografts. *Asian Pac. J. Cancer Prev.* **2017**, *18*, 707–713. [CrossRef] [PubMed]
4. Beninati, S.; Oliverio, S.; Cordella, M.; Rossi, S.; Senatore, C.; Liguori, I.; Lentini, A.; Piredda, L.; Tabolacci, C. Inhibition of cell proliferation, migration and invasion of B16-F10 melanoma cells by α-mangostin. *Biochem. Biophys. Res. Commun.* **2014**, *450*, 1512–1517. [CrossRef]
5. Hsieh, S.-C.; Huang, M.-H.; Cheng, C.-W.; Hung, J.-H.; Yang, S.-F.; Hsieh, Y.-H. α-Mangostin induces mitochondrial dependent apoptosis in human hepatoma SK-Hep-1 cells through inhibition of p38 MAPK pathway. *Apoptosis* **2013**, *18*, 1548–1560. [CrossRef]
6. Shibata, M.-A.; Iinuma, M.; Morimoto, J.; Kurose, H.; Akamatsu, K.; Okuno, Y.; Akao, Y.; Otsuki, Y. α-Mangostin extracted from the pericarp of the mangosteen (*Garcinia mangostana* Linn) reduces tumor growth and lymph node metastasis in an immunocompetent xenograft model of metastatic mammary cancer carrying a p53 mutation. *BMC Med.* **2011**, *9*, 69. [CrossRef]
7. Chao, A.-C.; Hsu, Y.-L.; Liu, C.-K.; Kuo, P.-L. α-Mangostin, a Dietary Xanthone, Induces Autophagic Cell Death by Activating the AMP-Activated Protein Kinase Pathway in Glioblastoma Cells. *J. Agric. Food Chem.* **2011**, *59*, 2086–2096. [CrossRef]
8. Bin Hafeez, B.; Mustafa, A.; Fischer, J.W.; Singh, A.; Zhong, W.; Shekhani, M.O.; Meske, L.; Havighurst, T.; Kim, K.; Verma, A.K. α-Mangostin: A Dietary Antioxidant Derived from the Pericarp of *Garcinia mangostana* L. Inhibits Pancreatic Tumor Growth in Xenograft Mouse Model. *Antioxid. Redox Signal.* **2014**, *21*, 682–699. [CrossRef]
9. Cai, N.; Xie, S.-J.; Qiu, D.-B.; Jia, C.-C.; Du, C.; Liu, W.; Chen, J.-J.; Zhang, Q. Potential effects of α-mangostin in the prevention and treatment of hepatocellular carcinoma. *J. Funct. Foods* **2016**, *26*, 309–318. [CrossRef]
10. Lee, C.-H.; Ying, T.-H.; Chiou, H.-L.; Hsieh, S.-C.; Wen, S.-H.; Chou, R.-H.; Hsieh, Y.-H. Alpha-mangostin induces apoptosis through activation of reactive oxygen species and ASK1/p38 signaling pathway in cervical cancer cells. *Oncotarget* **2017**, *8*, 47425–47439. [CrossRef]
11. Johnson, J.J.; Petiwala, S.M.; Syed, D.N.; Rasmussen, J.T.; Adhami, V.M.; Siddiqui, I.A.; Kohl, A.M.; Mukhtar, H. α-Mangostin, a xanthone from mangosteen fruit, promotes cell cycle arrest in prostate cancer and decreases xenograft tumor growth. *Carcinogenesis* **2011**, *33*, 413–419. [CrossRef]
12. Chitchumroonchokchai, C.; Thomas-Ahner, J.M.; Li, J.; Riedl, K.M.; Nontakham, J.; Suksumrarn, S.; Clinton, S.K.; Kinghorn, A.D.; Failla, M.L. Anti-tumorigenicity of dietary α-mangostin in an HT-29 colon cell xenograft model and the tissue distribution of xanthones and their phase II metabolites. *Mol. Nutr. Food Res.* **2013**, *57*, 203–211. [CrossRef]
13. Bissoli, I.; Muscari, C. Doxorubicin and α-Mangostin oppositely affect luminal breast cancer cell stemness evaluated by a new retinaldehyde-dependent ALDH assay in MCF-7 tumor spheroids. *Biomed. Pharmacother.* **2020**, *124*, 109927. [CrossRef]
14. Adli, A.D.F.; Jahanban-Esfahlan, R.; Seidi, K.; Samandari-Rad, S.; Zarghami, N. An overview on Vadimezan (DMXAA): The vascular disrupting agent. *Chem. Biol. Drug Des.* **2018**, *91*, 996–1006. [CrossRef]
15. Baguley, B.C.; McKeage, M.J. ASA404: A tumor vascular-disrupting agent with broad potential for cancer therapy. *Future Oncol.* **2010**, *6*, 1537–1543. [CrossRef]
16. Le Naour, J.; Zitvogel, L.; Galluzzi, L.; Vacchelli, E.; Kroemer, G. Trial watch: STING agonists in cancer therapy. *OncoImmunology* **2020**, *9*, 1777624. [CrossRef]
17. Shih, A.Y.; Damm-Ganamet, K.L.; Mirzadegan, T. Dynamic Structural Differences between Human and Mouse STING Lead to Differing Sensitivity to DMXAA. *Biophys. J.* **2018**, *114*, 32–39. [CrossRef]
18. Liu, W.; Kim, G.B.; Krump, N.A.; Zhou, Y.; Riley, J.L.; You, J. Selective reactivation of STING signaling to target Merkel cell carcinoma. *Proc. Natl. Acad. Sci. USA* **2020**, *117*, 13730–13739. [CrossRef]

19. Chen, D.; Yu, Q.; Huang, X.; Dai, H.; Luo, T.; Shao, J.; Chen, J.; Huang, W.; Dong, X. A Highly-Efficient Type I Photosensitizer with Robust Vascular-Disruption Activity for Hypoxic-and-Metastatic Tumor Specific Photodynamic Therapy. *Small* **2020**, *16*, e2001059. [CrossRef]
20. Patra, J.K.; Das, G.; Fraceto, L.F.; Campos, E.V.R.; del Pilar Rodriguez-Torres, M.; Acosta-Torres, L.S.; Diaz-Torres, L.A.; Grillo, R.; Swamy, M.K.; Sharma, S.; et al. Nano based drug delivery systems: Recent developments and future prospects. *J. Nanobiotechnol.* **2018**, *16*, 71. [CrossRef]
21. Ambekar, R.S.; Choudhary, M.; Kandasubramanian, B. Recent advances in dendrimer-based nanoplatform for cancer treatment: A review. *Eur. Polym. J.* **2020**, *126*, 109546. [CrossRef]
22. Tunki, L.; Kulhari, H.; Sistla, R.; Pooja, D. 5—Dendrimer-Based Targeted Drug Delivery. In *Pharmaceutical Applications of Dendrimers*; Chauhan, A., Kulhari, H., Eds.; Micro and Nano Technologies; Elsevier: Amsterdam, The Netherlands, 2020; pp. 107–129. ISBN 978-0-12-814527-2.
23. Mahesh, S.; Tang, K.-C.; Raj, M. Amide Bond Activation of Biological Molecules. *Molecules* **2018**, *23*, 2615. [CrossRef]
24. Luo, G.-F.; Chen, W.-H.; Liu, Y.; Lei, Q.; Zhuo, R.-X.; Zhang, X.-Z. Multifunctional Enveloped Mesoporous Silica Nanoparticles for Subcellular Co-delivery of Drug and Therapeutic Peptide. *Sci. Rep.* **2014**, *4*, 6064. [CrossRef]
25. Bradshaw, P.R.; Wilson, I.D.; Gill, R.U.; Butler, P.J.; Dilworth, C.; Athersuch, T.J. Metabolic Hydrolysis of Aromatic Amides in Selected Rat, Minipig, and Human In Vitro Systems. *Sci. Rep.* **2018**, *8*, 2405. [CrossRef]
26. Kumari, R.; Majumder, M.M.; Lievonen, J.; Silvennoinen, R.; Anttila, P.; Nupponen, N.N.; Lehmann, F.; Heckman, C.A. Prognostic significance of esterase gene expression in multiple myeloma. *Br. J. Cancer* **2021**, *124*, 1428–1436. [CrossRef]
27. Dong, H.; Pang, L.; Cong, H.; Shen, Y.; Yu, B. Application and design of esterase-responsive nanoparticles for cancer therapy. *Drug Deliv.* **2019**, *26*, 416–432. [CrossRef]
28. Kurtoglu, Y.E.; Mishra, M.K.; Kannan, S.; Kannan, R.M. Drug release characteristics of PAMAM dendrimer–drug conjugates with different linkers. *Int. J. Pharm.* **2010**, *384*, 189–194. [CrossRef]
29. Markowicz, J.; Uram, Ł.; Wołowiec, S.; Rode, W. Biotin Transport-Targeting Polysaccharide-Modified PAMAM G3 Dendrimer as System Delivering α-Mangostin into Cancer Cells and *C. elegans* Worms. *Int. J. Mol. Sci.* **2021**, *22*, 12925. [CrossRef]
30. Perumal, D.; Golla, M.; Pillai, K.S.; Raj, G.; Krishna, P.K.A.; Varghese, R. Biotin-decorated NIR-absorbing nanosheets for targeted photodynamic cancer therapy. *Org. Biomol. Chem.* **2021**, *19*, 2804–2810. [CrossRef]
31. Uram, Ł.; Szuster, M.; Filipowicz, A.; Zaręba, M.; Wałajtys-Rode, E.; Wolowiec, S. Cellular uptake of glucoheptoamidated poly(amidoamine) PAMAM G3 dendrimer with amide-conjugated biotin, a potential carrier of anticancer drugs. *Bioorg. Med. Chem.* **2017**, *25*, 706–713. [CrossRef]
32. Yang, W.; Cheng, Y.; Xu, T.; Wang, X.; Wen, L.-P. Targeting cancer cells with biotin–dendrimer conjugates. *Eur. J. Med. Chem.* **2009**, *44*, 862–868. [CrossRef] [PubMed]
33. Yellepeddi, V.; Kumar, A.; Palakurthi, S. Biotinylated poly(amido)amine (PAMAM) dendrimers as carriers for drug delivery to ovarian cancer cells in vitro. *Anticancer Res.* **2009**, *29*, 2933–2943. [PubMed]
34. Ma, J.; Yao, H. Dendrimer-paclitaxel complexes for efficient treatment in ovarian cancer: Study on OVCAR-3 and HEK293T cells. *Acta Biochim. Pol.* **2018**, *65*, 219–225. [CrossRef] [PubMed]
35. Hemmer, R.; Hall, A.; Spaulding, R.; Rossow, B.; Hester, M.; Caroway, M.; Haskamp, A.; Wall, S.; Bullen, H.A.; Morris, C.; et al. Analysis of Biotinylated Generation 4 Poly(amidoamine) (PAMAM) Dendrimer Distribution in the Rat Brain and Toxicity in a Cellular Model of the Blood-Brain Barrier. *Molecules* **2013**, *18*, 11537–11552. [CrossRef]
36. Smith, P.E.S.; Brender, J.R.; Dürr, U.H.N.; Xu, J.; Mullen, D.G.; Holl, M.M.B.; Ramamoorthy, A. Solid-State NMR Reveals the Hydrophobic-Core Location of Poly(amidoamine) Dendrimers in Biomembranes. *J. Am. Chem. Soc.* **2010**, *132*, 8087–8097. [CrossRef]
37. Honnen, S. *Caenorhabditis elegans* as a powerful alternative model organism to promote research in genetic toxicology and biomedicine. *Arch. Toxicol.* **2017**, *91*, 2029–2044. [CrossRef]
38. Tomalia, D.A.; Baker, H.; Dewald, J.; Hall, M.; Kallos, G.; Martin, S.; Roeck, J.; Ryder, J.; Smith, P. A New Class of Polymers: Starburst-Dendritic Macromolecules. *Polym. J.* **1985**, *17*, 117–132. [CrossRef]
39. Czarnik-Kwaśniak, J.; Kwaśniak, K.; Tutaj, K.; Filiks, I.; Uram, Ł.; Stompor, M.; Wołowiec, S. Glucoheptoamidated polyamidoamine PAMAM G3 dendrimer as a vehicle for succinate linked doxorubicin; enhanced toxicity of DOX against grade IV glioblastoma U-118 MG cells. *J. Drug Deliv. Sci. Technol.* **2020**, *55*, 101424. [CrossRef]
40. Stiernagle, T. Maintenance of *C. elegans*. In *WormBook*; The *C. elegans* Research Community, Ed.; WormBook: Pasadena, CA, USA, 2006. [CrossRef]
41. Crosignani, S.; Gonzalez, A.J.; Swinnen, D. Polymer-Supported Mukaiyama Reagent: A Useful Coupling Reagent for the Synthesis of Esters and Amides. *Org. Lett.* **2004**, *6*, 4579–4582. [CrossRef]
42. Czerniecka-Kubicka, A.; Tutka, P.; Pyda, M.; Walczak, M.; Uram, Ł.; Misiorek, M.; Chmiel, E.; Wołowiec, S. Stepwise Glucoheptoamidation of Poly(Amidoamine) Dendrimer G3 to Tune Physicochemical Properties of the Potential Drug Carrier: In Vitro Tests for Cytisine Conjugates. *Pharmaceutics* **2020**, *12*, 473. [CrossRef]
43. Martinho, N.; Florindo, H.; Silva, L.; Brocchini, S.; Zloh, M.; Barata, T. Molecular Modeling to Study Dendrimers for Biomedical Applications. *Molecules* **2014**, *19*, 20424–20467. [CrossRef]
44. Zhang, S.-J.; Ding, Z.-S.; Jiang, F.-S.; Ge, Q.-F.; Guo, D.-W.; Li, H.-B.; Hu, W.-X. Synthesis, anticancer evaluation and docking study of vadimezan derivatives with carboxyl substitution. *MedChemComm* **2014**, *5*, 512–520. [CrossRef]

45. Lv, S.; Tang, Z.; Song, W.; Zhang, D.; Li, M.; Liu, H.; Cheng, J.; Zhong, W.; Chen, X. Inhibiting Solid Tumor Growth In Vivo by Non-Tumor-Penetrating Nanomedicine. *Small* **2017**, *13*, 1600954. [CrossRef]
46. AAT Bioquest. Available online: https://www.aatbio.com/tools/ic50-calculator (accessed on 6 January 2022).
47. Kurniawan, Y.S.; Priyangga, K.T.A.; Jumina; Pranowo, H.D.; Sholikhah, E.N.; Zulkarnain, A.K.; Fatimi, H.A.; Julianus, J. An Update on the Anticancer Activity of Xanthone Derivatives: A Review. *Pharmaceuticals* **2021**, *14*, 1144. [CrossRef]
48. Castanheiro, R.A.P.; Silva, A.M.S.; Campos, N.A.N.; Nascimento, M.S.J.; Pinto, M.M.M. Antitumor Activity of Some Prenylated Xanthones. *Pharmaceuticals* **2009**, *2*, 33–43. [CrossRef]
49. Teh, S.S.; Ee, G.C.L.; Mah, S.H.; Lim, Y.M.; Ahmad, Z. Cytotoxicity and Structure-Activity Relationships of Xanthone Derivatives from *Mesua beccariana*, *Mesua ferrea* and *Mesua congestiflora* towards Nine Human Cancer Cell Lines. *Molecules* **2013**, *18*, 1985–1994. [CrossRef]
50. Singh, J.; Jain, K.; Mehra, N.K.; Jain, N.K. Dendrimers in anticancer drug delivery: Mechanism of interaction of drug and dendrimers. *Artif. Cells Nanomed. Biotechnol.* **2016**, *44*, 1626–1634. [CrossRef]
51. Zeng, Y.; Kurokawa, Y.; Win-Shwe, T.-T.; Zeng, Q.; Hirano, S.; Zhang, Z.; Sone, H. Effects of PAMAM dendrimers with various surface functional groups and multiple generations on cytotoxicity and neuronal differentiation using human neural progenitor cells. *J. Toxicol. Sci.* **2016**, *41*, 351–370. [CrossRef]
52. Janaszewska, A.; Lazniewska, J.; Trzepiński, P.; Marcinkowska, M.; Klajnert-Maculewicz, B. Cytotoxicity of Dendrimers. *Biomolecules* **2019**, *9*, 330. [CrossRef]
53. Quintana, A.; Raczka, E.; Piehler, L.; Lee, I.; Myc, A.; Majoros, I.; Patri, A.K.; Thomas, T.P.; Mulé, J.; Baker, J.R., Jr. Design and Function of a Dendrimer-Based Therapeutic Nanodevice Targeted to Tumor Cells Through the Folate Receptor. *Pharm. Res.* **2002**, *19*, 1310–1316. [CrossRef]
54. Thomas, T.P.; Majoros, I.J.; Kotlyar, A.; Kukowska-Latallo, J.F.; Bielinska, A.; Myc, A.A.; Baker, J.J.R. Targeting and Inhibition of Cell Growth by an Engineered Dendritic Nanodevice. *J. Med. Chem.* **2005**, *48*, 3729–3735. [CrossRef]
55. de Almeida, M.S.; Susnik, E.; Drasler, B.; Taladriz-Blanco, P.; Petri-Fink, A.; Rothen-Rutishauser, B. Understanding nanoparticle endocytosis to improve targeting strategies in nanomedicine. *Chem. Soc. Rev.* **2021**, *50*, 5397–5434. [CrossRef]
56. Adli, A.D.F.; Jahanban-Esfahlan, R.; Seidi, K.; Farajzadeh, D.; Behzadi, R.; Zarghami, N. Co-Administration of Vadimezan and Recombinant Coagulase-NGR Inhibits Growth of Melanoma Tumor in Mice. *Adv. Pharm. Bull.* **2021**, *11*, 385–392. [CrossRef]
57. van Dongen, M.A.; Vaidyanathan, S.; Holl, M.M.B. PAMAM dendrimers as quantized building blocks for novel nanostructures. *Soft Matter* **2013**, *9*, 11188–11196. [CrossRef]
58. Uram, Ł.; Szuster, M.; Misiorek, M.; Filipowicz, A.; Wołowiec, S.; Wałajtys-Rode, E. The effect of G3 PAMAM dendrimer conjugated with B-group vitamins on cell morphology, motility and ATP level in normal and cancer cells. *Eur. J. Pharm. Sci.* **2017**, *102*, 275–283. [CrossRef]
59. Kurose, H.; Shibata, M.-A.; Iinuma, M.; Otsuki, Y. Alterations in Cell Cycle and Induction of Apoptotic Cell Death in Breast Cancer Cells Treated with α-Mangostin Extracted from Mangosteen Pericarp. *J. Biomed. Biotechnol.* **2012**, *2012*, 672428. [CrossRef]
60. Kwak, H.-H.; Kim, I.-R.; Kim, H.-J.; Park, B.-S.; Yu, S.-B. α-Mangostin Induces Apoptosis and Cell Cycle Arrest in Oral Squamous Cell Carcinoma Cell. *Evid.-Based Complement. Altern. Med.* **2016**, *2016*, 5352412. [CrossRef]
61. Lucio, D.; Martínez-Ohárriz, M.C.; Gu, Z.; He, Y.; Aranaz, P.; Vizmanos, J.L.; Irache, J.M. Cyclodextrin-grafted poly(anhydride) nanoparticles for oral glibenclamide administration. In vivo evaluation using *C. elegans*. *Int. J. Pharm.* **2018**, *547*, 97–105. [CrossRef]
62. Martínez-López, A.L.; González-Navarro, C.J.; Aranaz, P.; Vizmanos, J.L.; Irache, J.M. In vivo testing of mucus-permeating nanoparticles for oral insulin delivery using *Caenorhabditis elegans* as a model under hyperglycemic conditions. *Acta Pharm. Sin. B* **2021**, *11*, 989–1002. [CrossRef]
63. Ma, H.; Bertsch, P.M.; Glenn, T.C.; Kabengi, N.; Williams, P.L. Toxicity of manufactured zinc oxide nanoparticles in the nematode *Caenorhabditis elegans*. *Environ. Toxicol. Chem.* **2009**, *28*, 1324–1330. [CrossRef]
64. Marcelino, M.Y.; Borges, F.A.; Scorzoni, L.; Singulani, J.D.L.; Garms, B.C.; Niemeyer, J.C.; Guerra, N.B.; Brasil, G.S.P.; Mussagy, C.U.; Carvalho, F.A.D.O.; et al. Synthesis and characterization of gold nanoparticles and their toxicity in alternative methods to the use of mammals. *J. Environ. Chem. Eng.* **2021**, *9*, 106779. [CrossRef]

pharmaceutics

Supplementary materials: Synthesis and Properties of α-Mangostin and Vadimezan Conjugates with Glucoheptoamidated and Biotinylated 3rd Generation Poly(amidoamine) Dendrimer, and Conjugation Effect on Their Anticancer and Anti-Nematode Activities

Joanna Markowicz, Stanisław Wołowiec, Wojciech Rode and Łukasz Uram

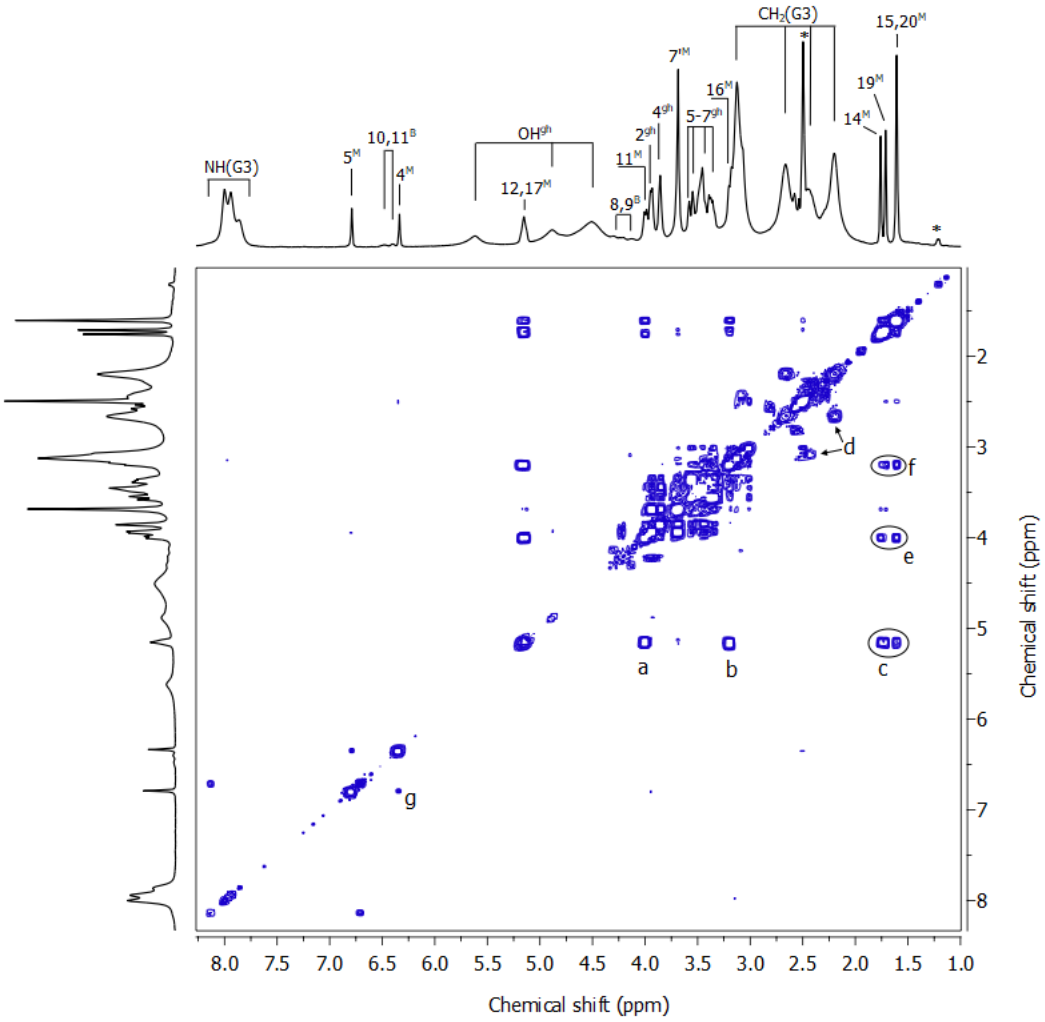

Figure S1. The ^{1}H-^{1}H COSY spectrum of G3^{gh2B5M} in DMSO-d$_6$. The relevant cross-peaks are labeled as follows: a – 11H^{M}/12H^{M}; b – 16H^{M}/17H^{M}; c – a group of scalar coupling peaks between 14H^{M}, 15H^{M}, 19H^{M}, 20H^{M} (methyl group singlets) and 12H^{M}, 17H^{M} (overlapping methylene triplets); d – a group of internal PAMAM G3 cross-peaks; e – 14H^{M},15H^{M}/11H^{M}; f – 19H^{M},20H^{M}/16H^{M}; g – 4H^{M}/5H^{M}. The chemical shifts of ^{1}H peaks are collected in Table S1.

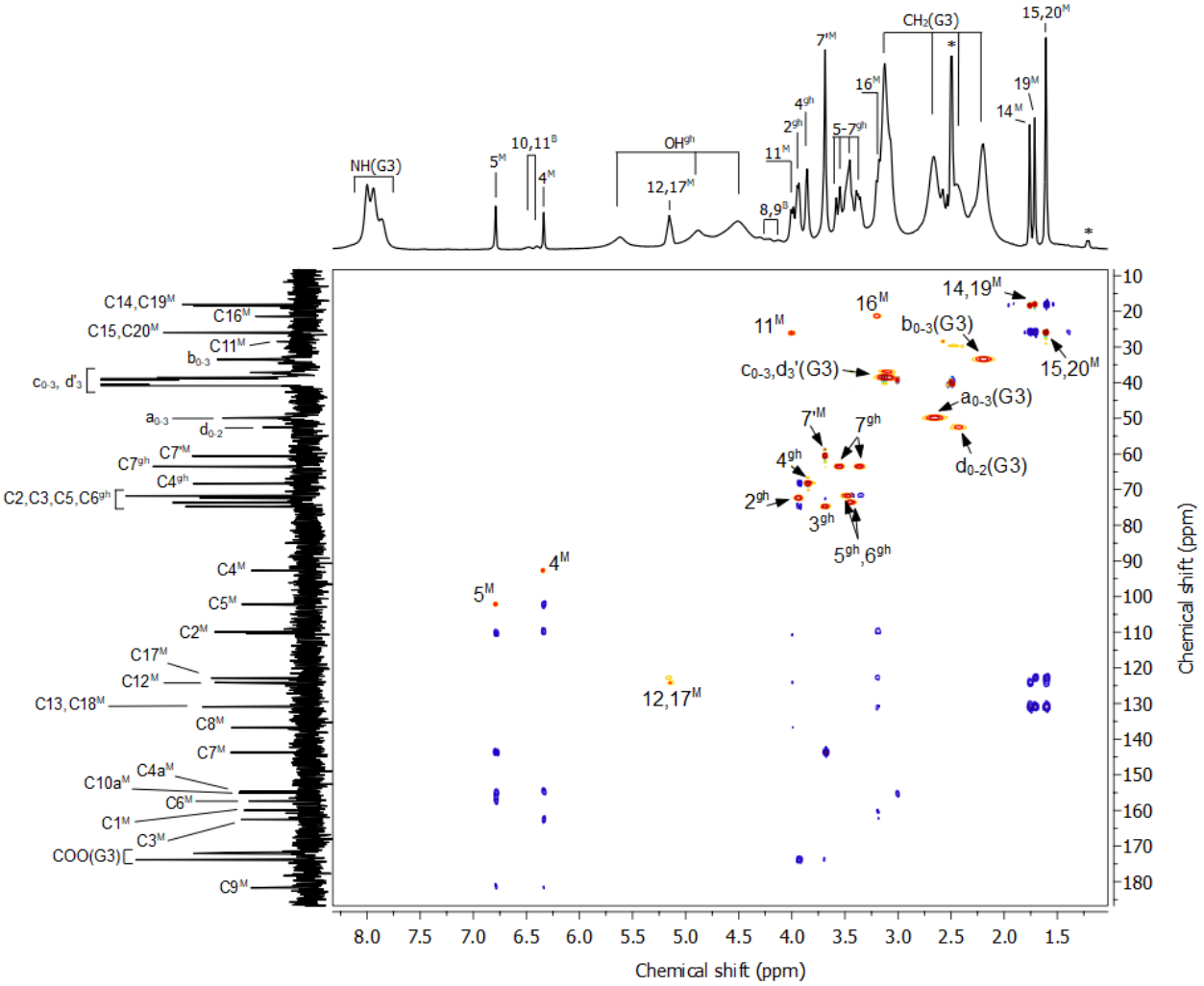

Figure S2. The HSQC/HMBC combined spectra for G3^{gh2B5M} in DMSO-d$_6$. HSQC peaks are marked yellow-red and HMBC peaks are marked blue. The one-bond ^{1}H-^{13}C peaks are labeled with locant and substituents with upper case (^{M}, ^{B}, and ^{gh}), while the peaks within PAMAM G3 arms are labeled according to numbering shown in Fig.2 in [29]. The chemical shifts of ^{1}H and ^{13}C peaks are collected in Table S1.

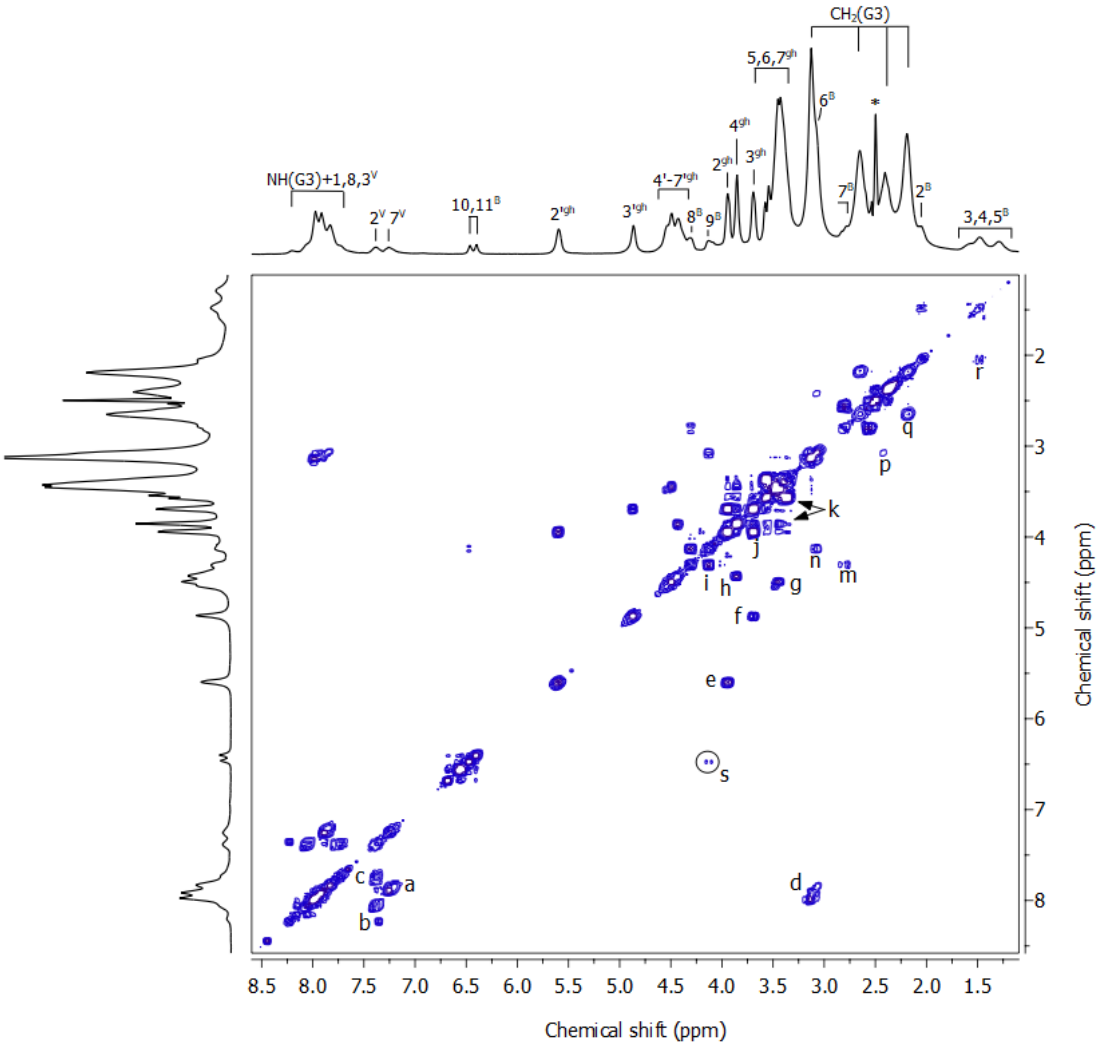

Figure S3. The ^{1}H-^{1}H COSY spectrum of **G3^{gh4B5V}** in DMSO-d$_6$. The relevant cross-peaks are labeled as follows: a – 7H^{V}/8H^{V}; b – 2H^{V}/1H^{V}; c – 2H^{V}/3H^{V}; d – c$_{0\text{-}3}$/NH (internal PAMAM G3 cross-peak; for detailed assignment see Fig. 2 in [29]); e – 2H^{gh}/2′H^{gh}; f – 3H^{gh}/3′H^{gh}; g – cross-peak between group of gh CH protons (5^{gh}, 6^{gh}, 7^{gh}) and group of OH protons (5′^{gh}, 6′^{gh}, 7′^{gh}) in gh; h – 4H^{gh}/4′H^{gh}; i – 9H^{B}/8H^{B}; j – 3H^{gh}/2H^{gh},4H^{gh}; k – 5H^{gh}/4H^{gh}; m – 7H^{B}/8H^{B}; n – 6H^{B}/9H^{B}; p – d$_{0\text{-}2}$/c$_{0\text{-}3}$ and q – b$_{0\text{-}3}$/a$_{0\text{-}3}$ (internal PAMAM G3 cross-peaks); r – 3H^{B}/2H^{B}; s – 9H^{B}/11H^{B}. The chemical shifts of ^{1}H peaks are collected in Table S1.

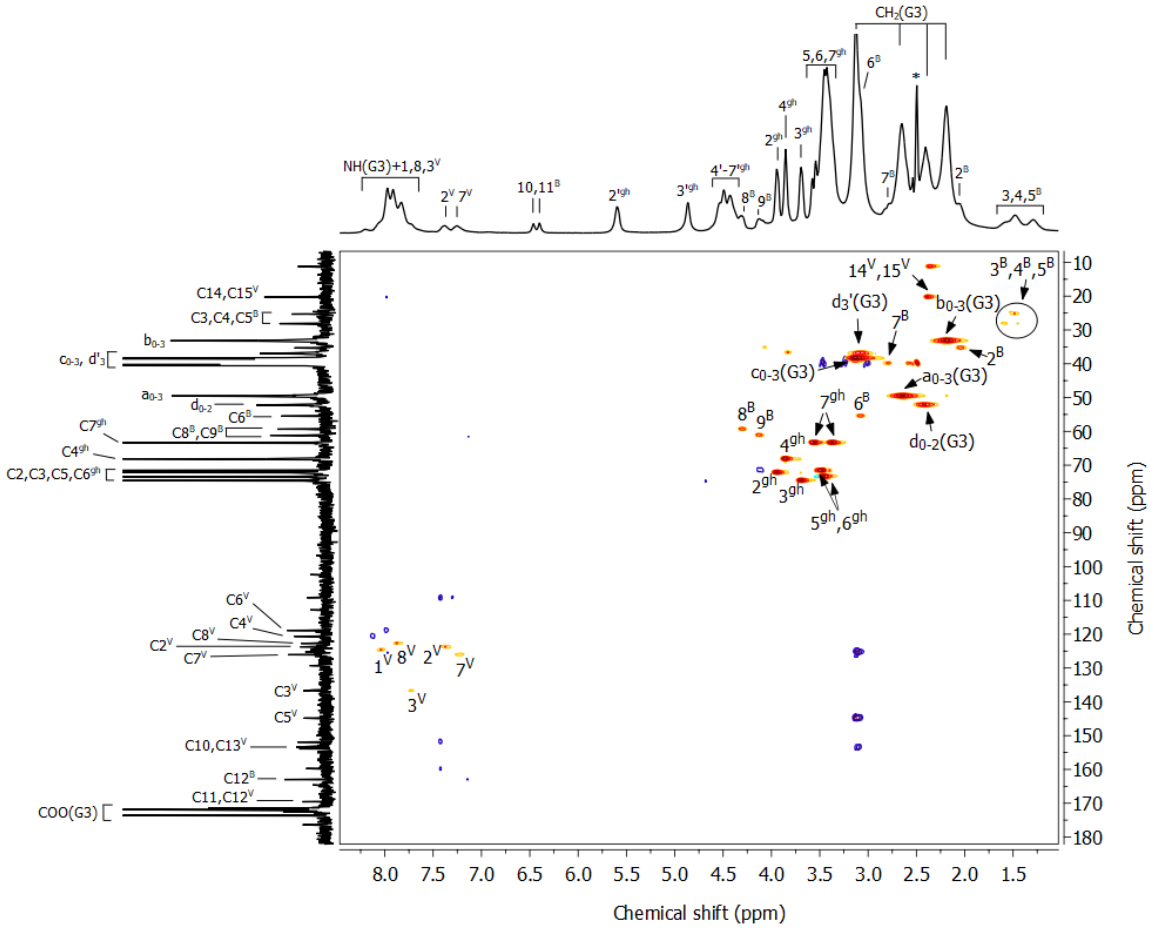

Figure S4. The HSQC/HMBC combined spectra for **G3^{gh4B5V}** in DMSO-d_6. HSQC peaks are marked yellow-red and HMBC peaks are marked blue. The one-bond ^{1}H-^{13}C peaks are labeled with locant and substituents with upper case (^{V}, ^{B}, and ^{gh}), while the peaks within PAMAM G3 arms are labeled according to numbering shown in Fig.2 in [29]. The group of HSQC peaks between 3, 4, and 5 proton nuclei of biotin and corresponding carbon nuclei are grouped within the circle on the map. The chemical shifts of ^{1}H and ^{13}C peaks are collected in Table S1.

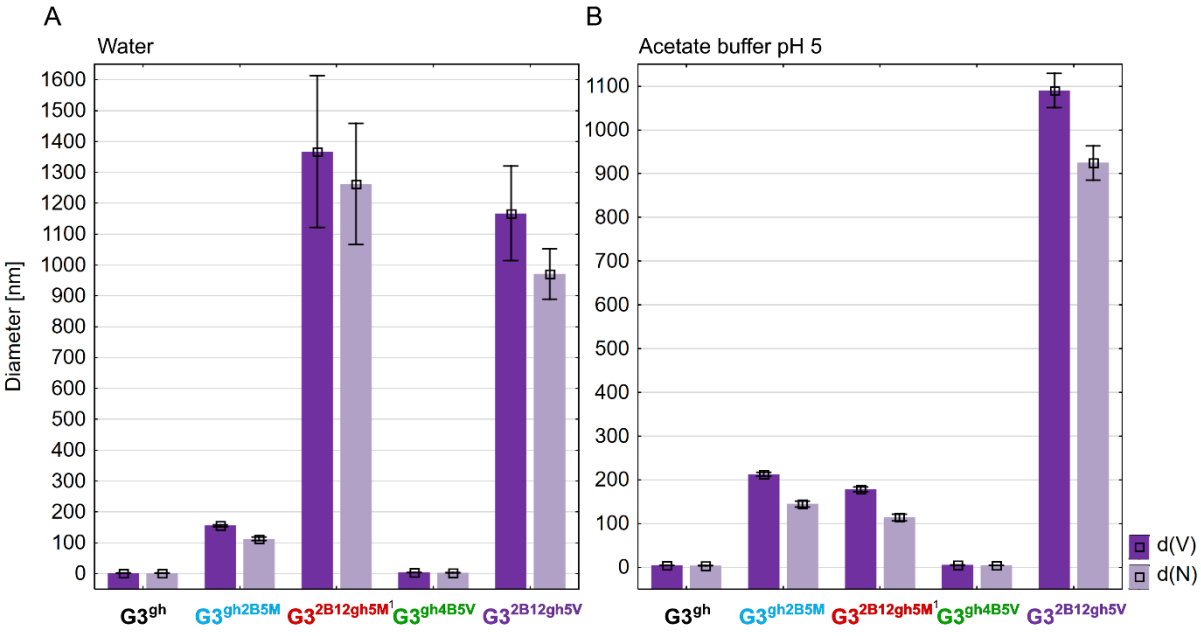

Figure S5. Diameter of conjugates averaged by volume (d(V)) and by number of molecules (d(N)) measured in water (A) and in acetate buffer pH 5 (B). Data are presented as a mean ± standard deviation. [1] Values for $G3^{2B12gh5M}$ were reproduced from [29].

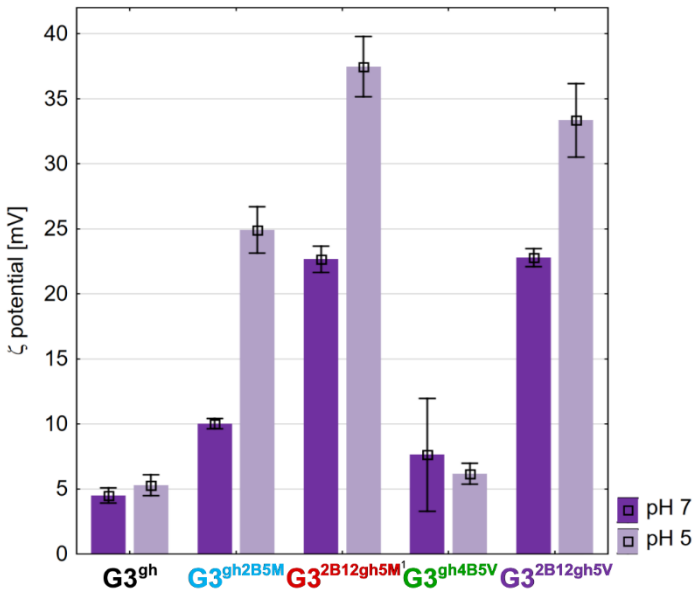

Figure S6. Zeta potential of conjugates measured in water (pH 7) and acetate buffer (pH 5). Data are presented as a mean ± standard deviation. [1] Values for $G3^{2B12gh5M}$ were taken from [29].

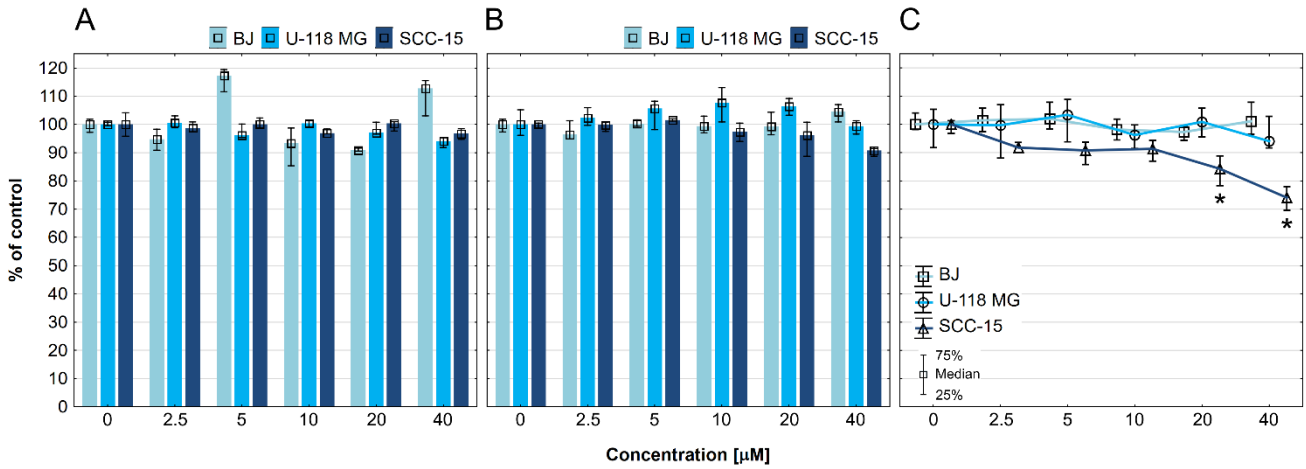

Figure S7. Cytotoxicity of **G3^{gh}** vehicle estimated with NR (**A**) and XTT (**B**) assay after 48 h incubation with normal fibroblasts (BJ), glioblastoma cells (U-118 MG) and squamous carcinoma cells (SCC-15). Anti-proliferative activity (**C**) of **G3^{gh}** against BJ, U-118 MG, and SCC-15 cells after 72 h of incubation, determined with Hoechst 33342 staining. Results are presented as medians of a percent against non-treated control (control expressed as 100%). The whiskers indicate lower (25%) and upper (75%) quartile ranges. * $p \leq 0.05$; Kruskal-Wallis test (against non-treated control).

Table S1. The ^{1}H and ^{13}C resonance assignments of the **G3^{gh4B5V}**, V, **G3^{gh2B5M}** and αM based on COSY and HSQC/HMBC spectra in DMSO-d$_6$. The superscripts: ^{B}, ^{gh}, ^{V} and ^{M} are related to Biotin, glucoheptoamide, Vadimezan and α-Mangostin, respectively. The annotation nd means not determined due to low intensity of resonances or overlapping with high intensity peaks from PAMAM.

Species	G3^{gh4B5V}		Vadimezan		G3^{gh2B5M}		α-Mangostin	
Locant	^{1}H	^{13}C	^{1}H	^{13}C	^{1}H	^{13}C	^{1}H	^{13}C
b$_{0\text{-}3}$(PAMAM)	2.19	33.2			2.20	33.5		
d$_{0\text{-}2}$(PAMAM)	2.42	52.2			2.45	52.6		
a$_{0\text{-}3}$ (PAMAM)	2.65	49.5			2.66	49.9		
d$_3$'(PAMAM)	3.08	37.0			3.07	37.2		
c$_{0\text{-}3}$(PAMAM)	3.13	38.3			3.13	38.6		
-COO(G3)	-	171.5			-	171.9		
-COO(G3)	-	171.8			-	173.8		
NH(G3)	7.98				7.93			
2^{B}	2.05	35.3			nd	nd		
3^{B}, 4^{B}, 5^{B}	1.20-1.65	25.3			1.21	nd		
3^{B}, 4^{B}, 5^{B}	1.20-1.65	28.1						
3^{B}, 4^{B}, 5^{B}	1.20-1.65	28.3						
6^{B}	3.08	55.5			nd			
7^{B}	2.78	nd			nd			
8^{B}	4.31	59.4			4.30	nd		
9^{B}	4.13	61.2			4.12	nd		
10^{B}	6.40	nd			6.40	nd		
11^{B}	6.46	nd			6.48	nd		
12^{B}	-	163.0			-	nd		
1^{gh}	-	172.5			-	nd		
2^{gh}	3.94	72.2			3.94	72.4		
3^{gh}	3.69	74.6			3.69	74.8		
4^{gh}	3.85	68.1			3.86	68.3		
5^{gh} or 6^{gh}	3.46	73.4			3.45	73.7		
5^{gh} or 6^{gh}	3.48	71.6			3.48	71.8		
7^{gh}	3.60-3.30	63.3			3.60-3.30	63.5		
4'^{gh}, 5'^{gh}, 6'^{gh}, 7'^{gh}	4.54-4.43	-			5.62-4.51	-		

3′^{gh}	4.86	-				-		
2′^{gh}	5.60	-				-		
1^{V}	7.98	124.5	8.09	124.6				
2^{V}	7.38	123.7	7.41	123.8				
3^{V}	7.73	136.7	7.79	136.7				
4^{V}	-	120.6	-	120.6				
5^{V}	-	144.8	-	144.8				
6^{V}	-	118.9	-	118.9				
7^{V}	7.26	126.1	7.30	126.1				
8^{V}	7.88	122.7	7.92	122.7				
9^{V}	-	176.5	-	176.3				
10^{V}	-	153.9	-	154.0				
11^{V} or 12^{V}	-	169.6	-	169.3				
13^{V}	-	153.4	-	153.5				
14^{V}, 15^{V}	2.37	20.3	2.41	11.15 20.25				
16^{V}	nd	nd	3.98	35.7				
17^{V}	-	173.6	-	172.0				
1^{M}					-	159.9	-	160.0
1′^{M}					13.73	-	13.72	-
2^{M}					-	109.8	-	109.7
3^{M}					-	162.6	-	162.9
3′^{M}					-	-	11.01	-
4^{M}					6.34	92.7	6.34	92.6
4a^{M}					-	154.5	-	154.5
9a^{M}					-	nd	-	154.9
9^{M}					-	181.7	-	181.2
8a^{M}					-	nd	-	108.0
10a^{M}					-	155.1	-	155.8
5^{M}					6.79	102.1	6.80	101.9
6^{M}					-	157.3	-	161.6
6′^{M}					-	-	10.82	-
7^{M}					-	143.7	-	145.1
7′^{M}					3.69	60.5	3.70	60.2
8^{M}					-	136.7	-	135.6
11^{M}					3.99	26.0	4.01	26.2
12^{M}					5.15	124.1	5.16	124.8
13^{M}					-	130.8	-	130.2
14^{M}					1.76	18.6	1.77	18.4
15^{M}					1.61	26.1	1.62	26.1
16^{M}					3.19	21.4	3.21	21.6
17^{M}					5.15	122.8	5.16	123.3
18^{M}					-	130.9	-	130.6
19^{M}					1.71	18.1	1.72	18.2
20^{M}					1.61	26.0	1.62	26.0